

NASA-CR-193151

FINAL TECHNICAL REPORT

BASALTIC VOLCANISM AND ANCIENT PLANETARY CRUSTS

NASA GRANT NAG9-102

GRANT PERIOD: 6/1/86 to 5/31/93

PRINCIPAL INVESTIGATOR: JOHN W. SHERVAIS, Ph.D.

Department of Geological Sciences
University of South Carolina
Columbia, SC 29208

GRANT
1N-46-CR
170680

(NASA-CR-193151) BASALTIC
VOLCANISM AND ANCIENT PLANETARY
CRUSTS Final Technical Report, 1
Jun. 1986 - 31 May 1993 (South
Carolina Univ.) 123 p

N94-24363
--THRU--
N94-24373
Unclas

G3/91 0170680



BASALTIC VOLCANISM AND ANCIENT PLANETARY CRUSTS

The purpose of this project is to decipher the origin of rocks which form the ancient lunar crust. Our goal is to better understand the how the moon evolved chemically and, more generally, the processes involved in the chemical fractionation of terrestrial planetoids. This research has implications for other planetary bodies besides the Moon, especially smaller planetoids which evolved early in the history of the solar system and are now thermally stable.

The three main areas focused on in our work (lunar mare basalts, KREEP basalts, and plutonic rocks of the lunar highlands) provide complementary information on the lunar interior and the processes that formed it. Mare basalts are important because they form by melting of the lunar mantle and thus provide information on its chemical and mineralogical constitution. In order to obtain this information, however, we must be able to see through any low pressure fractionation that has affected these rocks and back to the original parent magma composition. This means that the effects of fractional crystallization and assimilation must be determined and accounted for. KREEP basalts are important because they appear to represent the final product of magma ocean crystallization (Warren and Wasson, 1979) and because they constitute a ubiquitous mixing component in many (if not most) lunar rocks. Highland plutonic rocks are important because they tell us about flotation cumulates of the magma ocean and about subsequent crust-forming magmatic events that preceded mare basalt genesis.

My work has focused to a large extent on the western lunar areas because it is in these areas that the most interesting petrologic and chemical variations are observed. As part of this project, I have studied mare basalts and KREEP basalts from the Apollo 15 site, and mare basalts and highland rocks from the Apollo 14 site. In the following sections I summarize our work in these areas, and present whole rock geochemical data generated during this project. Abundant mineral chemical data have also been produced, but are not presented in this report.

Petrogenesis of Mare Basalts

Despite the fact that mare basalts comprise less than 1% of the lunar crust, they constitute our primary source of information on the moon's upper mantle. Compositional variations between mare basalt suites reflect variations in the mineralogical and geochemical make-up of the lunar mantle that formed during the earliest stages of lunar differentiation. Mare basalt model ages show that their source region underwent a major fractionation early in the moon's history (4.5-4.4 b.y.), coeval with the formation of the lunar highlands crust.

The mare basalt source region has geochemical characteristics that are complementary to the highlands crust, and it is generally thought to comprise mafic cumulates from the magma ocean (e.g., Taylor and Jakes, 1977; Taylor, 1982). The progressive enrichment of mare basalts in Fe/Mg, alkalis, and incompatible trace elements in the sequence very low-Ti basalt --> low-Ti basalt --> high-Ti basalt is explained by the remelting of cumulates formed at progressively shallower depths in the evolving magma ocean (Taylor and Jakes, 1977; Taylor, 1982; BSVP, 1981). This

model is also consistent with the observed decrease in compatible element concentrations and the progressive increase in negative Eu anomalies.

Recent models of mare basalt petrogenesis have stressed two dominant themes: (1) the assimilation of crustal components, e.g., KREEP or granite (Binder, 1985; Shervais et al, 1985a, 1985b; Shih et al, 1984, 1986; Dickinson et al, 1985; Neal et al, 1987, 1988), and (2) melting of complex, hybrid source regions (Hughes et al, 1988). Assimilation of granite by at least one Apollo 14 mare basalt has been well established (Shervais et al, 1985b; Shih et al, 1984, 1986; Neal et al, 1988a). Assimilation of KREEP by mare basalts has also been well established at the Apollo 14 site (Dickinson et al, 1985; Shervais et al, 1985a; Neal et al, 1987, 1988b). Binder (1985) suggests that all mare basalts have undergone modification by a KREEPy component, but no specific studies have been made of individual basalt suites except at the Apollo 14 site.

Apollo 15 Mare basalts: Twenty-five clasts of mare basalt from lunar breccia 15498 were analyzed to determine (a) the compositional range of mare basalt suites at the Apollo 15 site and (b) if mare basalt types not found among previously analyzed large samples exist at this site. All samples were studied petrographically and representative suites of minerals analyzed by EMP; whole rock major and trace element compositions were determined by fused bead EMP analysis and by INAA (Shervais et al., 1988, 1990; Vetter et al., 1988). Our data show that the Apollo 15 QNB suite extends to more evolved compositions than previously recognized, and that the ONB suite contains some high-SiO₂ members which are probably parental to the QNB group (Vetter et al., 1988). No exotic mare basalt types were found, in contrast to the Apollo 14 site, where a wide range of distinct mare basalt types exist only as clasts in breccia (e.g., Shervais et al., 1985a).

Our data show that assimilation of KREEP at low pressures is not important at the Apollo 15 site (Vetter and Shervais, 1989). KREEP assimilation models which succeed at the Apollo 14 site will not work at Apollo 15 because the A-15 basalts have LREE/MREE slopes < 1. The Apollo 15 basalts also have low overall concentrations of incompatible elements which differ little between the two main suites present -- the ONB suite and the QNB suite. These suites differ mainly in their major element chemistry (unlike the Apollo 14 basalts, which have nearly identical major element compositions but a wide range in trace element concentrations). We have tried a variety of KREEP assimilation models for Apollo 15 basalts and none have proved satisfactory.

We have proposed that major and trace element chemical variations in the Apollo 15 mare basalt suites are consistent with a dynamic melting model (Vetter and Shervais, 1989). In this model, an earlier melting event depletes the basalt source region in incompatible elements, but this depletion is incomplete because a small fraction of the melt produced (typically 10% to 20%) is retained in the refractory residue (most likely as dikes and veins). Later melting events tap this combined source region (refractory phases plus trapped melt). Our preliminary results indicate that dynamic melting is capable of reproducing the peculiar hump-shaped pattern of the Apollo 15 mare basalts without recourse to KREEP assimilation (Vetter and Shervais, 1989). We have written a computer model to investigate dynamic melting which includes nine trace

elements (5 REE, Ba, Th, Sc, Ti) which range from very incompatible to compatible. The computer model also calculates the trace element composition of magma ocean cumulates in equilibrium with the liquid (the phases and proportions must be input) and factors in any specified amount of trapped liquid requested. The dynamic melting model appears to be capable of generating the ONB and QNB trace element patterns with a range of assumed mantle compositions, from pyroxene-rich to olivine-rich (Vetter and Shervais, 1989).

We have also modeled major element compositions using the MAGPOX and MAGFOX programs of John Longhi. These calculations are not as robust as the trace element models because melting relations are not well constrained at high pressures and because the mineralogic compositions of magma ocean cumulates are not well known. Nonetheless, our calculations show that the major element compositions of primitive olivine normative and quartz normative basalts can be reproduced approximately by successive melting events in the same ultramafic source region.



Table 1. Whole rock major and trace element analyses of Apollo 15 mare basalt clasts from lunar breccia 15498. Major elements by fused bead electron microprobe analysis (EMPA), trace elements by instrumental neutron activation analysis (INAA). nd = not detected, na = not analyzed.

	B-1	B-2	B-40	B-20	B-6	B-24	B-43	B-5	B-3
SiO ₂	48.8	47.89	47.62	48.03	47.52	48.06	47.86	47.74	48.09
TiO ₂	1.82	2.35	1.95	1.95	2.14	2.17	2	2.14	1.93
Al ₂ O ₃	9.64	9.14	9.66	9.68	9.82	10.67	10.07	10.27	10.37
FeO	18.75	20.19	19.76	19.06	19.98	18.96	19.09	19.43	18.96
MnO	0.22	0.24	0.3	0.25	0.3	0.23	0.26	0.26	0.24
MgO	9.27	9.25	9.48	9.09	9.42	8.12	8.43	8.04	8.56
CaO	10.58	10.34	10.27	10.44	10.26	10.78	10.82	11.01	10.68
Na ₂ O	0.24	0.23	0.26	0.23	0.25	0.37	0.26	0.24	0.25
K ₂ O	0.04	0.04	0.04	0.04	0.05	0.04	0.04	0.02	0.04
P ₂ O ₅	0.06	0.05	0.06	0.06	0.06	0.08	0.06	0.09	0.05
Cr ₂ O ₃	0.51	0.48	0.55	0.6	0.56	0.54	0.59	0.47	0.58
Sum	99.93	100.2	99.95	99.43	100.36	100.02	99.48	99.71	99.75
Na ₂ O	0.223	0.222	0.244	0.236	0.243	0.237	0.246	0.255	0.254
FeO	19.12	20.04	19.55	18.58	9.2	19.15	19.06	18.63	18.84
Sc	48.3	46.7	42.7	41.3	41.3	43.8	43.3	44.2	43.3
Cr	3100	3100	3500	3500	3400	3500	3700	3200	3600
Co	37	47.5	42	39.2	40.6	40.8	39.6	39.3	40
Rb	20	nd	20	nd	nd	nd	9	nd	nd
Sr	180	150	120	nd	nd	nd	130	150	110
Cs	nd	nd	nd	nd	0.24	nd	nd	nd	nd
Ba	89	90	90	90	90	90	130	100	90
La	4.93	4.41	5.68	5.63	5.85	5.7	5.48	5.43	5.02
Ce	4.1	12.1	17.1	16.4	8	17.2	16	15.5	14
Nd	16	16	13	11	16	16	19	19	20
Sm	3.15	3.14	3.54	3.39	3.67	3.57	3.51	3.43	3.27
Eu	0.68	0.723	0.784	0.739	0.77	0.777	0.764	0.77	0.715
Tb	0.78	0.76	0.82	0.84	0.83	0.83	0.83	0.82	0.77
Yb	2.32	2.17	2.61	2.53	2.59	2.62	2.56	2.54	2.38
Lu	0.34	0.317	0.36	0.352	0.382	0.376	0.37	0.37	0.344
Zr	130	160	150	170	165	120	100	110	140
Hf	2.2	2.33	2.54	2.37	2.67	2.41	2.54	2.45	2.33
Ta	0.36	0.36	0.41	0.34	0.39	0.35	0.36	0.38	0.32
Th	0.58	0.43	0.67	0.6	0.67	0.65	0.64	0.65	0.65

Table 1. Whole rock major and trace element analyses of Apollo 15 mare basalt clasts from lunar breccia 15498 (continued).

	B-14	B-11	B-23	B-44	B-22	B-45	B-12	B-42
SiO ₂	47.67	46.82	46.59	47.18	47.49	46.88	43.07	44.44
TiO ₂	1.59	2.06	2.17	2.22	2.48	2.63	0.53	1.5
Al ₂ O ₃	10.2	10.35	11.62	11.03	13	12.71	4.42	7.76
FeO	18.99	20.27	20.55	20	19.67	21	19.67	20.77
MnO	0.28	0.26	0.22	0.26	0.22	0.26	0.26	0.22
MgO	8.56	7.92	5.95	6.98	4.61	4.92	24.1	16.41
CaO	11.32	10.88	11.8	11.24	11.52	11.56	6.84	7.84
Na ₂ O	0.27	0.26	0.37	0.26	0.31	0.27	0.1	0.18
K ₂ O	0.05	0.04	0.03	0.05	0.04	0.05	0.01	0.03
P ₂ O ₅	0.05	0.06	0.03	0.06	0.1	0.06	0.06	0.07
Cr ₂ O ₃	0.36	0.39	0.25	0.33	0.16	0.16	0.98	0.95
Sum	99.34	99.31	99.58	99.61	99.6	100.5	100.04	100.17
Na ₂ O	na	0.254	na	0.256	0.309	0.311	0.077	0.178
FeO	na	18.73	na	19.29	19.89	19.79	18.19	20.5
Sc	na	41.6	na	43.8	39.3	37.1	27.2	31.4
Cr	na	2700	na	2300	1100	1100	6500	4600
Co	na	37.9	na	36.7	36.9	37.6	85.2	65.4
Rb	na	nd	na	nd	nd	nd	27	nd
Sr	na	150	na	140	150	nd	nd	nd
Cs	na	nd	na	nd	0.21	nd	nd	nd
Ba	na	60	na	100	87	100	75	160
La	na	5.74	na	6.15	7.39	7.67	2.11	3.99
Ce	na	16.6	na	18.5	21.1	22.5	7.9	12.2
Nd	na	14	na	13	17	22	11	11
Sm	na	3.54	na	3.55	4.55	4.77	1.25	2.49
Eu	na	0.803	na	0.839	0.98	1.001	0.211	0.544
Tb	na	0.82	na	0.85	0.99	1.11	0.28	0.6
Yb	na	2.59	na	2.86	3.08	3.29	0.91	1.75
Lu	na	0.384	na	0.41	0.47	0.48	0.15	0.266
Zr	na	110	na	100	100	200	nd	120
Hf	na	2.5	na	2.71	3.09	3.36	0.86	1.73
Ta	na	0.32	na	0.4	0.45	0.47	0.2	0.26
Th	na	0.66	na	0.74	0.87	1.01	nd	0.35



Table 1. Whole rock major and trace element analyses of Apollo 15 mare basalt clasts from lunar breccia 15498 (continued).

	B-27	B-9	B-4	B-26	B-29	B-41	B-25	B-10
SiO ₂	44.71	45.14	44.54	45.83	45.19	46.98	47.7	47.39
TiO ₂	1.49	2.25	2.46	2.28	2.47	1.65	1.9	1.73
Al ₂ O ₃	8.13	9.37	7.75	8.7	7.96	8.25	8.35	9.01
FeO	20.83	20.13	23.44	21.57	23.26	19.71	19.75	20.19
MnO	0.24	0.24	0.26	0.28	0.3	0.26	0.22	0.28
MgO	13.63	9.31	11.65	7.87	9.49	12.74	11.83	9.73
CaO	8.92	10.67	9.2	11.47	9.93	8.91	9.15	10.3
Na ₂ O	0.2	0.25	0.2	0.24	0.26	0.21	0.19	0.23
K ₂ O	0.03	0.03	0.03	0.04	0.03	0.03	0.03	0.03
P ₂ O ₅	0.04	0.08	0.03	0.05	0.05	0.04	0.06	0.05
Cr ₂ O ₃	0.91	0.56	0.71	0.32	0.54	0.9	0.77	0.54
Sum	99.13	98.03	100.27	98.65	99.48	99.68	99.95	99.48
Na ₂ O	na	0.239	0.238	na	na	0.184	0.201	na
FeO	na	18.3	22.84	na	na	19.19	20.05	na
Sc	na	42.3	37.8	na	na	38.6	41.7	na
Cr	na	3600	4200	na	na	6200	5000	na
Co	na	40.3	58.9	na	na	55	53.3	na
Rb	na	nd	nd	na	na	nd	35	na
Sr	na	130	nd	na	na	120	nd	na
Cs	na	nd	nd	na	na	nd	nd	na
Ba	na	110	80	na	na	78	90	na
La	na	5.3	4.63	na	na	4.34	4.62	na
Ce	na	15.5	13.7	na	na	11.5	14.4	na
Nd	na	13	nd	na	na	15	7	na
Sm	na	3.29	3.43	na	na	2.67	2.94	na
Eu	na	0.705	0.828	na	na	0.54	0.609	na
Tb	na	0.76	0.78	na	na	0.63	0.69	na
Yb	na	2.41	2.04	na	na	1.98	2.24	na
Lu	na	0.358	0.292	na	na	0.286	0.332	na
Zr	na	120	220	na	na	110	160	na
Hf	na	236	2.49	na	na	1.96	2.04	na
Ta	na	0.37	0.37	na	na	0.3	0.36	na
Th	na	0.59	0.42	na	na	0.47	0.47	na



Sample Heterogeneity in Clast Studies: A major problem with the analysis of small clast samples is that the material analyzed may not be representative of the "whole rock" from which it was originally derived (Shervais et al., 1990). In order to address this problem, and to provide additional new data on the range of mare basalt compositions, two splits each from nine small samples of previously unanalyzed olivine-normative Apollo 15 mare basalts were analyzed for major and trace elements by combined fused bead EMPA and INAA (Shervais et al., 1990.) These samples overlapped in part with a study by Ryder and Schuraytz, who produced homogenous powders of 10 gram splits from several samples of Apollo 15 olivine normative basalt in order to produce representative analyses of the parent rocks. We obtained splits of the sample powders which we analyzed by the same methods used for our smaller sample aliquots, in order to evaluate how much our aliquots deviated from a true "representative" sample aliquot. We also analyzed representative suites of minerals in each basalt sample using existing probe mounts. These analyses were used in mass balance calculations to determine how the modal mineralogy affects the major element chemical variations (Shervais et al., 1990).

As expected, we found the largest variations in coarse-grained microgabbro samples, but we also observed significant variations in the compositions of the finer-grained mare basalts. These compositional variations result from the heterogeneous distribution of late mesostasis phases, and from the relatively coarse grain size of many samples (Shervais et al., 1990). In most cases the chemical variations shift sample compositions along olivine control lines in composition space, making them appear to be either more or less fractionated than a true representative sample aliquot. In extreme cases, the coarser-grained microgabbros may be shifted off of mineralogic control lines, so that they appear unrelated to their parent samples. Our data show that breccia clast studies using small sample aliquots must be approached with caution, especially if the samples have coarse grain sizes. Nonetheless, these data can provide useful constraints for petrogenetic modeling if the uncertainties are taken into account (Shervais et al., 1990).



Table 2. Whole rock major and trace element analyses of Apollo 15 olivine normative mare basalts. Samples labeled "A" and "B" represent separate aliquots of each sample which are similar in size to clasts taken from lunar breccias. The additional samples without corresponding trace element analyses (,9003 et cetera) are aliquots from the large homogenized samples (10 grams or more) prepared by Ryder and Schuraytz. Major elements by fused bead electron microprobe analysis (EMPA), trace elements by instrumental neutron activation analysis (INAA).

Sample #	15536A	15536B	15536 ,9003	15537A	15537B	15538A	15538B
weight mg	101	101		146	143	159	145
SiO ₂	44.6	44.7	44.4	44.6	44.5	44.8	45.6
TiO ₂	2.05	2.23	2.30	2.18	2.31	1.82	2.00
Al ₂ O ₃	7.46	7.57	7.66	7.28	7.17	8.90	8.78
FeO	23.56	23.02	23.24	22.31	23.07	21.67	21.44
MnO	0.29	0.29	0.31	0.310	0.320	0.30	0.300
MgO	11.89	11.36	11.11	13.00	12.96	11.50	11.01
CaO	9.23	9.42	9.53	9.09	8.77	9.65	10.16
Na ₂ O	0.22	0.21	0.25	0.200	0.210	0.26	0.250
K ₂ O	0.02	0.04	0.04	0.030	0.030	0.02	0.020
P ₂ O ₅	0.04	0.04	0.04	0.050	0.060	0.06	0.030
Cr ₂ O ₃	0.69	0.65	0.60	0.700	0.720	0.58	0.580
Total	100.02	99.48	99.47	99.78	100.07	99.57	100.12
Na ₂ O %	0.234	0.255		0.225	0.224	0.274	0.246
FeO %	22.4	22		21.5	23.1	20.5	22.2
Sc ppm	40	41.1		41.3	39.7	39.8	40.9
Cr	4700	4590		5100	5414	4300	3980
Co	55.9	55.4		56.7	61.9	53.3	55.8
Ni	60	70		80	78	61	90
Sr	90	120		90	93	124	130
Ba	41	23		47	50	34	45
La	3.82	4.27		5.26	5.15	3.25	5.38
Ce	12.3	12.1		14.6	14.6	10.3	14
Sm	2.87	3.07		3.64	3.59	2.37	3.74
Eu	0.739	0.81		0.811	0.790	0.746	0.89
Tb	0.64	0.74		0.78	0.78	0.52	0.84
Yb	1.87	1.94		2.25	2.30	1.6	2.35
Lu	0.255	0.273		0.308	0.314	0.212	0.311
Zr	70	<190		80	<150	60	120
Hf	2.25	2.3		2.66	2.61	1.79	2.7
Ta	0.31	0.32		0.352	0.376	0.237	0.36
U	0.06	<.2		0.24	0.12	<.2	<.3
Th	0.29	0.3		0.44	0.44	0.25	0.4

Table 2. Whole rock major and trace element analyses of Apollo 15 olivine normative mare basalts (continued).

Sample #	15546A	15546B	15546 ,9003	15547A	15547B	15547 ,9003
weight mg	152	147		154	151	
SiO ₂	45.3	45.1	45.2	42.5	45.2	44.3
TiO ₂	1.90	2.07	2.41	3.21	1.73	2.22
Al ₂ O ₃	9.54	8.03	8.15	5.48	9.38	8.03
FeO	20.72	21.44	22.54	28.21	20.68	22.65
MnO	0.29	0.27	0.30	0.34	0.31	0.28
MgO	10.96	11.85	10.75	10.68	11.78	11.46
CaO	10.05	9.78	9.83	8.52	9.79	9.40
Na ₂ O	0.29	0.25	0.23	0.20	0.28	0.21
K ₂ O	0.02	0.02	0.03	0.05	0.02	0.03
P ₂ O ₅	0.05	0.03	0.04	0.11	0.03	0.06
Cr ₂ O ₃	0.64	0.67	0.58	0.62	0.63	0.64
Total	99.76	99.52	100.04	99.88	99.87	99.33
Na ₂ O	0.282	0.28		0.183	0.274	
FeO	20.1	20.2		27.8	20.6	
Sc	40.9	42.3		45.1	38.7	
Cr	4360	4180		4170	4450	
Co	50.4	51.6		58.7	56.5	
Ni	80	70		60	70	
Sr	120	120		130	80	
Ba	33	45		72	32	
La	2.64	2.64		7.89	2.79	
Ce	8.5	7.7		22.2	8.2	
Sm	2.02	1.99		5.54	2.11	
Eu	0.706	0.71		1.03	0.721	
Tb	0.46	0.46		1.2	0.51	
Yb	1.39	1.42		3.3	1.41	
Lu	0.199	0.187		0.468	0.196	
Zr	<150	<130		110	110	
Hf	1.59	1.51		4.25	1.52	
Ta	0.218	0.19		0.62	0.2	
U	0.13	<.3		0.15	<.23	
Th	0.16	0.17		0.76	0.23	

Table 2. Whole rock major and trace element analyses of Apollo 15 olivine normative mare basalts (continued).

Sample #	15548A	15548B	15598A	15598B	15598 ,9003	15605A	15605B	15605 ,3
weight mg	158	145	100	101		93	91	
SiO ₂	45.0	44.6	44.7	45.3	45.1	44.9	45.1	
TiO ₂	2.39	2.63	2.48	2.65	2.45	2.27	2.27	2.1
Al ₂ O ₃	8.65	8.13	7.92	8.19	8.47	8.55	7.73	9.1
FeO	22.13	22.96	23.42	22.74	22.56	22.23	22.77	22.3
MnO	0.30	0.28	0.32	0.31	0.28	0.30	0.33	
MgO	9.72	9.84	10.35	9.39	9.82	10.22	10.70	11
CaO	10.29	9.95	9.66	10.21	10.16	10.05	9.80	10.1
Na ₂ O	0.27	0.25	0.24	0.25	0.23	0.25	0.22	0.257
K ₂ O	0.03	0.04	0.03	0.03	0.03	0.04	0.03	0.051
P ₂ O ₅	0.07	0.06	0.04	0.06	0.05	0.05	0.06	
Cr ₂ O ₃	0.60	0.55	0.66	0.49	0.54	0.64	0.60	
Total	99.43	99.32	99.79	99.65	99.72	99.49	99.62	
Na ₂ O	0.261	0.252	0.254	0.28		0.261	0.255	
FeO	21.8	22.7	22.6	22		22.1	21.9	
Sc	47.7	45.6	44.2	45.6		43.8	44	42
Cr	4170	4100	4460	3710		4530	4310	4150
Co	48.6	50.5	53.6	47.2		49.9	51.3	51
Ni	<100	n.d.	<90	<100		50	60	40
Sr	110	140	170	130		140	90	
Ba	50	39	48	55		52	49	45
La	4.62	5.17	4.44	4.97		5.95	5.45	5.4
Ce	13.8	15	13.8	14.3		16.2	15.7	
Sm	3.44	3.78	3.33	3.6		4.19	3.82	3.6
Eu	0.86	0.92	0.82	0.93		0.96	0.93	0.84
Tb	0.79	0.86	0.74	0.83		0.95	0.86	
Yb	2.16	2.33	2.12	2.3		2.55	2.4	0.7
Lu	0.338	0.318	0.299	0.313		0.36	0.322	0.29
Zr	90	90	160	110		130	130	
Hf	2.55	2.72	2.54	2.7		3.14	2.85	2.5
Ta	0.33	0.38	0.34	0.38		0.45	0.38	450
U	<.27	<.3	<.12	<.3		0.11	0.24	
Th	0.37	0.39	0.414	0.41		0.48	0.42	

Table 2. Whole rock major and trace element analyses of Apollo 15 olivine normative mare basalts (continued).

Sample #	15636A	15636B	15636 ,9003	15636 composite	W-2	One sigma
weight mg	101	100				
SiO ₂	45.3	42.3	44.8	44.6	53.07	0.2
TiO ₂	2.26	3.60	1.93	2.22	1.01	0.12
Al ₂ O ₃	6.73	5.01	9.14	8.55	15.47	0.6
FeO	23.99	28.77	21.22	22.67	9.58	0.29
MnO	0.32	0.34	0.27		0.17	0.02
MgO	11.08	10.36	11.60	11.32	6.53	0.23
CaO	9.45	8.54	9.63	9.58	11.04	0.12
Na ₂ O	0.17	0.16	0.23	0.26	2.29	0.06
K ₂ O	0.03	0.05	0.03	0.04	0.59	0.04
P ₂ O ₅	0.04	0.10	0.03	0.07	0.14	0.05
Cr ₂ O ₃	0.59	0.59	0.61			
Total	99.95	99.82	99.55	99.29	99.89	
Na ₂ O	0.221	0.175				0.005
FeO	24.4	29.1				0.25
Sc	45.3	47				0.5
Cr	4290	4160		3840		50
Co	54.1	57.1		52		0.6
Ni	<110	90				25
Sr	100	140				25
Ba	65	111				9
La	7.81	11.49		2.6		0.08
Ce	23.4	32.1				1
Sm	5.53	7.8		1.9		0.04
Eu	1.07	1.31		0.66		0.02
Tb	1.17	1.71				0.03
Yb	3.19	4.49		1.3		0.05
Lu	0.443	0.622		0.22		0.01
Zr	150	210		77		40
Hf	4.02	5.76		1.3		0.08
Ta	0.53	0.84				0.02
U	0.14	0.24				0.05
Th	0.71	0.99				0.04

Hybrid Source Regions: Our general review of compositional variations in mare basalts from all sites has revealed that two distinct mixing trends are present. One trend is delineated by high-Ti mare basalts, the other by all low-Ti basalts, VLT basalts, and high-Al basalts (Shervais and Vetter, 1989a, 1990). Both trends converge on a KREEP-like composition, but the other mixing component in each case is distinct (figure 1). The KREEP-like component is too evolved and too fractionated to be lunar magma ocean (LMO) trapped liquid in equilibrium with the mare source region cumulates. In addition, if this trend is due to simple low pressure assimilation of urKREEP, over 65% assimilation is indicated in some cases.

These observations suggest that the compositional variations observed in mare basalts result from a complex hybridization process similar to that proposed by Hughes et al (1988, 1989, 1990). Our model proposes that an incompatible element-rich ferrobalt component equivalent to KREEP sinks into earlier magma ocean cumulates and the resulting mixture undergoes partial melting to form the mare basalt parent magmas (Shervais and Vetter, 1990). The major difference between our model and that of Hughes et al (1988, 1989, 1990) is that the KREEPy component mixes with distinct high-Ti and low-Ti source regions, and there is little mixing between these two source regions. Each source region is internally heterogeneous and may mix with different amounts of the KREEP ferrobalt component. The distinct break between the two cumulate source regions is probably the caused by a change in cumulate phase assemblage (ilmenite + clinopyroxene in ?).

One problem with this model is that pristine KREEP compositions are not ferrobaltic and will not sink into LMO cumulates. This is probably because these KREEP compositions are themselves mixtures (e.g., Warren, 1988). In order to extract the "true" urKREEP composition from the mixtures, we are exploring the use of polytopic vector analysis (Shervais and Ehrlich, 1990). Polytopic vector analysis (PVA) differs from factor analysis in that it applies Q-mode analysis to non-orthogonal multivariate sample vectors to extract sample endmember compositions. The data are fit to a polytope of N-1 dimensions (where N = number of variables) and endmembers are defined as vertices of the polytope after it has been modified to eliminate negative values (Shervais and Ehrlich, 1990). Advantages of this method are that it works best with constant sum data (e.g., chemical analyses) and that it can define endmembers which lie outside the data cloud.

Our results using this technique on primitive mare basalts suggest that the KREEP component in mare basalts is an Fe-rich ferrobalt with very low MgO that is fractionated with respect to pristine KREEP 15386. The implications of these results are (1) the major element composition of KREEP varies depending on either the extent of magma ocean crystallization prior to its crystallization or mixing with other components, (2) the major element composition of the KREEP component in mare basalts is similar for all mare basalts (i.e., ferrobaltic), (3) the high Fe-content of this KREEP component suggests densities of 2.96 to 2.99 for the magma; this density will be higher if the magma contains suspended mafic crystals. Magma with this density will sink through felsic cumulates or mafic gabbros, but not through ultramafic cumulates unless the content of suspended mafic crystals is high.



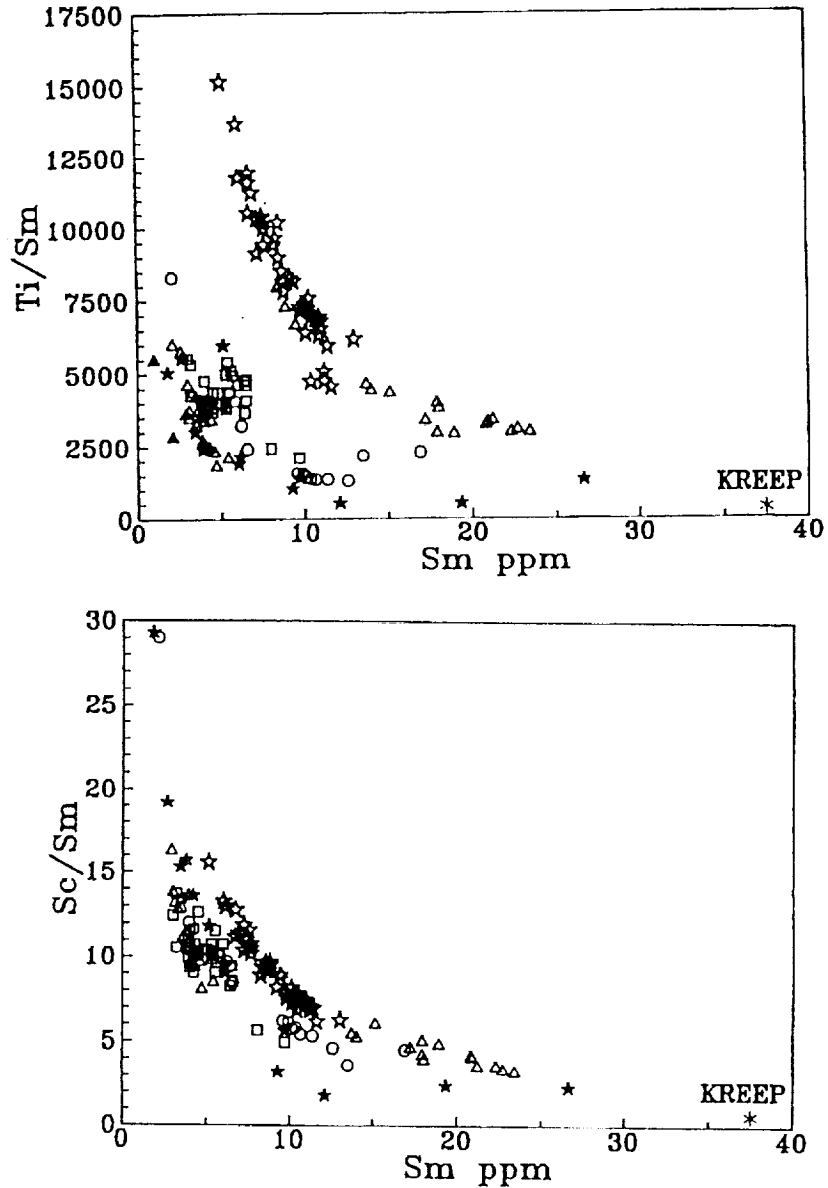


Figure 1. Ti/Sm and Sc/Sm versus Sm plots for lunar mare basalts. Open stars and open triangles = high-Ti mare basalts, other symbols all low-Ti mare basalts. Note that data define two mixing hyperbolas with KREEP at one end of each hyperbola. The upper intercepts of the mixing hyperbolas are inferred to represent the cumulate source regions of low-Ti and high-Ti mare basalts (or more precisely, melts derived from those source regions). Scatter in the mixing hyperbolas (especially in the low-Ti mare basalts) may represent heterogeneity in the source cumulates.



Pristine KREEP basalts

The primary aim of this study is to characterize pristine KREEP basalts petrographically, to establish the range in chemical compositions of KREEP basalts, and to test models that have been proposed for their origin. High quality major and trace element data on KREEP basalts are rare. Many samples have been analyzed by INAA only, resulting in partial major element analyses; many others are found only in thin section and have been analyzed for major elements using the electron microprobe defocused beam technique. The quality of these DBA analyses is poor, and no trace elements have been determined on these samples. As a result, our knowledge of compositional variations in pristine KREEP basalts is limited (e.g., Ryder, 1988).

Thirteen fragments of KREEP basalt from breccia 15205, representing 11 different clasts, have been analyzed. Trace elements were analyzed by INAA (Lindstrom and others, 1989). Major element compositions were determined by fused bead EMP analysis on the same splits used for trace elements (Vetter and Shervais, 1992). Corresponding probe mounts are available for 5 of these fragments; a petrographic/mineral chemical study was presented by Shervais and Vetter (1989).

Fractionation models using the least-squares mixing approach are not successful if the observed phenocryst phases (pigeonite, plagioclase) only are used. Successful models are obtained if olivine is added to the fractionating assemblage, but there is no evidence to suggest that these samples were ever olivine saturated (although olivine has been observed some KREEP basalts by Dymek et al, 1974, and Ryder, personal comm.). Two clasts were analyzed in two splits each. Each of these sample pairs spans approximately half of the total range observed in MgO and in most other elements. Tie-lines connecting these sample pairs generally parallel the apparent "fractionation" trend displayed by the sample set as a whole, suggesting that crystal fractionation may not be responsible for this trend.

Our results on these samples are consistent with the idea that one coarse-grained, texturally heterogeneous flow may have been sampled by the impact that created breccia 15205. Major element variations are consistent with differences in modal proportions of the silicate and oxide phases. In contrast, incompatible trace elements correlate well with one another but poorly with the major elements, suggesting that overall incompatible trace element concentrations are a function of mesostasis mode. The high degree of correlation between Sc and incompatible elements such as La and Hf implies a strong coupling of mesostasis phases with the augite rims on pigeonite.

Table 3. Major and trace element analyses of pristine KREEP basalt clasts from lunar breccia 15205. Major elements by fused bead electron microprobe analysis (EMPA), trace elements by instrumental neutron activation analysis (INAA).

SubSample#	,131	,132	,133	,135	,140	,142b	,146
SiO ₂	50.34	51.25	50.96	51.03	49.75	51.83	51.27
TiO ₂	1.99	1.92	2.41	2.07	1.40	1.78	2.07
Al ₂ O ₃	15.38	16.26	16.81	15.78	16.90	16.33	16.09
FeO	10.71	9.79	9.97	10.15	9.65	9.31	10.17
MnO	0.16	0.15	0.14	0.12	0.14	0.11	0.16
MgO	8.81	8.49	6.41	8.85	10.45	8.79	7.33
CaO	10.11	10.10	10.23	9.97	9.67	10.06	10.31
Na ₂ O	0.81	0.84	0.82	0.81	0.78	0.78	0.87
K ₂ O	0.51	0.58	0.67	0.56	0.40	0.55	0.67
P ₂ O ₅	0.29	0.22	0.47	0.29	0.11	0.23	0.35
Cr ₂ O ₃	0.34	0.32	0.26	0.31	0.36	0.31	0.27
SUM	99.45	99.92	99.15	99.94	99.61	100.08	99.56

INAA (PPM Except where noted)

Na ₂ O %	0.894	0.874	0.822	0.818	0.825	0.804	0.874
K ₂ O %	0.63	0.65	0.57	0.49	0.56	0.56	0.61
CaO %	11.0	11.0	10.6	9.9	9.2	9.5	10.1
FeO %	10.34	10.04	10.31	10.12	10.46	10.00	10.31
Sc	22.4	21.8	21.6	21.3	21.9	21.9	22.4
Cr	2930	2060	2470	2280	2260	2990	2190
Ce	19.5	19.2	22.3	20.4	20.3	20.4	19.9
Ba	870	840	810	760	820	780	860
La	81.6	79.1	76.2	71.1	76.3	71.8	79.3
Gd	207	205	197	185	199	185	204
Sm	37.8	36.0	36.2	32.6	36.1	32.8	36.4
Eu	2.72	2.67	2.72	2.63	2.65	2.59	2.78
Tb	7.46	7.18	6.90	6.49	6.89	6.47	7.29
Yb	23.3	24.2	22.9	21.0	22.4	22.2	24.4
Lu	3.35	3.28	3.10	2.84	3.06	3.00	3.31
Hf	30.1	29.4	28.1	26.3	27.8	26.5	30.1



Table 3. Major and trace element analyses of pristine KREEP basalt clasts from lunar breccia 15205. Major elements by fused bead electron microprobe analysis (EMPA), trace elements by instrumental neutron activation analysis (INAA).

SubSample#	,148	,158	,161b	,163	,165	,167
SiO ₂	50.76	48.34	50.66	50.04	52.88	50.15
TiO ₂	2.20	2.02	2.03	2.36	2.13	1.94
Al ₂ O ₃	15.87	15.37	16.98	14.61	15.38	15.92
FeO	10.23	10.80	9.85	11.52	10.11	10.33
MnO	0.15	0.16	0.18	0.18	0.14	0.15
MgO	8.53	11.31	8.27	8.19	7.18	9.32
CaO	10.14	9.43	10.58	10.16	9.70	9.99
Na ₂ O	0.82	0.72	0.79	0.81	0.91	0.76
K ₂ O	0.54	0.34	0.37	0.65	0.83	0.49
P ₂ O ₅	0.41	0.23	0.16	0.54	0.44	0.30
Cr ₂ O ₃	0.32	0.43	0.31	0.29	0.26	0.33
SUM	99.97	99.15	100.18	99.35	99.96	99.68

INAA (PPM Except where noted)

Na ₂ O %	0.799	0.798	0.827	0.9	0.888	0.796
K ₂ O %	0.56	0.58	0.42	0.75	0.73	0.41
CaO %	9.5	9.9	9.4	10.2	10.6	10.1
FeO %	10.34	10.31	9.19	9.90	10.20	10.10
Sc	21.7	21.6	19.5	22.0	22.3	21.1
Cr	2250	2140	2250	1860	1900	2910
Co	20.6	19.2	20.6	17.3	18.0	20.8
Ba	790	840	610	930	960	730
La	70.4	78.4	58.0	83.5	84.3	85.5
Ce	194	200	152	218	218	171
Sm	32.2	36.1	26.7	37.6	37.8	30.1
Eu	2.55	2.68	2.51	2.70	2.67	2.51
Tb	6.40	7.05	5.28	7.58	7.65	6.05
Yb	21.2	22.3	17.4	25.4	26.0	19.9
Lu	2.86	3.18	2.34	3.42	3.53	2.68
Hf	26.5	28.6	20.6	31.6	33.0	24.6



Apollo 14 Revisited

Our work at the Apollo 14 site has focused on producing new major element data for mare and highland samples analyzed previously by INAA, and a synthesis of data on highland lithologies at the Apollo 14 site. There is now a wealth of analytical and petrographic data on Apollo 14 highland rocks (e.g., Warren and Wasson, 1980; Warren et al., 1981, 1983a, 1983b, 1986, 1987, 1990; Goodrich et al, 1986; Morris et al., 1990; Lindstrom et al., 1984; Hunter and Taylor, 1982; Shervais et al., 1983, 1984; Snyder et al, 1991; Joliff, 1991), but so far no one has attempted to synthesize this data into a coherent picture of how the highland crust at this site formed, how it relates to ferroan anorthosite crust at other sites, or even how the various suites at Apollo 14 relate to one another.

My work to date suggests that the alkali suite and Mg-suite cannot be related to a common parent magma (Shervais, 1989, 1990). The Mg-suite parent magma probably mixed with urKREEP, as proposed by Warren (1988); the alkali suite represents either a separate magma system which also assimilated KREEP, or cumulates derived from the urKREEP magma itself (Shervais, 1989, 1990). Snyder et al (1991) reach the latter conclusion, based a study of 27 Apollo 14 soil fragments (mostly impact melt breccias).

The origin of REE-rich whitlockites in samples from both suites is controversial; Neal and Taylor (1989) have proposed a metasomatic origin by their "REE-frac" component. Alternatively, I have proposed that these whitlockites formed from the cumulate trapped liquid component after extensive closed system fractionation (Shervais, 1990; Shervais and Vetter, 1991). The similarity of REE concentrations in whitlockites of all suites is attributed to similar enrichment factors for the REE and for P to attain phosphate saturation, providing the magma starts out with KREEPy trace element ratios (Shervais and Vetter, 1991). Movement of this fractionated trapped liquid in response to compaction, major impacts, or tectonic stress would lead to "autometasomatism" of the cumulate by its own trapped liquid. Significantly, whitlockites differ most clearly in their Fe/Mg ratios, which are higher for the alkali suite rocks.

A major problem with interpreting Apollo 14 highland rocks and mare basalt is the lack of complete major element chemical data. Despite the importance of these clasts for petrogenetic models of mare basalt and highland evolution, many have not been analyzed for major element chemistry because of their small size. As a result, systematic chemical data are not available for most samples, which have only been studied by instrumental neutron activation analysis (INAA). Activation analysis has the advantage of producing excellent data for a large number of trace elements (including REE) and a few major elements (FeO, Al₂O₃, Na₂O) from small analytical samples. The primary disadvantage of INAA is that several important major elements cannot be analyzed accurately (CaO, MgO, TiO₂, K₂O), and SiO₂ cannot be determined at all. Several of these major elements produce short-lived isotopes which require special irradiation and counting techniques (Al₂O₃, MgO, TiO₂); as a result, these are not determined routinely. When these elements are determined, it is customary to calculate "SiO₂" by difference, assuming the major elements sum to 100 percent by weight. As a result, dunites and troctolites may have calculated SiO₂ as low as 34-36

wt%, despite the fact that they consist of Fo88 olivine and An94 plagioclase (Lindstrom et al, 1988).

We have attempted to overcome these problems by using fused bead electron microprobe analysis for major elements in conjunction with INAA for trace elements and selected major elements. Fused bead EMP analysis produces results comparable in quality to X-ray fluorescence analysis when basaltic samples are analyzed and can be applied to samples as small as 10 milligrams. Since INAA samples generally range from 10 to 100 mg in mass, both techniques can be applied to the same sample, either by splitting a homogenized powder, or by serial analysis (INAA followed by fused bead EMPA).

Twenty clasts from lunar breccia 14321 were analyzed as part of this effort. These clasts include 11 mare basalts, 3 olivine vitrophyres, 3 Mg-troctolites, 2 Mg-anorthosites, and one dunite. These clasts were analyzed for trace elements and selected major elements by INAA (Shervais et al, 1985a, 1988; Lindstrom et al, 1984). All 20 samples were fused in molybdenum foil boats and prepared for major element analysis using our normal procedures. The fused samples were analyzed for 12 elements (including molybdenum to monitor dissolution of Mo from the sample boats into the fused glass) on a Cameca SX-50 EMP at the University of South Carolina. This data set represents the first complete major element for these samples (Shervais and Vetter, 1992).

Differences between the INAA and EMPA data sets are generally smallest for those elements which can be measured accurately by INAA: Al₂O₃, FeO, MnO, and Na₂O (figure 1; table 1). Fused bead EMPA for Na₂O are systematically 5-10% lower than the INAA results, suggesting that Na was mobilized under the electron beam. INAA results for TiO₂ and MgO are systematically too high by 15% to 20% on average, while K₂O and SiO₂ (by difference) show significant scatter to both high and low values. Cr₂O₃ values correspond well for the mare basalts, but show significant differences in the highland samples.

Fused bead EMPA provides superior analytical results for the major elements SiO₂, TiO₂, MgO, CaO, and K₂O on small samples extracted from lunar breccias. This method can be applied to samples which have been irradiated for INAA and complements the data obtained by INAA. Fused bead EMPA eliminates the need for "rabbit runs", which are used primarily to obtain data for the major elements Al, Mg, and Ti. These data will allow us to refine petrogenetic models for 14321 mare basalts and highland rocks, and expand the range of clast sizes from which complete geochemical data may be obtained.

Table 4. Highland Plutonic and Impact Melt Rocks from Lunar Breccia 14321 Analyzed for Major Elements by Fused Bead EMPA.

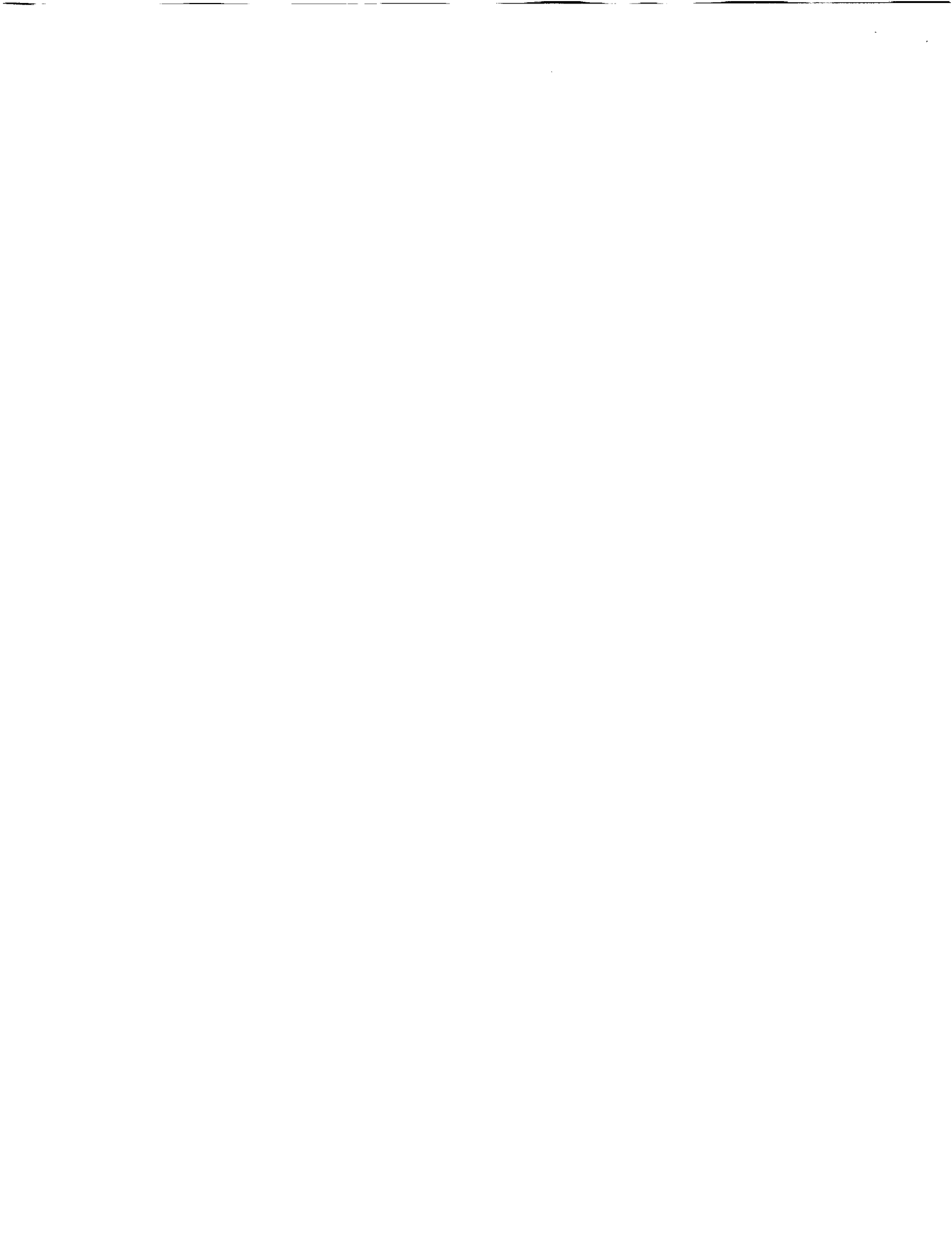
Sample Number	A14321 ,1140	A14321 ,1142	A14321 ,1154	A14321 ,1211	A14321 ,1205-A
Rock Name	Troctolite	Troctolite	Troctolite	Mg Anorth	Mg Anorth
SiO ₂	41.83	43.05	43.41	44.24	44.45
TiO ₂	0.05	0.18	0.04	0.36	0.17
Al ₂ O ₃	18.12	24.01	27.04	32.59	34.24
FeO	7.73	4.76	3.27	1.88	0.90
MnO	0.07	0.05	0.01	0.02	0.01
MgO	22.89	14.91	11.65	2.16	1.30
CaO	9.87	13.20	14.67	18.37	18.84
Na ₂ O	0.17	0.30	0.34	0.39	0.45
K ₂ O	0.02	0.05	0.06	0.11	0.11
Cr ₂ O ₃	0.03	0.10	0.01	0.02	0.00
P ₂ O ₅	0.01	0.01	0.01	0.07	0.12
Total	100.79	100.63	100.51	100.21	100.59

Sample Number	A14321 ,1141	A14321 ,1158	A14321 ,1159	A14321 ,1180
Rock Name	Dunite	Ol-Vitro	Ol-Vitro	Ol-Vitro
SiO ₂	41.80	47.12	47.07	47.22
TiO ₂	0.03	1.36	1.37	1.33
Al ₂ O ₃	0.30	12.72	12.61	12.35
FeO	7.49	9.81	10.02	9.97
MnO	0.09	0.12	0.12	0.12
MgO	50.18	19.50	19.48	20.10
CaO	0.24	8.03	8.04	7.75
Na ₂ O	0.00	0.72	0.74	0.77
K ₂ O	0.00	0.46	0.44	0.48
Cr ₂ O ₃	0.04	0.21	0.22	0.21
P ₂ O ₅	0.00	0.15	0.25	0.21
Total	100.16	100.20	100.36	100.50

Table 5. Mare Basalt Clasts from Lunar Breccia 14321 Analyzed for Major Elements by Fused Bead EMPA.

Sample Number	A14321,1143	A14321,1157	A14321,1160	A14321,1161	A14321,1162	A14321,1179
Rock Name	Basalt	Basalt	Basalt	Basalt	Basalt	Basalt
SiO ₂	48.16	47.97	45.73	44.47	44.89	47.24
TiO ₂	2.14	1.84	3.05	2.84	5.50	2.08
Al ₂ O ₃	13.49	12.76	12.25	11.69	9.07	12.69
FeO	15.34	15.21	17.61	17.62	23.66	15.93
MnO	0.24	0.25	0.27	0.27	0.32	0.23
MgO	8.56	9.55	8.28	11.36	5.71	9.75
CaO	11.39	11.52	11.05	10.39	10.12	10.76
Na ₂ O	0.50	0.44	0.52	0.42	0.27	0.49
K ₂ O	0.13	0.10	0.08	0.06	0.21	0.13
Cr ₂ O ₃	0.48	0.42	0.43	0.52	0.30	0.52
P ₂ O ₅	0.03	0.05	0.01	0.00	0.01	0.03
Total	100.45	100.13	99.28	99.64	100.06	99.85

Sample Number	A14321,1183	A14321,1184	A14321,1185	A14321,1210	A14321,1149
Rock Name	Basalt	Basalt	Basalt	Basalt	Basalt
SiO ₂	46.76	47.55	45.43	46.20	45.35
TiO ₂	2.25	2.62	2.42	2.28	3.25
Al ₂ O ₃	12.78	13.80	12.13	12.75	11.30
FeO	16.88	14.80	17.18	16.95	17.54
MnO	0.24	0.24	0.26	0.24	0.27
MgO	8.55	7.15	8.60	8.37	11.61
CaO	11.09	11.98	11.24	11.10	9.83
Na ₂ O	0.77	0.52	0.41	0.75	0.39
K ₂ O	0.17	0.15	0.14	0.17	0.21
Cr ₂ O ₃	0.41	0.30	0.46	0.37	0.41
P ₂ O ₅	0.03	0.02	0.05	0.07	0.00
Total	99.92	99.12	98.32	99.24	100.17



Publications Resulting from NASA Grant NAG9-169:

ARTICLES:

Shervais, J.W., Vetter, S.K., and Lindstrom, M.M. (1990) Chemical differences between small subsamples of Apollo 15 olivine-normative basalts, Proceedings of the 20th Lunar and Planetary Science Conference, Lunar and Planetary Institute, Houston, 109-126.

Shervais, J.W. (1989) Highland Crust at the Apollo 14 Site: A Review, *in* Taylor, G.J. and Warren, P.H., eds., Workshop on Moon in Transition: Apollo 14, KREEP, and Evolved Lunar Rocks, LPI Tech. Report 89-03, Lunar and Planetary Institute, Houston, p. 118-127.

Vetter, S.K., **Shervais, J.W.**, M.M. Lindstrom (1988) Petrology and Geochemistry of Olivine-normative and Quartz-normative basalts from Regolith Breccia 15498: New Diversity in Apollo 15 Mare Basalt. Proc. 18th Lunar Planetary Science Conference, Cambridge University Press, Cambridge, 255-272.

Shervais, J.W., L.A. Taylor, and M.M. Lindstrom (1988) Olivine vitrophyres: a non-pristine high-Mg component in lunar breccia 14321. Proc. 18th Lunar Planetary Science Conference, Cambridge University Press, Cambridge, 45-58.

Lindstrom, M.M., U.B. Marvin, S.K. Vetter, and **Shervais, J.W.** (1988) Apennine Front revisited: diversity of Apollo 15 highland rock types. Proc. 18th Lunar Planetary Science Conference, Cambridge University Press, Cambridge, 169-186.

Shervais, J.W. (1988) Clues emerge from Mars to Montana, *Geotimes*, June 1988, p. 22-24.

LUNAR & PLANETARY SCIENCE CONFERENCE EXTENDED ABSTRACTS

Shervais, J.W. and Vetter, S.K. (1992) Major element chemistry of Apollo 14 mare basalt clasts and highland plutonic clasts from lunar breccia 14321: comparison with neutron activation results. Lunar and Planetary Science XXIII, Lunar and Planetary Institute, Houston, 1287-1288.

Vetter, S.K. and **Shervais, J.W.** (1992) Whole rock major element chemistry of KREEP basalt clasts in lunar breccia 15205: Implications for the petrogenesis of volcanic KREEP basalts. Lunar and Planetary Science XXIII, Lunar and Planetary Institute, Houston, 1471-1472.

Shervais, J.W. and Vetter, S.K. (1991) Auto-metasomatism of the western lunar highlands: result of closed system fractionation and mobilization of a KREEPy trapped liquid, Lunar and Planetary Science XXII, Lunar and Planetary Institute, Houston, 1237-1238.



Shervais, J.W. and Erhlich, R. (1991) Polytopic vector analysis: application to lunar petrogenesis, Lunar and Planetary Science XXII, Lunar and Planetary Institute, Houston, 1235-1236.

Shervais, J.W. and Vetter, S.K. (1990) Lunar mare volcanism: mixing of distinct mantle source regions with KREEP-like component, Lunar and Planetary Science XXI, Lunar and Planetary Institute, Houston, 1142-1143.

Shervais, J.W. (1990) The western highland province at the Apollo 14 site, Lunar and Planetary Science XXI, Lunar and Planetary Institute, Houston, 1140-1141.

Shervais, J.W. and Vetter, S.K. (1989) Melt rock components in KREEPy breccia 15205 - Petrology and mineral chemistry of KREEP basalts and quartz-normative mare basalts, Lunar and Planetary Science XX, Lunar and Planetary Institute, Houston, 1000-1001.

Vetter, S.K. and **Shervais, J.W.** (1989) A dynamic melting model for the origin of Apollo 15 olivine normative and quartz normative basalts, Lunar and Planetary Science XX, Lunar and Planetary Institute, Houston, 1152-1153.

Shervais, J.W., Vetter, S.K. and Lindstrom, M.M. (1988), "Heterogeneity in small aliquots of Apollo 15 olivine normative basalt: implications for breccia clast studies", *in* Lunar and Planetary Science XIX, 1069-1070.

Vetter, S.K., **Shervais, J.W.**, and Lindstrom, M.M. (1987) Petrology of mare basalt and highland clasts from breccia 15498. Lunar and Planetary Science XVIII, Lunar and Planetary Institute, Houston, 1040-1041.

OTHER ABSTRACTS:

Shervais, J.W. and Vetter, S.K. (1990) Mare Basalts: Evidence for distinct hybrid source regions. LPI Workshop on Mare Basalts, Dallas, Texas.

Vetter, S.K. and **Shervais, J.W.** (1990) Dynamic melting in the genesis of mare basalts, LPI Workshop on Mare Basalts, Dallas, Texas.

Shervais, J.W. and Vetter, S.K. (1989) Lunar mare volcanism: new variations on old themes, Geological Society of America, Abstracts with Programs, 23/6, A300.

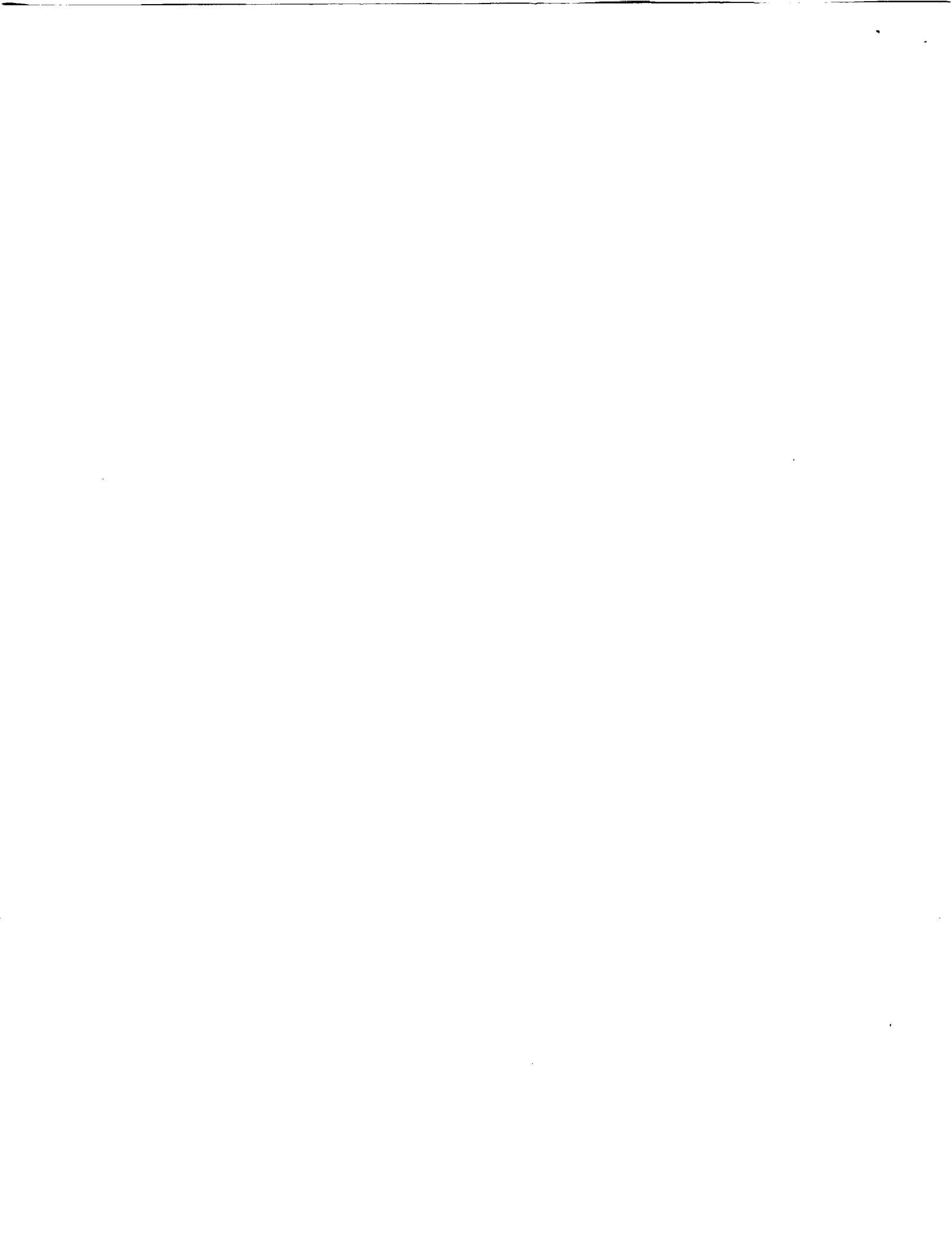
REFERENCES

- Binder, A.B. (1985) Mare basalt genesis: modeling trace elements and isotopic ratios. Proc. 16th Lunar Planet. Sci. Conf., J. Geophys. Res., 90, D19-D30.
- Dickinson, T., G.J. Taylor, K. Keil, Schmitt, R.A., S.S. Hughes, and M.R. Smith (1985) Apollo 14 aluminous mare basalts and their possible relationship to KREEP. Proc. 15th Lunar Planet. Sci. Conf., J. Geophys. Res., 90, C365-C374.
- Goodrich, C.A., Taylor, G.J., Keil, K., Kallemeyn, G.W., and Warren, P.H. (1986) Alkali norite, troctolites, and VHK mare basalts from breccia 14304, Proceedings Lunar and Planetary Science Conference 16th, J. Geophys. Res. Supl., 91, D319-D330.
- Hughes, S. S., Delano, J.W., and Schmidt, R.A. (1988) Apollo 15 yellow-brown volcanic glass: chemistry and petrogenetic relations to green volcanic glass and olivine normative mare basalts, *Geochimica cosmochimica acta*, 52, 2379-2391.
- Hughes, S. S., Delano, J.W., and Schmidt, R.A. (1989) Petrogenetic modeling of 74220 high-Ti orange volcanic glasses and the Apollo 11 and 17 high-Ti mare basalts, Proc. Lunar and Planetary Science Conf. 19th, 175-188.
- Hughes, S. S., Delano, J.W., and Schmidt, R.A. (1990) Chemistries of individual mare volcanic glasses: evidence for distinct regions of hybridized mantle and a KREEP component in Apollo 14 magmatic sources, Proc. 20th Lunar and Planetary Science Conf, 127-138.
- Hunter, R.H. and Taylor, L.A. (1983) The magma ocean from the Fra Mauro shoreline: An overview of the Apollo 14 crust; Proc. 13th Lunar and Planet. Sci. Conf., J. Geophys. Res. Supl., 88, A591-A602.
- Lindstrom, M.M., Knapp, S.A., Shervais, J.W. and Taylor, L.A. (1984) Magnesian anorthosites and associated troctolites and dunite in Apollo 14 breccias; Proc. 15th Lunar and Planet. Sci. Conf., J. Geophys. Res. Supl, 89, C41-C49.
- Morris, R.W., Taylor, G.J., Newsom, H.E., Keil, K, and Garcia, S.R. (1990) Highly evolved and ultramafic lithologies from Apollo 14 soils, Proceedings 20th Lunar and Planetary Science Conference, Lunar and Planetary Institute, Houston, 61-75.
- Neal, C.R. and Taylor, L.A. (1990) REEP metasomatism of the Apollo 14 highlands: evidence from the Mg suite, Lunar and Planetary Science XXI, Lunar and Planetary Institute, Houston, 851-852.
- Neal C.R., Taylor, L.A., and Lindstrom, M.M. (1987) Mare basalt evolution: The influence of KREEP-like components, Lunar Planet. Sci., XVIII, 706-707.
- Neal C.R., Taylor, L.A., and Lindstrom, M.M. (1988a) Importance of lunar granite and KREEP in VHK basalt petrogenesis, Proc. 18th Lunar and Planetary Science Conf., Cambridge Univ. Press, 121-137.
- Neal C.R., Taylor, L.A., and Lindstrom, M.M. (1988b) Apollo 14 Mare Petrogenesis: Assimilation of KREEP-like components by a fractioning magma, Proc. 18th Lunar and Planetary Science Conf., Cambridge Univ. Press, 139-1153.
- Ryder, G. (1988) Limited chemical variation of Apollo 15 KREEP basalts, Lunar and Planetary Science XIX, 1011-1012.



- Shervais, J.W. (1989) Highland Crust at the Apollo 14 Site: A Review, *in* Taylor, G.J. and Warren, P.H., eds., Workshop on Moon in Transition: Apollo 14, KREEP, and Evolved Lunar Rocks, LPI Tech. Report 89-03, Lunar and Planetary Institute, Houston, p. 118-127.
- Shervais, J.W. (1990) The western highland province at the Apollo 14 site, Lunar and Planetary Science XXI, Lunar and Planetary Institute, Houston, 1140-1141.
- Shervais, J.W. and Taylor, L.A. (1986) Petrologic constraints on the origin of the Moon; in W.K. Hartman, R.J. Phillips, and G.J. Taylor (eds) Origin of the Moon, LPI Houston, 173-202.
- Shervais, J.W. and Vetter, S.K. (1989a) Lunar mare volcanism: new variations on old themes, Geological Society of America, Abstracts with Programs, 23/6, A300.
- Shervais, J.W. and Vetter, S.K. (1989b) Melt rock components in KREEPy breccia 15205 - Petrology and mineral chemistry of KREEP basalts and quartz-normative mare basalts, Lunar and Planetary Science XX, Lunar and Planetary Institute, Houston, 1000-1001.
- Shervais, J.W. and Vetter, S.K. (1990) Lunar mare volcanism: mixing of distinct mantle source regions with KREEP-like component, Lunar and Planetary Science XXI, Lunar and Planetary Institute, Houston, 1142-1143.
- Shervais, J.W., Taylor, L.A. and Laul, J.C. (1983) Ancient crustal components in the Fra Mauro breccias: implications for igneous processes; Proc. 14th Lunar and Planet. Sci. Conf., J. Geophys. Res. Suppl., 88, B177-B192.
- Shervais, J.W., Taylor, L.A., Laul, J.C., and Smith, M.R. (1984b) Pristine highland class in consortium breccia 14305: Petrology and geochemistry; Proc. 15th Lunar and Planet. Sci. Conf., J. Geophys. Res. Suppl., 89, C25-C40.
- Shervais J.W., Taylor L.A., and Lindstrom M.M. (1985a) Apollo 14 mare basalts: Petrology and geochemistry of clasts from consortium breccia 14321, Jour. Geophys. Res., 90, C375-C395.
- Shervais J.W., Taylor L.A., Laul J.C., Shih C.-Y., and Nyquist L.E. (1985b) Very high potassium (VHK) basalt: Complications in mare basalt petrogenesis, Jour. Geophys. Res., 90, D3-D18.
- Shervais, J.W., Vetter, S.K., and Lindstrom, M.M. (1990) "Heterogeneity in small sub-samples of Apollo 15 Olivine Normative Basalt: Implications for breccia clast studies", Proceedings 20th Lunar and Planetary Science Conference, Lunar and Planetary Institute, Houston, 109-126.
- Shih, C-Y., Bansal, B.M., Weisman, H., and Nyquist, L.E. (1984) Rb-Sr Chronology and petrogenesis of VHK basalts. Lunar Planet. Sci. XV, 774-775.
- Shih, C-Y., Nyquist, L.E., Bogard, D.D., Bansal, B.M., Weisman, H., Johnson, P., Shervais, J.W., and Taylor, L.A. (1986) Geochronology and petrogenesis of Apollo 14 Very High Potassium mare basalts. Proc. 16th Lunar and Planet. Sci. Conf., J. Geophys. Res., 91, D214-D228.
- Vetter, S.K., J.W. Shervais, M.M. Lindstrom (1988) Petrology and Geochemistry of Olivine-normative and Quartz-normative basalts from Regolith Breccia 15498: New Diversity in Apollo 15 Mare Basalt. Proc. 18th Lunar Planetary Science Conference, Cambridge University Press, Cambridge, 255-272.
- Vetter, S.K. and Shervais, J.W. (1989) A dynamic melting model for the origin of Apollo 15 olivine normative and quartz normative basalts, Lunar and Planetary Science XX, Lunar and Planetary Institute, Houston, 1152-1153.

- Warren, P.H. (1988) Origin of pristine KREEP: effects of mixing between urKREEP and magmas parental to the Mg-rich cumulates. Proc. 18th Lunar Planet Sci Conf., 233-242.
- Warren P.H. and Wasson, J.T. (1979) The origin of KREEP; Rev. Geophys. Space Phys., 17, 73-88.
- Warren, P.H. and Wasson, J.T. (1980) Further foraging for pristine nonmare rocks: correlations between geochemistry and longitude, Proc. Lunar Planetary Science Conf. 11th, 431-470.
- Warren, P.H., Taylor, G.J., Keil, K., Marshall, C., and Wasson, J.T. (1981) Foraging westward for pristine nonmare rocks: complications in petrogenetic models, Proc. Lunar Planetary Science Conf., 12B, 21-40.
- Warren, P.H., Taylor, G.J., Keil, K., Kallemeyn, G.W., Rosener, P.S. and Wasson, J.T. (1983a) Sixth foray for pristine nonmare rocks and an assessment of the diversity of lunar anorthosites; Proc. 13th Lunar and Planet. Sci. Conf., J. Geophys. Res. Supl., 88, A615-A630.
- Warren, P.H., Taylor, G.J., Keil, K., Kallemeyn, G.W., Shirley, D. and Wasson, J.T. (1983b) Seventh foray: whitlockite-rich lithologies, a diopside bearing troctolitic anorthosite, ferroan anorthosites, and KREEP, Proc. 14th Lunar and Planet. Sci. Conf., J. Geophys. Res. Supl., 88, A615-A630.
- Warren, P.H., Shirley, D.N., and Kallemeyn, G.W. (1986) A potpourri of pristine moon rocks, including a VHK mare basalt and a unique, augite-rich Apollo 17 anorthosite, Proceedings Lunar and Planetary Science Conference 16th, J. Geophys. Res. Supl., 91, D319-D330.
- Warren, P.H., Jerde, E.A., and Kallemeyn, G.W. (1987) Pristine moon rocks: a large felsite and a metal rich ferroan anorthosite, Proceedings Lunar and Planetary Science Conference 17th, J. Geophys. Res. Supl., 92, E303-E313.
- Warren, P.H., Jerde, E.A., and Kallemeyn, G.W. (1990) Pristine moon rocks: an alkali anorthosite with coarse augite exsolution from plagioclase, a magnesian harzburgite, and other oddities, Proceedings 20th Lunar and Planetary Science Conference, Lunar and Planetary Institute, Houston, 31-59.



Chemical Differences Between Small Subsamples of Apollo 15 Olivine-Normative Basalts

J. W. Shervais

Department of Geological Sciences, University of South Carolina,
Columbia, SC 29208

S. K. Vetter

Department of Geological Sciences, University of South Carolina,
Columbia, SC 29208

M. M. Lindstrom

Planetary Science Branch, Mail Code SN2, NASA Johnson Space Center,
Houston, TX 77058

PREV. ANN
90A 33465

Nine samples of Apollo 15 mare basalt have been analyzed to assess chemical and petrological variations within the mare basalt suite at this site. All nine (15536, 15537, 15538, 15546, 15547, 15548, 15598, 15605, and 15636) are low-silica olivine normative basalts (ONBs) that correlate with the ONB suite as defined in previous studies. Partial analyses have been published for two of these samples, but the other seven have not been analyzed previously. Five of these samples are part of a concurrent study by Schuraytz and Ryder (1988). The nine samples vary in texture and grain size from fine-grained, intergranular or subophitic basalts to coarse-grained, granular "microgabbros." Six of these samples are small (original sample weights 1.9 g to 27.8 g) but three are relatively large (original sample weights 135.7 g to 336.7 g). Two splits from each sample were analyzed separately to assess chemical differences between small subsamples of the same rock as a function of grain size and texture. Seven of the basalts have subsample pairs that are similar in composition and plot on olivine control lines with other Apollo 15 low-silica ONBs. Two of the basalts (15547 and 15636) have subsample pairs that differ significantly in composition from each other and from large subsamples of the same basalt. They also deviate from the overall trend of well-analyzed ONBs (Rhodes and Hubbard, 1973). These samples are coarse-grained microgabbros characterized by the heterogeneous distribution of late-forming mesostasis phases (glass, ilmenite, fayalite, whitlockite, troilite, Fe-metal) that are rich in FeO, TiO₂, and incompatible trace elements. Our data support the conclusions of Ryder and Steele (1988) that the ONB suite (referred to here as the low-silica ONB suite) to distinguish it from high-silica ONBs parental to the quartz-normative basalt suite) represents a single chemical group related by fractional crystallization of olivine. Chemical variations observed within the low-silica ONB suite that did not form by olivine removal are probably the result of nonrepresentative sampling and analytical uncertainty. These problems are most acute for small subsamples of coarse-grained granular basalts with heterogeneously distributed mesostasis phases. These data can be applied to breccia clast studies to infer the extent to which small clasts can be considered representative of their parent rock. The high-silica ONBs of Vetter et al. (1988) fall on olivine control lines with primitive quartz-normative basalts and are probably related to the QNB suite by olivine fractionation. The high-silica ONBs do not exhibit variations of the same magnitude or type as the low-silica ONBs studied here, which are affected primarily by mesostasis enrichments or depletions. We conclude that the high-silica ONBs of Vetter et al. (1988) are indeed a distinct rock type unrelated to the more common low-silica ONBs at the Apollo 15 site.

INTRODUCTION

Early studies of the Apollo 15 mare basalt suite established the presence of two distinct groups: the olivine-normative basalts and quartz-normative basalts (e.g., *Rhodes and Hubbard, 1973; Chappell and Green, 1973*). Olivine normative basalts (ONBs) are the more common variety and are inferred to overlie quartz-normative basalts (QNBs) at the Apollo 15 site (*ALGIT, 1972; Ryder, 1989*). These groups cannot be related to one another by fractional crystallization, so at least two separate parental magmas are needed (*Rhodes and Hubbard, 1973; Chappell and Green, 1973*).

Recent studies of mare basalts at the Apollo 14 site have revealed a wide variety of previously unrecognized mare basalt types (e.g., *Shervais et al., 1985a,b; Dickinson et al., 1985; Neal et al., 1988a,b*). The new basalts, which occur as clasts in

breccias or as coarse-fine fragments, have considerably broadened our views on mare basalt petrogenesis. These studies show that the lunar crust is far more complex than suspected previously, and that processes such as magma-mixing and wall-rock assimilation were important in its petrogenesis (e.g., *Warren et al., 1983; Shervais et al., 1985a,b; Neal et al., 1988a,b; Warren, 1988*). However, in many cases the samples may be only a few grain diameters across and weigh less than 50 mg. This can create problems in obtaining a representative sample. These problems are most acute for coarse-grained highland rocks, but can also cause considerable uncertainty in the analysis of mare basalt clasts.

Similar problems may arise when small subsamples of individual hand samples are allocated for analysis. *Mason et al. (1972)* discuss this problem in regard to the Apollo 15 mare basalt suite. They report that their analysis of 15085, which

has an average grain size of about 3 mm, deviates significantly from the trend of other analyzed mare basalts, and that this deviation is not in the direction expected by normal igneous processes. *Rhodes and Hubbard* (1973) note differences in separate analyses of coarse-grained mare basalt 15555 by different laboratories that were too large to be caused by interlaboratory analytical error. They also find large differences in their own replicate analyses of 15076, a coarse-grained basalt or microgabbro. *Mason et al.*, (1972) and *Rhodes and Hubbard* (1973) both attribute these discrepancies to inadequate sampling of the coarse-grained rocks. *Helmke et al.* (1973) discuss sampling problems in their study of Apollo 15 basalts, which includes 24 "walnut" and "peanut" sized samples from the rake samples and coarse-fines. They note that the compatible elements display relatively little scatter, but that the incompatible elements are more sensitive to the distribution of late mesostasis phases.

Clanton and Fletcher (1976) developed a model for major element variations in small samples based on Monte Carlo simulations of mineral grain distribution, observed grain size, mode, and sample weight. The model is designed to convert uncertainties in the mineral grain distribution into uncertainties in the abundance of the major elements. It does not consider the distribution of mesostasis phases, however, and thus cannot explain variations in the incompatible trace elements.

Ryder and Steele (1988) and *Schuraytz and Ryder* (1988) have attempted to minimize this problem for the Apollo 15 ONB suite by analyzing splits taken from large, homogenized subsamples. *Ryder and Steele* (1988) homogenized subsamples weighing 200 to 500 mg for 12 of their analyses. *Schuraytz and Ryder* (1988) increased that by an order of magnitude, homogenizing 4 to 5 g per sample. This approach is impractical for breccia clast studies, where the weight of sample extracted from the breccia matrix may be 100 mg or less.

We report here new chemical and petrographic data on nine samples of Apollo 15 ONB. Seven of these samples have not been analyzed previously; one has been analyzed by INAA only (15605; *Ma et al.*, 1978), and another has been analyzed by XRF and INAA (15636; *Compston et al.*, 1972; *Frichter et al.*, 1973). These basalts exhibit a range in average grain size from coarse to fine, and several display macroscopic heterogeneity. Our approach is to analyze subsamples similar in size to those

commonly used in breccia clast studies (100 to 150 mg), and to analyze two separate rock fragments from each sample. In addition, we received subsamples from five of the large samples studied by *Schuraytz and Ryder* (1988). Our goal is to present new data on the Apollo 15 olivine basalt suite, and to assess the effects of small sample size on the apparent bulk chemistry of mare basalt samples. We extend our conclusions to analyses of small clasts in breccia 15498 reported by *Vetter et al.* (1988).

METHODS

Nine mare basalts were sampled in this study: 15536, 15537, 15538, 15546, 15547, 15548, 15598, 15605, and 15636. Existing thin sections and probe mounts of each sample were studied using standard petrographic techniques, and their constituent mineral phases analyzed using the SX-50 electron microprobe at the University of South Carolina. Minerals were analyzed at 15 kV with a 25 nA beam current and a 1-2- μ spot size; representative mineral analyses are reported in the Appendix, and complete analytical data are on file in the datapacks at NASA-JSC. A suite of natural and synthetic minerals provided by E. Jarosewich of the National Museum of Natural History at the Smithsonian Institution were used as standards. Modes were determined by point counts on one to three thin sections of each sample; these data are reported in Table 1. The number of sections counted for the modes was a function of the number of sections available for each sample, not their grain size. Grain size distributions were determined using color photomicrographs; for each sample, *all* of the mineral grains in one or more photos were measured.

Five of the nine samples studied here were received as two separate subsamples, each weighing approximately 150 mg, taken from different parts of the parent sample. The other four samples were received as single 200-mg samples (15536, 15598, 15605, 15636) and were split into two 100-mg subsamples prior to further processing. Each subsample was crushed to a fine powder in an agate mortar and further subdivided into two fractions: 35-50 mg for major element analysis using the fused bead-electron microprobe technique (*Broun*, 1977) and 60-100 mg for trace element analysis by instrumental neutron activation analysis (INAA). FeO, Na₂O, and Cr were also determined by INAA. Subsamples for fused

TABLE 1. Modal composition of Apollo 15 olivine normative basalts based on petrographic analysis.

Sample	15536 .7	15536 .8	15536 Avg	15537 .4	15538 .4	15538 .5	15538 Avg	15546 .6	15546 .7	15546 .8	15546 Avg	15547 .6	15547 .7	15547 .8	15547 Avg
Points Counted	6750	6079	12829	831	532	563	1095	1211	1162	1398	3771	719	1218	1086	3023
Modal %															
Olivine	28.0	20.2	24.3	17.7	18.0	20.2	19.2	7.8	20.8	10.6	12.9	19.5	16.2	16.5	17.1
Pyroxene	35.9	40.2	37.9	41.2	41.0	35.7	38.3	51.6	39.1	53.6	48.5	47.6	45.4	49.0	47.2
Plagioclase	31.2	30.3	30.8	32.3	31.4	29.3	30.3	34.2	27.5	26.5	29.3	26.8	30.2	23.8	27.1
Opacues	3.1	5.4	4.2	6.5	0.8	2.3	1.6	3.7	5.8	5.1	4.9	1.0	5.1	2.2	3.1
Mesostasis	0.2	0.7	0.5	0.7	2.6	2.8	2.7	0.6	3.4	1.6	1.8	0.7	1.1	2.1	1.4
Fayalite	0.2	0.8	0.5	0.0	0.6	1.1	0.8	2.1	2.2	0.1	1.4	0.1	1.6	0.9	1.0
Cristobalite	1.4	2.4	1.9	1.7	5.6	8.5	7.1	0.0	1.2	2.5	1.3	4.3	0.3	5.4	3.1

TABLE 1. (continued).

Sample	15548 ,4	15598 ,10	15598 ,11	15598 ,12	15598 Avg.	15605 ,5	15605 ,6	15605 Avg.	15636 ,8	15636 ,9	15636 Avg.
Points Counted	532	1836	2300	2286	6422	1488	1480	2968	1058	858	1916
Modal %											
Olivine	22.4	15.3	14.7	12.7	14.2	16.3	15.3	15.8	16.2	20.3	18.0
Pyroxene	41.4	42.6	40.8	45.1	42.8	47.6	48.0	47.8	47.9	40.8	44.7
Plagioclase	28.2	32.2	35.0	32.7	33.4	27.0	23.9	25.4	24.0	29.1	26.3
Opacues	5.6	7.1	6.9	5.7	6.5	4.5	8.3	6.4	6.1	6.2	6.2
Mesostasis	0.9	2.1	0.8	2.4	1.7	1.2	1.7	1.4	1.6	1.4	1.5
Fayalite	0.2	0.6	1.6	1.3	1.2	2.8	2.2	2.5	2.6	1.0	1.9
Cristobalite	1.3	0.2	0.1	0.0	0.1	0.5	0.7	0.6	1.6	1.2	1.4

bead EMP analysis were fused in an electric strip furnace at the University of South Carolina, using Mo foil sample boats and a dry nitrogen gas atmosphere. Fusion time was generally 20 seconds or less. The fused beads were analyzed at 15 kV with a 15 nA beam current and a 15-20- μ -diameter spot size on a Cameca SX-50 electron microprobe at the University of South Carolina (Table 2). Natural and synthetic minerals and glasses provided by E. Jarosewich of the National Museum of Natural History at the Smithsonian Institution were used as standards.

In order to test this method, ten separate fractions of USGS basalt standard W-2 were fused into glass beads and analyzed using the same conditions and standards as the mare basalts. The results were averaged and a standard deviation for each element determined (Table 2). This estimate of analytical uncertainty includes counting error, sample preparation, and matrix correction effects, which are the most important sources of error inherent in the analytical technique.

The trace element subsamples were analyzed at NASA-JSC using the procedures outlined by *Liudstrom et al.* (1989); the results are reported in Table 2 along with the major element data. The analytical uncertainties listed in the rightmost column reflect both counting errors and 1% uncertainty for noncounting errors. The silica glass tube containing one sample, 15537B, broke during irradiation or transport, resulting in the loss of about one-third of the sample. The mass of sample remaining was obtained by comparing the apparent FeO in the INAA sample to the concentration of FeO determined by fused bead electron microprobe analysis of powder from the same split.

PETROGRAPHY AND MINERAL CHEMISTRY

All the samples studied here are low-SiO₂ ONBs typical of the Apollo 15 site. Six of these samples are medium- or coarse-grained granular basalts and probably best classified as olivine microgabbros; the other three (15536, 15548, and 15598) are olivine-phyric basalts with medium- or fine-grained groundmass. The grain size designations used here differ from those used by *Ryder* (1985): fine-grained <0.35 mm average, medium-grained = 0.35-0.5 mm average, and coarse-grained >0.5 mm average. The reason for these differences is that the

average grain size determined by counting *all* the grains in a given area is smaller than that estimated from random measurements because very small grains tend to be ignored in random measurements. The average grain size here was determined by calculating the area of each measured grain, averaging the areas, and determining the equivalent length of the average grain. This results in a slightly larger average grain size than simply averaging the grain diameters. Photomicrographs of each sample, all made at the same magnification, are shown in Fig. 1.

Petrography

Basalt 15536. 15536 is a medium-grained olivine-phyric basalt, with olivine phenocrysts 0.5 to 1.5 mm in diameter (Fig. 1a). Olivine is less common than pyroxene in the groundmass, where both minerals range from 0.1 to 1.1 mm across (average about 0.4 mm). The mafic phases are enclosed by plagioclase laths up to 1.7 \times 0.5 mm in size (0.5 \times 0.2 mm average) that form a subophitic to poikilitic texture, with small pyroxene chadacrysts in plagioclase oikocrysts. Ilmenite, ulvospinel, fayalite, cristobalite, glass, and troilite all crystallized late and are interstitial to the mafic phases, but are not generally associated with plagioclase. *Ryder* (1985) noted that 15536 contains mafic and felsic bands in hand specimen, but these bands are not obvious in thin section.

Basalt 15537. 15537 is a medium-grained, vesicular olivine basalt with rounded olivine grains, 0.20 to 1.5 mm across, forming chadacrysts in large, subhedral pigeonite oikocrysts (Fig. 1b). Small chadacrysts of plagioclase in pyroxene are less common. Pigeonite forms blocky prisms up to 4 mm long, but most are 0.2 to 1 mm in length with subhedral to anhedral outlines (0.41 mm average). The pigeonite is surrounded by plagioclase laths 0.1 to 0.8 mm in length (about 1.5 mm maximum, 0.38 mm average) that enclose pyroxene subophitically, but some laths are partly enclosed by pyroxene. Late pyroxene-plagioclase intergrowths are finer-grained and have variolitic textures. Mesostasis phases, which include ilmenite, ulvospinel, chromite, glass, and fayalite, are relatively scarce and evenly distributed throughout the sections.

Basalt 15538. 15538 is medium-grained granular olivine basalt or microgabbro with a poikilitic, cumulus texture (Fig.

TABLE 2. Whole rock major and trace element analyses of Apollo 15 mare basalts

Sample wt. (mg)	15536		15536		15536		15536		15536		15536		15536		15536		15536			
	A	B	A+B	9003	A	B	A+B	9003	A	B	A+B	9003	A	B	A+B	9003	A	B	A+B	9003
SiO ₂	44.6	44.7	44.6	44.4	44.6	44.5	44.5	45.2	45.3	45.1	45.2	45.2	42.5	45.2	45.2	45.2	42.5	45.2	45.2	44.3
TiO ₂	2.05	2.23	2.14	2.30	2.18	2.31	2.25	1.82	2.00	1.91	1.98	2.41	3.21	1.73	2.47	2.22	3.21	1.73	2.47	2.22
Al ₂ O ₃	7.46	7.57	7.52	7.66	7.28	7.17	7.22	8.90	8.78	8.84	9.54	8.15	5.48	9.38	7.43	8.03	5.48	9.38	7.43	8.03
FeO	23.56	23.02	23.29	23.24	22.31	23.07	22.69	21.67	21.44	21.56	20.72	22.54	28.21	20.68	24.44	22.65	28.21	20.68	24.44	22.65
MnO	0.29	0.29	0.29	0.31	0.310	0.320	0.32	0.30	0.300	0.30	0.29	0.28	0.30	0.34	0.31	0.28	0.30	0.34	0.31	0.28
MgO	11.89	11.36	11.63	11.11	13.00	12.96	12.98	11.50	11.01	11.26	10.96	11.41	10.75	10.68	11.78	11.46	10.68	11.78	11.23	11.46
CaO	9.23	9.42	9.32	9.53	9.09	8.77	8.93	9.65	10.16	9.90	10.05	9.83	8.52	9.79	9.15	9.40	8.52	9.79	9.15	9.40
Na ₂ O	0.22	0.21	0.21	0.25	0.200	0.210	0.21	0.26	0.250	0.26	0.29	0.23	0.20	0.28	0.24	0.21	0.20	0.28	0.24	0.21
K ₂ O	0.02	0.04	0.03	0.04	0.030	0.030	0.03	0.02	0.020	0.02	0.02	0.03	0.05	0.02	0.04	0.03	0.05	0.02	0.04	0.03
P ₂ O ₅	0.04	0.04	0.04	0.04	0.050	0.060	0.06	0.06	0.030	0.04	0.05	0.04	0.11	0.03	0.07	0.06	0.11	0.03	0.07	0.06
Cr ₂ O ₃	0.69	0.65	0.67	0.60	0.700	0.720	0.71	0.58	0.580	0.58	0.64	0.58	0.62	0.63	0.62	0.64	0.62	0.63	0.62	0.64
Total	100.02	99.48	99.75	99.47	99.78	100.07	99.93	99.57	100.12	99.85	99.76	99.52	99.64	99.88	99.87	99.33	99.88	99.87	99.87	99.33
Na ₂ O	0.234	0.255	0.244		0.225	0.224	0.225	0.274	0.246	0.260	0.282	0.28	0.281	0.183	0.274	0.229	0.183	0.274	0.229	
FeO	22.4	22	22.2		21.5	23.1	22.3	20.5	22.2	21.4	20.1	20.2	20.1	27.8	20.6	24.2	27.8	20.6	24.2	
Sc	40	41.1	40.5		41.3	39.7	40.5	39.8	40.9	40.3	40.9	42.3	41.6	45.1	38.7	41.9	45.1	38.7	41.9	
Cr	4700	4590	4645		5100	5114	5257	4300	3980	4140	4360	4180	4270	4170	4450	4310	4170	4450	4310	
Co	55.9	55.4	55.6		56.7	61.9	59.3	53.3	55.8	54.5	50.4	51.6	51.0	58.7	56.5	57.6	58.7	56.5	57.6	
Ni	60	70	65		80	78	79	61	90	76	80	70	75	60	70	65	60	70	65	
Sr	90	120	105		90	93	92	124	130	127	120	120	120	130	80	105	130	80	105	
Ba	41	23	32		47	50	48	34	45	40	33	45	39	72	32	52	72	32	52	
La	3.82	4.27	4.04		5.26	5.15	5.20	3.25	5.38	4.31	2.64	2.64	2.64	7.89	2.79	5.34	7.89	2.79	5.34	
Ce	12.3	12.1	12.2		14.6	14.6	14.6	10.3	14	12.2	8.5	7.7	8.1	22.2	8.2	15.2	22.2	8.2	15.2	
Sm	2.87	3.07	2.97		3.64	3.59	3.62	2.37	3.74	3.06	2.02	1.99	2.00	5.54	2.11	3.83	5.54	2.11	3.83	
Eu	0.739	0.81	0.774		0.811	0.790	0.801	0.746	0.89	0.818	0.706	0.71	0.708	1.03	0.721	0.875	1.03	0.721	0.875	
Tb	0.64	0.74	0.69		0.78	0.78	0.78	0.52	0.84	0.68	0.46	0.46	0.46	1.2	0.51	0.85	1.2	0.51	0.85	
Yb	1.87	1.94	1.91		2.25	2.30	2.28	1.6	2.35	1.98	1.39	1.42	1.40	3.3	1.41	2.35	3.3	1.41	2.35	
Lu	0.255	0.273	0.264		0.308	0.314	0.311	0.212	0.311	0.262	0.199	0.187	0.193	0.468	0.196	0.332	0.468	0.196	0.332	
Zr	70	<190	70		80	<150	80	60	120	90	<130	<130	<150	110	110	110	110	110	110	
Hf	2.25	2.3	2.27		2.66	2.61	2.61	1.79	2.7	2.25	1.59	1.51	1.55	4.25	1.52	2.88	4.25	1.52	2.88	
Ta	0.31	0.32	0.32		0.352	0.376	0.36	0.237	0.36	0.30	0.218	0.19	0.20	0.62	0.2	0.41	0.62	0.2	0.41	
U	0.06	<0.2	0.06		0.24	0.12	0.18	<0.2	<0.3	<0.3	0.13	<0.3	0.13	0.15	<0.23	0.15	0.15	<0.23	0.15	
Th	0.29	0.3	0.29		0.44	0.44	0.44	0.25	0.4	0.33	0.16	0.17	0.17	0.76	0.23	0.49	0.76	0.23	0.49	

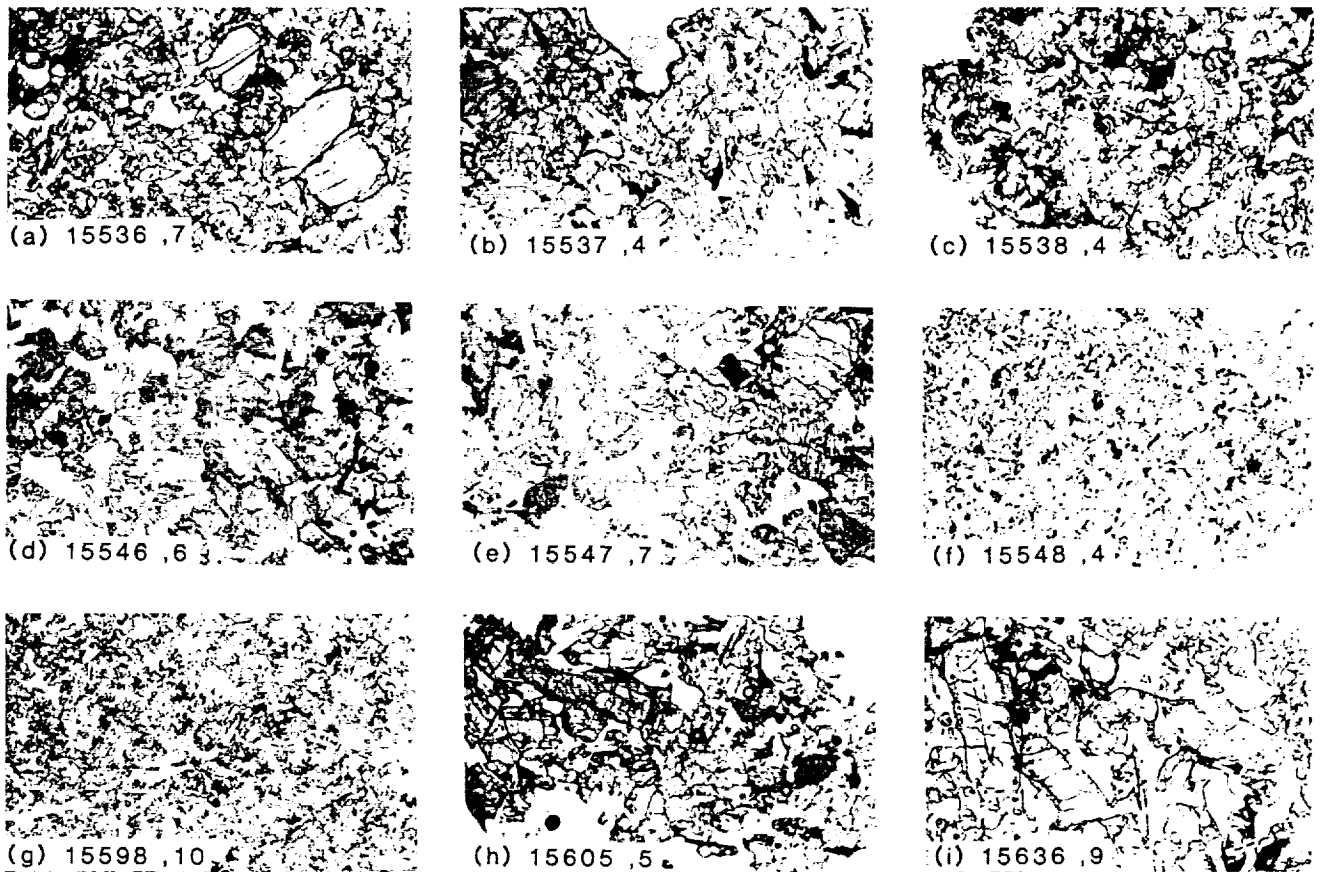


Fig. 1. Photomicrographs of the nine mare basalt samples studied here, all at the same scale (field of view = 5.6 mm). (a) 15536 .7; (b) 15537 .4; (c) 15538 .4; (d) 15546 .6; (e) 15547 .7; (f) 15548 .4; (g) 15598 .10; (h) 15605 .5; (i) 15636 .9.

1c). Rounded olivine and pyroxene grains 0.1 to 0.8 mm across are poikilitically enclosed by blocky, lath-shaped plagioclase oikocrysts 1.0 to 2.5 mm long, and up to 1.0 mm wide. Smaller plagioclase laths are interstitial to both plagioclase and pyroxene. Magnesian olivine also occurs as small (0.3 mm average) rounded inclusions in pigeonite, which zones outward to augite. The pigeonites contain very thin exsolution lamellae of a pale brown phase, possibly spinel.

Half of thin section .4 is mafic and the other half is plagioclase-rich; this banding was also noted in hand specimens by *Ryder* (1985). The mafic half contains abundant pigeonite, olivine, ulvospinel, and ilmenite surrounded by 25-30% interstitial plagioclase. The other half of the section contains larger lath-shaped plagioclase oikocrysts that comprise 50-60% of the basalt, with small, rounded chadacrysts of olivine and pigeonite. Mesostasis clots consisting of ilmenite, fayalite, cristobalite, and brown glass are common in the mafic half of the section, but are rare in the plagioclase-rich half.

Basalt 15546. 15546 is a medium- to coarse-grained, granular-textured olivine basalt (Fig. 1d). Olivine forms blocky or rounded crystals less than 1 mm across (0.4 mm average) that generally are either overgrown by pigeonite or form inclusions within single pigeonite grains. Pigeonite forms blocky, subhedral crystals, mostly 0.1 to 1.0 mm long, although

some are as large as 2 mm (0.4 mm average). The mafic phases are surrounded by interstitial plagioclase laths approximately 0.8×0.2 mm in size that enclose pyroxene subophitically, but in some cases this relationship is reversed and pyroxene molds around plagioclase.

Except for a few chromite inclusions, opaque phases are generally interstitial to pyroxene and mold around pyroxene crystal faces. The opaques, ilmenite and ulvospinel, are usually small (0.1 to 0.2 mm) but a few ilmenite blades are as large as 1.2×0.4 mm. Late-forming mesostasis phases such as cristobalite, fayalite, and pale brown glass are commonly associated with the opaques, but these mesostasis-rich areas are small and evenly distributed throughout the section.

Basalt 15547. 15547 is a coarse-grained, granular-textured olivine basalt or microgabbro (Fig. 1e). Pyroxene and plagioclase form an interlocking network of subhedral to anhedral prisms and laths 0.5 to 2 mm long (0.58 mm average), with the plagioclase commonly enclosing pyroxene subophitically. The pyroxene (0.62 mm average) is strongly zoned from pigeonite cores to reddish-brown ferroaugite rims that are rich in opaque inclusions. The pigeonites commonly contain very thin exsolution lamellae of a pale brown phase that are too thin to analyze but which may be spinel; similar lamellae are found in 15605 and 15538. Olivine occurs as tiny

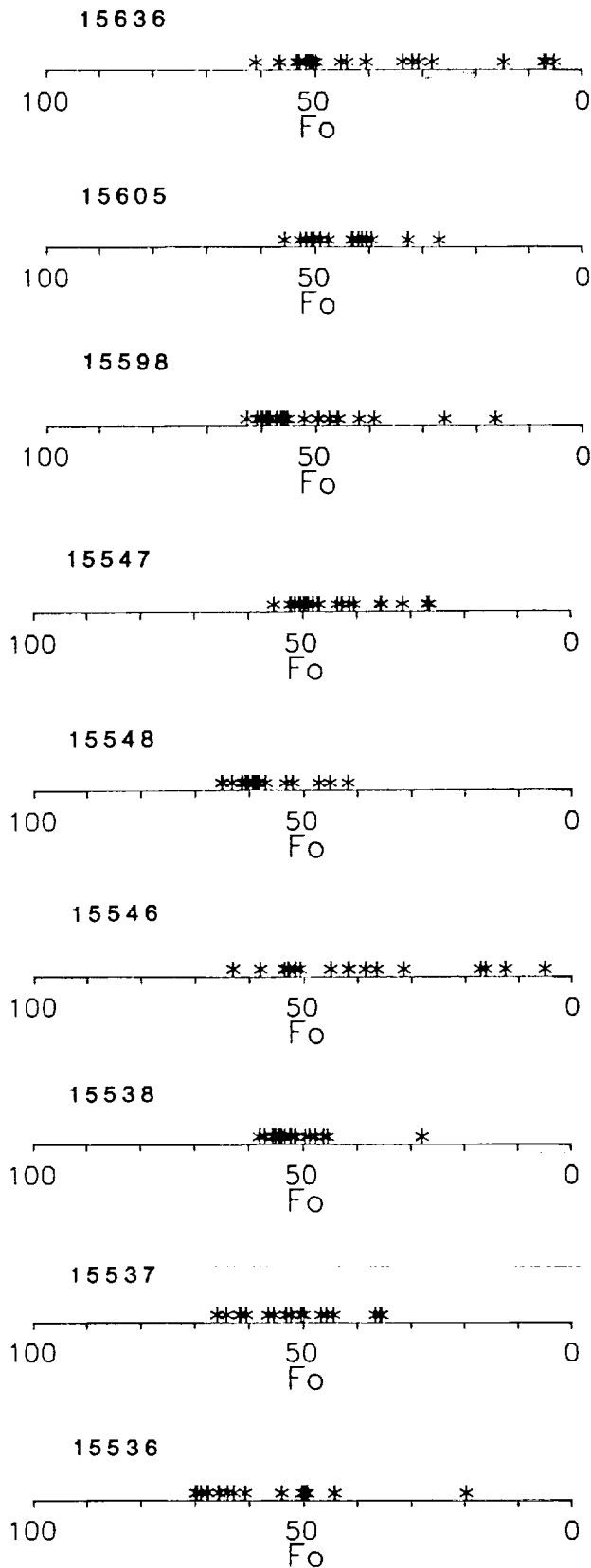


Fig. 2. Olivine compositions in mol.% forsterite component.

(0.1 to 0.5 mm) rounded inclusions in pigeonite and plagioclase. Ilmenite and ulvospinel occur interstitially either as individual grains or in clots with other mesostasis phases.

Mesostasis phases typically occur as clots up to 0.6 mm across that are irregularly distributed throughout the thin sections. The clots are scarce and small in sections ,6 and ,7, whereas in section ,8 they are abundant. The clots generally consist of fayalite, ilmenite, cristobalite, pale brown glass, ulvospinel, whitlockite, troilite, and Fe-metal; fayalite and glass are commonly associated in vermicular intergrowths.

Basalt 15548. 15548 is a very fine-grained, olivine-microphyric basalt with an intergranular to subophitic texture in which plagioclase laths partially enclose smaller pyroxene grains (Fig. 1f). The olivine microphenocrysts are 0.25 to 1.25 mm across (0.4 mm average) and have subhedral to nearly euhedral outlines with ragged grain boundaries. A few olivines are embayed and the embayment is filled with groundmass phases. The groundmass consists of a framework of plagioclase laths 0.05 to 0.55 mm long (0.23 mm average) with interstices that are filled with granular aggregates of pyroxene (0.17 mm average) and opaques (0.09 mm average). A few of the larger plagioclase grains are poikilitic and enclose small pyroxene grains, but partial molding of plagioclase around pyroxene is more common. The opaque phases, ilmenite and ulvospinel, are evenly distributed as small, anhedral grains that are interstitial to pyroxene; cristobalite and glass are scarce.

Basalt 15598. 15598 is a fine-grained, olivine-phyric basalt consisting of scattered olivine phenocrysts 0.6 to 1.3 mm across, set in an intergranular matrix of plagioclase, pyroxene, and opaques (Fig. 1g). The olivine phenocrysts are subhedral to anhedral in outline, with embayed rims and ragged or fritted grain boundaries (Fig. 1g). The groundmass consists of subhedral plagioclase laths 0.1 to 0.8 mm long (0.33 mm average) separated by a fine granular aggregate of pyroxene, ilmenite, and ulvospinel. Cristobalite, fayalite, and residual glass are distributed in residual patches, but these are generally small and evenly distributed throughout the sample. The groundmass pyroxene is generally only 0.1 to 0.4 mm in diameter (0.27 mm average), and forms a granular mosaic that fills in between plagioclase laths.

Basalt 15605. 15605 is a coarse-grained, vesicular olivine-bearing basalt with scarce, large, rounded olivines up to 1.25 mm across. Most olivines form small (<0.8 mm) rounded and embayed inclusions in pyroxene, but section ,5 contains a large skeletal olivine grain 3 mm long \times 0.3 mm wide with a hollow core (Ryder, 1985). Pigeonite forms subhedral prisms up to 2.5 \times 0.6 mm, but most are 0.2 to 2 mm in length (0.56 mm average). Chromite inclusions are common in both pigeonite and olivine. Many of the larger pigeonites have very thin exsolution lamellae of a pale brown phase—possibly spinel—that are too thin to analyze. Plagioclase forms laths up to 2 mm long that are interstitial to pyroxene and commonly mold around them to form a subophitic texture.

Mesostasis phases include fayalite, ilmenite, ulvospinel, cristobalite, brown glass, and a phosphate. These are generally concentrated in mesostasis-rich areas between the mafic silicate grains, but these areas are small and evenly distributed

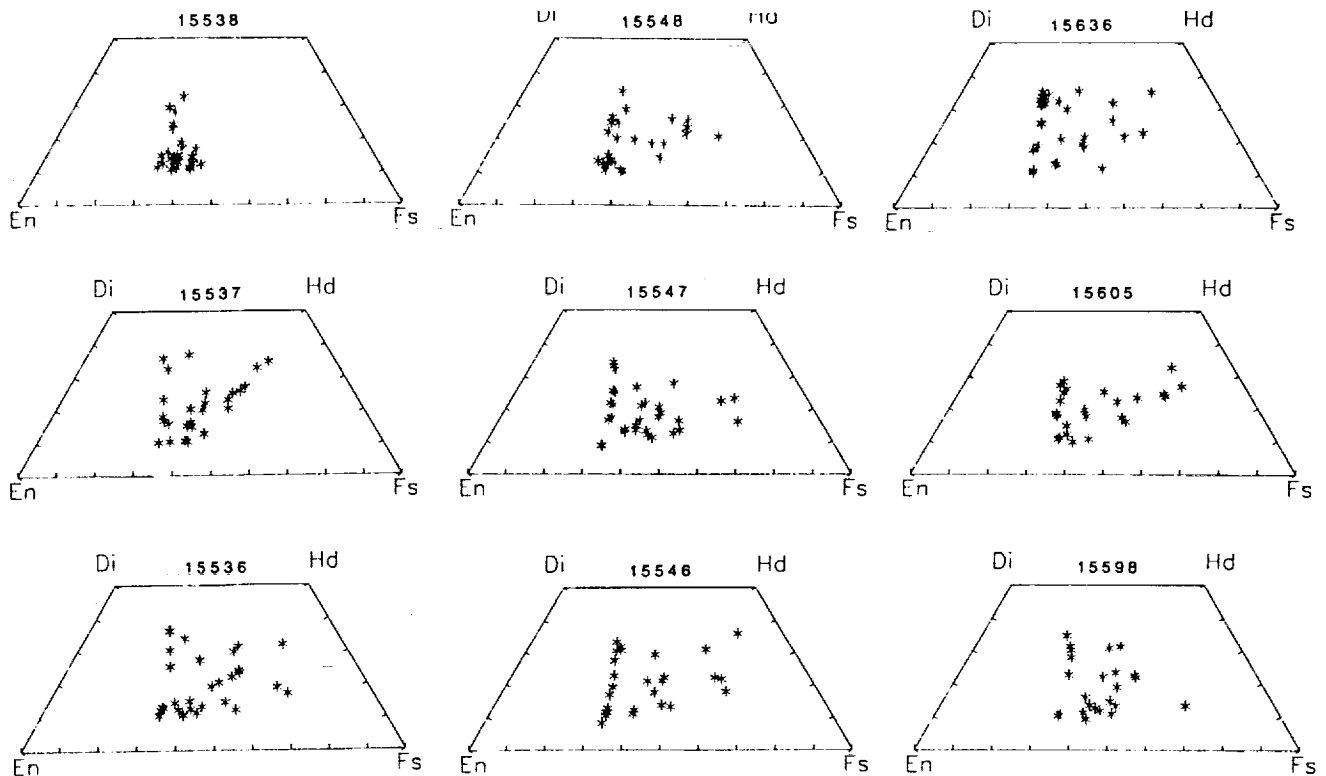


Fig. 3. Pyroxene compositions.

throughout the sample. One interesting textural feature found in section ,5 is a deformed pyroxene grain that has been curved around an adjacent olivine. The pyroxene has undulatory extinction where the cleavage is curved, and a sharp kink-band boundary with the undeformed termination of the crystal. Despite the strong curvature in the pyroxene, the adjacent plagioclase shows no indication of strain or deformation.

Basalt 15636. 15636 is a coarse-grained, granular-textured olivine basalt or microgabbro consisting of large subhedral to anhedral pyroxene and plagioclase laths up to 3.5 mm long (Fig. 1i). Pyroxene (0.74 mm average) is strongly zoned from pigeonite cores to reddish-brown, inclusion-rich ferroaugite rims. The pyroxenes are commonly twinned but no exsolution lamellae are evident. Blocky plagioclase laths (0.65 mm average) enclose pyroxenes subophitically, and also poikilitically enclose some of the smaller olivine and pyroxene grains. Olivine occurs as small (0.1 to 0.5 mm) subhedral to euhedral inclusions in plagioclase, or as rounded inclusions in pyroxene. Opaque phases include chromite, ilmenite, ulvospinel (which may contain ilmenite exsolution lamellae), troilite, and Fe-metal. Chromite generally occurs as inclusions in pigeonite or olivine; the other opaque phases are commonly associated with mesostasis clots that also include fayalite, cristobalite, brown glass, and whitlockite.

The mesostasis clots are up to 1.0×0.5 mm in size and are distributed irregularly throughout the sample. Their occurrence is generally restricted to plagioclase-free areas between

pyroxene grains, and they are commonly intergrown with the ferroaugite rims. 15636 resembles 15538 in the irregular distribution of mafic phases and plagioclase: two-thirds of thin section ,8 consists of plagioclase-rich basalt (45-50% plagioclase) with rare opaques; the other one-third of ,8 contains only 25-30% plagioclase. The mafic portion of ,8 and most of thin section ,9 contain abundant mesostasis clots, but even in section ,9 (which is relatively mafic) the mesostasis-rich areas are clustered in three distinct regions. This highly irregular distribution of opaque and mesostasis phases is also evident in hand specimen.

Mineral Chemistry

Olivine. Olivine phenocrysts in the three olivine-phyric basalts (15536, 15548, 15598) range in composition from Fo50 to Fo71, with rims that are somewhat richer in iron—Fo43 to Fo63 (Fig. 2). The cores of the olivine phenocrysts are generally more magnesian than the resorbed olivine chadacrysts in the coarser-grained olivine basalts and olivine microgabbros, which generally range from Fo40 to Fo57, although chadacrysts in one sample (15537) are more magnesian (Fo60 to Fo66). Fayalitic olivines associated with other late mesostasis phases in the coarse-grained basalts are greenish in color, and range in composition from Fo37 to Fo15.

Pyroxene. Pyroxenes in all the samples have similar compositional ranges, regardless of texture or grain size (Fig.

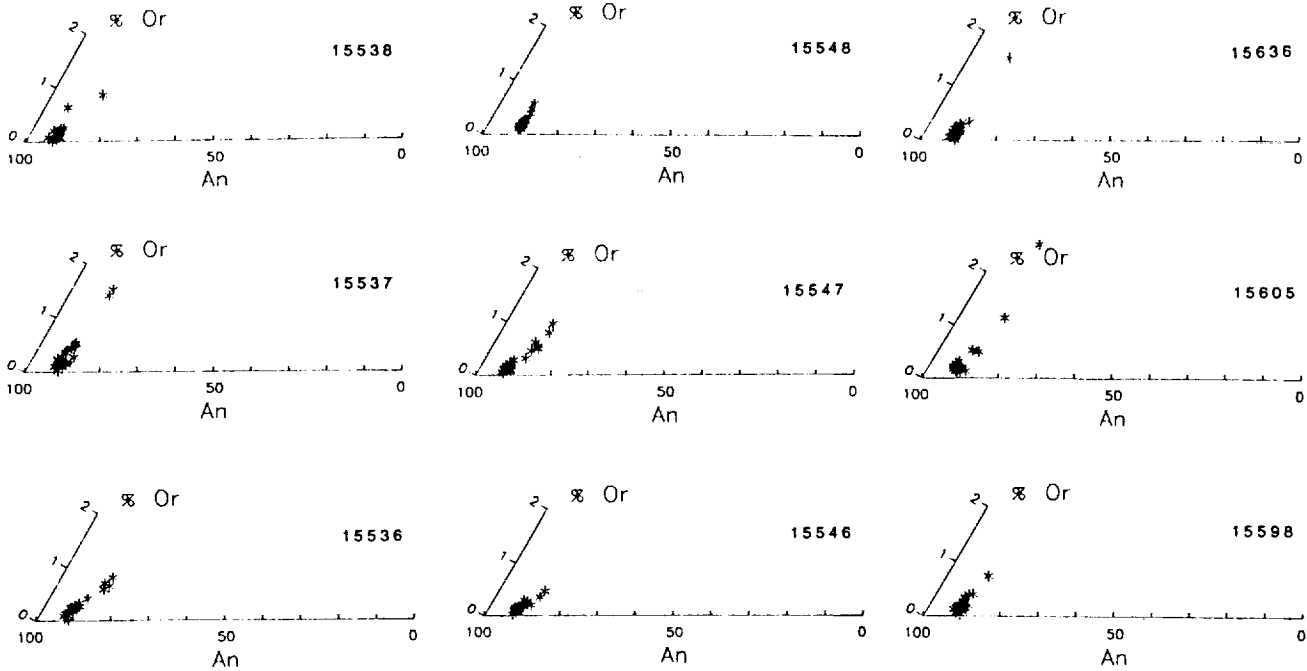


Fig. 4. Plagioclase compositions.

3). Groundmass pyroxenes in the olivine-phyric samples have $100^{\circ} \text{Mg}/(\text{Mg}+\text{Fe})$ ratios (MG#s) that range from 66 to 24. Large, subhedral pyroxenes in the coarse-grained olivine microgabbros have pigeonitic cores (MG#s = 67 to 46) that zone outwards toward augite or ferroaugite rims (MG#s = 63 to 24). Minor element concentrations are also similar, with $\text{Al}_2\text{O}_3 = 0.8$ to 3.1 and $\text{TiO}_2 = 0.3$ to 1.8 in all samples. In general, the highest minor element concentrations are associated with higher wollastonite components in the pyroxene.

Plagioclase. Plagioclase displays limited compositional variation, ranging from An93 to An85 and averaging about An91 in most samples (Fig. 4). One of the coarse-grained basalts (15547) seems to include a larger proportion of more sodic plagioclase, lowering the average composition to around An89 (Fig. 4). Potassium contents are uniformly low, with compositions ranging up to 2 mol.% Or maximum.

Opagues. Ilmenite and ulvospinel are the most common opaque phases in all samples; low-Ti chromite is much less abundant and generally occurs as small euhedral inclusions in olivine or pigeonite. Ilmenites display limited solid solution towards geikielite, with 0.1 to 1.5 wt.% MgO. Chromites include about 3 to 4 wt.% TiO_2 , the ulvospinels 20 to 30 wt.% TiO_2 .

Mesostasis glass. Mesostasis glass is scarce in the fine-grained samples, but is common in many of the coarser-grained rocks. This glass is rich in SiO_2 (74 to 79 wt.%), Al_2O_3 (10.7 to 12.9 wt.%), and K_2O (2.6 to 8.8 wt.%), with relatively minor TiO_2 (0.4 to 0.6 wt.%), FeO (0.9 to 2.15 wt.%), MgO (0 to 0.03 wt.%), CaO (0.6 to 4.0 wt.%), and Na_2O (0.12 to 0.3 wt.%).

WHOLE ROCK GEOCHEMISTRY

Whole rock geochemical data for the nine mare basalts studied here are presented in Table 2, along with additional data from the literature for samples 15605 and 15636 (Ma et al., 1978; Compston et al., 1972; Fruehter et al., 1973). Table 2 also includes major element data that we determined for five of the basalts studied here, using subsamples from the 4 to 5 g homogenized powders prepared by Schuraytz and Ryder (1988). These data, along with the previously published results for samples 15605, provide our best estimate of "true" bulk rock compositions for comparison with our analyses of the small subsamples.

Major Elements

All the samples studied here have major element geochemical characteristics typical of the Apollo 15 olivine-normative basalt suite. Data for the 18 small subsamples (2 per basalt sample) and 6 large subsamples are plotted on MgO variation diagrams in Fig. 5. All of the large subsamples and 16 of the small subsamples plot within the same region as the other Apollo 15 ONBs. Two of our small aliquots (15547A and 15636B) are enriched in FeO and TiO_2 , and depleted in SiO_2 and CaO; these samples fall outside the area of typical Apollo 15 ONBs and far from the other samples studied here (Fig. 5).

Five of the nine samples studied here (15536, 15537, 15538, 15548, 15605) have subsample pairs that are essentially the same within analytical uncertainty (assumed to be about twice the standard deviation of replicate analyses, Table 2). Two other samples (15546, 15598) have subsample pairs that differ

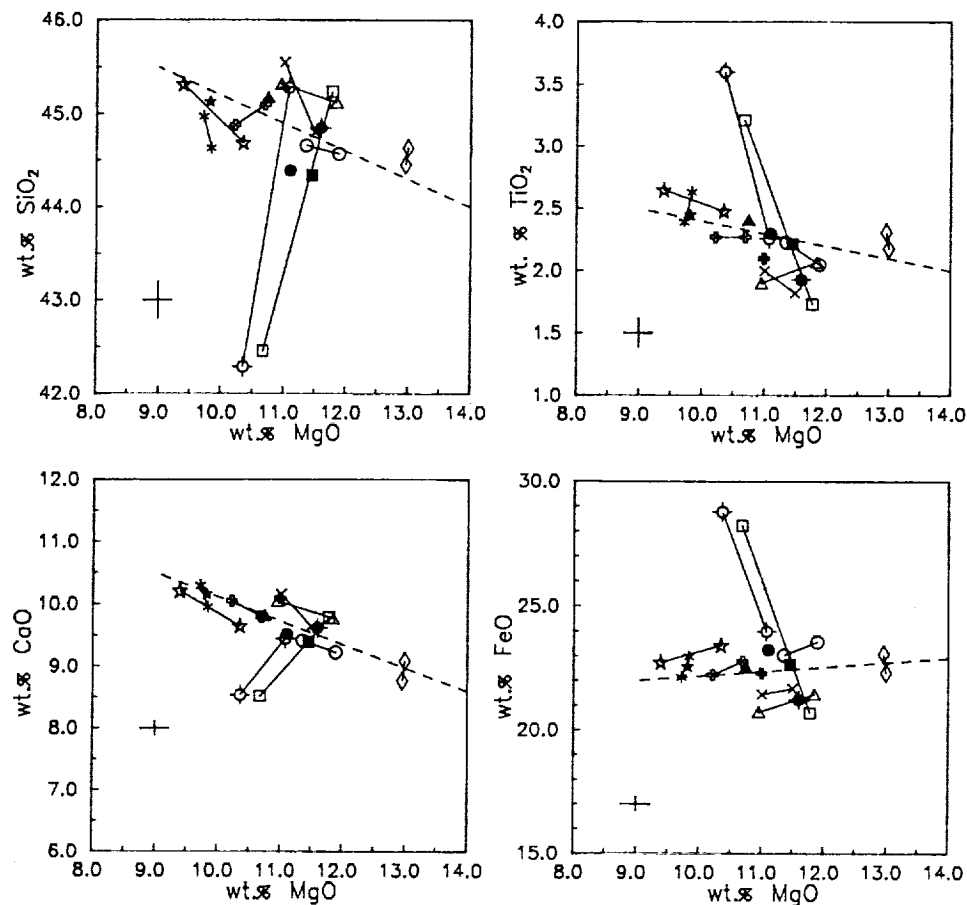


Fig. 5. MgO variation diagrams for SiO_2 , TiO_2 , FeO , and CaO . Open symbols connected by tie-lines are small subsamples analyzed here, closed symbols are large subsamples. Circles = 15536, diamonds = 15537, X = 15538, triangles = 15546, squares = 15547, asterisks = 15548, stars = 15598, cross = 15605, circle with cross = 15636. Dashed lines are olivine control lines projected from composition Fo70. Error bars in lower left corner of each diagram represent two-sigma analytical uncertainty (from Table 2).

by larger amounts, but still lie within the field of Apollo 15 ONBs. Of these seven samples, four have been analyzed as large samples (15536, 15546, 15598 analyzed here from the powders of Schuraytz and Ryder, 1988, and 15605 analyzed by Ma *et al.*, 1978). Three of these large samples are within analytical uncertainty of at least one corresponding subsample and within twice the analytical uncertainty of both subsamples (Fig. 5). The large sample of 15546 is much higher in FeO and TiO_2 than either corresponding subsample (Fig. 5).

Two of the nine samples studied here, 15547 and 15636, have subsamples that differ significantly from each other and from their corresponding large samples. Each of these has a subsample that deviates from the overall trend of Apollo 15 ONBs and does not lie along olivine control lines drawn through the other ONB data (Fig. 5). These large differences in composition affect all the important major elements—Fe, Ti, Si, Ca, Al, and Mg.

Trace Elements

Differences in trace element concentrations among the nine subsample pairs studied here are shown in Fig. 6 for six representative elements as a function of MgO content. MgO was chosen for the abscissa to facilitate comparison with the major element data in Fig. 5. Concentrations of compatible elements such as Cr and Co correlate positively with MgO overall, which probably reflects control by olivine (Co) and Cr-spinel (Cr). Several subsample pairs show distinct negative correlations within this overall trend (Fig. 6). Details of the Cr, Co, and MgO variations among the subsample pairs suggest some decoupling of olivine and chromite.

Incompatible trace elements such as La, Ta, Hf, and Sc correlate negatively with MgO overall (as expected) and most data scatter around simple olivine control lines (Fig. 6). Data for the small subsamples parallel that for the large samples but with somewhat greater scatter. However, subsamples that fall

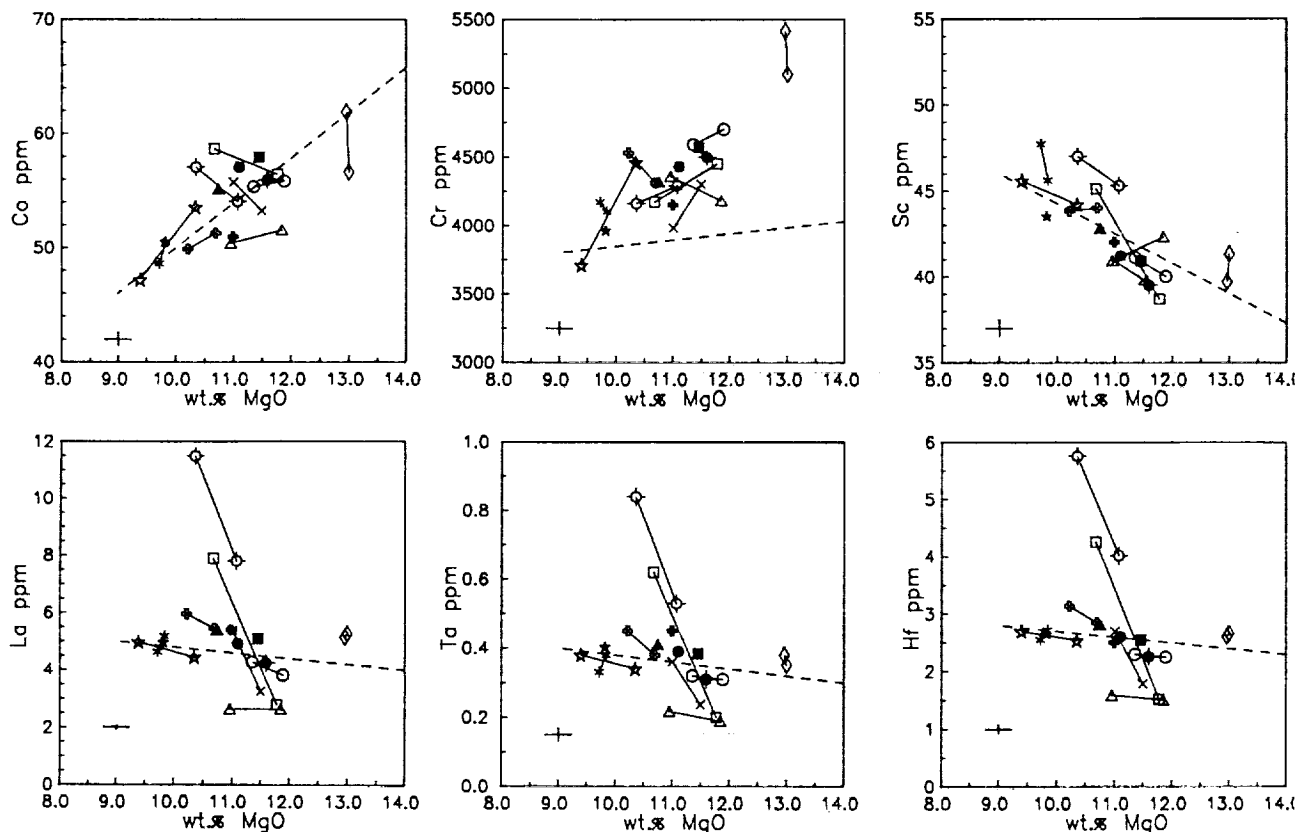


Fig. 6. MgO variation diagrams for six representative trace elements: Co, Cr, Sc, La, Ta, and Hf. Same symbols and conventions as Fig. 5.

outside the normal ONB fields on major element plots (Fig. 5) show strong enrichments in La, Ta, and Hf which are not consistent with subtraction of phenocrystic olivine or any other major silicate phase (Fig. 6).

DISCUSSION

Chemical Evolution of the Olivine Normative Basalt Suite

The chemical and petrologic data presented above show that all nine of the samples studied here are low-silica ONBs similar to those described earlier from the Apollo 15 site (e.g., *Rhodes and Hubbard, 1973; Chappell and Green, 1973; Helmke et al., 1973; Douty et al., 1973*). Variation diagrams show that the overall trend of the data is consistent with the fractionation of olivine (plus minor Cr-spinel) from a high-MgO parent magma (Figs. 5 and 6). Olivine control lines (dashed) are generally parallel to the trend of the data; the exact position of the control line depends on the olivine composition used (Fo70 in this case) and the low MgO projection point.

One sample analyzed here, 15537, contains ~13.0 wt.% MgO and is the most primitive Apollo 15 low-silica ONB described yet. The two small subsamples analyzed here have compositions that are nearly identical, despite the fact that these

subsamples were taken from different parts of the parent rock (see methods). As noted here and by *Ryder (1985)*, olivine in 15537 occurs as small chadacrysts in pyroxene, not as phenocrysts (Fig. 1b). Thus, it seems unlikely that the high MgO in these analyses is due to excess (nonrepresentative) olivine in the subsamples. This is supported by the observation that 15537 is not deficient in incompatible elements.

Least square mixing calculations using 15537 as the parent magma indicate that about 12% olivine fractionation is needed to model the most evolved sample analyzed here (15598); about 17% olivine fractionation is needed to model the most evolved Apollo 15 ONB analyzed previously (15085). These results are consistent with previous suggestions of <15% olivine fractionation (*Rhodes and Hubbard, 1973; Chappell and Green, 1973; Helmke et al., 1973*) when the more primitive nature of 15537 is considered.

Causes of Chemical Heterogeneity

The dispersion of chemical data in replicate analyses can be attributed to two basic causes: analytical error and nonrepresentative sampling. Deviations that exceed the expected analytical uncertainty may be due to sampling problems or to nonsystematic errors (e.g., human errors). Sampling problems can be reduced by analyzing samples that

are large enough to contain representative proportions of the constituent mineral phases, but this may be impractical in many situations.

The mare basalts studied here vary from very fine to medium or coarse in grain size, and from intergranular or subophitic to poikilitic-granular in texture. One of the fine-grained, olivine-phyric samples, 15598, shows significant variations in the compatible elements Mg, Cr, and Co, suggesting that the olivine phenocrysts (and chromite inclusions within them) were not sampled representatively. Chemical variations created by the nonrepresentative sampling of olivine are common even in large samples of terrestrial rocks. However, in samples that are saturated with olivine-only (such as the Apollo 15 ONB suite), the addition or subtraction of olivine does not remove the rock from its normal liquid line of descent—it merely moves the rock toward or away from more primitive compositions.

One result that is somewhat surprising is that the small subsamples of the medium-grained basalts are consistently within the compositional range of Apollo 15 ONBs defined by larger samples (Figs. 5 and 6). Compositional differences between subsample pairs may exceed the analytical uncertainty of the major elements somewhat (generally by a factor of less than two), but credible fractionation trends can be drawn through the data, which tend to form linear arrays trending away from olivine. Differences between the subsample pairs and corresponding large samples show that caution must be exercised against trying to squeeze too much from the data (e.g., *Binder, 1976*).

Subsample pairs of the coarse-grained basalts 15547 and 15636 differ dramatically in both their major element and trace element concentrations. The differences exceed the expected analytical uncertainty significantly and result in subsamples that do not plot with other Apollo 15 ONBs. These samples are characterized by the heterogeneous distribution of late-forming mesostasis phases such as fayalite and ilmenite, and one sample (15636) is also heterogeneous with respect to plagioclase and pyroxene. The mesostasis phases (fayalite, ilmenite, glass, cristobalite, ulvospinel, and whitlockite) tend to occur together in the interstices between mafic phases (generally pigeonite) where these interstices are not already filled by plagioclase (which crystallizes before the mesostasis phases). This competition between the mesostasis phases and plagioclase for the interstitial areas between the early forming mafic silicates is graphically illustrated by the scarcity of mesostasis phases in the plagioclase-rich zones of samples like 15538.

The mesostasis phases contain much of the Fe (fayalite, ilmenite) and almost all of the TiO_2 , Ta, and Hf (ilmenite, ulvospinel), P_2O_5 and REE (whitlockite), and U and Th (glass) found in these samples. This results in the positive correlation between FeO and TiO_2 , P_2O_5 , and La observed (Fig. 7). The trend of the data in Fig. 7 is at a high angle to possible olivine control lines and cannot be due to olivine subtraction or addition. Many of these phases are also low in SiO_2 (fayalite, ilmenite, spinel, whitlockite), resulting in a negative correlation between these elements and SiO_2 . Apparently the silica-rich glass and cristobalite are not abundant enough in these clots to cause silica enrichment.

The importance of mesostasis phase distribution is illustrated by the medium-grained basalts that have subsample pairs that are essentially identical to one another. These samples are characterized by small mesostasis clots that are more or less

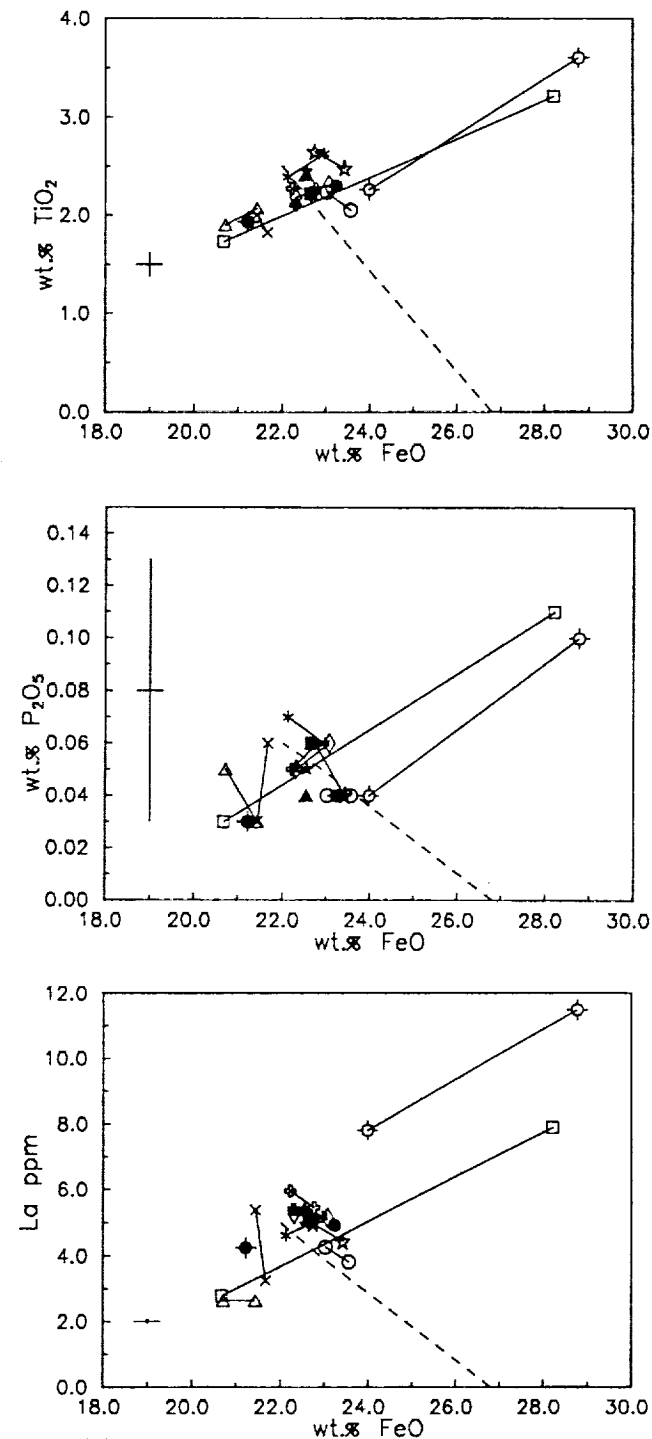


Fig. 7. FeO variation diagrams for TiO_2 , P_2O_5 , and La. Symbols and conventions same as Fig. 5. Note the strong positive correlation between these elements and FeO.

evenly distributed throughout the sample. The variation seen between some of these subsample pairs is not much larger than that observed by *Schuraytz and Ryder* (1988) between 4- or 5-g subsamples of 15555 and 15556. These samples can be used to model the geochemical evolution of the ONB suite despite the small size of the subsamples analyzed, as long as due consideration is given to the effects of analytical uncertainty on the results.

Haskin and Korotev (1977) were the first to document the effect of mesostasis distribution on bulk analyses of small mare basalt fragments. They found that small, 5- to 7-mg subsamples of basalt 70135 may differ by a factor of 20 or more in incompatible trace element concentrations, especially the REE, Ta, and Hf (*Haskin and Korotev*, 1977). They also found that separate subsamples of this basalt weighing 0.25 to 1.4 g may have trace element concentrations that vary by up to a factor of four—enough to significantly effect any trace element models based on these analyses (*Haskin and Korotev*, 1977). *Haskin and Korotev* attribute these chemical variations to differences in the proportions of mesostasis phases (primarily glass and ilmenite) present in each subsample.

These results are consistent with the so-called “short-range unmixing” model of *Lindstrom and Haskin* (1978, 1981). They proposed that chemical variations observed between hand samples from a single lava flow of Icelandic basalt, and within different suites of lunar mare basalt, could be explained by nonuniform distribution of the primary mineral phases and an incompatible-element-rich mesostasis. They show that nonrepresentative samples may be characterized by combina-

tions of minerals and mesostasis that are not petrologically likely (e.g., olivine plus glass) and that the mesostasis could separate from the other phases at any stage during crystallization. *Lindstrom and Haskin* (1978, 1981) note that much of the incompatible element variation between samples from a single flow can be attributed to the nonuniform distribution of the mesostasis (*Lindstrom and Haskin*, 1981). Our results support this conclusion for mare basalt samples, where distribution of the mesostasis in small subsamples appears to be even more important than in terrestrial rocks.

Application to Breccia Clast Studies

One goal of this study is to evaluate the reliability of the small subsamples normally used in breccia clast studies. The primary limitation in these studies is imposed by the size of the clast, not the Lunar and Planetary Sample Team. Breccia clast samples allocated for chemical analysis are commonly in the 100-mg range, and in some cases even smaller. Despite the problems inherent in analyzing small samples, the wide array of potential samples not available in the large sample suite make these studies necessary and even desirable.

Vetter et al. (1988) investigated 25 mare basalt clasts extracted from lunar breccia 15498. Eleven of these clasts proved to be olivine normative, but three are chemically distinct from all previously studied ONB suite samples. These three clasts, which constitute the “high silica ONB” group of *Vetter et al.* (1988), are lower than normal ONBs in TiO_2 and FeO , and higher in SiO_2 (Fig. 8). *Vetter et al.* (1988) noted that these three clasts closely resemble basalts of the QNB suite, but are olivine normative because of their high MgO concentrations. They propose that the high-silica ONB clasts in 15498 represent primitive magmas that were parental to basalts of the QNB suite. This view is supported by a single large sample, 15065, which is grouped with the QNB suite even though it is slightly olivine-normative (*Rhodes and Hubbard*, 1973).

Another possible explanation for the high-silica ONBs is that they are nonrepresentative samples of normal ONB suite basalt. In this scenario, the high-silica ONBs are interpreted as spurious samples which result from the analysis of small subsamples of coarse-grained, heterogeneous, low-silica ONBs. The samples analyzed by *Vetter et al.* (1988) weighed only 100-150 mg, which is common for breccia clast studies but much smaller than the 4 to 5 g preferred for normal hand specimens (e.g., *Schuraytz and Ryder*, 1988).

Our results reported here can be used to test this hypothesis. The high-silica ONBs are medium-grained basalts similar to several of those studied here, and the subsamples analyzed by *Vetter et al.* (1988) were the same size as ours. Several lines of evidence support the conclusion of *Vetter et al.* that the high-silica ONBs do represent a distinct rock type that is not related to the low-silica ONB suite.

1. The most deviant samples of ONB studied here (15547, 15636) are characterized by the concentration of mesostasis-enriched areas in the subsample analyzed. This concentration of the mesostasis clots results in subsamples that are higher in FeO , TiO_2 , and the incompatible trace elements such as La,

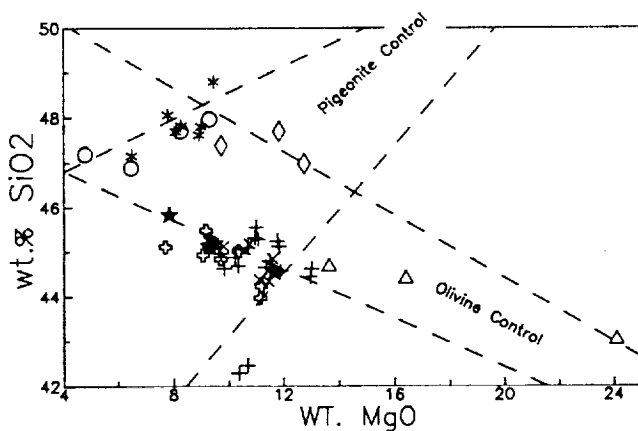


Fig. 8. MgO vs. SiO_2 plot for Apollo 15 mare basalts. Stars = low-silica ONB clasts in breccia 15498 (*Vetter et al.*, 1988); open crosses = low-silica ONBs (*Rhodes and Hubbard*, 1973); pluses = low-silica ONBs studied here (small subsamples); crosses = large subsamples of low-silica ONBs produced by *Schuraytz and Ryder* (1988), data from Table 2; open circles = QNB clasts in breccia 15498 (*Vetter et al.*, 1988); asterices = large QNB samples (*Rhodes and Hubbard*, 1973); diamonds = high-silica ONB clasts in breccia 15498 (*Vetter et al.*, 1988); triangles = olivine-pyroxene cumulate clasts in breccia 15498 (*Vetter et al.*, 1988). Dashed lines represent possible olivine control lines or pigeonite control lines based on high-Mg olivine and pigeonite phenocryst compositions.

Yb, and Hf, and lower in CaO, Al₂O₃, MgO, and SiO₂. The high-silica ONBs are lower in FeO and TiO₂ than the low-silica ONBs, suggesting a depletion in mesostasis, but have incompatible element concentrations that are similar to both the low-silica ONB suite and the QNB suite. Unlike the most deviant samples studied here, the high-silica ONBs have major and trace element concentrations that fall on smooth trends with other Apollo 15 mare basalts; they are not depleted in incompatible elements as would be expected if they formed by subtraction of mesostasis clots from the bulk rock.

2. The deviant ONB samples studied here are characterized by heterogeneous distribution of mesostasis-rich clots containing fayalite, ilmenite, cristobalite, glass, and whitlockite. The high-silica ONBs do not contain any fayalitic olivine, glass, or whitlockite. Ilmenite and cristobalite do occur, but they are evenly distributed through the sections and do not form large mesostasis clots.

3. One olivine-phyric ONB studied here (15598) exhibits variations in Mg, Co, and Cr that suggest that olivine may be heterogeneously distributed. Although the high-silica ONB samples studied by Vetter *et al.* (1988) may be enriched or depleted in olivine, this will not move the samples off of their normal liquid line of descent because olivine is the primary liquidus phase in both the ONB suite and primitive members of the QNB suite.

4. A cursory examination of Fig. 8 suggests that enrichment of a low-silica ONB in pigeonite could create a high-silica ONB. This suggestion is wrong for several reasons. First, thin sections of high-silica ONB samples are not noticeably enriched in pigeonite. Second, sufficient enrichment of a low-silica ONB with pigeonite would lower the incompatible element concentration of the rock significantly; this is not observed. Third, pigeonite enrichment would also enrich Sc; this is not observed. Fourth, least squares mixing models are not consistent with this explanation for the other chemical elements not shown on Fig. 8.

5. Short-range unmixing calculations (Vetter *et al.*, 1988) show that compositional ranges within 15498 basalt suites cannot be due to short-range unmixing, but must represent fractional crystallization of the liquidus phases. Differences between suites require at least two separate parent magmas (Vetter *et al.*, 1988).

In summary, our data on small subsamples of mare basalt suggest that certain systematic variations can be expected if these subsamples deviate from the bulk composition of their parent rock because of nonrepresentative sampling. The high-silica ONBs of Vetter *et al.* (1988) exhibit variations from the normal, low-silica ONB group that are *not* consistent with those caused by nonrepresentative sampling. This supports the conclusion of Vetter *et al.* (1988) that the high-silica ONB group is a distinct rock type that is not related to the normal, low-silica Apollo 15 ONB suite.

CONCLUSIONS

The nine samples studied here are all normal low-silica olivine normative basalts similar to other Apollo 15 ONBs described previously (Rhodes and Hubbard, 1973; Mason *et al.*, 1972; Chappell and Green, 1973; Helmke *et al.*, 1973).

One sample analyzed for this investigation (15537) is primitive in composition and may represent the ONB parent magma; other samples studied here can be related to it by up to 12% olivine fractionation. There is no evidence to suggest more than one low-silica ONB magma series.

Small subsamples of Apollo 15 ONBs may approximate the bulk rock if the late mesostasis phases are evenly distributed throughout the sample and do not form large clots that can be fractionated into or from the subsample during sampling. Where this does occur, systematic enrichment or depletion of the subsample in FeO, TiO₂, and the incompatible trace elements can result. Enrichment may also deplete the sample in SiO₂, Al₂O₃, and CaO; depletion will have the opposite effect. These trends are consistent with the short-range unmixing model of Lindstrom and Haskin (1978, 1981).

These results can be applied to breccia clast studies to show that a new group of high-silica ONBs described by Vetter *et al.* (1988) from breccia 15498 are a distinct rock type that is not related to the low-silica ONBs normally found at the Apollo 15 site. The high-silica ONBs have trace element concentrations that are in the range of Apollo 15 mare basalts, and so cannot represent low-silica ONBs that have been depleted in mesostasis-rich areas by the sampling process.

Acknowledgments. This work was supported by NASA's Planetary Materials and Geochemistry program through grant NAG9-169 to J. W. Shervais and RTOP 152-13-40-21 to M. M. Lindstrom. Curatorial work by C. Galindo of the JSC-LESC curatorial staff is greatly appreciated. This paper in its various incarnations was improved substantially by thorough reviews from R. Korotev, B. Schuraytz, D. Lindstrom, S. Hughes, and J. Jones.

REFERENCES

- ALGIT (Apollo Lunar Geology Investigation Team) (1972) Geological setting of the Apollo 15 samples. *Science*, 175, 407-415.
- Binder A. B. (1976) On the compositions and characteristics of the mare basalt magmas and their source regions. *The Moon*, 16, 115-150.
- Brown R. W. (1977) A sample fusion technique for whole rock analysis with the electron microprobe. *Geochim. Cosmochim. Acta*, 41, 435-438.
- Chappell B. W. and Green D. H. (1973) Chemical composition and petrogenetic relationships in the Apollo 15 mare basalts. *Earth Planet. Sci. Lett.*, 18, 237-246.
- Clanton U. S. and Fletcher C. R. (1976) Sample size and sampling errors as the source of dispersion in chemical analyses. *Proc. Lunar Sci. Conf. 7th*, pp. 1413-1428.
- Compston W., de Laeter J. R., and Veron M. J. (1972) Strontium isotope geology of Apollo 15 basalts. In *The Apollo 15 Lunar Samples* (J. W. Chamberlain and C. Watkins, eds), pp. 347-351. The Lunar Science Institute, Houston.
- Dickinson T., Taylor G. J., Keil K., Schmitt R. A., Hughes S. S., and Smith M. R. (1985) Apollo 14 aluminous mare basalts and their possible relationship to KREEP. *Proc. Lunar Planet. Sci. Conf. 15th*, in *J. Geophys. Res.*, 90, C365-C374.
- Dowty E., Prinz M., and Keil K. (1973) Composition, mineralogy, and petrology of 28 mare basalts from Apollo 15 rake samples. *Proc. Lunar Sci. Conf. 4th*, pp. 423-444.
- Fruchter J. S., Stoesser J. W., Lindstrom M. M., and Goles G. G. (1973) Apollo 15 clastic materials and their relationship to geological features. *Proc. Lunar Sci. Conf. 4th*, pp. 1227-1237.

Haskin L. A. and Korotev R. L. (1977) Test of a model for trace element partition during closed system solidification of a silicate liquid. *Geochim. Cosmochim. Acta*, 41, 921-939.

Helmke P. A., Blanchard D. P., Haskin L. A., Telander K., Weiss C., and Jacobs J. W. (1973) Major and trace elements in igneous rocks from Apollo 15. *The Moon*, 8, 129-148.

Lindstrom M. M. and Haskin L. A. (1978) Causes of compositional variations within mare basalt suites. *Proc. Lunar Planet. Sci. Conf. 9th*, pp. 465-486.

Lindstrom M. M. and Haskin L. A. (1981) Compositional inhomogeneities in a single Icelandic tholeiite flow. *Geochim. Cosmochim. Acta*, 45, 15-31.

Lindstrom M. M., Marvin U. B., and Mittlefehldt, D. W. (1989) Apollo 15 Mg and Fe norites: a redefinition of the Mg-suite differentiation trend. *Proc. Lunar Planet. Sci. Conf. 19th*, pp. 245-254.

Ma M.-S., Schmitt R. A., Warner R. D., Taylor G. J., and Keil K. (1978) Genesis of Apollo 15 olivine normative basalts: Trace element correlations. *Proc. Lunar Sci. Conf. 7th*, pp. 523-533.

Mason B., Jarosewich E., Melson W. G., and Thompson G. (1972) Mineralogy, petrology, and chemical composition of lunar samples 15085, 15256, 15271, 15471, 15475, 15476, 15535, and 15556. *Proc. Lunar Sci. Conf. 3rd*, pp. 785-796.

Neal C. R., Taylor, L. A., and Lindstrom, M. M. (1988a) Importance of lunar granite and KREEP in VHK basalt petrogenesis. *Proc. Lunar Planet. Sci. Conf. 18th*, pp. 121-137.

Neal C. R., Taylor L. A., and Lindstrom M. M. (1988b) Apollo 14 Mare Petrogenesis: Assimilation of KREEP-like components by a fractioning magma. *Proc. Lunar Planet. Sci. Conf. 18th*, pp. 139-153.

Rhodes J. M. and Hubbard N. J. (1973) Chemistry, classification, and petrogenesis of Apollo 15 mare basalts. *Proc. Lunar Sci. Conf. 4th*, pp. 1127-1148.

Ryder G. (1985) Catalog of Apollo 15 Rocks. *Curatorial Branch Publication 72, JSC 20787*. NASA-JSC, Houston. 1296 pp.

Ryder G. (1989) Mare basalts of the Apennine Front and the mare stratigraphy of the Apollo 15 site. *Proc. Lunar Planet. Sci. Conf. 19th*, pp. 43-50.

Ryder G. and Steele A. (1988) Chemical dispersion among Apollo 15 olivine- normative basalts. *Proc. Lunar Planet. Sci. Conf. 18th*, pp. 273-282.

Schuraytz B. and Ryder G. (1988) New petrochemical data base of Apollo 15 olivine normative mare basalts (abstract). In *Lunar and Planetary Science XIX*, pp. 1041-1042. Lunar and Planetary Institute, Houston.

Shervais J. W., Taylor L. A., and Lindstrom M. M. (1985a) Apollo 14 mare basalts: Petrology and geochemistry of clasts from consortium breccia 14321. *Proc. Lunar Planet. Sci. Conf. 15th*, in *J. Geophys. Res.*, 90, C375-C395.

Shervais J. W., Taylor L. A., Iaul J. C., Shih C.-Y., and Nyquist L. E. (1985b) Very high potassium (VHK) basalt: Complications in mare basalt petrogenesis. *Proc. Lunar Planet. Sci. Conf. 16th*, in *J. Geophys. Res.*, 90, D3-D18.

Vetter S. K., Shervais J. W., and Lindstrom M. M. (1988) Petrology and geochemistry of olivine-normative and quartz-normative basalts from regolith breccia 15498: new diversity in Apollo 15 mare basalts. *Proc. Lunar Planet. Sci. Conf. 18th*, pp. 255-271.

Warren P. H. (1988) The origin of pristine KREEP: effects of mixing between urKREEP and the magmas parental to the Mg-rich cumulates. *Proc. Lunar Planet. Sci. Conf. 18th*, pp. 233-241.

Warren P. H., Taylor G. J., Keil K., Kallemeyn G. W., Shirley D. S., and Wasson J. T. (1983) Seventh foray: whitlockite-rich lithologies, a diopside-bearing troctolitic anorthosite, ferroan anorthosites, and KREEP. *Proc. Lunar Planet. Sci. Conf. 14th*, in *J. Geophys. Res.*, 88, B151-B164.

APPENDIX 1. Representative olivine compositions for Apollo 15 mare basalts.

	15536		15538		15537		15546		15547						
			Avg.			Avg.		Avg.			Avg.				
SiO ₂	37.7	31.7	38.2	35.8	34.3	36.3	37.3	33.3	35.7	37.2	29.9	34.0	35.2	32.8	34.3
FeO	26.80	59.06	30.76	35.66	43.60	38.03	29.24	49.90	36.63	31.39	66.47	46.62	36.82	49.37	42.56
MnO	0.25	0.58	0.32	0.39	0.47	0.41	0.30	0.37	0.36	0.32	0.74	0.45	0.35	0.50	0.42
MgO	35.31	8.65	29.20	27.95	21.35	24.58	33.38	16.90	27.32	31.44	2.35	17.96	26.87	15.91	22.11
CaO	0.28	0.52	1.58	0.32	0.27	0.74	0.21	0.39	0.31	0.21	0.50	0.67	0.35	0.38	0.33
Cr ₂ O ₃	0.22	0.03	0.28	0.09	0.16	0.19	0.21	0.08	0.17	0.14	0.00	0.54	0.22	0.06	0.13
Total	100.59	100.65	100.75	100.29	100.22	100.40	100.68	101.03	100.56	100.75	100.27	100.43	99.83	99.12	99.94
Si	0.996	0.998	1.027	0.994	0.995	1.014	0.997	0.990	0.994	1.003	0.994	1.001	0.989	0.997	0.994
Fe	0.593	1.557	0.704	0.829	1.058	0.896	0.654	1.241	0.857	0.708	1.845	1.170	0.866	1.254	1.033
Mn	0.006	0.015	0.007	0.009	0.012	0.010	0.007	0.009	0.009	0.007	0.021	0.012	0.008	0.013	0.010
Mg	1.392	0.407	1.166	1.157	0.923	1.029	1.331	0.749	1.129	1.265	0.116	0.768	1.127	0.721	0.952
Ca	0.008	0.017	0.044	0.010	0.009	0.021	0.006	0.012	0.009	0.006	0.018	0.021	0.011	0.012	0.010
Cr	0.005	0.001	0.006	0.002	0.004	0.004	0.004	0.002	0.004	0.003	0.000	0.012	0.005	0.001	0.003
Sum	3.001	3.000	2.964	3.003	3.002	2.980	3.001	3.007	3.004	2.995	3.002	2.990	3.007	3.001	3.004
Fo	69.94	20.54	61.59	58.01	46.33	53.36	66.82	37.46	56.62	63.86	5.87	39.67	56.30	36.25	47.71
Fa	30.06	79.46	38.41	42.00	53.67	46.64	33.18	62.54	43.38	36.14	94.13	60.33	43.70	63.75	52.29

APPENDIX 1. (continued).

	15548		15598			15605			15636			
						Avg.						Avg.
SiO ₂	37.2	33.9	35.8	36.6	34.6	37.0	35.1	31.7	34.3	35.8	30.7	34.5
FeO	29.89	46.13	35.36	33.64	43.62	37.31	38.68	55.54	44.17	35.91	61.77	42.73
MnO	0.25	0.35	0.34	0.33	0.47	0.37	0.37	0.54	0.43	0.32	0.60	0.44
MgO	32.84	19.37	28.14	29.67	21.60	24.84	25.49	12.09	21.29	27.39	6.48	22.42
CaO	0.27	0.29	0.28	0.26	0.34	0.84	0.29	0.32	0.34	0.28	0.46	0.37
Cr ₂ O ₃	0.15	0.09	0.14	0.18	0.12	0.17	0.19	0.04	0.13	0.82	0.01	0.18
Total	100.67	100.30	100.10	100.52	100.82	100.79	100.22	100.38	100.71	100.64	100.17	100.76
Si	0.999	0.996	0.995	0.996	0.997	1.025	0.993	0.984	0.992	0.993	0.991	0.992
Fe	0.670	1.133	0.825	0.771	1.051	0.872	0.914	1.441	1.073	0.833	1.667	1.034
Mn	0.006	0.009	0.008	0.008	0.011	0.009	0.009	0.014	0.011	0.007	0.017	0.011
Mg	1.313	0.848	1.163	1.212	0.927	1.030	1.074	0.559	0.915	1.133	0.312	0.951
Ca	0.008	0.009	0.008	0.008	0.011	0.024	0.009	0.010	0.010	0.008	0.016	0.011
Cr	0.003	0.002	0.003	0.004	0.003	0.004	0.004	0.001	0.003	0.018	0.000	0.004
Sum	2.999	3.000	3.003	3.001	3.001	2.970	3.005	3.015	3.006	2.996	3.006	3.005
Fo	66.00	42.62	58.26	60.88	46.61	53.84	53.77	27.76	45.77	57.40	15.62	47.66
Fa	34.00	57.38	41.74	39.12	53.39	46.16	46.23	72.24	54.23	42.60	84.38	52.34

APPENDIX 2. Representative pyroxene compositions for Apollo 15 mare basalts.

	15536		15537			15538			15546			15547			
SiO ₂	52.5	51.2	47.6	51.9	49.9	49.0	51.8	50.2	50.5	52.4	51.6	48.3	53.6	50.9	47.3
TiO ₂	0.52	0.83	1.33	0.34	1.07	1.15	0.45	0.92	0.94	0.45	0.62	0.83	0.27	0.92	1.10
Al ₂ O ₃	1.32	2.39	1.62	1.08	3.38	1.62	0.94	2.44	2.26	1.31	1.87	0.84	0.73	2.79	1.32
FeO	19.13	14.35	29.43	19.61	13.63	24.93	21.95	16.91	17.23	18.38	17.02	31.46	18.99	12.40	32.77
MnO	0.25	0.27	0.51	0.28	0.22	0.38	0.43	0.39	0.34	0.35	0.33	0.42	0.26	0.30	0.46
MgO	20.90	15.88	5.10	20.71	15.02	10.39	18.85	16.37	16.60	20.39	18.20	7.47	21.42	15.05	5.98
CaO	5.10	14.50	14.36	4.94	15.15	11.42	5.42	11.54	10.89	5.61	9.19	9.72	4.22	16.08	10.32
Na ₂ O	0.02	0.07	0.06	0.00	0.04	0.04	0.02	0.02	0.04	0.03	0.03	0.04	0.05	0.04	0.03
Cr ₂ O ₃	0.78	0.86	0.17	0.51	0.88	0.27	0.38	0.82	0.74	0.76	0.85	0.11	0.43	1.05	0.14
Total	100.50	100.32	100.20	99.39	99.29	99.17	100.25	99.57	99.55	99.72	99.75	99.23	100.02	99.51	99.38
Si	1.945	1.914	1.926	1.951	1.886	1.936	1.954	1.902	1.913	1.956	1.936	1.962	1.985	1.912	1.936
Ti	0.015	0.023	0.040	0.010	0.031	0.034	0.013	0.026	0.027	0.013	0.017	0.025	0.008	0.026	0.034
Al	0.058	0.106	0.077	0.048	0.151	0.075	0.042	0.109	0.101	0.057	0.082	0.040	0.032	0.124	0.064
Fe	0.593	0.449	0.995	0.616	0.431	0.824	0.692	0.536	0.545	0.573	0.534	1.068	0.588	0.390	1.122
Mn	0.008	0.008	0.017	0.009	0.007	0.013	0.014	0.013	0.011	0.011	0.010	0.014	0.008	0.010	0.016
Mg	1.155	0.886	0.307	1.160	0.847	0.612	1.060	0.925	0.937	1.134	1.017	0.452	1.182	0.843	0.365
Ca	0.203	0.582	0.622	0.199	0.614	0.484	0.219	0.469	0.442	0.224	0.369	0.423	0.167	0.647	0.453
Na	0.002	0.005	0.004	0.000	0.003	0.003	0.001	0.001	0.003	0.002	0.002	0.003	0.004	0.003	0.002
Cr	0.023	0.025	0.006	0.015	0.026	0.008	0.011	0.024	0.022	0.022	0.025	0.004	0.013	0.031	0.005
Sum	4.000	3.999	3.995	4.008	3.996	3.989	4.007	4.005	4.000	3.992	3.993	3.992	3.987	3.986	3.997
Fe/ Fe+Mg	34.2	34.0	76.7	35.0	34.1	57.8	40.0	37.2	37.3	34.0	34.8	70.5	33.5	32.1	75.7
Wo	10.3	30.2	32.0	10.0	32.3	25.0	11.0	24.1	22.8	11.5	19.1	21.6	8.6	34.3	23.2
En	59.0	46.0	15.8	58.5	44.6	31.7	53.4	47.6	48.4	58.4	52.7	23.1	60.7	44.6	18.7
Fs	30.7	23.8	52.1	31.5	23.1	43.3	35.6	28.3	28.8	30.1	28.2	55.3	30.6	21.1	58.2

APPENDIX 2. (continued).

	15548		15598		15605		15636					
SiO ₂	52.6	50.4	48.2	52.4	51.2	47.7	52.8	50.4	47.9	52.9	51.6	48.6
TiO ₂	0.43	0.88	0.79	0.41	0.78	0.94	0.41	0.87	0.85	0.40	0.80	1.12
Al ₂ O ₃	1.29	2.50	0.87	1.19	2.33	1.20	1.08	2.64	0.81	1.04	2.20	1.38
FeO	20.33	16.81	33.23	19.96	17.18	36.29	20.36	16.41	32.07	19.09	15.33	31.03
MnO	0.39	0.30	0.40	0.39	0.33	0.43	0.34	0.28	0.41	0.31	0.29	0.40
MgO	19.69	17.00	7.12	20.51	16.71	7.44	19.91	15.91	5.19	20.70	16.94	7.89
CaO	5.09	10.31	9.37	5.07	10.81	5.99	5.18	12.33	11.88	5.22	12.33	10.29
Na ₂ O	0.00	0.07	0.02	0.00	0.03	0.02	0.04	0.05	0.04	0.03	0.02	0.02
Cr ₂ O ₃	0.66	0.91	0.07	0.51	0.85	0.17	0.41	0.74	0.19	0.56	0.82	0.20
Total	100.48	99.20	100.04	100.44	100.25	100.16	100.55	99.64	99.36	100.23	100.35	100.93
Si	1.960	1.909	1.953	1.951	1.922	1.941	1.965	1.907	1.963	1.964	1.925	1.935
Ti	0.012	0.025	0.024	0.012	0.022	0.029	0.012	0.025	0.026	0.011	0.022	0.034
Al	0.056	0.111	0.041	0.052	0.103	0.058	0.047	0.118	0.039	0.045	0.097	0.065
Fe	0.633	0.533	1.127	0.622	0.539	1.236	0.634	0.519	1.099	0.593	0.478	1.033
Mn	0.012	0.010	0.014	0.012	0.011	0.015	0.011	0.009	0.014	0.010	0.009	0.014
Mg	1.093	0.960	0.430	1.138	0.934	0.452	1.104	0.897	0.317	1.146	0.942	0.468
Ca	0.203	0.419	0.407	0.202	0.434	0.261	0.206	0.500	0.521	0.208	0.493	0.439
Na	0.000	0.006	0.001	0.000	0.002	0.002	0.003	0.004	0.003	0.002	0.001	0.002
Cr	0.020	0.027	0.002	0.015	0.025	0.005	0.012	0.022	0.006	0.016	0.024	0.006
Sum	3.990	4.000	4.001	4.004	3.992	3.999	3.994	4.000	3.989	3.995	3.993	3.996
Fe/Fe+Mg	37.1	36.1	72.6	35.8	37.0	73.5	36.8	37.1	77.8	34.5	34.1	69.1
Wo	10.5	21.8	20.6	10.2	22.6	13.3	10.6	26.0	26.7	10.6	25.6	22.5
En	56.3	50.0	21.8	57.6	48.7	23.0	56.5	46.6	16.2	58.6	49.0	24.0
Fs	33.2	28.2	57.7	32.1	28.6	63.7	33.0	27.4	57.0	30.8	25.4	53.6

APPENDIX 3. Representative plagioclase compositions for Apollo 15 mare basalts.

	15536		15537		15538		15546		15547						
			Avg.			Avg.			Avg.		Avg.			Avg.	
SiO ₂	46.5	49.6	47.7	46.4	48.4	47.7	46.0	49.0	48.3	46.4	48.8	47.3	46.6	49.5	47.7
Al ₂ O ₃	34.31	31.59	33.18	33.74	32.41	33.06	34.26	31.76	32.19	34.06	32.38	33.65	33.95	31.57	32.86
FeO	0.43	1.00	0.61	0.61	0.56	0.61	0.53	0.83	0.71	0.43	0.61	0.51	0.41	0.85	0.64
MgO	0.19	0.15	0.22	0.25	0.33	0.31	0.18	0.10	0.29	0.21	0.18	0.22	0.20	0.07	0.19
CaO	18.51	16.57	17.82	18.50	17.09	17.90	19.01	16.69	17.73	18.36	17.02	17.96	18.42	16.44	17.52
Na ₂ O	0.74	1.55	1.05	0.82	1.16	0.96	0.61	1.50	0.84	0.76	1.27	0.95	0.74	1.22	1.11
K ₂ O	0.02	0.11	0.05	0.02	0.04	0.03	0.01	0.14	0.03	0.03	0.06	0.03	0.03	0.50	0.10
Total	100.71	100.59	100.73	100.39	100.08	100.63	100.67	100.12	100.17	100.29	100.39	100.65	100.45	100.13	100.19
Si	2.125	2.261	2.180	2.134	2.217	2.179	2.112	2.247	2.212	2.132	2.228	2.161	2.138	2.266	2.190
Al	1.850	1.697	1.786	1.828	1.749	1.781	1.853	1.715	1.741	1.844	1.742	1.812	1.834	1.704	1.777
Fe	0.017	0.038	0.023	0.023	0.021	0.023	0.020	0.032	0.027	0.017	0.023	0.020	0.016	0.032	0.025
Mg	0.013	0.010	0.015	0.017	0.022	0.021	0.012	0.007	0.019	0.014	0.012	0.015	0.013	0.005	0.013
Ca	0.907	0.809	0.872	0.911	0.838	0.876	0.935	0.819	0.872	0.903	0.832	0.879	0.905	0.807	0.862
Na	0.066	0.137	0.093	0.073	0.103	0.085	0.054	0.133	0.075	0.067	0.112	0.084	0.066	0.108	0.099
K	0.001	0.006	0.003	0.001	0.003	0.002	0.001	0.008	0.002	0.001	0.003	0.002	0.002	0.029	0.006
Sum	4.981	4.960	4.973	4.989	4.958	4.971	4.988	4.964	4.952	4.980	4.957	4.975	4.976	4.951	4.972
Ab	6.8	14.4	9.6	7.4	10.9	8.9	5.5	13.9	7.8	6.9	11.9	8.7	6.8	11.5	10.2
Or	0.1	0.6	0.3	0.1	0.3	0.2	0.1	0.9	0.2	0.2	0.3	0.2	0.2	3.1	0.6
An	93.1	85.0	90.1	92.5	88.8	90.9	94.5	85.3	91.9	92.9	87.8	91.1	93.0	85.4	89.2

APPENDIX 3. (continued).

	15548		15598			15605			15636			
			Avg.			Avg.			Avg.			Avg.
SiO ₂	47.4	47.6	47.6	46.7	48.1	47.2	46.6	48.8	47.2	46.5	47.6	47.1
Al ₂ O ₃	33.16	32.12	32.81	34.17	32.70	33.65	34.02	32.14	33.38	33.76	33.51	33.49
FeO	0.69	0.87	0.78	0.56	0.60	0.61	0.51	1.11	0.67	0.48	0.64	0.53
MgO	0.30	0.28	0.26	0.17	0.36	0.23	0.20	0.07	0.20	0.25	0.20	0.25
CaO	18.13	17.50	17.85	18.27	17.61	18.14	18.41	17.08	18.06	18.33	17.72	18.13
Na ₂ O	0.95	1.04	1.01	0.83	1.06	0.94	0.70	1.07	0.91	0.78	1.11	0.94
K ₂ O	0.02	0.06	0.04	0.03	0.03	0.03	0.04	0.41	0.07	0.04	0.05	0.03
Total	100.72	99.58	100.43	100.77	100.51	100.87	100.47	100.79	100.54	100.16	100.88	100.55
Si	2.168	2.201	2.183	2.134	2.199	2.155	2.135	2.227	2.161	2.138	2.171	2.157
Al	1.787	1.749	1.772	1.841	1.761	1.811	1.838	1.730	1.803	1.831	1.801	1.807
Fe	0.027	0.034	0.030	0.021	0.023	0.023	0.019	0.043	0.026	0.019	0.024	0.020
Mg	0.020	0.019	0.018	0.012	0.025	0.015	0.013	0.005	0.014	0.017	0.013	0.017
Ca	0.888	0.866	0.877	0.895	0.862	0.887	0.905	0.836	0.887	0.904	0.866	0.890
Na	0.084	0.094	0.090	0.074	0.094	0.084	0.062	0.095	0.080	0.070	0.098	0.083
K	0.001	0.004	0.002	0.001	0.001	0.002	0.002	0.024	0.004	0.002	0.003	0.002
Sum	4.978	4.970	4.975	4.981	4.966	4.980	4.976	4.963	4.977	4.981	4.978	4.979
Ab	8.6	9.7	9.3	7.6	9.8	8.6	6.4	9.9	8.3	7.1	10.1	8.6
Or	0.1	0.4	0.2	0.2	0.2	0.2	0.2	2.5	0.4	0.2	0.3	0.2
An	91.3	89.9	90.5	92.3	90.0	91.2	93.4	87.6	91.3	92.7	89.5	91.3

Petrology and Geochemistry of Olivine-Normative and Quartz-Normative Basalts from Regolith Breccia 15498: New Diversity in Apollo 15 Mare Basalts

PREV. ANY
89 A 10868

Scott K. Vetter and John W. Shervais

Department of Geology, University of South Carolina, Columbia SC 29208

Marilyn M. Lindstrom

Planetary Materials Branch, Code SN2, NASA Johnson Space Center, Houston, TX 77058

Mare basalt clasts from regolith breccia 15498 are divided into olivine normative basalts (ONB) and quartz normative basalts (QNB), based on major element chemistry. The QNB are characterized by high SiO₂ (46.5-48%), FeO < 21%, TiO₂ of 1.6%-2.6%, and low compatible element concentrations. The QNB suite in 15498 extends to more evolved compositions than previously reported at Apollo 15, and can be divided into four groups: primitive, intermediate/1, intermediate/2, and evolved. Variations within each group can be explained by short-range unmixing of the modal components; variations between groups result from fractional crystallization of olivine (early), pigeonite, and augite (late). The ONB suite in 15498 is divided into three subgroups, based on variations in SiO₂, MgO, and TiO₂: (1) low-SiO₂ ONB, (2) high-SiO₂ ONB, and (3) olivine-pyroxene cumulates. The low-SiO₂ ONB are geochemically identical to the ONB suite described by earlier studies. They are characterized by low SiO₂ (44-46%), high FeO (20-23%), and TiO₂ of 2.2-2.5%. The high-SiO₂ ONB are characterized by high SiO₂ (47-48%), high MgO (9.7-12.7%), low TiO₂ (1.65-1.9%), and low FeO (19.7-20%). The olivine-pyroxene cumulates have the highest MgO and lowest incompatible element concentrations, and one sample contains cumulus augite. Least-squares mixing models show that the more evolved QNBs can be derived from parent magmas similar to the primitive QNBs by crystal fractionation of pigeonite, olivine, and spinel. Variations within the low-SiO₂ ONBs can be explained by olivine fractionation. However, the low-SiO₂ ONBs cannot be parental to any of the QNB lavas. Similar modeling calculations show that the high-SiO₂ ONBs may be parental to the QNB suite, documenting the first link between ONBs and QNBs at the Apollo 15 site. The composition of the high-SiO₂ ONB parent magma is the identical to the hypothetical QNB suite parent postulated by *Chappell and Green* (1973).

INTRODUCTION

A primary goal of the Apollo 15 mission was to sample mare basalts from Palus Putredinis, where mare stratigraphy is exposed to depths of over 500 meters in Hadley Rille, a major lava channel. Over 76 kg of basalt were returned from several widely spaced stations. Although the walls of Hadley Rille were not sampled directly, sampling of crater ejecta near the rille provides reasonable hope that some of the stratigraphic sequence visible in the walls of the rille was sampled.

Early studies of the Apollo 15 mare basalt suite (*Rhodes*, 1972; *Rhodes and Hubbard*, 1973; *Chappell and Green*, 1973; *Helmke et al.*, 1973; *Dowty et al.*, 1973) established that two distinct groups are represented: the olivine-normative basalts (ONB) and the quartz-normative basalts (QNB). Distinctions between these groups are based on both petrography and major element geochemistry. The ONB group is characterized by low SiO₂, higher TiO₂, higher FeO, and lower Mg#s than the QNB group. The ONB group is also characterized by both normative and modal olivine. Modal olivine commonly occurs as large phenocrysts that are apparently in equilibrium with their groundmass (*Papike et al.*, 1976). The QNB lavas have higher SiO₂ and Mg#s and lower TiO₂ and FeO than the ONB, and are characterized by quartz-normative compositions. Pigeonite is the most common phenocryst phase, but relicts of partly

resorbed olivine phenocrysts may be found in the more primitive samples (always accompanied by pigeonite).

Chemical variations observed within each of these suites are attributed to near surface crystal fractionation of the liquidus phases—olivine in the ONB, pigeonite in the QNB (*Rhodes and Hubbard*, 1973; *Mason et al.*, 1972; *Chappell and Green*, 1973). This conclusion is supported both by major element mixing calculations and by the small range in trace element concentrations.

The ONB and QNB groups as defined by these early studies cannot be related to one another by low pressure crystal fractionation (*Rhodes*, 1972; *Rhodes and Hubbard*, 1973; *Chappell and Green*, 1973; *Helmke et al.*, 1973; *Dowty et al.*, 1973). The combination of high Mg#, high SiO₂, low TiO₂, and silica saturation in the QNB precludes a relationship to the ONB suite by simple removal of the liquidus minerals (olivine and pigeonite). These characteristics also preclude a similar relationship to the low-Ti mare basalts of Apollo 12.

The average isotopic age data show that the ONB suite is slightly younger than the QNB (3.2 aeons versus 3.3 aeons; *BVSP*, 1981, p. 951). *Duncan et al.* (1975) and *LSPET* (1972) determined that the dominant mare component of the Apollo 15 soils is ONB. The younger isotopic ages and regolith compositions lead to the conclusion that the ONB represents a thin flow or series of flows that stratigraphically overlie the

QNB flow. The number of QNB flows and thus possible number of parent magmas, however, remains ambiguous. Comparison of textural variations in the QNB suite with experimental crystallization studies (*Lofgren et al., 1975*) suggests that all of these samples may be derived from a single flow two to three meters thick. This conclusion is supported by the small range in major element compositions. However, *Helmke et al. (1973)* cite variations in REE concentrations and Sm/Eu ratio to suggest two or three parent magmas. Further progress on the origin of this important basalt group has been thwarted, however, by the small number of samples available for study.

Several of the regolith breccias returned by the Apollo 15 mission contain abundant clasts of mare basalt that can be used to expand our knowledge of the range of basalt types present and their petrogenesis. The clasts in these breccias were essentially overlooked during the first selection and analysis of Apollo 15 samples in the early 1970's. Recent studies have shown that these breccia clasts can dramatically increase our database at a particular site and yield significant new insights into the origin of mare basalts (e.g., *Taylor et al., 1983; Sbervais et al., 1985a,b; Neal et al., 1987*).

This report presents results of a consortium investigation of 25 mare basalt clasts from a new slab (.141) and existing chips of lunar breccia 15498. Our data show that the olivine-normative basalts at Apollo 15 can be subdivided into three groups: (1) a low-silica group identical to the ONB suite characterized by earlier studies; (2) a high-silica group that is parental to the quartz-normative basalts, and (3) olivine-pyroxene cumulates that may be related to the evolved QNBs. Our data also show that the QNB suite extends to more evolved compositions than were previously recognized. Major element fractionation models for the combined QNB/high-SiO₂ ONB groups show that they can be related by early olivine fractionation, followed by pigeonite and then augite fractionation. The low-SiO₂ ONB group cannot be related to either of the other groups by low pressure fractionation, as shown by major element models and trace element data.

GEOLOGIC SETTING

The Apollo 15 lunar module landed in Palus Putredinis, a small outlier of mare basalt in the lunar highlands located on the SE margin of the Imbrium Basin. This site offered several important mission objectives, among them the opportunity to observe *in situ* mare basalt stratigraphy in the walls of Hadley Rille. Panoramic photographs of the western wall of the Rille, coupled with astronaut descriptions, show that at least three flows are present in the upper 60 m of the mare across from Stations 9 and 10.

The uppermost flow forms dark hackly outcrops ~6 m thick immediately below the regolith. Based on the high proportion of olivine-normative basalt in the regolith, this flow is commonly interpreted to represent the ONB flow sampled at several locations (*ALGIT, 1972*). Below this flow, and separated from it by a short covered interval, is a massive outcrop, 15-20 m thick, of light-colored basalt. This may represent a single flow since no internal layering is apparent, and because talus blocks thought to derive from it are more than 10 m across.

The lowest exposed "flow" is a layered outcrop 8 to 16 m thick that contains at least 12 distinct layers 1-3 meters thick. These may represent separate flows or flow units, or merely fracture surfaces within a single flow. The lower and middle units may comprise the QNB suite samples that dominate the mare basalt suite at this site (*ALGIT, 1972*).



Fig. 1. View of the new 15498 slab (.141) with representative clasts.

Regolith breccia 15498 was collected on the south rim of Dune Crater (Station 4), approximately 1 km north of the Apennine Front, near boulder samples 15485, 15486, and 15499. Weighing 2.34 kg, 15498 is one of the largest regolith breccias returned by the Apollo 15 mission. Sample 15498 is a coherent glassy-matrix regolith breccia consisting of approximately 16% clasts in a matrix of glass and finely comminuted minerals (Fig. 1). The majority of clasts are mare basalts, although some highland clasts can be observed. Little previous data exist on this breccia, aside from random analyses of matrix material and one clast (*Wänke et al., 1977; Laul and Schmitt, 1973*).

Dune Crater may sample bedrock to a depth of 90 m (*ALGIT, 1972*), making Station 4 an ideal setting to sample and analyze deeper flows. Stratigraphic layering was observed in the walls of Hadley Rille across from Station 9, but could not be sampled there. The hope is that Dune crater penetrated far enough into the mare to sample several of these elusive flows.

METHODS

A new slab of regolith breccia 15498 (.141) was mapped during a visit to the pristine sample lab at JSC to determine the distribution and textural variations of the clasts. Clasts were selected from this slab and existing chips to include the complete textural range observed. The genealogy of each clast is listed in Table 1, which documents the corresponding whole rock and probe mount numbers with the clast # used in this report.

The clasts range from 0.5-3 cm in diameter. Approximately 100-150 mg of matrix-free material was extracted from each clast for whole rock analysis. This sample was ground and

TABLE 1. Genealogy of 15498 basaltic clasts.

Type Clast #	Whole rock #	Probe #	Parent #
QNB			
Primitive			
B-1	,178	,240	,141
B-2	,180	,241	,141
B-6	,190	,245	,141
B-20	,206	,249	,141
B-40	,173	,239	,24
Intermediate- 1			
B-3	,183	,242	,141
B-5	,188	,244	,141
B-11	,198	,246	,141
B-14	,204	,248*	,141
B-24	,219	,252	,141
Intermediate- 2			
B-23	,217	,218*	,141
B-44	,155	,235	,14
Evolved			
B-22	,212	,251	,141
B-45	,151	,234	,14
ONB			
Low-SiO ₂			
B-4	,186	,243	,141
B-9	,194	,195	,141
B-26	,224	,225*	,141
B-29	,228	,229*	,141
B-43	,166	,238	,19
High-SiO ₂			
B-10	,196	,197	,141
B-25	,222	,253	,141
B-41	,148	,233	,13
Cumulates			
B-12	,201	,247	,141
B-27	,226	,227*	,141
B-24	,163	,237	,19

*Indicates major elements only.

split into two aliquots for major element (10-40 mg) and trace element (100-120 mg) analyses. Additional material (\pm matrix) was extracted to make a corresponding probe mount.

All whole rock major element analyses were made on fused glass beads with a Cameca SX-50 electron microprobe at the University of South Carolina. Samples weighing 10-40 mg were crushed in an agate mortar to ensure homogeneity during melting and then fused in Mo boats on an electric strip furnace at NASA/JSC. High purity Ar at 40 psi was used as the surrounding atmosphere. The samples melted within 10-20 sec ensuring little volatilization. Operating conditions for the EMP analyses were 15 KV accelerating potential and beam current of 10 nA. A natural glass standard (VG-2, Smithsonian Institution) was used for all elements except for Cr, Mn, and Mo, for which pure metals were employed. The electron microprobe data was reduced using Cameca's online PAP routine. Twenty points were taken on each bead and averaged for the final analysis. A minor Mo correction (usually less than 0.02%) was made on all of the samples.

Mineral analyses were made at either USC or NASA/JSC. The analyses at NASA/JSC were made with a Cameca MBX EMP system using natural and synthetic mineral standards at 15 KV, 30 A. At USC the operating conditions were 15 KV accelerating potential and beam current of 15 nA. Natural mineral standards were used except for Cr and Mn, for which pure metals were used.

Instrumental neutron activation analyses (INAA) were done on 19 selected clasts at NASA/JSC (6 clasts were too small or had sufficient matrix contamination). Uncertainties based on counting statistics at the 1 sigma level are: 1%-2%—Co, Cr, Fe, Sc, Sm, Eu, La, Na; 3%-5%—Ce, Hf, Lu, Yb, Tb, Ta; 20%—Ba, Th; and 30%—Nd and Zr. Both Ir and Au occur below the detection limit of 2 ppb, supporting the textural evidence that these clasts were not formed by impact melting events.

CLASSIFICATION

All of the clasts studied are low-Ti mare basalts similar to those described from the Apollo 15 site by earlier studies (*Rhodes and Hubbard, 1973; Chappell and Green, 1973; Dowty et al., 1973*). As recognized by these earlier studies, two groups may be distinguished—one group is olivine normative, the other quartz normative. Petrographically, these samples show a wide range in textures from vitrophyric to coarse grained granular-subophitic.

Geochemically, the 15498 mare basalt suite (Table 2) has a range in FeO content (18.8-23.4 wt %) and Mg# [$100\text{Mg}/(\text{Mg}+\text{Fe}) = 29.5-68.6$] which is larger than reported previously for Apollo 15 mare basalt (*Rhodes and Hubbard, 1973; Dowty et al., 1973; Chappell and Green, 1973*). Based on the geochemical variations, we recognize three subdivisions within the ONB suite, and four subdivisions within the QNB suite:

A. OLIVINE-NORMATIVE BASALTS (ONB)

- (1) Low-SiO₂ ONB
- (2) High-SiO₂ ONB
- (3) Olivine-pyroxene cumulates

B. QUARTZ-NORMATIVE BASALTS (QNB)

- (1) Primitive QNB
- (2) Intermediate Group 1 QNB
- (3) Intermediate Group 2 QNB
- (4) Evolved QNB

Table 1 summarizes the genealogies of these clasts, and Table 3 presents thin section modes based on approximately 500 points per section.

PETROGRAPHY AND MINERAL CHEMISTRY

A. Olivine-Normative Basalts

1. *Low-SiO₂ ONB: (B-4, B-9, B-26, B-29)*. The low-SiO₂ ONBs form two distinct textural types. Fine-grained olivine-phryric basalt is represented solely by clast B-4. This clast is characterized by large subhedral olivine phenocrysts (up to

TABLE 2. Whole rock geochemistry and norm calculations of 15498; major elements by EMP, trace elements by INAA.

	Quartz-Normative Basalts (QNB)														
	Primitive					Intermediate- 1					Intermediate- 2			Evolved	
	B-1	B-2	B-40	B-20	B-6	B-24	B-43	B-5	B-3	B-14	B-11	B-23	B-44	B-22	B-45
SiO ₂	48.80	47.89	47.62	48.03	47.52	48.06	47.86	47.74	48.09	47.67	46.82	46.59	47.18	47.49	46.88
TiO ₂	1.82	2.35	1.95	1.95	2.14	2.17	2.00	2.14	1.93	1.59	2.06	2.17	2.22	2.48	2.63
Al ₂ O ₃	9.64	9.14	9.66	9.68	9.82	10.67	10.07	10.27	10.37	10.20	10.35	11.62	11.03	13.00	12.71
FeO	18.75	20.19	19.76	19.06	19.98	18.96	19.09	19.43	18.96	18.99	20.27	20.55	20.00	19.67	21.00
MnO	0.22	0.24	0.30	0.25	0.30	0.23	0.26	0.26	0.24	0.28	0.26	0.22	0.26	0.22	0.26
MgO	9.27	9.25	9.48	9.09	9.42	8.12	8.43	8.04	8.56	8.56	7.92	5.95	6.98	4.61	4.92
CaO	10.58	10.34	10.27	10.44	10.26	10.78	10.82	11.01	10.68	11.32	10.88	11.80	11.24	11.52	11.56
Na ₂ O	0.24	0.23	0.26	0.23	0.25	0.37	0.26	0.24	0.25	0.27	0.26	0.37	0.26	0.31	0.27
K ₂ O	0.04	0.04	0.04	0.04	0.05	0.04	0.04	0.02	0.04	0.05	0.04	0.03	0.05	0.04	0.05
P ₂ O ₅	0.06	0.05	0.06	0.06	0.06	0.08	0.06	0.09	0.05	0.05	0.06	0.03	0.06	0.10	0.06
Cr ₂ O ₃	0.51	0.48	0.55	0.60	0.56	0.54	0.59	0.47	0.58	0.36	0.39	0.25	0.33	0.16	0.16
Total	99.93	100.19	99.94	99.54	100.37	99.79	99.24	99.70	99.76	99.34	99.29	99.35	99.63	99.60	100.50
Mg#	46.9	45.0	46.1	46.0	45.7	43.3	44.1	42.5	44.6	44.5	41.0	34.0	38.4	29.5	29.5
Norms															
Q	2.46	1.33	0.39	2.07	0.27	2.23	2.14	2.13	2.12	0.66	0.45	0.63	1.75	4.41	2.54
Or	0.24	0.24	0.24	0.24	0.30	0.24	0.24	0.12	0.24	0.30	0.24	0.18	0.30	0.24	0.30
Ab	2.03	1.95	2.20	1.95	2.12	3.13	2.20	2.03	2.12	2.28	2.20	3.13	2.20	2.62	2.28
An	25.11	23.79	25.07	25.26	25.53	26.71	25.59	26.89	27.06	26.47	26.96	29.96	28.78	33.96	33.32
Di	22.56	22.77	21.33	21.87	20.92	22.04	23.24	22.82	21.47	24.64	22.44	24.15	22.48	19.28	20.23
Hy	43.19	44.85	46.08	43.22	46.21	40.34	41.05	40.76	42.12	41.24	42.41	36.65	39.27	33.91	36.46
Ol	0.00	0.00	0.00	0.00	0.00	0.00	0.00	0.00	0.00	0.00	0.00	0.00	0.00	0.00	0.00
Il	3.46	4.46	3.70	3.93	4.06	4.12	3.80	4.06	3.67	3.21	3.91	4.39	4.22	4.71	5.00
Ap	0.13	0.11	0.13	0.13	0.13	0.17	0.13	0.20	0.11	0.11	0.13	0.07	0.13	0.22	0.13
<i>Selected Major and Trace Elements (INAA)</i>															
Na ₂ O	0.223	0.222	0.244	0.236	0.243	0.237	0.246	0.255	0.254		0.254		0.256	0.309	0.311
FeO	19.12	20.04	19.55	18.58	19.20	19.15	19.06	18.63	18.84		18.73		19.29	19.89	19.79
Sc	48.3	46.7	42.7	41.3	41.3	43.8	43.3	44.2	43.3		41.6		43.8	39.3	37.1
Cr	3100	3100	3500	3500	3400	3500	3700	3200	3600		2700		2300	1100	1100
Co	37	47.5	42	39.2	40.6	40.8	39.6	39.3	40		37.9		36.7	36.9	37.6
Rb	20		20				9								
Sr	180	150	120				130	150	110		150		140	150	
Cs					0.24									0.21	
Ba	89	90	90	90	90	90	130	100	90		60		100	87	100
La	4.93	4.41	5.68	5.63	5.85	5.70	5.48	5.43	5.02		5.74		6.15	7.39	7.67
Ce	14.1	12.1	17.1	16.4	18.0	17.2	16.0	15.5	14.0		16.6		18.5	21.1	22.5
Nd	16	16	13	11	16	16	19	19	20		14		13	17	22
Sm	3.15	3.14	3.54	3.39	3.67	3.57	3.51	3.43	3.27		3.54		3.55	4.55	4.77
Eu	0.68	0.723	0.784	0.739	0.77	0.777	0.764	0.770	0.715		0.803		0.839	0.98	1.001
Th	0.78	0.76	0.82	0.84	0.83	0.83	0.83	0.82	0.77		0.82		0.85	0.99	1.11
Yb	2.32	2.17	2.61	2.53	2.59	2.62	2.56	2.54	2.38		2.59		2.86	3.08	3.29
Lu	0.34	0.317	0.360	0.352	0.382	0.376	0.37	0.37	0.344		0.384		0.410	0.47	0.48
Zr	130	160	150	170	165	120	100	110	140		110		100	100	200
Hf	2.20	2.33	2.54	2.37	2.67	2.41	2.54	2.45	2.33		2.50		2.71	3.09	3.36
Ta	0.36	0.36	0.41	0.34	0.39	0.35	0.36	0.38	0.32		0.32		0.40	0.45	0.47
Th	0.58	0.43	0.67	0.60	0.67	0.65	0.64	0.65	0.65		0.66		0.74	0.87	1.01

0.9 mm across) set in an aphanitic to fine-grained granular matrix of pigeonite, subcalcic augite, plagioclase, and ilmenite (Fig. 2a). Olivine phenocrysts are sparse (< 5% modally) and range in composition from Fo₆₆ to Fo₆₈ with no apparent zoning.

The other three low-SiO₂ ONB clasts have coarse ophitic textures with small plagioclase laths (up to 0.5 mm long)

totally enclosed by large (up to 1.2 mm long) blocky pyroxene crystals. Ilmenite and Cr-spinel occur both interstitially and intergrown with pyroxene. Olivine comprises up to 10% of the mode in some rocks, but is not found in all of our sections. This may be due in part to sampling problems (our probe mounts of the coarse ophitic low-SiO₂ ONBs all contain less

TABLE 2. (continued)

	Olivine-Normative Basalts (ONB)									
	Cumulates			Low-SiO ₂ ONB				High-SiO ₂ ONB		
	B-12	B-42	B-27	B-9	B-4	B-26	B-29	B-41	B-25	B-10
SiO ₂	43.07	44.44	44.71	45.14	44.54	45.83	45.19	46.98	47.70	47.39
TiO ₂	0.53	1.50	1.49	2.25	2.46	2.28	2.47	1.65	1.90	1.73
Al ₂ O ₃	4.42	7.76	8.13	9.37	7.75	8.70	7.96	8.25	8.35	9.01
FeO	19.67	20.77	20.83	20.13	23.44	21.57	23.26	19.71	19.75	20.19
MnO	0.26	0.22	0.24	0.24	0.26	0.28	0.30	0.26	0.22	0.28
MgO	24.10	16.41	13.63	9.31	11.65	7.87	9.49	12.74	11.83	9.73
CaO	6.84	7.84	8.92	10.67	9.20	11.47	9.93	8.91	9.15	10.30
Na ₂ O	0.10	0.18	0.20	0.25	0.20	0.24	0.26	0.21	0.19	0.23
K ₂ O	0.01	0.03	0.03	0.03	0.03	0.04	0.03	0.03	0.03	0.03
P ₂ O ₅	0.06	0.07	0.04	0.08	0.03	0.05	0.05	0.04	0.06	0.05
Cr ₂ O ₃	0.98	0.95	0.91	0.56	0.71	0.32	0.54	0.90	0.77	0.54
Total	100.08	100.04	99.13	99.35	100.25	98.65	99.48	99.69	100.08	99.48
Mg#	68.6	58.5	53.8	45.2	47.0	39.4	42.1	53.5	51.6	46.2
Norms										
Q	0.00	0.00	0.00	0.00	0.00	0.00	0.00	0.00	0.00	0.00
Or	0.09	0.18	0.18	0.18	0.18	0.24	0.18	0.18	0.18	0.18
Ab	0.85	1.52	1.69	2.12	1.69	2.03	2.20	1.78	1.61	1.95
An	11.57	19.92	21.20	24.60	20.11	22.54	20.44	21.48	21.84	23.46
Di	17.87	15.24	18.88	23.29	21.17	28.74	21.59	18.61	19.23	22.86
Hy	16.19	31.61	33.11	41.46	34.20	37.50	41.62	45.82	50.76	46.37
Ol	50.87	27.16	19.74	2.43	17.11	2.55	7.12	7.27	1.35	0.37
Il	1.08	2.85	3.00	4.27	4.67	4.62	5.00	3.13	3.84	3.49
Ap	0.13	0.15	0.09	0.17	0.07	0.11	0.11	0.09	0.13	0.11
<i>Selected Major and Trace Elements (INAA)</i>										
Na ₂ O	0.077	0.178		0.239	0.238			0.184	0.201	
FeO	18.19	20.5		18.3	22.84			19.19	20.05	
Sc	27.2	31.4		42.3	37.8			38.6	41.7	
Cr	6500	4600		3600	4200			6200	5000	
Co	85.2	65.4		40.3	58.9			55	53.3	
Rb	27								35	
Sr				130				120		
Cs										
Ba	75	160		110	80			78	90	
La	2.11	3.99		5.30	4.63			4.34	4.62	
Ce	7.9	12.2		15.5	13.7			11.5	14.4	
Nd	11	11		13	12			15	7	
Sm	1.25	2.49		3.29	3.43			2.67	2.94	
Eu	0.211	0.544		0.705	0.828			0.54	0.609	
Tb	0.28	0.60		0.76	0.78			0.63	0.69	
Yb	0.91	1.75		2.41	2.04			1.98	2.24	
Lu	0.15	0.266		0.358	0.292			0.286	0.332	
Zr		120		120	220			110	160	
Hf	0.86	1.73		2.36	2.49			1.96	2.04	
Ta	0.20	0.26		0.37	0.37			0.30	0.36	
Th		0.35		0.59	0.42			0.47	0.47	

than 2.5 sq. mm of basalt). The olivine in the coarse ophitic low-SiO₂ ONBs is Fo₅₅ to Fo₆₂—more Fe-rich than in B-4. Pyroxenes span a wide range of compositions, from magnesian pigeonite to subcalcic ferroaugite, but are generally more Fe-rich than pyroxene in the high-SiO₂ ONBs (Table 4, Fig. 3a). A few pyroxene grains contain thin exsolution lamellae of

another pyroxene, but these are too small to analyze. Plagioclase in all low-SiO₂ ONBs ranges from An₉₇ to An₈₅ in composition (Fig. 4a).

2. *High-SiO₂ ONB: (B-10, B-25, B-41).* The high-SiO₂ ONBs are all medium to coarse-grained, with subophitic to ophitic textures. Small plagioclase laths (up to 0.6 mm long)

TABLE 3. Modal compositions of representative mare basalt clasts from Apollo 15 breccia 15498.

	Pyroxene	Olivine	Plagioclase	Opaque	Silica	Groundmass	Other
QNB							
Primitive							
B-1	56	-	39	6	<1	-	-
B-2	55	-	41	2	<1	-	-
B-6	1	7	-	-	-	92	-
B-20	-	7	-	-	-	93	-
B-40*	-	-	-	-	-	100	-
Intermediate-1							
B-3	56	10	28	5	<1	-	<1
B-5	53	-	35	10	<1	-	-
B-11	60	-	36	3	-	-	<1
B-14	54	-	37	8	<1	-	-
B-24	64	-	26	9	1	-	-
B-43	59	-	34	7	<1	-	-
Intermediate-2							
B-23	52	-	46	3	-	-	-
B-44	56	-	35	6	3	-	-
Evolved							
B-22	54	-	35	7	4	-	5
B-45	61	-	30	6	3	-	<1
ONB							
Low-SiO ₂							
B-4	52	9	31	9	-	-	-
B-9 [†]	50	6	37	7	<1	-	-
B-26 [†]	62	-	33	5	-	-	-
B-29 [†]	62	-	33	5	-	-	-
High-SiO ₂							
B-10 [†]	50	-	32	13	-	-	-
B-25 [†]	65	-	31	4	-	-	-
B-41	68	10	18	4	-	-	2
Cumulates							
B-12	55	38	1	5	-	-	-
B-27 [†]	75	25	-	-	-	-	-
B-42	45	31	23	5	-	-	4

Groundmass = devitrified glass/fine-grained quenched textured.

Others = late-stage residual areas.

*No phenocryst in probe mount; however, pyroxene (?) phenocryst seen in hand sample.

[†]Small probe mount with matrix attached. Less than 200 points.

are partly to totally enclosed in pyroxene grains that average about 0.5 mm across. Olivine forms rounded grains up to 0.7 mm across and may include small euhedral Cr-spinels (Fig. 2b). Olivine cores are Fo₅₇ to Fo_{67.5}, rims Fo₄₅ to Fo₅₅. Pyroxene ranges from Wo₇En₆₆ to Wo₂₅En₃₄ and is generally more magnesian than pyroxene in the low-SiO₂ ONBs (Table 4, Fig. 3b). Plagioclase ranges from An₉₄ to An₈₇ and is lower in potassium than plagioclase with the same An content in the low-SiO₂ ONB suite (Fig. 4a).

A major difference in the mineralogy of the high-SiO₂ ONBs that distinguishes them from the low-SiO₂ ONBs is the presence in two clasts (B-10, B-25) of minor cristobalite as a late, interstitial phase. This indicates that the residual liquids in the high-SiO₂ ONBs evolved to silica-oversaturated compositions prior to final crystallization.

3. Olivine-pyroxene cumulates: (B-12, B-27, B-42).

These rocks are characterized by cumulus textures with primocrysts of olivine, magnesian pigeonite, Cr-spinel, and (in clast B-12) augite, surrounded by intercumulus plagioclase, ilmenite, and pyroxene (Fig. 5c,d). Postcumulate pyroxene most commonly forms by adcumulate enlargement of cumulate pyroxene grains or as mantles on cumulate olivine. Olivine and pyroxene primocrysts are generally about 1.0 mm in diameter, with blocky euhedral to subhedral outlines. Modal plagioclase is less abundant in these rocks than in the basalts (Table 3), reflecting cumulate enrichment in mafic phases.

In contrast to the basalts, the cores of the cumulus phases in the cumulate rocks exhibit restricted compositional ranges. Olivine cores range from Fo₇₁ to Fo₆₄ (Fo₇₁ to Fo₆₉ in B-12); rims are somewhat more Fe-rich in B-27 (Fo₅₈ to Fo₄₅).

TABLE 4. Representative pyroxene compositions in 15498 basalts.

	Quartz-Normative Basalts (QNB)						Olivine-Normative Basalts (ONB)						
	Evolved (B-45)		Intermediate (B-44)		Primitive (B-1)		Cumulate (B-12)		High-SiO ₂ (B-4)		Low-SiO ₂ (B-41)		
	Pheno-cryst	Ground-mass	Pheno-cryst	Ground-mass	Pheno-cryst	Pheno-cryst	Ground-mass	Pigeonite	Augite	Pheno-cryst	Ground-mass	Pheno-cryst	Ground-mass
					(core)	(rim)							
SiO ₂	52.51	47.52	49.23	48.59	51.93	49.95	46.96	53.45	51.00	53.55	49.40	53.27	48.90
TiO ₂	0.42	1.05	1.25	0.89	0.49	1.05	1.11	0.31	0.54	0.36	1.06	0.33	1.40
Al ₂ O ₃	1.66	1.14	4.55	1.39	2.08	3.65	1.17	1.32	3.49	1.34	1.78	1.45	1.75
Cr ₂ O ₃	0.82	0.11	1.04	0.33	0.99	1.04	0.03	0.74	1.25	0.91	0.49	0.83	0.19
FeO	17.80	35.35	14.17	27.77	17.48	13.83	37.05	16.88	9.34	16.61	25.48	17.03	26.29
MnO	0.34	0.47	0.23	0.41	0.28	0.36	0.45	0.28	0.20	0.32	0.41	0.31	0.34
MgO	21.57	3.99	13.41	11.84	21.09	14.60	3.11	23.02	16.67	23.67	14.15	22.41	10.99
CaO	4.08	10.51	16.93	7.56	4.76	15.39	10.05	3.83	17.87	3.43	6.88	4.53	9.75
Na ₂ O	0.03	0.00	0.03	0.01	0.01	0.94	0.05	0.01	0.06	0.02	0.03	0.02	0.03
Total	99.23	100.14	100.84	98.79	99.11	99.91	99.98	99.84	100.42	100.21	99.68	100.18	99.64
<i>Formula Based on 24 Oxygens</i>													
Si	7.810	7.815	7.393	7.739	7.747	7.530	7.798	7.853	7.532	7.825	7.685	7.825	7.703
Al	0.290	0.221	0.806	0.261	0.366	0.647	0.229	0.228	0.608	0.231	0.327	0.252	0.324
Ti	0.047	0.129	0.141	0.106	0.055	0.118	0.139	0.034	0.060	0.040	0.124	0.037	0.166
Cr	0.096	0.014	0.124	0.041	0.117	0.124	0.004	0.086	0.146	0.106	0.060	0.096	0.023
Fe	2.215	4.862	1.779	3.699	2.181	1.743	5.145	2.074	1.154	2.030	3.314	2.092	3.463
Mn	0.043	0.065	0.029	0.055	0.035	0.046	0.063	0.035	0.025	0.039	0.055	0.039	0.046
Mg	4.783	0.979	3.002	2.811	4.690	3.278	0.769	5.040	3.670	5.155	3.280	4.907	2.581
Ca	0.650	1.851	2.724	1.290	0.762	2.483	1.788	0.603	2.827	0.537	1.146	0.712	1.645
Na	0.009	0.000	0.008	0.003	0.002	0.010	0.016	0.002	0.016	0.005	0.010	0.005	0.009

Pigeonite primocrysts cluster around Wo₇En₆ with postcumulus rims of Wo₂₆En₄₅ (Table 4, Fig. 3c). Clast B12 is unusual in that it contains cumulus augite (Wo₃₇En₄₆) that zones outward towards magnesian pigeonite (Wo₁₇En₆₂). The apparent cosaturation with both pigeonite and augite is uncommon in mare cumulates (e.g., Taylor *et al.*, 1983).

Plagioclase compositions are generally similar to those in the other ONBs, except in clast B-12, where the plagioclase is more potassic than in the other two ONB groups (Fig. 4a).

These clasts are similar to the feldspathic peridotites and olivine microgabbros described by Douty *et al.* (1973) from the Apollo 15 rake samples, but their constituent minerals have

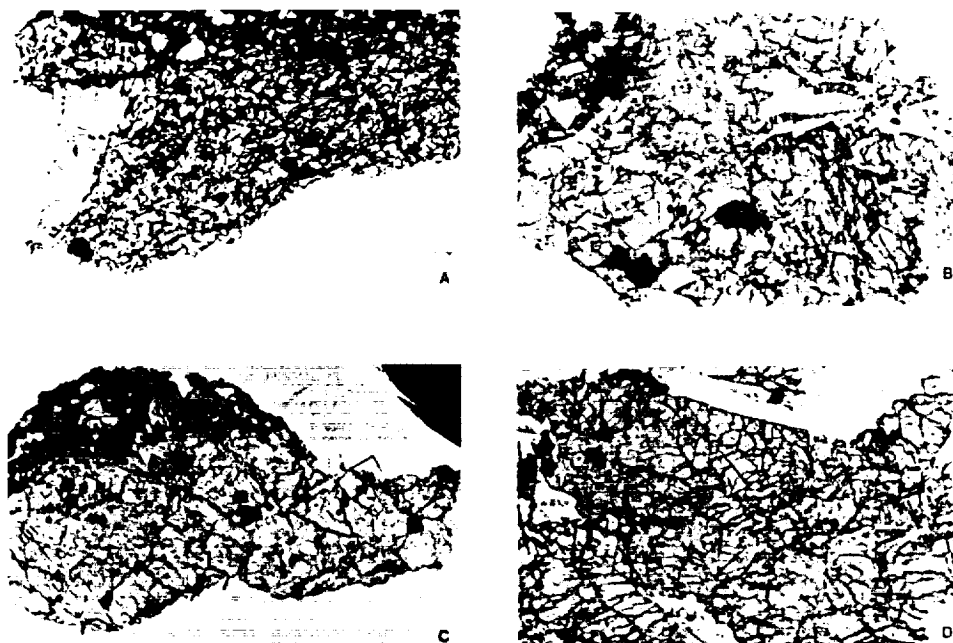


Fig. 2. Plane-polarized light photomicrographs of the ONB suite from 15498. Field of view is 3 mm across. (a) = B-4, low-SiO₂ ONB; (b) = B-41, high-SiO₂ ONB; (c) = B-12, cumulate ONB; (d) = B-42, cumulate ONB.

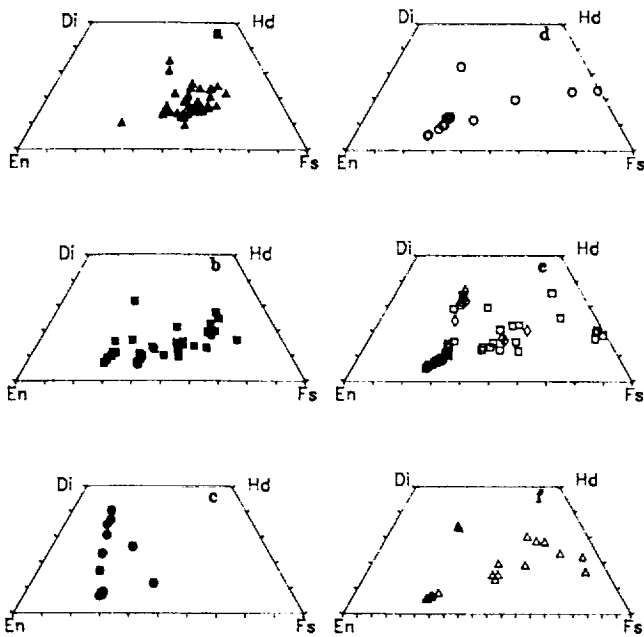


Fig. 3. Pyroxene compositions in the 15498 basalts. (a) = low-SiO₂ ONBs; (b) = high-SiO₂ ONBs; (c) = cumulate ONBs; (d) = primitive QNBs; (e) = intermediate-1 and intermediate-2 QNBs; (f) = evolved QNBs.

more restricted compositional ranges than the rocks described by Dowty. The origin of these rocks as cumulates from mare basalt parent magmas is suggested by their magnesian mineral compositions, restricted compositional ranges, and low modal feldspar contents.

B. Quartz-Normative Basalts

1. Primitive QNB: (B1, B2, B6, B20, B40). The primitive QNBs exhibit a wide range of textures, including vitrophyric, ophitic, and radial-ophitic. Clasts B-6 and B-20 exhibit textures characteristic of quenched liquids, although they are not true vitrophyres because the groundmass is only partly glass (Fig. 5a,b). These rocks consist of sparse olivine phenocrysts (0.25-0.75 mm across) in an aphanitic to fine-grained variolitic groundmass of pyroxene, plagioclase, opaques, and glass. The olivine phenocrysts, which comprise less than 2% of the mode, have rounded to subhedral shapes and Mg-rich core compositions (Fo₆₆ to Fo₇₀ in B-6; Fo₇₁ to Fo₇₃ in B-20). Olivine rim compositions are more Fe-rich in B-6 (Fo₄₈ to Fo₅₈) but are unzoned in B-20. B-6 also contains a small (0.25 mm), subhedral pigeonite microphenocryst (Wo₄ En₇₀) that appears to be in equilibrium with the olivine microphenocrysts.

Clast B-40 differs somewhat from the other vitrophyric clasts. The groundmass of B-40 consists of randomly arranged, euhedral to subhedral pigeonite laths surrounded by quench pyroxene (radiating pyroxene grains intergrown with glass and opaques), plagioclase, opaque oxides, and glass. The glass is opaque, with abundant tiny inclusions. The slender pyroxene

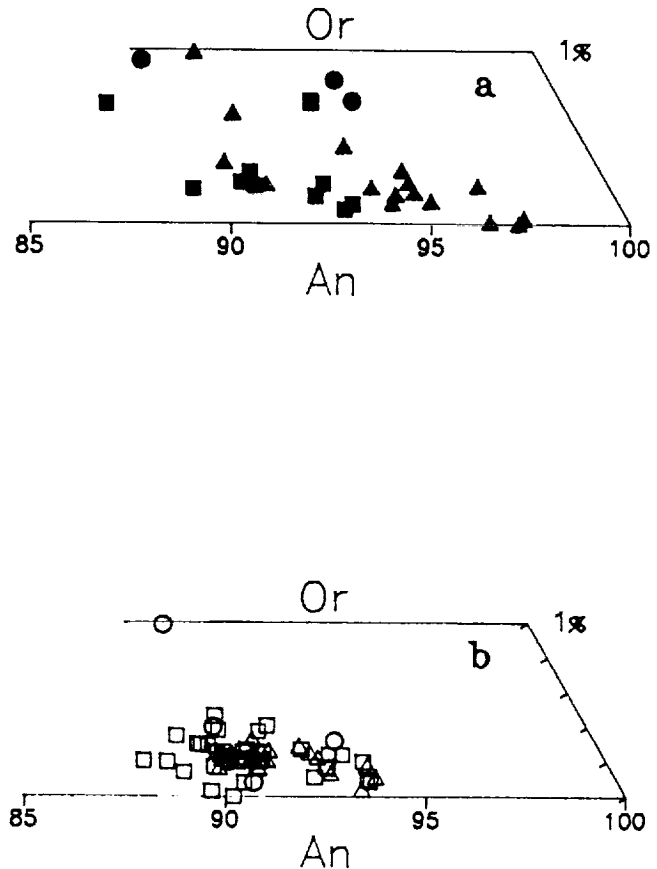


Fig. 4. Plagioclase compositions of the 15498 basalts. (a) = ONBs; (b) = QNBs. Symbols same as Fig. 6.

laths decrease in abundance towards one end of the clast, where glass and quench pyroxene become dominant. This may represent a cooling-rate gradient within the parent lava flow, suggesting proximity to a cooling surface (either top or bottom). Clast B-40 was observed to contain large (< 2.0 mm) phenocrysts of either olivine or pyroxene in hand specimen, but no phenocrysts were included in our probe mount.

The other two primitive QNB clasts (B-1, B-2) have medium to coarse-grained ophitic textures. In B-1, the ophitic texture consists of radiating, fan-like arrays of pyroxene and plagioclase that surround phenocrysts of magnesian pigeonite. Groundmass pyroxene and plagioclase in these clasts and in the vitrophyric clasts have the same compositional ranges as in the other QNB suite clasts (figure 3c and figure 4b).

The textural evidence indicates that B-6, B-20, and B-40 probably represent quenched liquid compositions with little or no olivine accumulation. This conclusion is supported by the composition of the olivine phenocrysts and microphenocrysts, which are Mg-rich and appear to be in equilibrium with the bulk rock Mg/Fe ratios (based on an equilibrium Kd = 0.33). The presence of olivine in these quartz-normative basalts suggests that their compositions are relatively primitive and may be parental to more evolved pyroxene-phyric basalts.

2. Intermediate group 1 QNB: (B-3, B-5, B-11, B-14, B-24, B-43). Four of these clasts (B-3, B-11, B-24, B-43)

are characterized by the common occurrence of large pigeonite phenocrysts (and more rarely olivine) set in a finer-grained groundmass of pyroxene, plagioclase, opaques, cristobalite, and glass (Fig. 5c,d). Two samples are aphyric (B-5, B-14), but have textures that are identical to the groundmass in the other intermediate/1 QNBs. The aphyric samples are most likely phenocryst-free portions of normal pyroxene-phyric flows.

Pigeonite phenocrysts have subhedral, blocky shapes and range in size from 0.5-5.0 mm, with aspect ratios of about 2/1. Olivine phenocrysts range from 0.5-0.7 mm across and have irregular, partly resorbed shapes. Groundmass textures vary from ophitic (Fig. 5c) to radial-ophitic, with radiating fans of slender plagioclase laths enclosed by similar, radiating pyroxene crystals (Fig. 5d). The plagioclase laths may be as long as 1.0 mm, but are rarely wider than 50 microns. Groundmass pyroxene is generally coarser than the plagioclase, but also forms granular aggregates between the feldspar laths. Ilmenite, Ti-rich Cr-spinel, and cristobalite are intergrown with groundmass plagioclase and pyroxene, but Cr-rich spinel also forms inclusions in pigeonite phenocrysts.

Olivine phenocrysts range in composition from $Fe_{0.7}$ to $Fe_{0.67}$. Pyroxene phenocrysts show small compositional ranges, with cores of magnesian pigeonite (Wo_6En_{68} to $Wo_{11}En_{59}$) that commonly display epitactic rims of augite ($Wo_{34}En_{42}$ to $Wo_{31}En_{41}$). Groundmass pyroxenes are more Fe-rich and range in composition from subcalcic ferroaugite to ferrohedenbergite (Fig. 3e). Plagioclase compositions range from An_{94} to An_{89} (Fig. 4b).

3. Intermediate group 2 QNB: (B-23, B-44). The intermediate/2 QNBs display the same range in textures and mineral chemistry as the intermediate/1 QNBs. Major differences in the phenocryst assemblages distinguish the two groups: The intermediate/2 QNBs lack olivine phenocrysts, and one clast (B-44) contains large euhedral augite phenocrysts in addition to phenocrysts of magnesian pigeonite. The augite phenocrysts are generally similar to epitactic augite in composition, but exhibit a wider range, from $Wo_{35}En_{40}$ to $Wo_{31}En_{41}$ (Fig. 3e). Plagioclase ranges in composition from An_{94} to An_{89} (Fig. 4b).

4. Evolved QNB: (B-22, B-45). The evolved QNB clasts studied here are more evolved chemically than any reported previously. One of these clasts (B-45) contains sparse large pyroxene phenocrysts in a radial-ophitic to radial-subophitic groundmass. The other clast (B-22) lacks phenocrysts, but its texture is nearly identical to the groundmass in clast B-45, except that it is coarser-grained. In addition to pyroxene and plagioclase, both of the aphyric QNB contain ilmenite, Ti-rich Cr-spinel, and cristobalite.

The coarser-grained aphyric clast, B-22, is a textbook example of radial subophitic texture. This clast consists of fan-like arrays of slender plagioclase laths up to 2.0 mm long and 50 microns wide intergrown with splays of prismatic pyroxene needles that mold around the ends of the laths, or are molded by adjacent plagioclase (Fig. 5f). The common occurrence of plagioclase laths that mold around pyroxene prisms, despite the modal predominance and larger size of the pyroxene, suggests that pyroxene nucleated before plagioclase or simultaneously with it. The latter hypothesis is supported by

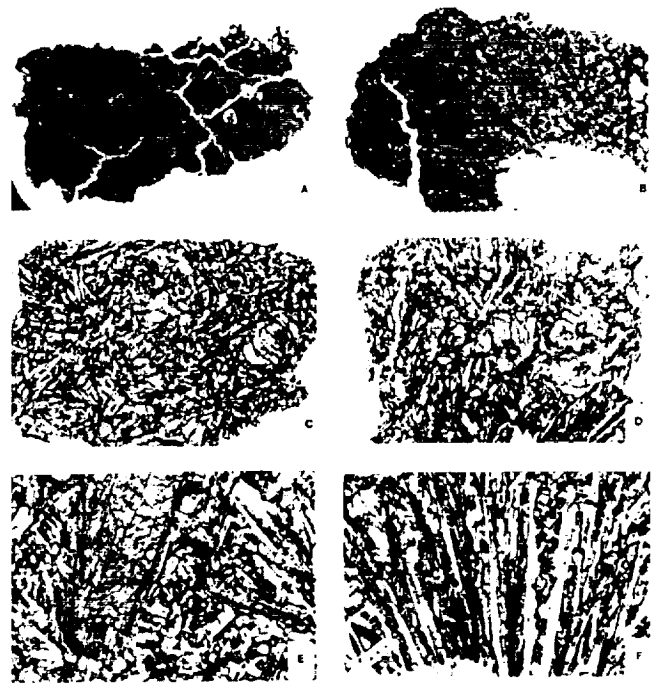


Fig. 5. Plane-polarized light photomicrographs of the QNB suite in the 15498 basalts. (a) = B-6, primitive QNB; (b) = B-20, primitive QNB. Both primitive QNB contain no significant phenocryst phases. (c) = B-3, intermediate-1 QNB; (d) = B-11, intermediate-1 QNB. Both intermediate-1 QNBs contain large pigeonite phenocrysts set in a medium grained groundmass of pigeonite, plagioclase, and residual liquid. (e) = B-44, intermediate-2 QNB (the large phenocryst on the left side is an augite phenocryst); (f) = B-22, evolved QNB; note the radiating intergrowths of pyroxene and plagioclases.

analyses of the cores of pyroxene splays, which show that the cores consist of finely intergrown pyroxene and plagioclase that cannot be resolved optically.

Pyroxenes in the evolved QNB show the same compositional ranges displayed by pyroxene in the intermediate QNBs, from subcalcic augite to ferrohedenbergite (Fig. 3f). The only major difference between pyroxenes of the evolved QNB group and the other QNBs is a tendency towards more Fe-rich compositions, and fewer magnesian pigeonite phenocrysts. Plagioclase (An_{90} to An_{94}), ilmenite, and Ti-rich Cr-spinel likewise exhibit compositional ranges similar to their counterparts in the intermediate QNB groups.

WHOLE ROCK GEOCHEMISTRY

Major and trace element analyses of the twenty-five mare basalt clasts studied here are presented in Table 2. Major element variations as a function of MgO are shown in Fig. 6, trace element variations in Fig. 7, and chondrite-normalized REE concentrations in Fig. 8.

A. Olivine-Normative Basalts

Major element variations in the ONB suite are generally consistent with olivine control (either subtraction or addition):

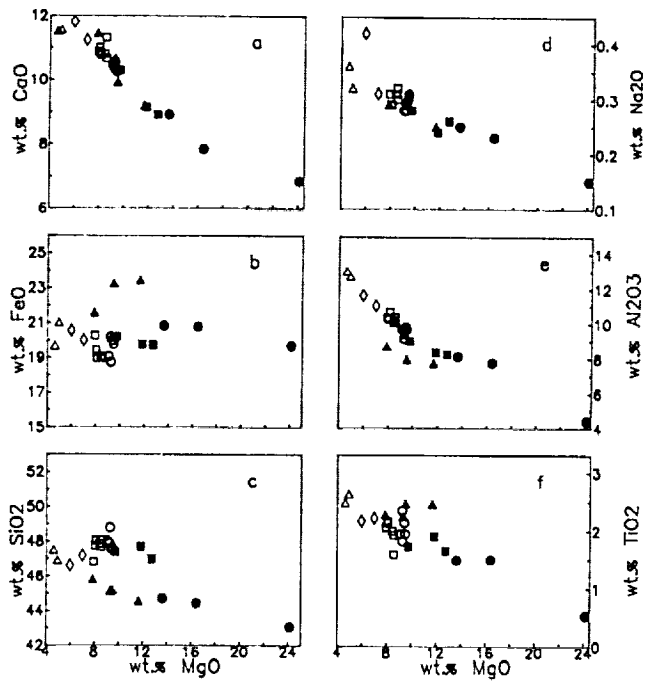


Fig. 6. Major element variations in 15498 basalts, using MgO as a fractionation index. Symbols: Open circles = primitive QNBs; open boxes = intermediate-1 QNBs; open diamonds = intermediate-2 QNBs; open triangles = evolved QNBs; filled circles = cumulate ONBs; filled boxes = high-SiO₂ ONBs; filled triangles = low SiO₂ ONBs.

SiO₂, Al₂O₃, CaO, Na₂O, and TiO₂ all increase with decreasing MgO, whereas FeO remains constant or decreases slightly (Fig. 6). Trace element variations show similar trends—the REE, Hf, and Sc all increase with decreasing MgO, whereas Cr and Co decrease sharply (Fig. 7). REE concentrations are the same in both the low and high-SiO₂ ONBs (La = 13-16 × chondrite) but are lower in the olivine-pyroxene cumulates (La = 6-12 × chondrite; Fig. 8). Despite this overall similarity, significant differences exist between the three ONB groups described earlier.

1. **Low-SiO₂ ONB.** The low-SiO₂ ONBs recognized here are identical to the ONB suite described by earlier studies (Rhodes and Hubbard, 1973; Chappell and Green, 1973; Dowty et al., 1973). The low-SiO₂ ONBs have low SiO₂ contents (44-46 wt %), high TiO₂ (2.2-2.5 wt %), and high FeO (20.1-23.4 wt %) compared to the high-SiO₂ ONB suite and to the QNB suite. Alumina is also low in the low-SiO₂ ONBs relative to these other groups (Fig. 6). MgO concentrations are relatively low (7.9-11.7 wt %), so that their Mg#s range from 47.0-39.4.

2. **High-SiO₂ ONB.** The high-SiO₂ suite is characterized by high SiO₂ contents (47-48 wt %), low TiO₂ (1.65-1.9 wt %), low FeO (19.7-20.2 wt %), and MgO of 9.7-12.7 % (Fig. 6). Because the low FeO concentrations are coupled with relatively high MgO, Mg#s for these rocks (46.2-53.5) are higher than the low-SiO₂ ONB suite. The amount of normative olivine in the high-SiO₂ group (0.4 to 7.3 wt%) is less than in the low-SiO₂ group (2.6-17 wt %), and is due to the high Mg content, despite their high silica.

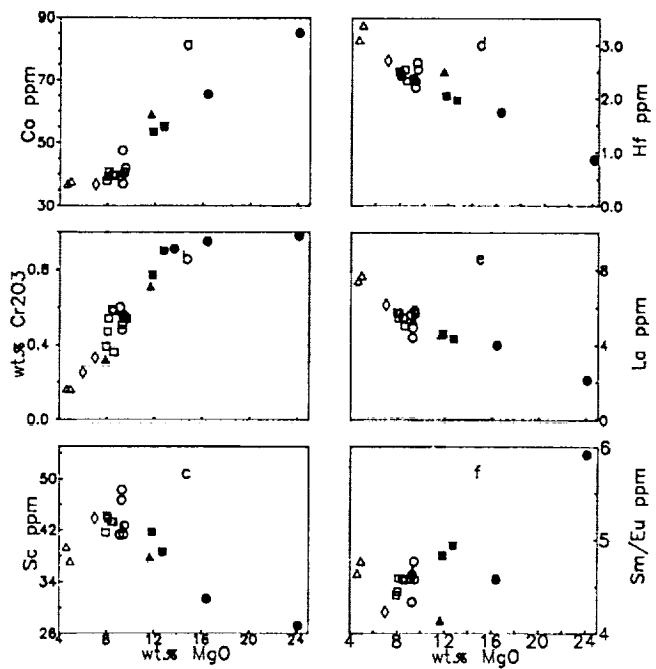


Fig. 7. Trace element variations in 15498 basalts, using MgO as a fractionation index. (a,b,c) = compatible trace elements (Co, Cr, Sc); (d,e,f) = incompatible trace elements (Hf, La, Sm/Eu). See Fig. 6 for symbols.

3. **Olivine-pyroxene cumulates.** These cumulates are characterized by low SiO₂ (43-44 wt %), low TiO₂ (0.5-1.5 wt %), and high MgO (16-24 wt %). Their high normative olivine concentrations (up to 50 wt%) are matched by high modal olivine and pyroxene (Table 3). These rocks have high concentrations of Cr and Co (which are compatible elements in spinel and olivine) but are low in Sc (which concentrates in pyroxene; Fig. 7). Incompatible element concentrations are the lowest observed in any ONB or QNB analyzed here, which is consistent with dilution by cumulate mafic phases. REE concentrations range from 6-12 × chondrite (Fig. 8). The data show that these clasts accumulated olivine and thus do not represent liquid compositions.

B. Quartz-Normative Basalts

The QNBs are characterized by high SiO₂ concentrations of 46.5-48 wt %, FeO abundances of < 21 wt %, and TiO₂ of 1.6-2.6 wt %. Mg#s range from 29.5-47, with MgO concentrations between 4.6-9.5 wt %. Two of the QNB clasts studied here have more evolved compositions than any QNBs described previously (Rhodes and Hubbard, 1973; Helmke et al., 1973).

Major and trace element variation trends in the QNB suite are not consistent with simple olivine control: CaO, Al₂O₃, FeO, Na₂O, and TiO₂ all increase with decreasing MgO, but SiO₂ decreases (Fig. 6). The REE, Hf, Ta, and Th increase with decreasing MgO, and Cr continues to decrease, as in the ONB suite. In contrast to the ONBs, however, Co concentrations remain constant and Sc concentrations decrease with decreasing MgO (Fig. 7). These trends are consistent with

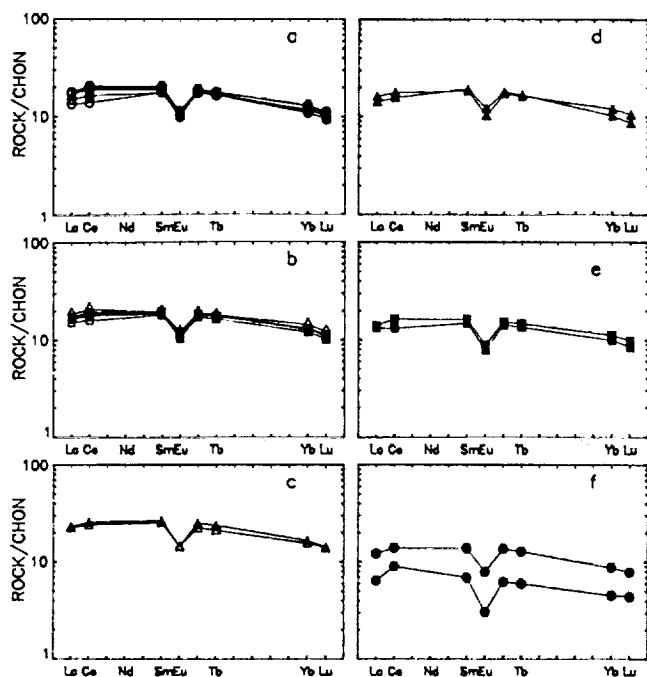


Fig. 8. Chondrite-normalized REE concentrations for 15498 basalts. (a) = primitive QNBs; (b) = intermediate-1 (boxes) and intermediate-2 (diamonds) QNBs; (c) = evolved QNBs; (d) = low-SiO₂ ONBs; (e) = high-SiO₂ ONBs; (f) = cumulate ONBs.

pyroxene fractionation.

REE concentrations are generally lowest in the primitive QNBs (La = 13–17 × chondrite), and highest in the evolved QNBs (La = 22 × chondrite). Sm/Eu ratios vary from 4.2–4.8 (Fig. 7), and the slopes of the REE patterns show little variation.

1. Primitive QNB. The primitive QNBs are characterized by Mg#s between 45.0 and 47.0 (Table 2). They have SiO₂ contents of 47.5–48.8 wt %, FeO of 18.8–20.3 wt %, and CaO of 10.2–10.6 wt %. These samples have the highest compatible element concentrations (Co, Cr, Sc) in the QNB suite and the lowest incompatible element concentrations.

2. Intermediate group 1 QNB. The intermediate/1 QNBs are slightly more evolved than the primitive QNBs, with Mg#s between 44.5 and 41 (Table 2). They have SiO₂ contents of 46.6–48.1 wt %, FeO of 19.0–20.6 wt %, and CaO of 10.8–11.3 wt %. Compatible element concentrations are similar to the primitive QNBs or slightly lower; incompatible elements concentrations are slightly higher than the primitive QNBs.

3. Intermediate group 2 QNB. The intermediate/2 QNBs are slightly more evolved than the intermediate/1 QNBs, with Mg#s of 34 and 38 (Table 2). The SiO₂ content is 46.2–47.2 wt %, FeO of 20.0–20.6 wt %, and CaO of 11.2–11.8 wt %. Compatible element concentrations are slightly lower than in the intermediate/1 QNBs, and incompatible element concentrations slightly higher (Fig. 7). REE concentrations are available for only one sample from this group (B-44); these concentrations are slightly higher than the intermediate/1 QNBs and lower than the evolved QNBs (Fig. 8).

4. Evolved QNB. These basalts are more evolved than any reported previously, with Mg#s of 29.5, and 2.5–4.4% normative quartz (Table 2). The SiO₂ contents are 46.8–47.5 wt %, FeO of 19.7–21.0 wt %, and CaO of 11.5 to 11.6 wt %. Compatible trace element abundances are the lowest and the incompatible element abundances the highest (e.g., La = 22 × chondrite) among the QNBs.

The drop in CaO relative to the most Ca-rich intermediate/2 QNB terminates the Ca-enrichment trend seen in the less evolved samples (Fig. 6). This drop in CaO is not accompanied by a coincident drop in alumina, suggesting that augite fractionation may be involved.

DISCUSSION

The quartz-normative basalt (QNB) clasts studied here include samples more evolved than recognized before (with up to 4.4 wt % normative quartz), and olivine-phyric quenched liquids that are more primitive than any found in previous studies. The olivine-normative basalt (ONB) suite is considerably more complex. Basalts in the low-SiO₂ ONB group are identical to Apollo 15 basalts classified as "ONB" by earlier studies (e.g., Rhodes and Hubbard, 1973; Chappell and Green, 1973; Dowty et al., 1973). Basalts in the high-SiO₂ ONB group do not correspond to any previously described basalt suite at Apollo 15. Their chemical characteristics are similar to those of the QNB suite, suggesting that the high-SiO₂ ONBs may be related to that group. The olivine-pyroxene cumulates are enriched in mafic phases and cannot represent liquid compositions.

The relationships between these basalt groups are more complex than has been observed in previous studies of Apollo 15 basalts, and enable us to study the evolution of the Apollo 15 basalt suites over a wider compositional range. These relationships also raise some important questions:

- (1) Are the observed variations real, i.e., are they due to fractionation processes or do they merely reflect inadequate sample size (short-range unmixing)?
- (2) Are the primitive, olivine-phyric QNBs parental to the more evolved QNBs by normal processes such as crystal fractionation?
- (3) Are the QNBs related to the ONB by fractional crystallization? If so, are they related to the low-SiO₂ ONB or the high-SiO₂ ONB?
- (4) Are the high-SiO₂ ONB and low-SiO₂ ONB related by crystal fractionation?
- (5) Are the olivine-pyroxene cumulates related to the high-SiO₂ ONBs, the low-SiO₂ ONBs, or the QNBs?
- (6) How do these basalts relate to other Apollo 15 basalts?

Short Range Unmixing

A major source of uncertainty in the analysis of lunar mare basalts derives from the small size of the samples available for analysis. Lindstrom and Haskin (1981) have shown that small samples from a single flow of Icelandic basalt exhibit significant compositional differences that can not be related to fractional crystallization. They propose that these variations are caused by a process they termed "short-range unmixing,"

in which each sample contains different relative proportions of mafic and felsic phenocrysts, groundmass, and residual liquids.

Lindstrom and Haskin (1978) used the short-range unmixing model to show that among the Apollo 15 ONBs studied previously, variations in chemical modes were ~10% for pyroxene and plagioclase, 20% for spinel and residual liquid, and 20-30% for olivine, small enough to be accounted for by short-range unmixing of a single, undifferentiated flow. *Lindstrom and Haskin* (1978) also show that the QNB suite samples studied previously are too variable to be accounted for by short-range unmixing of a single, undifferentiated flow, or by fractional crystallization. They suggest that at least two separate flows may have been sampled.

We applied the short range unmixing model of Lindstrom and Haskin to Apollo 15 basalts studied here to test whether or not the intragroup variations observed in the QNB and ONB samples could be explained by short range unmixing, or if these variations require other explanations (e.g., fractional crystallization). Chemical modes were calculated for each rock using a least-squares mixing program and the average phase compositions used by *Lindstrom and Haskin* (1978); these modes were compared to the "average mode" of each group to evaluate the relative modal variations.

Variations observed within both the low-SiO₂ and high-SiO₂ ONB groups are too large to be accounted for solely by short-range unmixing. Olivine shows a variation of greater than 100%, spinel greater than 40%, pyroxene between 2 and 75%, plagioclase up to 50%, and residual liquid of up to 250%. Thus, although each of these groups may represent a single lava, these flows have differentiated by crystal fractionation to create the range in compositions observed. It is also important to note that these groups cannot be related to one another by short-range unmixing either. Two distinct groups are required.

The short-range unmixing model accounts for the variations observed within each of the four QNB groups described above, but cannot account for variations observed between these groups. Thus, the four QNB groups may represent four distinct, undifferentiated flows. The composition of the primitive flow is represented by the average of the primitive QNBs, which include three vitrophyric samples, enriched in residual liquid and two crystalline samples that are depleted in residual liquid relative to the average.

The intermediate/1 QNBs show considerable scatter on major and trace element variation plots (e.g., Fig. 6, 7), but variations in the calculated mode are less than 10% from the average for pyroxene, 10-20% for plagioclase and residual liquid (except for B-14 residual liquid). Thus, these samples may be related to a single, undifferentiated flow whose composition is best represented by the average of all six analyses.

The intermediate/2 and evolved QNB groups have modal compositions that fall far from the average of all QNBs, but modal variations between the two groups are more equivocal. The largest difference is seen in the residual liquid component: when compared to the average of both groups, the intermediate/2 sample B-44 deviates by 4% and the evolved samples deviate by 39%. This suggests that the differences between these samples are real, and result from processes other

than short-range unmixing. However, the small number of evolved samples for which we have data (two in each group) means that the averages calculated for each group may vary somewhat from the parent lava flows.

Fractional Crystallization Relationships

Major and trace element variations in both ONB and QNB suites exhibit trends that are consistent with crystal fractionation of the observed liquidus minerals—olivine in ONB suite and pyroxene in QNB suite (Fig. 6 and 7). Our evaluation of short-range unmixing effects, however, shows that much of the scatter evident on these diagrams is the result of modal variations in small samples that may not represent the average composition of their parent lava flow. This effect is most pronounced on the QNB suite samples. In order to avoid the problems associated with limited sample sizes, we have averaged the compositions of all the samples within each QNB group to derive a "best" estimate for the composition of the parent lava flow. These averages are presented in Table 5, and will be used in all of the calculations that follow. Because the ONB suite clasts exhibit differences that are too large to be explained by short-range unmixing, we will continue to consider these compositions individually. It is important to keep in mind, however, that the compositions of these clasts may also deviate somewhat from that of their parent lava flow.

Figure 9 is an MgO variation diagram for SiO₂ which illustrates fractionation trends in the ONB and QNB samples studied here. The large open symbols represent the average QNB data from Table 5, the stars are QNB analyses of *Rhodes and Hubbard* (1973), the closed symbols are ONBs studied here, and the crosses are ONB analyses from *Rhodes and Hubbard* (1973). Representative control lines for olivine (Fo₇₀) and pigeonite (Wo₇En₆₇Fs₂₆) fractionation are drawn from the observed liquidus minerals through the most primitive basalt of each group. This

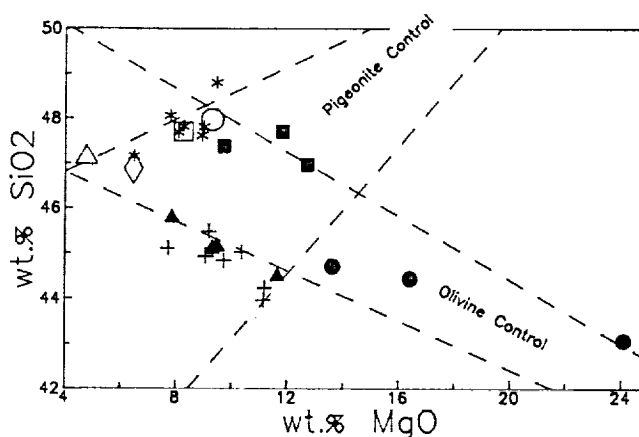


Fig. 9. SiO₂ wt % versus MgO wt % of 15498 basalts. Dashed lines represents olivine (Fo₇₀) and pigeonite (Wo₇En₆₇Fs₂₆) fractionation control lines. Symbols same as Fig. 6. Larger symbols: Circle = average of the primitive QNBs; box = average of the intermediate-1 QNBs; diamond = average of the intermediate-2 QNBs; triangle = average of evolved QNBs. Previous data of *Rhodes and Hubbard* (1973) are represented by the stars (QNBs) and crosses (ONBs).

diagram is useful because the olivine and pigeonite control lines intersect at high angles, resulting in residual liquid trends that diverge from the presumed parent magma composition.

This diagram illustrates several important points. First, the QNB clasts studied here, and the QNB data of Rhodes and Hubbard, plot on or near a pigeonite control line, suggesting that these samples may be related by pigeonite fractionation. Second, the ONB clasts studied here plot on or near two distinct olivine control lines (Fig. 9). The high-SiO₂ ONBs plot near an olivine control line that intersects the QNB array at its primitive (high MgO) end; the low-SiO₂ ONBs and the ONB data of Rhodes and Hubbard plot near an olivine control line that intersects the QNB array at its evolved (low MgO) end. Thus, the high-SiO₂ ONBs may be parental to QNB suite lavas, but only the most evolved QNBs could be related to the low-SiO₂ ONBs. Finally, the olivine-pyroxene cumulates plot between the high-SiO₂ ONB and low-SiO₂ ONB olivine control lines and may be related to either suite. These trends are evaluated quantitatively in the next section.

Least-Squares Modeling

Least-squares calculations were made for the major elements using the most primitive basalts as parental magmas for each group and the observed liquidus phases (olivine, pigeonite, augite, and Cr-spinel). The calculations take the form parent magma = daughter magma + liquidus phases, with the parent magma as the dependent variable.

Calculations involving the QNB suite use the average group compositions from Table 5. Clast B-4 is chosen to represent the low-SiO₂ parent magma because it lies at the high-Mg end of the low-SiO₂ ONB trend, and because its texture (very fine-grained, olivine-phyric; Fig. 2a) is likely to represent that of a quenched liquid. Clast B-41 is chosen to represent the high-SiO₂ parent magma for the same reasons, although its texture (medium-grained ophitic) makes this interpretation more uncertain. The results of these models are summarized in Table 6 (lavas) and Table 7 (cumulates).

The major element fractionation models calculated here were cross-checked by calculating the relative enrichment of La between the parent and daughter compositions. This fractionation factor, termed F^* in the results, calculates the fraction of liquid remaining for Rayleigh fractionation if the bulk partition coefficient for La = 0 (i.e., $F^* = L_{\text{parent}}/L_{\text{daughter}}$).

QNB parent magmas. Several possible combinations were tested in which QNB parent magmas fractionate to QNB daughters (Table 6). A parent magma similar to the average primitive QNB requires about 5% fractionation of either olivine or olivine + pigeonite to generate the intermediate/1 QNB group. The results for both cases are equally good (the "olivine-only" solution has a smaller error in the sum, but a larger residual than the "olivine + pigeonite" solution); it is not possible to choose between these two options. Although the primitive QNBs contain phenocrystic olivine, several also contain pigeonite phenocrysts. We favor the two phase fractionation result.

Primitive QNB parents may also fractionate to intermediate/2 QNB (17% crystallization) and evolved QNB (27% crystalli-

TABLE 5. Average of the QNB groups used in least-squares modeling.

	Primitive	Intermediate- 1	Intermediate- 2	Evolved
SiO ₂	47.97	47.71	46.89	47.18
TiO ₂	2.04	1.98	2.20	2.55
Al ₂ O ₃	9.59	10.32	11.33	12.85
FeO	19.55	19.28	20.27	20.33
MnO	0.26	0.25	0.24	0.24
MgO	9.30	8.27	6.47	4.77
CaO	10.38	10.91	11.52	11.54
Na ₂ O	0.24	0.27	0.32	0.29
K ₂ O	0.04	0.04	0.038	0.05
P ₂ O ₅	0.06	0.06	0.05	0.08
Cr ₂ O ₃	0.54	0.49	0.29	0.16
Total	99.97	99.52	99.49	100.05
Mg#	45.9	43.3	36.2	29.5
Norms				
Q	1.30	1.62	1.19	3.48
Or	0.25	0.23	0.24	0.27
Ab	2.05	2.33	2.67	2.45
An	24.95	26.61	29.37	33.64
Di	21.89	22.78	23.32	19.755
Hy	44.71	41.32	37.96	35.19
Ol	0.0	0.0	0.0	0.0
Il	3.92	3.80	4.31	4.86
Ap	0.13	0.14	0.1	0.18
Trace Elements				
Sc	44.06	43.24	43.80	38.20
Cr	3320	3340	2300	1100
Co	41.26	39.52	36.70	37.25
Rb	8.0	1.80		0.0
Sr	90	108		145
Cs	0.05	0.0		0.11
Ba	89.8	94.0	100.0	93.5
La	5.30	5.47	6.15	7.53
Ce	15.54	15.86	18.50	21.8
Nd	14.40	18	13	19
Sm	3.38	3.46	3.55	4.66
Eu	0.74	0.77	0.84	0.99
Tb	0.81	0.85	1.05	
Yb	2.44	2.54	2.86	3.18
Lu	0.35	0.37	0.41	0.475
Zr	155	116	100	150
Hf	2.42	2.45	2.71	3.23
Ta	0.37	0.35	0.40	0.46
Th	0.59	0.65	0.74	0.94

zation) magma compositions (Table 6). These results are corroborated by the La fractionation factors, which indicate 14% and 30% crystallization, respectively. When more evolved parent magmas are chosen (e.g., intermediate/1 QNB), similar results are obtained (Table 6). Note that these results are additive, so that the result for primitive QNB → evolved QNB is approximately the same as the sum of primitive QNB → intermediate/1 QNB plus intermediate/1 QNB → evolved QNB. Note also that all solutions for evolved QNB and intermediate/2 QNB require augite fractionation. These solutions are consistent

TABLE 6. Representative major element least-squares calculations for 15498 basalts.

Parent	Daughter	% Daughter	% Phases			Cr-Spinel	Sum	Error	Residuals	F*
			Olivine	Pigeonite	Augite					
QNB	QNB									
Prim	Inter-1	93.7	0.9	5.4	-	.06	100.0	3.1	.134	96.9
Prim	Inter-1	95.8	4.1	-	-	.12	100.0	1.0	.700	96.9
Prim	Inter-2	82.5	-	15.5	1.9	.26	100.0	1.7	.033	86.2
Prim	Evolved	73.0	2.4	16.5	7.3	.32	99.50	5.0	.540	70.4
Inter-1	Inter-2	87.9	-	9.2	2.6	.22	99.90	1.2	.188	88.9
Inter-1	Evolved	77.6	1.6	11.8	8.0	.27	99.22	4.1	.230	72.6
Inter-1	Evolved	77.0	-	14.1	7.9	.25	99.25	2.0	.430	72.6
Inter-2	Evolved	88.9	3.0	0.8	6.3	.08	99.17	6.2	.730	82.0
Inter-2	Evolved	89.1	3.5	-	6.4	.09	99.14	2.6	.710	82.0
Low-SiO ₂										
ONB	Low-SiO ₂ ONB									
B-4	B-29	93.4	7.3	-	-	.04	101.1	1.7	.460	-
B-4	B-26	85.1	14.1	-	-	.09	100.0	3.1	1.77	-
Low-SiO ₂										
ONB	QNB									
B-4	Evolved	66.6	14.7	15.4	-	.85	97.6	26.6	13.5	61.5
High-SiO ₂										
ONB	Low-SiO ₂ ONB									
B-41	B-4	87.0	-11.1	24.6	-	.02	100.6	16.9	6.00	93.7
B-25	B-4	90.4	-14.3	24.8	-	.01	100.0	13.1	4.39	99.8
B-25	B-29	84.1	-7.1	24.0	-	.26	101.3	15.0	6.30	-
High-SiO ₂										
ONB	QNB									
B-41	Prim	82.6	8.4	8.1	-	.73	99.80	3.8	.090	81.9
B-41	Inter-1	77.5	9.5	11.9	0.08	.80	99.90	1.6	.003	79.3
B-41	Inter-2	68.0	8.5	20.6	1.8	.96	99.80	2.0	.050	70.5
B-41	Inter-2	69.9	7.8	21.7	-	.95	100.0	3.1	.330	70.5
B-41	Evolved	59.8	11.2	20.7	-	1.0	99.10	5.7	.160	57.6
B-41	Evolved	59.8	10.9	21.0	6.6	.99	99.20	3.5	.140	57.6

Residual* = sum of the squares of the residuals.

F* = fraction of liquid remaining based on concentration of La in parent/concentration in daughter with bulk La D = 0.

* Indicates mineral not used in fit.

with the occurrence of augite phenocrysts in one of the intermediate/2 basalts, and with the termination of CaO enrichment seen at low MgO-contents in Fig. 6. We will return to this important point later when we discuss the cumulates.

ONB parent magmas. Four separate problems must be considered here: (1) Can the assumed low-SiO₂ ONB parent (clast B-4) fractionate to form more evolved low-SiO₂ ONBs? (2) Can a low-SiO₂ parent fractionate to form the evolved QNBs? (3) Can a high-SiO₂ parent magma fractionate to form the low-SiO₂ basalts? and (4) Can the assumed high-SiO₂ parent magma (clast B-41) fractionate to form various members of the QNB suite?

The modeling calculations show that the more evolved low-SiO₂ ONBs (B-26, B-29) can be derived from a low-SiO₂ parent magma similar to B-4 by 7-15% olivine fractionation, with minor Cr-spinel (Table 6). No pigeonite is required, consistent with its absence as an early liquidus phase. However, a low-SiO₂ parent magma similar to B-4 cannot be parental to the evolved

QNB suite samples. While a parent-daughter relationship appears possible in Fig. 9, the mixing calculations show extremely poor fits, with totals \cong 98% and the sum of the square of the residuals > 10 (Table 6).

The calculations also show that high-SiO₂ ONB parent magmas cannot be parental to the low-SiO₂ ONBs (e.g., B-4, B-29). Not only are the fits for these mixes exceptionally bad (sum of the square of the residuals = 4-6), but the solutions all require negative olivine fractionation and substantial pigeonite fractionation (~ 25%) despite the fact that pigeonite is not a liquidus phase in either suite.

Fractionation of the assumed high-SiO₂ ONB parent magma (B-41) results in excellent fits for all QNB suite samples. The primitive QNBs require about 8% each olivine and pigeonite fractionation, a result supported by the La fractionation factor, which indicates 16% crystallization (Table 6). The more evolved QNB samples (intermediate/1, intermediate/2, and evolved QNB) require progressively more pigeonite fractionation of

TABLE 7. Representative major element least-squares calculations for 15498 cumulates.

Cumulate	Trapped Liquid	Trapped Liquid %	% Phases				Sum	Error	Residual*	T.L.*
			Olivine	Pigeonite	Augite	Cr-Spinel				
Cumulates QNB										
B-12	Prim	33.3	42.5	1.3	19.5	.91	97.5	19.7	.544	40.0
B-12	Prim	33.5	43.5	-	19.6	.91	97.5	7.3	.707	40.0
B-27	Prim	81.4	20.0	-6.7	3.2	.92	98.8	5.5	.096	-
B-42	Prim	74.9	27.4	-3.9	.56	1.1	100.0	6.2	.994	75.3
B-12	Inter-1	32.7	45.0	-	19.2	.92	97.8	5.9	.798	38.6
B-27	Inter-1	76.1	19.3	-	2.7	.96	99.0	1.5	.304	-
B-42	Inter-1	70.4	28.2	.15	.39	1.1	100.2	4.8	.641	72.9
B-12	Inter-2	28.3	42.3	6.4	19.6	.99	97.7	16.4	.385	34.3
B-27	Inter-2	67.4	19.8	6.1	4.5	1.1	99.0	2.8	.030	-
B-42	Inter-2	61.8	27.1	8.1	1.9	1.3	100.2	5.9	.977	64.9
B-12	Evolved	24.5	43.9	6.3	21.9	.99	97.5	16.8	.476	28.0
B-27	Evolved	59.0	22.1	6.8	9.3	1.2	98.4	5.1	.550	-
B-42	Evolved	54.2	29.6	8.3	6.3	1.3	99.7	2.8	.207	53.0
Cumulates Low-SiO ₂ ONB										
B-12	B-4	30.6	41.9	-	23.7	.97	97.1	12.6	4.89	45.6
B-27	B-4	81.6	2.4	8.3	6.1	.41	98.8	22.4	3.34	-
B-42	B-4	76.1	10.4	10.1	2.7	.64	100.0	22.9	6.71	86.2
Cumulates High-SiO ₂ ONB										
B-12	B-41	40.7	37.6	-	18.9	.59	97.7	7.3	.333	48.6
B-27	B-41	98.9	11.4	-14.1	2.8	.19	99.2	3.7	.143	-
B-42	B-41	91.3	19.3	-10.6	-	.40	100.4	4.8	.621	91.9

Residual* = sum of squares of the residuals.

T.L.* = amount of trapped liquid based on concentration of La in whole rock/concentration in T.L. with bulk La D = O.

*Indicates mineral not used in fit.

a high-SiO₂ parent magma, along with 8%-11% olivine and minor Cr-spinel (Table 6). Although B-41 can fractionate to Inter-2 and Evolved with or without augite, the presence of augite phenocrysts supports the model with augite. La fractionation factors are within 2% of the major element mixing results, which confirms the solutions.

Cumulates. The olivine-pyroxene cumulates are best modeled as cumulate rocks that reflect the mixing of cumulus phases (olivine, pigeonite, augite, Cr-spinel) with trapped intercumulus magma. These calculations take the form: cumulate rock = cumulus phases + trapped liquid. The amount of trapped liquid calculated from the major element modeling can be cross-checked using La to calculate the fraction of trapped liquid by mass balance, assuming the bulk partition coefficient for La is zero (i.e., $[La_{WR}/La_{TL}] = \text{mass fraction trapped liquid}$). This is shown in Table 7 as T.L.*.

Mixing liquid calculations which assume a trapped liquid composition similar to the low-SiO₂ parent magma B-4 all result in poor fits to the actual cumulate rock compositions (Table 7). Errors about the sum are large, and the sums of the squares of the residuals range from 3.3-6.7 on the best solutions. Models which assume a high-SiO₂ parent magma (B-41) have negative pigeonite, except for cumulate clast B-12. This clast can be modeled reasonably well if pigeonite is excluded from the fit, but this is not consistent with petrographic evidence for cumulus pigeonite.

The best fits to these cumulates are achieved using QNB suite magmas for the trapped liquid component. Even here, fits which use the primitive and intermediate/1 QNBs as the trapped liquid component yield poor fits (Table 7). The best solutions result when the trapped liquid component is assumed to have an evolved composition, similar to intermediate/2 QNB or evolved QNB (Table 7). These results are confirmed by the La mass balance calculations, which show the closest correspondences for evolved trapped liquids.

Derivation of at least one of these cumulates (B-12) from an evolved parent magma is supported petrographically by presence of cumulus augite. Augite occurs as a phenocryst phase in the intermediate/2 QNBs, but not in less evolved QNBs. The onset of augite saturation at this point is further supported by the termination of the Ca-enrichment trend in the evolved QNBs (Fig. 6).

Relationships to Other Apollo 15 Mare Basalts

Two of the seven mare basalt groups described above have not been reported by previous studies of Apollo 15 mare basalts—the evolved QNB group, and the high-SiO₂ ONB group. There are probably two important reasons for this: (1) the geographic location of the sample site, and (2) analytical limitations of the previous data set.

Mare basalts were collected at three main locations: Station 1 (Elbow crater), Station 4 (Dune crater), and Station 9a (Hadley Rille rim). Pyroxene basalts (QNB) were common at all three sites, but olivine basalts were found only at Station 9a. In addition, a few mare cumulates were collected at Station 7. This distribution suggests that pyroxene basalts are laterally contiguous and underlie the entire mare plateau (ALGIT, 1972). The olivine basalts are interpreted as a thin flow unit that overlies the pyroxene basalt layer locally, but does not occur near the Apennine Front. Because 15498 was collected from the rim of Dune Crater (Station 4), the basalts present in this sample may come from as deep as 90 m—below the pyroxene basalt flows that underlie most of the site (ALGIT, 1972). Thus, the ONB and QNB clasts in 15498 may represent flows that predate the more common mare basalt samples studied previously. This interpretation is strengthened by the fact that 15498 is a breccia produced by impact processes containing random fragments of mare basalt. Thus, a wider range of compositions, from deeper stratigraphic levels, is more likely to be found.

Another possibility is that chemical differences between subgroups within each mare basalt suite (ONB versus QNB) have been masked by limited analytical data, and by chemical data of poor quality. For example, 15065 is a slightly olivine-normative basalt that *Rhodes and Hubbard* (1973) group with the QNBs, based on its chemical similarity to that suite. This rock is very similar chemically to the high-SiO₂ ONBs described here, and may represent the largest single sample of this group (but not necessarily from the same flow).

Ryder and Steele (1987) have recently re-analyzed several Apollo 15 ONBs, and calculated mass-weighted averages of the new and existing analyses. They used the same technique which we employed (fused bead EMP analysis), so our data sets should be comparable. Several of the analyses presented by *Ryder and Steele* have chemical characteristics similar to the high-SiO₂ ONBs described here: 15274, 15387, 15641, 15651, and possibly 15672. These samples have high SiO₂ for their MgO content, higher Al₂O₃, and lower TiO₂ than the "normal," low-SiO₂ ONBs with which they are correlated. Curiously, three of these samples (15641, 15651, 15672) were classified as "Olivine microgabbro B" by *Binder et al.* (1980), who noted their deviation from the other olivine-phyric samples. The other two samples (15274, 15387) are picrite basalts ("feldspathic peridotite" of *Dowty et al.*, 1973) that are similar to the olivine-pyroxene cumulate B-12. Although these rocks may not be directly related to the high-SiO₂ ONB group studied here, they may represent primitive, olivine-normative parent magmas to other QNB lava flows (or cumulates derived from these QNB flows). In any case, the data imply that more than one suite of olivine-normative basalt is present at the Apollo 15 site. Resolving these distinct ONB groups will be difficult, however, because basalts of the surface-outcropping units dominate the sample suite.

CONCLUSIONS

The data presented here document a greater diversity in Apollo 15 mare basalts than was recognized in earlier studies and provide important new constraints on mare basalt

petrogenesis at this site. The wider range of basalt types found here allow us to identify potential parent magmas, test interrelationships between sample groups, and define probable lines of descent. Our main conclusions are:

1. The Apollo 15 quartz-normative basalts (QNB) may be subdivided into four groups based on chemical variations: (a) primitive QNB, (b) intermediate/1 QNB, (c) intermediate/2 QNB, and (4) evolved QNB. The primitive QNB are commonly olivine-phyric and may be parental to the more evolved QNBs. The intermediate/1, intermediate/2, and evolved QNBs represent progressively more evolved compositions that may be related to the primitive QNB group by crystal fractionation of olivine (early), pigeonite, and augite (late). Chemical variations within each of these four groups can be explained by the short-range unmixing model of *Lindstrom and Haskin* (1978, 1981).

2. The Apollo 15 olivine-normative basalts (ONB) comprise three distinct groups: (a) low-SiO₂ ONB, (b) high-SiO₂ ONB, and (c) olivine-pyroxene cumulates. The low-SiO₂ ONBs are the same as the ONB suite described by earlier studies. The high-SiO₂ ONBs are a new type of mare basalt that were not recognized by previous studies. The olivine-pyroxene cumulates correspond to the feldspathic peridotites and olivine gabbros described by *Dowty et al.* (1973).

3. Least-squares mixing calculations show that the high-SiO₂ ONBs may be parental to the QNB suite, documenting the first link between ONBs and QNBs at the Apollo 15 site. The composition of the high-SiO₂ ONB clast B-41 is the identical to the hypothetical QNB suite parent postulated by *Chappell and Green* (1973).

4. Least-squares mixing models show that variations within the low-SiO₂ ONBs can be explained by olivine fractionation. However, the low-SiO₂ ONBs cannot be parental to any of the QNB lavas, nor can the low-SiO₂ ONBs and high-SiO₂ ONBs be related by either short-range unmixing or fractional crystallization.

5. The discovery of new basalt types in breccia 15498 may result from its geographic position near the edge of the mare plain, where normal ONBs are scarce, and from its presumed origin as ejecta from Dune Crater. The ejecta from this crater may come from as deep as 90 m, well below the ONB and QNB flows exposed at the surface. In addition, new data on mare basalts from other stations suggests that the new basalt groups may be more widespread than previously recognized.

6. The cumulates are similar to Apollo 15 picritic basalts (*Ryder and Steele*, 1987) and feldspathic peridotites (*Dowty et al.*, 1973). They also have characteristics similar to ultramafic rocks from the Apennine Front (M. M. Lindstrom, personal communication, 1987). The presence of *cumulus* augite in clast B-12 suggests a relationship to the more evolved QNBs, which is supported by our fractionation models. However, the relationship of the cumulates to the basalts is still imprecise due to the large uncertainties in the results.

Acknowledgments. We wish to thank Charlie Galindo for curatorial assistance in the Pristine Sample Lab, Gordon McKay for access to the JSC EMP and Jerry Wagstaff for help in running it, and Jim Wittke for assistance with the EMP analyses at USC. Discussions with Graham Ryder, John Delano, and Larry Taylor on mare basalt

petrogenesis were both educational and appreciated. Gary Lofgren provided access to the strip furnace at JSC, without which this paper would not be possible. We would also like to thank Odette James and Jeff Taylor for their careful reviews which improved the manuscript significantly. This work was supported by NASA grant NAG 9-169 to J.W. Shervais.

REFERENCES

- ALGIT (Apollo Lunar Geology Investigation Team) (1972) Geological setting of the Apollo 15 samples. *Science*, *175*, 407-415.
- Binder A. B. (1976) On the compositions and characteristics of the mare basalt magmas and their source regions. *The Moon*, *16*, 115-150.
- Binder A. B., Lange M. A., Brant H. J., and Kahler S. (1980) Mare basalt units and the compositions of their magmas. *Moon and Planets*, *23*, 445-481.
- BVSP (Basaltic Volcanism Study Project) (1981) *Basaltic Volcanism on the Terrestrial Planets*. Pergamon, New York. 1286 pp.
- Chappell B. W. and Green D. H. (1973) Chemical composition and petrogenetic relationships in the Apollo 15 mare basalts. *Earth Planet. Sci. Lett.*, *18*, 237-246.
- Dowty E., Prinz M., and Keil K. (1973) Composition, mineralogy, and petrology of 28 mare basalts from Apollo 15 rake samples. *Proc. Lunar Sci. Conf. 4th*, 423-444.
- Duncan A. R., Sher M. K., Abraham Y. C., Erlank A. J., Willis J. P., and Ahrens L. H. (1975) Compositional variability of the Apollo 15 regolith (abstract). In *Lunar Science VI*, pp. 220-222. The Lunar Science Institute, Houston.
- Helmke P. A., Blanchard D. P., Haskin L. A., Telander K., Weiss C., and Jacobs J. W. (1973) Major and trace elements in igneous rocks from Apollo 15. *The Moon*, *8*, 129-148.
- Laul J. C. and Schmitt R. A. (1973) Chemical composition of Apollo 15, 16, and 17 samples. *Proc. Lunar Sci. Conf. 4th*, 1349-1367.
- Lindstrom M. M. and Haskin L. A. (1978) Causes of compositional variations within mare basalt suites. *Proc. Lunar Planet. Sci. Conf. 9th*, 465-486.
- Lindstrom M. M. and Haskin L. A. (1981) Compositional inhomogeneities in a single Icelandic tholeiite flow. *Geochim. Cosmochim. Acta*, *45*, 15-31.
- Lofgren G. E., Donaldson C. H., and Usselman T. M. (1975) Geology, petrology, and crystallization of Apollo 15 quartz-normative basalts. *Proc. Lunar Sci. Conf. 6th*, 79-99.
- LSPET (Lunar Sample Preliminary Examination Team) (1972) The Apollo 15 lunar samples: A preliminary description. *Science*, *175*, 363-375.
- Mason B., Jarosewich E., Melson W. G., and Thompson G. (1972) Mineralogy, petrology, and chemical composition of lunar samples 15085, 15256, 15271, 15471, 15475, 15476, 15535, and 15556. *Proc. Lunar Sci. Conf. 3rd*, 785-796.
- Neal C. R., Taylor L. A., and Lindstrom M. M. (1987) Mare basalt evolution: The influence of KREEP-like components (abstract). In *Lunar and Planetary Science XVIII*, pp. 706-707. Lunar and Planetary Institute, Houston.
- Papike J. J., Hodges F. N., Bence A. E., Cameron M., and Rhodes J. M. (1976) Mare basalts: Crystal chemistry, mineralogy, and petrology. *Rev. Geophys. Space Phys.*, *14*, 475-540.
- Rhodes J. M. (1972) Major element chemistry of Apollo 15 mare basalts (abstract). In *The Apollo 15 Lunar Samples*, pp. 250-252. The Lunar Science Institute, Houston.
- Rhodes J. M. and Hubbard N. J. (1973) Chemistry, classification, and petrogenesis of Apollo 15 mare basalts. *Proc. Lunar Sci. Conf. 4th*, 1127-1148.
- Ryder G. and Steele A. (1987) Chemical dispersion among Apollo 15 olivine-normative basalts. *Proc. Lunar Planet. Sci. Conf. 18th*, this volume.
- Shervais J. W., Taylor L. A., and Lindstrom M. M. (1985a) Apollo 14 mare basalts: Petrology and geochemistry of clasts from consortium breccia 14321. *Proc. Lunar Planet. Sci. Conf. 15th*, in *J. Geophys. Res.*, *90*, C375-C395.
- Shervais J. W., Taylor L. A., Laul J. C., Shih C.-Y., and Nyquist L. E. (1985b) Very high potassium (VHK) basalt: Complications in mare basalt petrogenesis. *Proc. Lunar Planet. Sci. Conf. 16th*, in *J. Geophys. Res.*, *90*, D3-D18.
- Taylor L. A., Shervais J. W., Hunter R. H., Shih C.-Y., Nyquist L., Bansal B., Wooden J., and Laul J. C. (1983) Pre-4.2 AE mare basalt volcanism in the lunar highlands. *Earth Planet. Sci. Lett.*, *66*, 33-47.
- Wanke H., Baddenhausen H., Blum K., Cendales M., Dreibus G., Hofmeister H., Kruse H., Jagoutz E., Palme C., Spettel B., Thacker R., and Vilcsek E. (1977) On the chemistry of lunar samples and achondrites Primary matter in the lunar highlands: A re-evaluation. *Proc. Lunar Sci. Conf.*, *8th*, 2191-2213.

Note added in proof:

It has been pointed out to us that our modeling of the primitive QNB group by fractionation of olivine in pigeonite from a high-Si ONB parent is in conflict with experimental data showing the primitive QNB group to have olivine as the sole liquidous phase. Fractionation models with olivine and CR-spinel as the liquidous phases in a high-Si ONB give results similar to the olivine pigeonite models, although the fits are not quite as good (13% olivine, 0.3% spinel, 86% daughter melt, with 1.3% error and 1.6% residual). The poorer fit probably reflects minor deviations of B-41 from a true liquid composition as a result of short range unmixing. This does not, however, invalidate our basic conclusion that high-Si ONB magmas similar to B-41 are parental to the QNB suite. More samples are needed to better define this liquid composition.

HOUSE
COMMITTEE ON APPROPRIATIONS
SUBCOMMITTEE ON VA-HUD-INDEPENDENT AGENCIES

Subcommittee on VA- HUD-Independent Agencies
H143 Capitol
Washington, DC 20515
(202) 225-3241

(202) 225- Address

Democrats

Louis Stokes (OH) CHMN	7032	2365 RHOB
Alan B. Mollohan (WV)	4172	2242 RHOB
Jim Chapman (TX)	3035	2417 RHOB
Marcy Kaptur (OH)	4146	2104 RHOB
*Esteban Torres (CA)	5256	1740 LHOB
*Ray Thornton (AR)	2506	1214 LHOB

Republicans

Jerry Lewis (CA) RMM	5861	2312 RHOB
*Tom DeLay (TX)	5951	407 CHOB
*Dean A. Gallo (NJ)	5034	2447 RHOB

HOUSE
COMMITTEE ON SCIENCE, SPACE, AND TECHNOLOGY
SUBCOMMITTEE ON SPACE

Subcommittee on Space
2320 Rayburn House Office Building
Washington, DC 20515
(202) 225-7858

(202) 225- Address

Democrats

Ralph M. Hall (TX) CHRM	6673	2236 RHOB
Harold L. Volkmer (MO)	2956	2409 RHOB
Robert G. Torricelli (NJ)	5061	2159 RHOB
James A. Traficant, Jr. (OH)	5261	2446 RHOB
Glen Browder (AL)	5751	1221 LHOB
Jim Bacchus (FL)	3671	432 CHOB
Bud Cramer (AL)	4801	1318 LHOB
*James A. Barcia (MI)	8171	1719 LHOB
*Eric D. Fingerhut (OH)	5731	431 CHOB
James A. Hayes (LA)	2031	2432 RHOB
John S. Tanner (TN)	4714	1009 LHOB
Pete Geren (TX)	5071	1730 LHOB
*Tim Roemer (IN)	3915	415 CHOB
*Jane Harman (CA)	8220	325 CHOB
*Anna G. Eshoo (CA)	8104	1505 LHOB

Republicans

Jim Sensenbrenner, Jr. (WI) RMM	5101	2332 RHOB
Dana Rohrabacher (CA)	2415	1027 LHOB
Dick Zimmer (NJ)	5801	228 CHOB
Sam Johnson (TX)	4201	1030 LHOB
*Martin R. Hoke (OH)	5871	212 CHOB
*Ed Royce (CA)	4111	1404 LHOB
*Jennifer Dunn (WA)	7761	1641 LHOB
*Steven H. Schiff (NM)	6316	1009 LHOB
*Ken Calvert (CA)	1986	1523 LHOB

* Denotes New Subcommittee Member

HOUSE
COMMITTEE ON SCIENCE, SPACE, AND TECHNOLOGY

Committee on Science, Space, and Technology
2321 Rayburn House Office Building
Washington, DC 20515
(202) 225-6371

(202) 225- Address

Democrats

George E. Brown, Jr. (CA) CHRM	6161	2300 RHOB
Marilyn Lloyd (TN)	3271	2406 RHOB
Dan Glickman (KS)	6216	2371 RHOB
Harold L. Volkmer (MO)	2956	2409 RHOB
Ralph M. Hall (TX)	6673	2236 RHOB
Dave McCurdy (OK)	6165	2344 RHOB
Tim Valentine (NC)	4531	2229 RHOB
Robert G. Torricelli (NJ)	5061	2159 RHOB
Rick Boucher (VA)	3861	2245 RHOB
James A. Traficant, Jr. (OH)	5261	2446 RHOB
James A. Hayes (LA)	2031	2432 RHOB

John Tanner (TN)	4714	1009 LHOB
Glen Browder (AL)	3261	1221 LHOB
Pete Geren (TX)	5071	1730 LHOB
Jim Bacchus (FL)	3671	432 CHOB
Tim Roemer (IN)	3915	415 CHOB
Bud Cramer (AL)	4801	1318 LHOB
Dick Swett (NH)	5206	230 CHOB
*James A. Barcia (MI)	8171	1719 LHOB
*Herbert C. Klein (NJ)	5751	1728 LHOB
*Eric D. Fingerhut (OH)	5731	431 CHOB
*Paul McHale (PA)	6411	511 CHOB
*Jane Harman (CA)	8220	325 CHOB
*Don Johnson (GA)	4101	226 CHOB
*Sam Coppersmith (AZ)	2635	1607 LHOB
*Anna G. Eshoo (CA)	8104	1505 LHOB
*Jay Inslee (WA)	5816	1431 LHOB
*Eddie Bernice Johnson (TX)	8885	1721 LHOB
*David Minge (MN)	2331	1508 LHOB
*Lynn C. Woolsey (CA)	5161	439 CHOB
*Nathan Deal (GA)	5211	1406 LHOB
*Robert C. Scott (VA)	8351	501 CHOB
*Xavier Becerra (CA)	6235	1710 LHOB

Republicans

Robert S. Walker (PA) RMM	2411	2369 RHOB
F. James Sensenbrenner, Jr. (WI)	5101	2332 RHOB
Sherwood L. Boehlert (NY)	3665	1127 LHOB
Tom Lewis (FL)	5792	2351 RHOB
Paul B. Henry (MI)	3831	1526 LHOB
Harris W. Fawell (IL)	3515	2342 RHOB
Constance A. Morella (MD)	5341	223 CHOB
Dana Rohrabacher (CA)	2415	1027 LHOB
Steven H. Schiff (NM)	6316	1009 LHOB
Joe Barton (TX)	2002	1514 LHOB
Dick Zimmer (NJ)	5801	228 CHOB
Sam Johnson (TX)	4201	1030 LHOB
*Ken Calvert (CA)	1986	1523 LHOB
*Martin R. Hoke (OH)	5871	212 CHOB
*Nick Smith (MI)	6276	1708 LHOB
*Ed Royce (CA)	4111	1404 LHOB
*Rod Grams (MN)	2271	1713 LHOB
*John Linder (GA)	4272	1605 LHOB
*Peter I. Blute (MA)	6101	1029 LHOB
*Jennifer Dunn (WA)	7761	1641 LHOB
*Bill Baker (CA)	1880	1724 LHOB
*Roscoe G. Bartlett (MD)	2721	312 CHOB

SENATE
 COMMITTEE ON APPROPRIATIONS
 SUBCOMMITTEE ON VA - HUD - INDEPENDENT AGENCIES

Subcommittee on VA - HUD - Independent Agencies
 142 Dirksen Senate Office Building
 Washington, DC 20510
 (202) 224-7211

(202) 224- Address

Democrats:

Barbara A. Mikulski (MD) CHMN	4654	SH-320
Partick J. Leahy (VT)	4242	SR-433
J. Bennett Johnston (LA)	5824	SH-136
Frank R. Lautenberg (NJ)	4744	SH-506
J. Robert Kerrey (NE)	6551	SH-302
*Dianne Feinstein (CA)	3841	SD-367

Republicans:

Phil Gramm (TX) RMM	2934	SR-370
Alfonse M. D'Amato (NY)	6542	SH-520
Don Nickles (OK)	5754	SH-713
Christopher Bond (MO)	5721	SR-293
*Conrad Burns (ND)	2644	SD-183

SENATE
 COMMITTEE ON COMMERCE, SCIENCE, AND TRANSPORTATION

Committee on Commerce, Science, and Transportation
 508 Dirksen Senate Office Building
 Washington, DC 20510
 (202) 224-5115

(202) 224- Address

Democrats

Ernest F. Hollings (SC) CHMN	6121	SR-125
Daniel K. Inouye (HI)	3934	SH-722
Wendell H. Ford (KY)	4343	SR-173A
J. James Exon (NE)	4224	SH-528
John D. Rockefeller IV (WV)	6472	SH-109
John F. Kerry (MA)	2742	SR-421
John B. Breaux (LA)	4623	SH-516
Richard H. Bryan (NV)	6244	SR-364
Charles S. Robb (VA)	4024	SR-493
*Byron Dorgan (ND)	2551	SD-427
*Robert Krueger (TX)	5922	SH-703

Republicans

John C. Danforth (MO) RMM	6154	SR-249
Bob Packwood (OR)	5244	SR-259
Larry Pressler (SD)	5842	SH-133
Ted Stevens (AR)	3004	SH-522
John McCain (AZ)	2235	SR-111
Conrad Burns (MT)	2644	SD-183
Slade Gorton (WA)	3441	SH-730
Trent Lott (MS)	6253	SR-487
*Judd Gregg (NH)	3324	SH-513

SENATE
 COMMITTEE ON COMMERCE, SCIENCE, AND TRANSPORTATION
 SUBCOMMITTEE ON SCIENCE, TECHNOLOGY, AND SPACE

Subcommittee on Science, Technology, and Space
 427 Hart Senate Office Building
 Washington, DC 20510
 (202) 224-9360

(202) 224- Address

Democrats

John D. Rockefeller IV (WV)	6472	SH-724
*Ernest F. Hollings (SC) CHMN	6121	SR-125
John F. Kerry (MA)	2742	SR-421
Richard H. Bryan (NV)	6244	SR-364
Charles S. Robb (VA)	4024	SR-493
*Robert Krueger (TX)	5922	SH-703

* Indicates New Committee Member

SR = Russell Senate Office Building
 SD = Dirksen Senate Office Building
 SH = Hart Senate Office Building

Republicans

*Conrad Burns (MT) RMM	2644	SD-183
Larry Pressler (SD)	5842	SH-133
Trent Lott (MS)	6253	SR-487
*Judd Gregg (NH)	3324	SH-513

!!URGENT ACTION REQUIRED FOR THOSE INTERESTED IN LUNAR SCIENCE!!

Dear Colleague:

May 17, 1993

There is a fundamentally important opportunity for lunar science in the present NASA FY 94 budget before Congress, and the purpose of this letter is to alert you to actions on your part that are necessary to translate this opportunity into reality. *These actions are very time-critical and involve the LOW-COST, RAPID DATA RETURN, LUNAR SCOUT MISSIONS; it is imperative that a significant segment of the scientific community act in the very nearest future.*

Background:

*In 1992, the NASA Office of Exploration proposed two low-cost Lunar Scout missions, consulted with LExSWG and the scientific community, chose instruments, and manifested payloads. These missions are excellent examples of NASA's 'faster, cheaper, better' new way of doing business and they have been extremely well managed by the Johnson Space Center. The details of the missions have been described at several special sessions at scientific conferences, and there are abstracts describing the mission and instruments in LPSC XXIV, as well as a Dear Colleague letter from Lunar Scout Program Scientist Don Morrison that we all received early this year. "Faster, cheaper, better" means that the missions cost about \$150M, will be at the Moon in less than three years, and will have an excellent payload returning data to the Planetary Data System almost instantaneously.

*The resulting missions were rated as Excellent (the highest rating) by LExSWG and the Solar System Exploration Subcommittee in meeting the highest lunar orbital measurement objectives outlined by LExSWG (1. Global elemental composition, 2a. Global gravity, 2b. Global topography, 3. Global mineralogy, 5. Global imaging).

*Galileo Lunar Encounter data and potential Clementine data were viewed as complementary, but clearly can not achieve the highest scientific objective (1. Global elemental composition) and rank only poorly to moderately in addressing the other objectives.

*Recently, during the ongoing reorganization of NASA, the Office of Exploration was disbanded and the Lunar Scout Missions were transferred back to the Office of Space Science under Associate Administrator, Wes Huntress.

*The Lunar Scout mission concept was born under Wes Huntress' leadership in Code SL prior to being transferred to the Office of Exploration and follows a long line of pre-Apollo automated missions from that office (Ranger, Surveyor, Lunar Orbiter). While the Lunar Scouts were important precursors to the now-defunct Space Exploration Initiative (SEI), it is crucial to point out to Congress that they are fundamentally important science missions, and not tied to SEI.

*These missions are key examples of the emphasis on technology development and should be viewed as an important contribution to President Clinton's plan to provide significant scientific return while simultaneously developing and using new technology.

*Presently, the Lunar Scout missions are in the budget under the New Technology Investments and Space Station line and a total of \$2.3B has been requested for the two items with the details left TBD. When the NASA Administrator released the budget, he described "small lunar orbiters that could carry out the first post-Apollo scientific discovery flights to the Moon." Unfortunately because of the lack of knowledge of the Space Station configuration and thus the remaining money in this line, the Scouts, and any other items in this part of the budget, are not called out in the submitted budget as line items with specific budget numbers.

Summary: In contrast to almost all previous years since Apollo, the lunar science community is on the verge of completing the basic measurements necessary to provide the global geochemical, mineralogical, geological, topographic, and gravity context for the Apollo, Luna, and meteorite samples and related data. It goes without saying that these data will breathe new life into one of the most fundamental laboratories for the study of comparative planetology in the Solar System. We have waited over twenty years to obtain the global context and coverage that will permit us to make major new advances in lunar and planetary science.

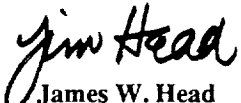
(over)

Concerns and Actions:


1. Because these missions were switched very recently from the Space Exploration Initiative back to Code S and SL, **it is imperative to let NASA Administrator Dan Goldin know, and to reiterate to Wes Huntress (Associate Administrator for Space Science) and Bill Piotrowski (Acting Head of the Solar System Exploration Division) that the Lunar Scout Missions are very important to the scientific community and that they should be supported in the FY 94 budget.** Key items to mention are the scientific merit and the fact that there is a large number of investigators supporting the mission concept and utilizing the returned data. Don't assume that your views are known!

2. Because the budget is so inexplicit in detail due to the Space Station redesign effort, most members of Congress are not fully aware of the opportunity that the Lunar Scouts present. In addition, there are many new members of Congress, and they need to be informed of the significance of these missions. **It is imperative to write your Congressional delegation and the leaders and members of the key Congressional committees to let them know of the significance of lunar science and the Lunar Scout missions.** This will let them know that there is a constituency, and that there is something really important to do with the money remaining after the Space Station redesign. Following is a list of possible points that you might mention.

Please let JWH know (Internet: Head@pggipl.geo.brown.edu - Telephone 401-863-2526 - FAX 401-863-3978) if we can provide any further information and please send copies of any letters that you write. Remember, without these letters, these missions will not happen!


James W. Head
Brown University


Carle Pieters
Brown University


Malcolm Rutherford
Brown University


E. Marc Parmentier
Brown University

Some Characteristics and Benefits of Lunar Scout Missions:

*The Moon is a cornerstone in comparative planetology made even more valuable by the samples returned from known and well characterized landing sites.

*There have been no dedicated lunar polar orbital missions in the last 20 years.

***Lunar Scout:**

- Provides global elemental, mineralogical, image, topographic and gravity data.
- Provides context for existing data from Apollo and Luna missions and lunar meteorites.
- Permits fundamental questions of lunar formation and evolution to be addressed.
- Allows us to fully utilize the existing lunar sample collection.
- Allows real synthesis of lunar geochemical, geological, and geophysical data.
- Provides an important basis for asking the next level of scientific questions about the Moon and formulating the important measurement requirements and mission strategies.
- Provides the data base to consider the next appropriate level of human lunar exploration.
- Provides a basis for the development of small high-technology experimental missions to the Moon.
- Achieves first-order scientific objectives and measurement requirements not met by the Galileo Lunar Encounters and Clementine.

*The data from Lunar Scouts will go to the Planetary Data System and be available to the full scientific community virtually immediately.

*NASA will very likely have a Lunar Data Analysis Program for these data.

*The Lunar Scouts meet all the criteria for new NASA missions: they are small, low cost, have focused science objectives, develop new technology, can be ready rapidly, and are of short duration.

*A new start in FY 94 could result in a spacecraft orbiting the Moon in 2.5 years and a second spacecraft there in another six months.

*The Lunar Scouts are supported by the scientific community and advisory panels (LExSWG, SSES).

*The lunar science community consists of a large number of individuals in many different disciplines (sample studies, geochemistry, petrology, mineralogy, geology, geophysics, remote sensing, etc.).

!!URGENT ACTION REQUIRED FOR THOSE INTERESTED IN LUNAR SCIENCE!!

Apennine Front Revisited: Diversity of Apollo 15 Highland Rock Types

Marilyn M. Lindstrom*

Code SN2, NASA Johnson Space Center, Houston, TX 77058

Ursula B. Marvin

Harvard-Smithsonian Center for Astrophysics, Cambridge, MA 02138

Scott K. Vetter and John W. Shervais

Department of Geology, University of South Carolina, Columbia, SC 29208

*Also at Department of Earth and Planetary Sciences, Washington University, St. Louis, MO 63130

PREV. ANN
89A 10863

The Apollo 15 landing site is geologically the most complex of the Apollo sites, situated at a mare-highland interface within the rings of two of the last major basin-forming impacts. Few of the Apollo 15 samples are ancient highland rocks derived from the early differentiation of the Moon, or impact melts from major basin impacts. Most of the samples are regolith breccias containing abundant clasts of younger volcanic mare and KREEP basalts. The early geologic evolution of the region can be understood only by examining the small fragments of highland rocks found in regolith breccias and soils. Geochemical and petrologic studies of clasts and matrices of three impact melt breccias and four regolith breccias are presented. Twelve igneous and metamorphic rocks show extreme diversity and include a new type of ferroan norite. Twenty-five samples of highland impact melt are divided into groups based on composition. These impact melts form nearly a continuum over more than an order of magnitude in REE concentrations. This continuum may result from both major basin impacts and younger local events. Highland rocks from the Apennine Front include most of the highland rock types found at all of the other sites. An extreme diversity of highland rocks is a fundamental characteristic of the Apennine Front and is a natural result of its complex geologic evolution.

INTRODUCTION

The Apollo 15 landing site is at the interface between the mare basalts of Palus Putredinus, which are exposed at Hadley Rille, and the highlands of the Apennine Front, exposed at Hadley Delta (ALGIT, 1972). The Apennine Front represents the rim of the Imbrium basin, but also falls within the Serenitatis basin (Spudis and Ryder, 1985). Highlands materials at the Front are therefore expected to consist of Imbrium ejecta overlying Serenitatis ejecta and possibly pre-Serenitatis materials (Spudis, 1980). Although some of the returned samples are rocks from the ancient highland crust or melt breccias representing major basin impacts, most of the samples are younger mare and KREEP basalts or regolith breccias, which are complex mixtures of lithic fragments, glasses, and soils (A15PET, 1972; Chamberlain and Watkins, 1972). The Apollo 15 Workshop (Spudis and Ryder, 1986) focused attention on the unsolved problems of the provenance and petrogenesis of Apollo 15 samples. Numerous research projects, including this one, were undertaken to resolve the unanswered questions at the Hadley-Apennine site. Results of some of those studies have already been published (Korotev, 1987a; Ryder, 1987; Ryder and Spudis, 1987; Simon et al., 1986). This volume contains reports of several other studies. This paper presents petrologic and compositional studies of matrices and clasts from seven Apollo 15 polymict breccias, which demonstrate the diversity of rock types at the site in comparison with rocks found at other sites.

CHARACTERIZATION OF APENNINE FRONT HIGHLAND ROCKS

Sampling and Analytical Procedures

This paper presents the results of a survey of Apennine Front slabs from two regolith breccias: 15459, from the Apennine Front (Lindstrom and Marvin, 1987), and 15498, from the mare plain (Vetter et al., 1987a). Sampling techniques and experimental procedures of the three studies differ.

Six polymict breccias collected at Station 7 on the Apennine Front were chosen to survey the materials at the Front. These included three regolith breccias (15426, 15435, 15459) and three impact melt breccias (15405, 15445, 15455). The impact melt breccias were studied previously by Ridley (1977; Ridley et al., 1973) and by the Imbrium Consortium (Wood, 1976). Ryder and Bower (1977) described the black and white breccias (15445, 15455) as LKFM impact melts containing clasts of Mg-suite plutonic rocks. Sufficient major and trace element analyses of these clasts were available (Ryder, 1985), so no new clast studies were done. Further characterization of the bulk compositions of the impact melt matrices was done on three matrix splits from each breccia. Breccia 15405 was described by Ryder (1976) as an impact melt rock consisting of KREEP basalt and its differentiates. He identified its most conspicuous clasts as quartz monzodiorite, and they have since been studied extensively (Nyquist et al., 1977; Taylor et al.,

TABLE 1. Compositional and petrographic characterization of samples.

Generic	INAA*	Pet [†]	Type [‡]	Composition/Texture
15405	170	170	C	Plutonic alkali norite
	171	9010	C	LKFM/ungrouped impact melt
	173		M	KREEP/A impact melt
	174		M	KREEP/A impact melt
	175		M	KREEP/A impact melt
	181	9009	C	Cataclastic alkali anorthosite
15426	137	9010	C	Plutonic Mg-troctolite
15435	54-1		C	LKFM/B impact melt
	54-2		C	LKFM/B impact melt
15445	244		M	LKFM/D impact melt
	245		M	LKFM/D impact melt
	246		M	LKFM/D impact melt
15455	258		M	LKFM/D impact melt
	259		M	LKFM/D impact melt
	260		M	LKFM/D impact melt
15459	231	231-2	C	LKFM/E impact melt
	231W	9008	C	Cataclastic Mg-anorthosite
	237	237	C	MKFM green glass
	238	9012	C	Granular Fe-anorthositic norite
	239A	9009	C	Contaminated Fe-anorthosite
	239W	9010	C	LKFM/D impact melt
	241		C	KREEP/A impact melt
	242	9011	C	KREEP/A impact melt
	274	337	C	Cataclastic Fe-anorthosite
	279	339	C	Granular Fe-norite
	286	340	C	LKFM/D impact melt
	288	289	C	Fe-granulitic breccia
	290	342	C	LKFM/A impact melt
	292	343	C	Granular Fe-norite
	305	345	C	LKFM/B impact melt
	309	346	C	Mg-poikilitic granulite
	313	347	C	LKFM/B impact melt
	315	316	C	Quartz monzodiorite
	317	318	C	LKFM/ungrouped impact melt
		320	348	C
	329	349	C	LKFM/B impact melt
15498	158	236	C	MKFM green glass
	192	193	C	LKFM/C impact melt
	209	210	C	LKFM/C impact melt

*INAA subsample number.

[†]Thin section subsample number.[‡]Clast (C) or matrix (M) sample.

1980). We analyzed three splits of matrix and three white clasts, none of which had been studied previously.

The regolith breccias included two friable clods (15426 and 15435) and one brown glass matrix breccia (15459). 15426 consists mostly of primitive mare green glass (Delano, 1979; Ma et al., 1981; Ryder, 1985). We analyzed a bulk sample

of the clod and two clasts. Only one of the clasts is a highland rock. Results for the mare materials will be presented elsewhere. 15435 was the pedestal for anorthosite 15415. We analyzed a bulk sample and two coherent clasts. Brown glass matrix breccia 15459 was the largest highland rock returned from the Apollo 15 site. It contains two large clasts, a 5-cm

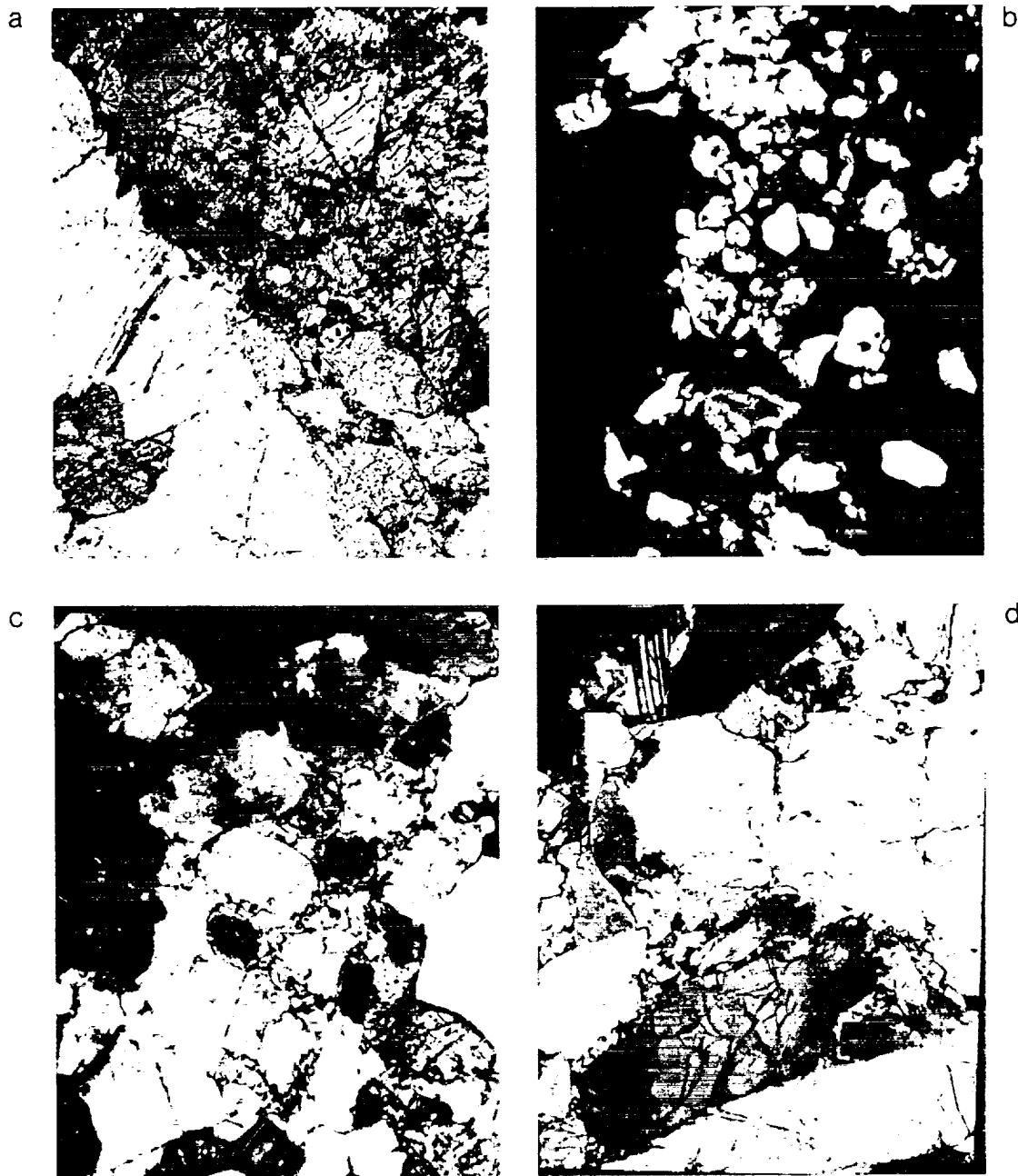


Fig. 1. Photomicrographs of igneous and metamorphic rocks (field of view approximately 1 mm for each photo). (a) Ferroan anorthosite 15459,337 (partially cross-polarized light) showing cataclastic texture, crushed mosaic grains without granulitic recrystallization. Note offset of twin lamellae. (b) Ferroan noritic anorthosite 15459,239a (cross-polarized light) showing crushed granular texture and matrix contamination. (c) Ferroan anorthositic norite 15459,238 (cross-polarized light) showing blocky plagioclase grains with intergranular pyroxene. (d) Magnesian troctolite 15426,137 (cross-polarized light) showing large blocky olivine grains with scattered twinned plagioclase. (e) Magnesian anorthosite 15459,231w (crossed polarized light) showing strained coarse plagioclase and exsolved pyroxene in granular groundmass. (f) Alkali anorthosite 15405,181 (cross-polarized light) showing large blocky plagioclase grains in granular groundmass. Note large exsolved pyroxene grain at left. (g) Alkali gabbronorite 15405,170 (cross-polarized light) showing coarse grains of plagioclase and pyroxene. (h) Quartz monzodiorite 15459,316 (backscattered electron image, field of view 4 microns) showing exsolved pyroxene and interstitial minerals. (i) Ferroan norite 15459,339 (partially cross-polarized light) showing cataclastic texture and lack of recrystallization of plagioclase (gray to white) and pyroxene (bright with dark rims). (j) Ferroan norite 15459,343 (transmitted light) showing coarse igneous texture offset along a fault plane indicated by arrows. The plagioclase (white) is granulitic, the darker material is predominantly orthopyroxene. (k) Granulite 15459,289 (partially polarized light) showing fine-grained granular recrystallized texture. (l) Poikilitic granulite 15459,346 (Partially polarized light) showing coarse poikilitic texture.

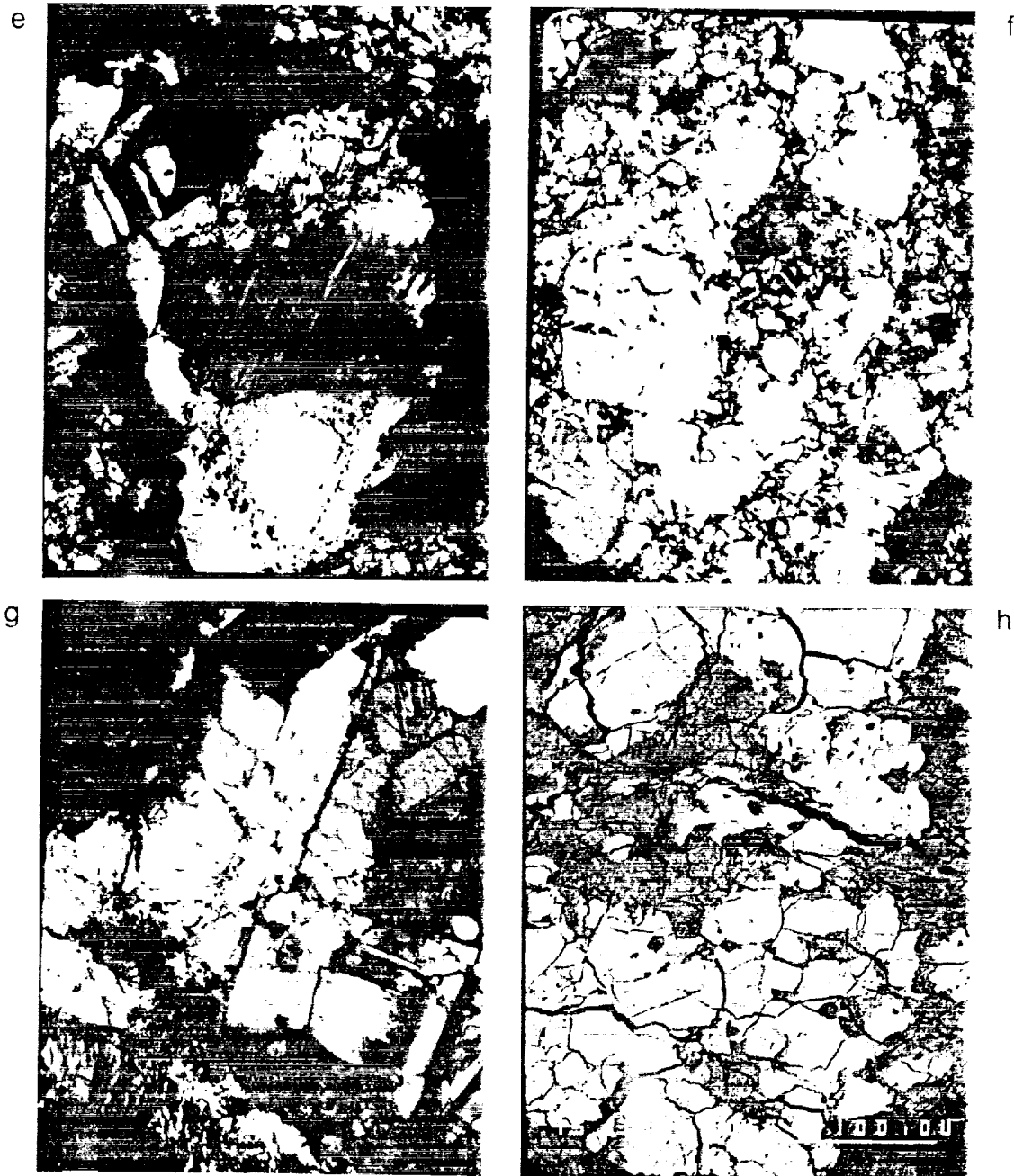


Fig. 1. (continued)

greenish mare basalt and a 3 cm white highland clast. The brief petrographic description (Ridley, 1977), and comparison of its bulk composition to those of other Apollo 15 regolith breccias (Korotev, 1985 and unpublished data), suggested that clasts of highland plutonic and impact melt lithologies might be more abundant than in other breccias. We selected 14 samples of clasts and matrix of 15459 for analysis.

The Apennine Front survey samples were analyzed by INAA at Washington University using the procedures of Korotev (1987c). Selected samples were later analyzed at the University of Missouri, Columbia for short-lived isotopes. Most of these

samples were then thin-sectioned for petrographic studies. Petrographic characterization and microprobe analyses of 15405 clasts were done by Shervais and Vetter. Similar studies of the 15426 clast were done by D. Mittlefehldt at JSC (personal communication, 1987), while studies of 15459 clasts were done by Marvin.

The initial study of breccia 15459 was sufficiently productive that a consortium study of a slab was initiated by Lindstrom. The slab was mapped by Marvin and samples selected for extraction. Larger clasts were split for thin sections and INAA. Petrographic characterization was done by Marvin using a

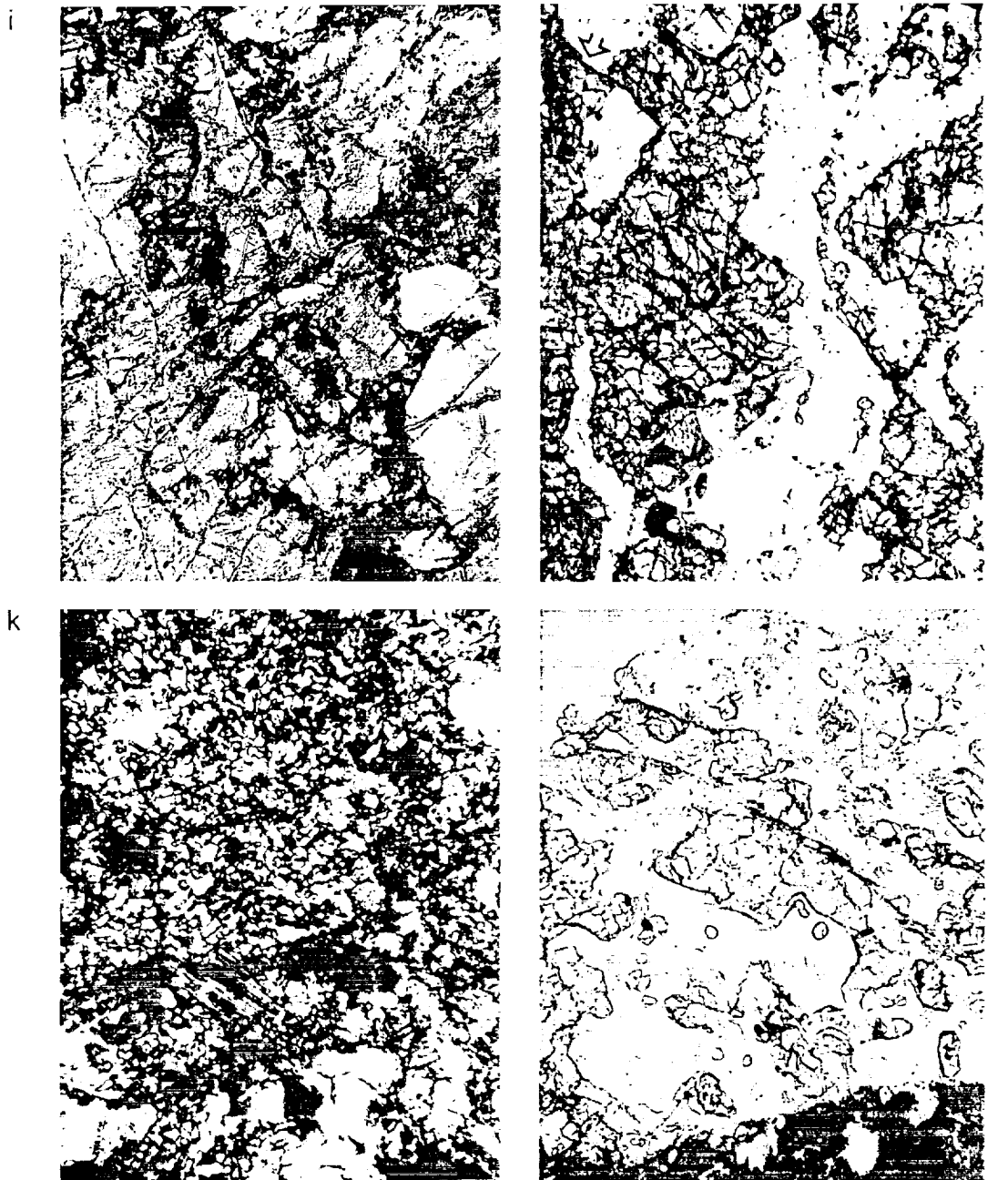


Fig. 1. (continued)

JEOL733 microprobe. Trace element analyses were done by INAA at Washington University. Major element analyses of two clasts (15459,279 and ,292) were determined by Shervais and Vetter using microprobe analyses of fused beads.

Consortium study of breccia 15498 from Station 4 on the mare plain was organized by Shervais, who mapped the slab and selected clasts. Studies of the mare clasts are reported in Vetter *et al.* (1987b). Analyses of three highland clasts from this mare breccia are reported here. The clasts were split for thin sectioning prior to analysis. Petrographic studies were done by Shervais and Vetter. Splits for bulk analyses were ground

and split again for major element analysis of fused beads and INAA, which was done at JSC using the procedures of Jacobs *et al.* (1977).

Table 1 presents a brief petrologic and compositional characterization of each of the samples. Samples are listed in Table 1 by generic sample number. When a clast was split for duplicate analyses it is listed only once, but both analyses are given later. When a polymict sample was separated into several lithologies, they are listed separately in Table 1. Detailed discussions in the following sections are organized by rock classification based on a combination of compositional and

petrographic characteristics. This paper describes clasts of highland origin and includes 12 igneous and metamorphic rocks, 25 melt breccias, and 2 glasses. Studies of seven clasts of mare origin will be reported elsewhere.

Igneous and Metamorphic Rocks

Twelve clasts of highland crustal rocks are characterized in the following section. Ten of the rocks have at least relict plutonic textures, while two are more recrystallized metamorphic rocks. Photomicrographs of these clasts are shown in Fig. 1. Major mineral compositions are compared to previously defined fields for pristine rocks in Fig. 2, a plot of Mg' in mafic minerals versus An in plagioclase (Warren *et al.*, 1983; Lindstrom *et al.*, 1984). Bulk compositions of the clasts are presented in Table 2. Many of the clasts are examples of familiar rock types. There are plutonic samples belonging to ferroan, magnesian, and alkali suites of highlands rocks. One rock is a highly differentiated quartz monzodiorite. Metamorphic rocks are lunar granulites similar to those found at all highland sites and in the lunar meteorites (Warner *et al.*, 1977; Lindstrom and Lindstrom, 1986). Two clasts are plutonic-textured ferroan norites with mineral compositions falling between the fields of the familiar pristine rock suites. These are discussed in detail here, while petrographic and compositional characteristics of rocks belonging to the familiar suites are only briefly summarized and compared to other examples of similar rock types.

Ferroan anorthositic rocks. Three of the clasts are ferroan anorthosites. Cataclastic anorthosite 15459,274/337 has a coarse-grained (up to 1.5 mm) mosaic texture (Fig. 1a), consisting almost entirely of plagioclase of uniform composition (An_{97}). Minute (1 micron) inclusions of pyroxene ($En_{66}Fs_{32}Wo_2$; $En_{44}Fs_{11}Wo_{45}$) occur in the plagioclases, and tiny interstitial grains of ilmenite are also present. The bulk composition of this anorthosite is very nearly that of pure plagioclase. Concentrations of transition metals, incompatible elements, and meteoritic siderophiles are all very low. The REE pattern (Fig. 3a) shows the low concentrations and positive Eu anomaly characteristic of plagioclase. The bulk and mineral compositions of this anorthosite are similar to those of 15415 (James, 1972; Haskin *et al.*, 1981), but its texture shows less recrystallization and annealing.

Clast 15459,239a is a cataclastic anorthosite with a small amount of matrix contamination. The thin section contains numerous mineral and lithic fragments, most of which are plagioclase (Fig. 1b). Some plagioclase fragments are crushed, others have a fine-grained granulitic texture. Scattered mafic minerals are found in small patches of matrix contamination and not associated with the bulk of the plagioclase. The bulk composition reflects the matrix contamination in its lower Al_2O_3 and CaO concentrations and higher transition metal and incompatible element concentrations. The REE pattern (Fig. 3a) is flat, with a positive Eu anomaly and concentrations higher than those of most mafic anorthosites. However, the plagioclase-dominated REE pattern limits matrix contamination to a few percent.

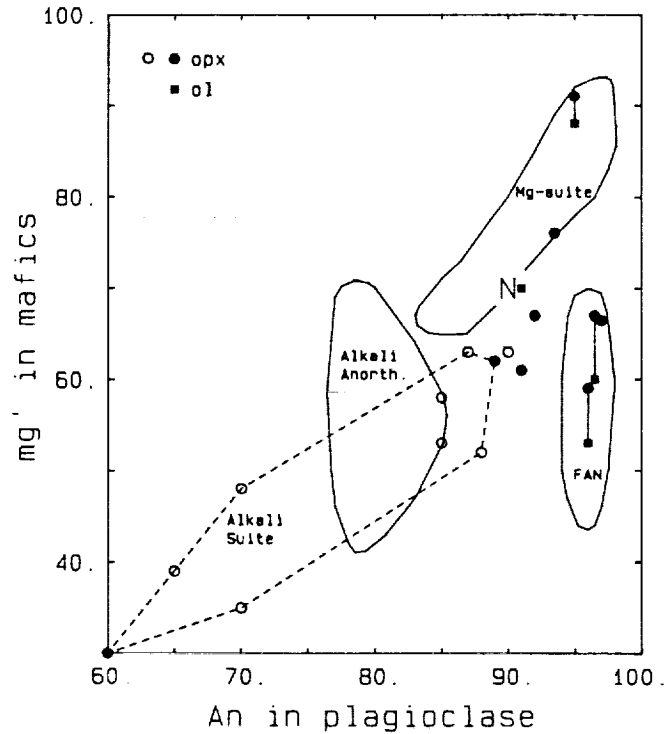


Fig. 2. Compositions of major minerals in igneous and metamorphic rocks compared to those of pristine rocks (Warren *et al.*, 1983). Plotted are $Mg' = [Molar\ Mg/(Mg + Fe) \times 100]$ versus $An = [Molar\ Ca/(Ca + Na) \times 100]$ for Apennine Front samples. Shaded symbols are from this study, open symbols represent other related rocks: ferroan norites (Ridley, 1977); alkali gabbroanorthosites (James *et al.*, 1987); and quartz monzodiorite (Ryder, 1976). Alkali norite, gabbroanorthosite, and quartz monzodiorite define a new alkali-suite field. Ferroan norites plot at the extension of this field. Ferroan norites plot at the extension of this field. N is Apollo 17 norites.

Clast 15459,238 is a cataclastic anorthositic norite consisting of 61% plagioclase, 29% pyroxene, and 10% olivine with accessory Al-Ti-Mg-chromite and Mg-ilmenite. Plagioclase ($An_{95.98}$) occurs predominantly in grains up to 1.4 mm long that have been crushed and partially randomized optically. Other patches of plagioclase approach granulitic texture (Fig. 1c). Irregular grains of pyroxene, up to 600 microns across, show fine exsolution lamellae with compositions of $En_{67}Fs_{31}Wo_2$ and $En_{41}Fs_{13}Wo_{46}$. Olivine (dominantly $Fo_{59.61}$) occurs in individual grains, up to 100 microns long, that are brownish-orange in color. Although crushed and partially recrystallized, the relict texture of this rock indicates a plutonic origin. The bulk composition is that of a mafic anorthosite. Concentrations of transition metals are three to four times higher than 15459,239a mafic anorthosite, but LREE concentrations are lower and reflect little or no contamination (Fig. 3a). The composition and texture of this plutonic anorthositic norite are similar to those of 15243,17 (Ryder *et al.*, 1987). The composition is almost identical to that of 15418, the large severely shocked and recrystallized

TABLE 2. Compositions of Apennine Front igneous and metamorphic rocks.

	Ferroan Anorthosites			Mg-suite		Alkali Suite			Ferroan Norites		Metamorphic	
	FA	FAN	FAN	Mgt	MgA	AA	AN	QMD	FN	FN	GRAN	POIK
	15459	15459	15459	15426	15459	15405	15405	15459	15459	15459	15459	15459
	,274	,239a	,238	,137	,231w	,181	,170	,315	,279	,292	,288	,309
TiO ₂ (%)			0.17	0.31	0.48		0.36					
Al ₂ O ₃		27.8	24.2	12.7	30.7	30.4	24.4		24.4	30.4		
FeO	0.226	1.71	6.27	7.47	1.51	0.302	4.30	12.9	6.88	10.9	4.22	5.82
MgO		1.5	6.1	31.3	1.8	1.0	4.4					
CaO	19.0	17.0	15.1	5.8	17.4	17.6	16.4	11.3	13.1	10.9	16.3	12.6
Na ₂ O	0.334	0.452	0.297	0.177	1.02	1.81	0.91	0.86	0.607	0.525	0.384	0.578
K ₂ O			<12	<14	<7							
Sc (ppm)	0.676	3.46	11.92	5.41	3.53	0.591	9.25	29.6	9.84	18.6	6.60	7.17
Cr	26.0	520	740	630	170	5.6	570	1180	2730	2360	390	660
Co	0.235	6.60	14.4	38.9	5.05	0.36	18.0	10.0	26.4	30.1	6.09	18.0
Ni	<6	145	65	110	35		<50	<40	28	51	<40	88
Rb	0.36	<8		<10	<3	<2	5	46	<9	9	<4	<7
Sr	170	150	150	80	340	580	230	190	160	120	170	170
Cs	0.097	0.52	0.11	0.05	0.14	0.19	0.26	1.25	0.12	0.13	0.034	0.073
Ba	7.2	80	28	180	140	180	890	1100	140	110	30	160
La	0.183	2.16	1.43	17.1	8.03	15.1	470	108	5.77	4.46	2.36	8.35
Ce	0.47	6.10	3.80	38.3	19.7	39.2	1254	280	16.6	14.5	6.26	20.7
Nd		2.37	2.00	15.7	9.4	24.0	780	160	7.7	5.5	4.1	13
Sm	0.105	0.84	0.71	4.10	2.72	7.08	213	47.2	2.29	2.98	1.12	3.41
Eu	0.80	0.94	0.74	1.23	2.37	4.85	4.00	2.26	1.40	1.78	0.820	1.34
Tb	0.143	0.151	0.166	0.80	0.53	1.48	42.0	10.7	0.59	1.03	0.224	0.74
Yb	0.052	0.63	0.61	5.69	1.24	2.08	94.0	36.9	2.33	5.15	0.750	2.80
Lu	0.0069	0.112	0.104	1.00	0.187	0.320	11.9	5.07	0.361	0.775	0.119	0.448
Zr	<6	110	<80	1030	50	80	220	1510	120	50	40	100
Hf	0.029	1.65	0.55	22.9	1.42	2.29	11.0	36.5	2.63	1.05	0.74	2.65
Ta	0.0045	0.12	0.37	2.73	0.216	0.08	0.96	4.77	0.48	0.058	0.110	0.395
Th	0.0048	0.23	0.14	2.4	0.76	0.53	39.4	22.3	1.23	0.15	0.258	0.83
U	<0.01	0.06	<0.7	3.64	0.21	0.07	1.6	6.4	0.60	0.05	0.064	0.17
Ir (ppb)	<1	<2	1.8	<2	<2	<1	<3	<4	<2	<2	<2	<3
Au	<1	<2	<1	<1	<1	<1	<6	<7	<2	<2	<2	<2

Analyses by INAA, one sigma uncertainties based on counting statistics are: 1-2% for Al₂O₃, FeO, Na₂O, Sc, Cr, Co, La, Sm, Eu; 3-10% for CaO, Sr, Ba, Ce, Tb, Yb, Lu, Hf, Ta, Th; 10-40% for TiO₂, MgO, K₂O, Ni, Cs, Nd, U, (Ir, Au).

anorthositic gabbro (A15PET, 1972). This similarity in composition supports suggestions by Nord *et al.* (1977) and Lindstrom and Lindstrom (1986) that 15418 is a metamorphosed plutonic rock.

Magnesian suite rocks. Clast 15426,137 is a magnesian troctolite. It is a coarse-grained plutonic rock (Fig. 1d) consisting of 65% olivine (Fo₈₈), 35% plagioclase (An₉₅), minor pyroxene and chromite, and accessory Fe-metal and apatite. The olivine is orange, with the color intensifying toward the margins of crystals. However, the cores and rims show no difference in composition that might reflect alteration. Rare pyroxene occurs as interstitial grains of orthopyroxene (En₈₈) and augite (En₄₉Fs₄Wo₄₇). The bulk composition of the clast is highly magnesian with high concentrations of Co and Ni, which are incorporated into olivine, but not Sc and Cr, which enter pyroxene or chromite. The REE pattern is unusual for such a magnesian rock (Fig. 3a). Concentrations are high for a Mg-troctolite and the pattern has an unusual U-shape. The presence of accessory apatite, which was observed in thin section, and zircon, not observed but undoubtedly the cause of high Zr and Hf concentrations, account for the unusual

REE pattern. Other clasts of Mg-suite troctolite were found in impact melt breccias 15445 and 15455 (Ryder and Bower, 1977; Ryder, 1985). These show large variations in major and REE abundances due to variations in proportions of both major and accessory phases.

15459,231w is a magnesian anorthosite. The thin section of the sample analyzed by INAA is essentially a grain mount (Fig. 1e). It consists mainly of plagioclase (An₉₀₋₉₃) with scattered olivines (Fo₆₉₋₇₂) and clinopyroxenes (En₄₇Fs₁₁Wo₄₂). Mineral compositions are more evolved than those of Apollo 14 magnesian anorthosites (Lindstrom *et al.*, 1984) and more similar to those of Mg-norites than Mg-troctolites. The bulk composition is similar to those of slightly mafic magnesian anorthosites. The REE pattern is like that of REE-poor Apollo 14 magnesian anorthosites (Lindstrom *et al.*, 1984), but falls between those of Mg-troctolite 15426,137 and Mg-norites and troctolites from 15445-15455 (Fig. 3a). Simon *et al.* (1987) report mineral compositions, but no bulk composition, for a Mg-anorthosite fragment.

Clasts of Mg-suite norites are also found at the Apennine Front, notably as clasts in the black and white breccias 15445-

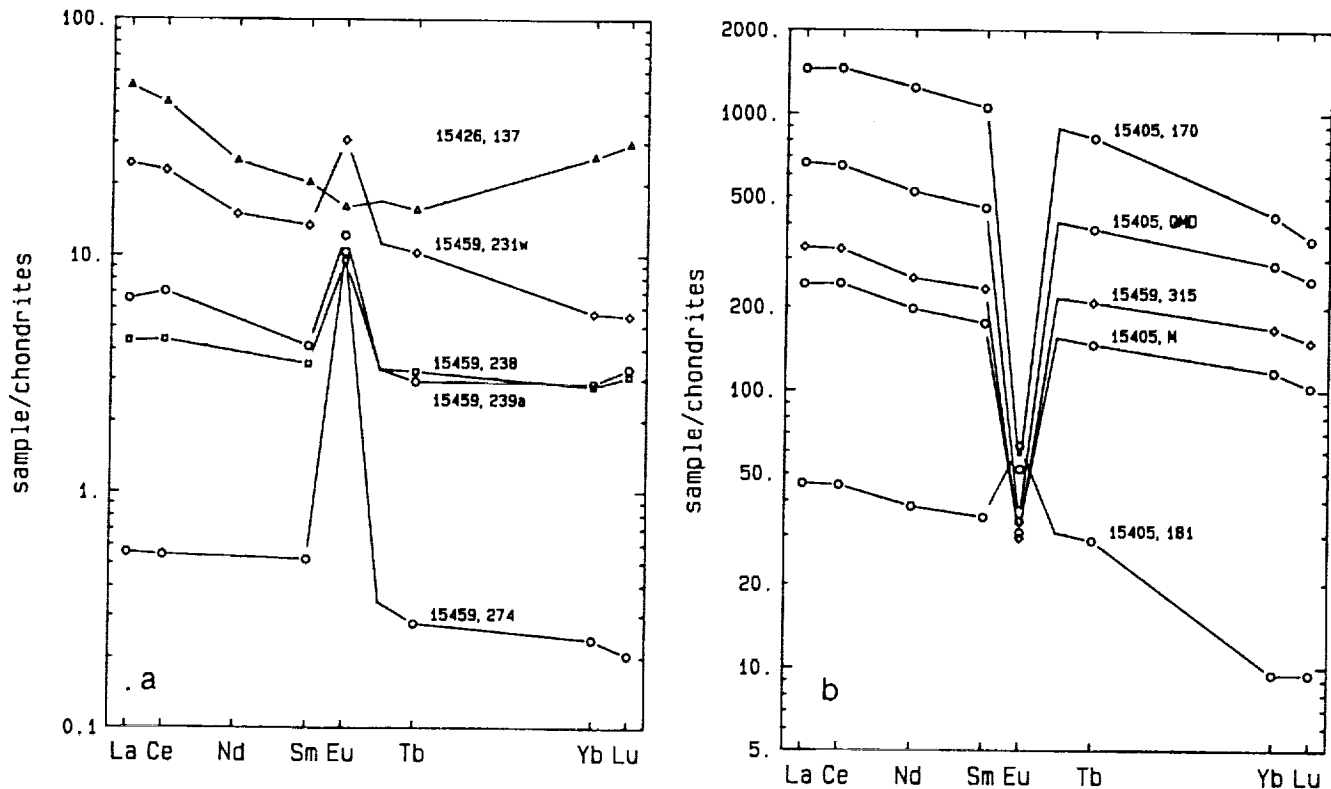


Fig. 3. Chondrite-normalized REE patterns for Apennine Front samples. (a) Ferroan anorthosites and Mg-suite rocks. Ferroan anorthositic rocks have low REE concentrations with large positive Eu anomalies, while magnesian anorthosite has a plagioclase pattern with much higher concentrations and a smaller Eu anomaly. Mg-troctolite has a REE-enriched pattern with unusual U-shape. (b) Alkali-suite rocks. Samples include clasts and matrix for 15405 and QMD 15459,315 compared with literature data for 15405 QMD clast (Nyquist *et al.*, 1977). Alkali anorthosite 15405,181 is similar to Apollo 14 alkali anorthosites in composition. Alkali norite 15405,170 has twice the REE concentrations as 15405 QMD clast. (c) Ferroan norites. Data for ferroan norites 15459,279 and ,292 are compared to literature data for 15405 QMD clast (Nyquist *et al.*, 1977). (d) Impact melt rocks. Means of individual analyses of representative melt rocks from this study are plotted as points. Ranges of analyses for each group are plotted and show the continuum of melt compositions in B-C-D region.

15455. Analyses of these clasts are reported by Ridley (1977; Ridley *et al.*, 1973), Blanchard *et al.* (1976), and Warren and Wasson (1978, 1979, 1980). Other clasts have been found in Apennine Front regolith breccias 15306, 15465, and 15565. These clasts tend to be fairly feldspathic norites with 20-25% Al_2O_3 and REE concentrations lower than those of the troctolite presented here.

Alkali suite rocks. Three clasts are members of the alkali suite. These include an alkali anorthosite, an alkali norite, and a quartz monzodiorite. 15405,181 is a cataclastic alkali anorthosite. The sample consists almost entirely of plagioclase (An_{84}) with large relict twinned grains (up to 0.6 mm) in a matrix of granulated plagioclase. Minor ilmenite and rare phosphate are the only accessory minerals, no mafic silicates were observed in thin section (Fig. 1f). The plagioclase composition falls at the Ca-rich end of the range for alkali anorthosites, but the absence of mafic silicates precludes plotting the sample in Fig. 2. The bulk composition is similar to that of other alkali anorthosites with very high concentrations of Al and Ca and very low concentrations of transition metals and siderophiles. REE concentrations are moderate, with LREE

enrichment and a positive Eu anomaly (Fig. 3b), as is observed for other alkali anorthosites (Lindstrom *et al.*, 1984).

15405,170 is a feldspathic alkali norite with plutonic texture. Cumulus plagioclase (An_{89} , up to 0.6×0.25 mm) and pigeonite ($En_{61}Fs_{37}Wo_2$ with minor exsolution of $En_{42}Fs_{15}Wo_{43}$, up to 1.0×0.4 mm) are enclosed by postcumulate plagioclase and pyroxene (Fig. 1g). Interstices between the major minerals contain an abundance of accessory minerals, including large ilmenites and small grains of Fe-metal and troilite, an intergrowth of K-feldspar and silica, zircon, ZrO_2 , and a large (300×500 micron) whitlockite. The bulk composition of the clast is that of a moderately feldspathic alkalic rock. Al_2O_3 is moderately high (24%) but transition metal concentrations are distinctly higher than in alkali anorthosites. Trace element characteristics of this clast are dependent on the amounts of accessory minerals. REE concentrations are extremely high (Fig. 3b) due to the abundance of whitlockite. Concentrations are a factor of five higher than KREEP basalt, a factor of two to five higher than quartz monzodiorite and alkali anorthosites (Warren *et al.*, 1983), and nearly as high as unique alkali anorthosite 14313c (Huskin *et al.*, 1973). Concentrations of

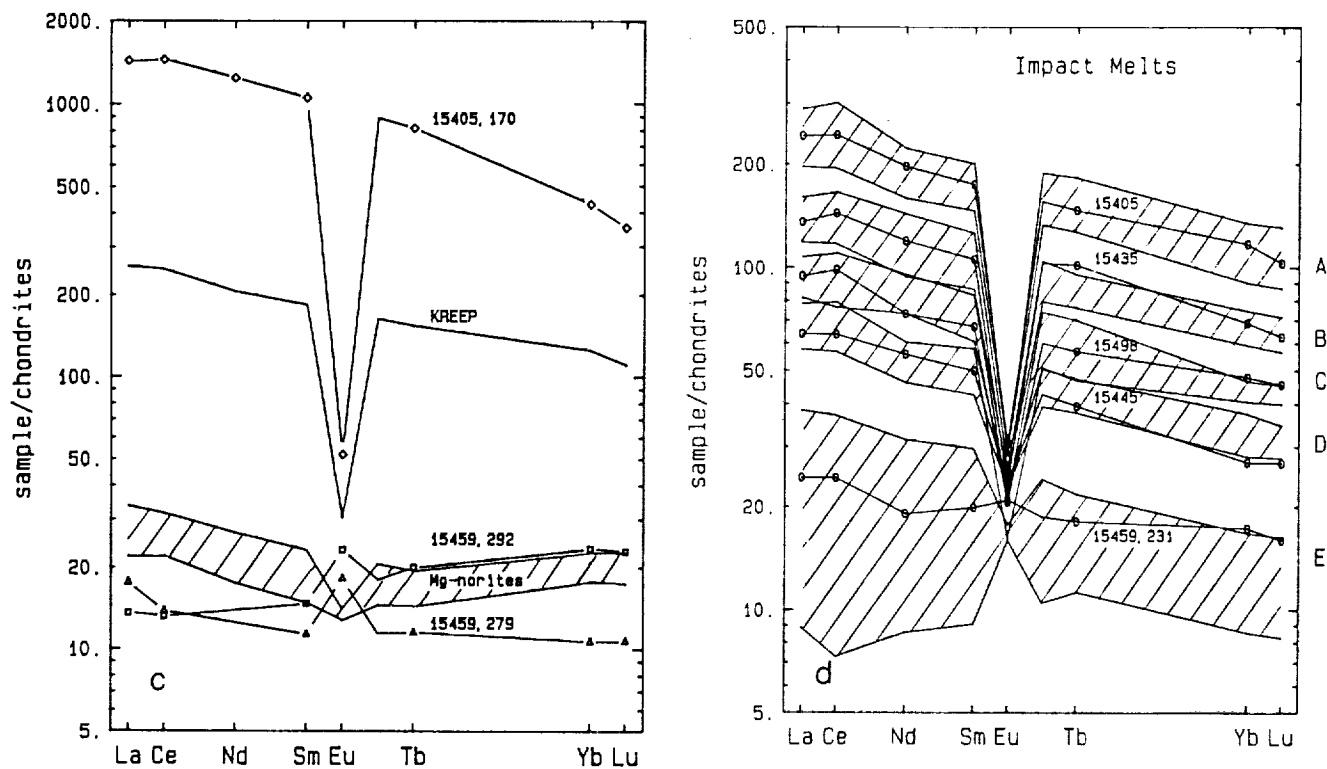


Fig. 3. (continued)

other incompatible elements are variable. Th is a factor of three enriched over KREEP basalt, while Sr and Ba are at the same level, and Rb, Cs, U, Zr, Hf, and Ta are depleted relative to KREEP basalts. This clast bears much similarity to alkali gabbronorite clasts in 67975 (*James et al.*, 1987), but it has slightly more primitive plagioclase and pyroxene compositions than the magnesian alkali gabbronorites and contains very little clinopyroxene. The high and variable trace element characteristics resemble some members of that suite.

15459,315/316 is a somewhat recrystallized quartz monzodiorite consisting of 59% feldspar, 39% pyroxene, 2% silica, and accessory ilmenite, whitlockite, and zircon. Crushing and deformation have obscured the original texture, reduced the grain size, and produced wavy extinction in both the feldspars and pyroxenes, but have not homogenized the mineral compositions (Fig. 1h). The most abundant feldspar is sodic plagioclase (An_{59-88}), but ternary feldspar ($An_{2-2}Ab_{20}Or_7$ to $An_{44}Ab_{10}Or_{46}$) and orthoclase ($An_1Ab_2Or_{97}$) are also present. Pyroxene grains have closely-spaced exsolution lamellae with end-member compositions of $En_{28}Fs_{68}Wo_4$ and $En_{23}Fs_{36}Wo_{41}$. These mineral compositions are very similar to those of quartz monzodiorite clasts in 15405 (*Ryder*, 1976). The bulk composition of our clast is somewhat more mafic than that of the 15405 clasts (*Ryder*, 1985), and a factor of two lower in REE concentrations (Fig. 3b).

These three clasts are the first true alkali suite clasts reported from Apollo 15. Two of the clasts were found in KREEP impact melt breccia 15405. *Ryder* (1976) describes KREEP basalts, quartz monzodiorite, and granite clasts in that breccia. He also

mentions seeing granular anorthositic clasts in hand specimen, but not finding any in thin section. He comments on a high-K white clast analyzed by *Ganapathy et al.* (1973) and speculates on whether to assign it to the ANT suite or the KREEP basalt suite. The wide range of clast types in this breccia (KREEP basalt, alkali anorthosite, alkali norite, quartz monzodiorite, and granite) represent extrusive KREEP basalt and its plutonic equivalents and differentiates. *Ryder* (1976) recognized that the differentiates were related to the basalts, but did not identify the alkali anorthosite or norite and relate the alkali suite to KREEP basalts. The alkali suite forms an extensive differentiation trend on Fig. 2 from alkali norite through gabbronorite and anorthosite to quartz monzodiorite. Breccia 15405 provides concrete evidence for a genetic link between KREEP basalt and alkali suite plutonic rocks.

While providing important information on KREEP and alkali suite rocks, breccia 15405 is so unusual that *Ryder* [1976] considered it to be exotic to the site. *Ryder and Spudis* (1987) suggest that it is a young (1 b.y.) impact melt from the Apennine Bench. It is by no means typical of Apennine Front material. The third alkali suite rock in this study was not a clast in this unique breccia, but was instead a clast in a typical Apennine Front regolith breccia. This clast is also the first QMD clast not found in 15405, suggesting that alkali suite rocks are not as uncommon at Apollo 15 as previously assumed, and that 15405 may not be exotic. Certainly KREEP basalts are common at the Apollo 15 site (*Ryder*, 1987) and the link between alkali suite rocks and KREEP basalts would suggest that alkali suite rocks may also be present near the site.

Ferroan norites. Two ferroan norites having unusual mineral compositions were found in 15459. 15459,279/339 is a shocked and granulated norite consisting of 65% plagioclase (An_{93}), 33% pyroxene (dominantly orthopyroxene $En_{66}Fs_{32}Wo_{2}$, with rare augite $En_{42}Fs_{13}Wo_{45}$) with accessory ilmenite, chromite, silica, K-feldspar, whitlockite, zircon, and an unidentified Fe-Ca-Zr-Ti oxide. Chromite compositions cluster around $(Mg_{0.10}Fe_{0.90})(Al_{0.18}Ti_{0.07}Cr_{0.75})_2O_4$, and Mg-ilmenites around $(Mg_{0.10}Fe_{0.90})TiO_3$. Original 1-2 mm grains of plagioclase and pyroxene have been shocked and granulated to subsets of angular fragments 500 to 700 microns long, with wavy extinction (Fig. 1i).

15459,292/343 is a coarse-grained norite consisting of 50% pyroxene (dominantly orthopyroxene $En_{60}Fs_{37}Wo_{3}$, with minor augite $En_{41}Fs_{15}Wo_{44}$), 48% plagioclase (An_{91}), and accessory ilmenite, chromite, zircon, silica, K-feldspar, troilite, and metal. Individual pyroxene grains originally 1-2 mm have been granulated to blocky mosaics, and plagioclase crushed and recrystallized to granular texture. At a later stage the fabric was offset by 0.5 mm along a smoothly curving fault trace (Fig. 1j). Patches rich in silica and K-feldspar occur in the crushed zones, but most of the accessory minerals over 10 microns in size are embedded in the pyroxene. These include zircon in euhedral or subhedral crystals, chromite ($Mg_{0.12}Fe_{0.88}$) ($Al_{0.18}Ti_{0.11}Cr_{0.71}$) $_2O_4$, and ilmenite ($Mg_{0.14}Fe_{0.86}$) TiO_3 . Sparse grains of Fe metal and troilite, about 10 microns across, occur mainly in plagioclase.

These two norites are petrographically very similar, both in the compositions of their major minerals and in their suites of accessory minerals. Another ferroan norite clast was found in 15459 by *Ridley* (1977). The compositions of the major minerals in the norites are plotted in Fig. 2 compared to familiar plutonic rocks. The ferroan norites plot in a region intermediate to the ferroan, magnesian, and alkali suites. A few other unusual rocks also plot in this region: alkali norite 15405,170 and Mg-anorthosite 15459,231w (this study), Apollo 17 ferroan anorthosite 76504,18 (*Warren et al.*, 1986), and mare gabbros in 15459 (*Ridley*, 1977) and mare peridotite rake samples 15385 and 15387 (*Douty et al.*, 1973; *Ryder*, 1987). The significance of these similarities will be discussed after the compositional characterization of the norites.

The modes of the two norite clasts differ, and that difference is reflected in their bulk compositions and normative mineralogies (Table 3). The norms correspond quite well to the modes of the norites. Norite 279/339 is a felsic norite with 22.9% Al_2O_3 , while clast 292/343 is more mafic with 16.9% Al_2O_3 . Concentrations of transition metals are moderate, while those of meteoritic siderophiles are low. Concentrations of Co and Ni are reasonable for pristine norites and those of Ir and Au are below detection limits for INAA. Concentrations of REE are also moderate. The REE patterns (Fig. 3c) reveal a flat pattern with a positive Eu anomaly for the felsic norite and a HREE-enriched pattern with a positive Eu anomaly for the mafic sample. This HREE-enrichment reflects the moderately high pyroxene distribution coefficients for HREE. The REE pattern of the felsic norite is similar to that of Mg-norites such as those in 15445-15455, but mafic Mg-norites do not display HREE-enrichment as observed in the mafic

TABLE 3. Bulk analyses and cation % norms of Fe norites.

Wt %	15459, 279/339	15459, 292/343
SiO ₂	48.50	49.50
TiO ₂	0.25	0.31
Al ₂ O ₃	22.90	16.90
FeO	6.97	10.99
MgO	7.35	10.03
CaO	13.38	11.28
Na ₂ O	0.613	0.506
K ₂ O	0.095	0.118
Cr ₂ O ₃	0.365	0.286
MnO	0.142	0.201
P ₂ O ₅	0.065	0.039
Total	100.63	100.16
Mg' atomic	0.65	0.62
<i>Norm</i>		
Olivine	0	0
Pyroxene	33%	50%
En	62	57
Fs	30	33
Wo	8	10
Plagioclase	65%	49%
An	91	89
Ab	8	9
Or	0.8	1.4
Quartz	0.8	0.6
Ilmenite	0.3	0.4
Chromite	0.4	0.3
Apatite	0.1	0.08

ferroan norite. Some mafic ferroan anorthositic rocks do show HREE-enrichments at an order of magnitude lower concentrations.

Relationships between the ferroan norites and other lunar endogenous rocks can be evaluated based on petrographic and compositional characteristics. Among the samples noted as having mineral compositions intermediate to major ferroan, magnesian, and alkali suites, relationships with ferroan anorthosite 76504,18, Mg-anorthosite 15459,231w, and mare gabbros and peridotites are unlikely because these samples all have olivine and augite as their dominant mafic minerals, and not low-Ca pyroxene which is dominant in the norites.

Some relationship may exist between the ferroan norites and either Mg-norites or alkali norite 15405,170. The alkali norite has mineral compositions quite similar to those of the feldspathic norite, while several Apollo 17 Mg-norites [77075, 77077 (*Warren and Wasson*, 1978); 77215 (*Chao et al.*, 1976)] have mineral compositions only slightly more magnesian than the mafic norite. All of these norites have low-Ca pyroxenes as the dominant mafic mineral, with only rare augite as lamellae in orthopyroxene or in small separate grains. The rocks all display a similar assemblage of accessory minerals usually found in mesostasis. These include ilmenite, troilite, Fe-metal, K-feldspar, silica, zircon, and whitlockite. Bulk compositions of the ferroan norites are plotted on the pseudoternary diagram

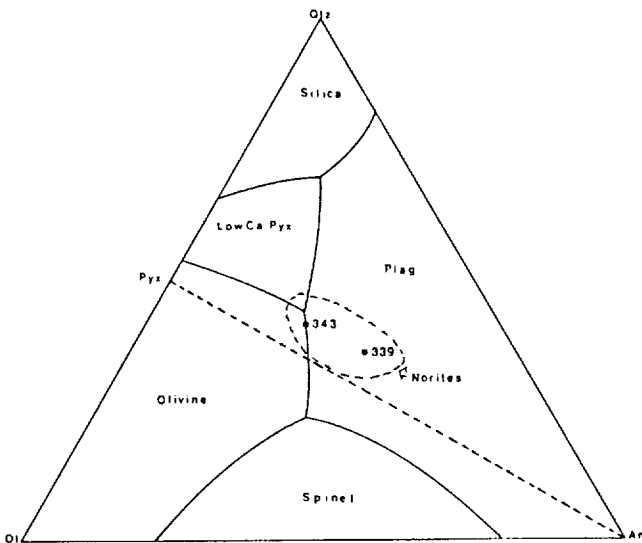


Fig. 4. Pseudoternary diagram of Walker *et al.* (1973) showing that bulk compositions of ferroan norites both plot in the norite field of Taylor (1982). The igneous texture and cotectic composition of 15459,292/343 suggest that it is a simple plutonic rock. Clast 15459,279/339 is a plagioclase-rich norite.

of Walker *et al.* (1973) in Fig. 4. Both lie in the norite field as depicted by Taylor (1982). Mafic norite 15459,343 plots on the cotectic line, while feldspathic norite 15459,339 falls in the plagioclase field. Alkali norite 15405,170 also lies in the plagioclase-rich part of the norite field, while KREEP basalts and norites plot near the peritectic point. This suggests that all these norites may be plutonic norites, with samples 15459,279/339 and 15405,170 being somewhat enriched in plagioclase.

Comparison of the norite REE patterns in Fig. 3c reveals some complications. The REE concentrations of the alkali norite are extremely high and, as noted above, are due to an unusually high abundance of whitlockite (calculated as 5% from the bulk and whitlockite concentrations of La). REE patterns of the Mg-norites overlap with those of the Fe-norites, but their pattern shapes are clearly distinct. The Mg-norites and 15459,279 have LREE-enriched patterns, while norite 15459,292 has a HREE-enriched pattern. The Mg-norites have negative Eu anomalies, while both Fe-norites have positive Eu anomalies. Preliminary model calculations were done to evaluate the possibility that Mg and Fe norites might be derived from similar parent norite but contain different proportions of minerals and residual liquid. The Mg-norites would contain a higher proportion of residual liquid to account for the LREE-enriched patterns and the Fe-norites would contain a higher proportion of plagioclase to account for the positive Eu anomalies. Although it is possible to generate both LREE- and HREE-enriched patterns and positive and negative Eu anomalies by varying the proportions of minerals and residual liquid, we have not been able to match the patterns in detail. Another problem is that the calculated variations in mineral proportions are larger than allowed by observed modal proportions or bulk compositions. We cannot

at this point resolve the question of possible relationships between ferroan norites and Mg- and alkali-suite norites. The ferroan norites may be unusually ferroan Mg-norites, or they may represent the Mg-rich end of the alkali suite, which now forms an extensive differentiation trend subparallel to the Mg-suite (Fig. 2).

Metamorphic rocks. The two metamorphic clasts are granulitic breccias as discussed by Warner *et al.* (1977) and Lindstrom and Lindstrom (1986). Clast 15459,288/289 is a highly feldspathic granulite consisting of 90% plagioclase ($An_{94.96}$), 10% olivine and pyroxene, and accessory Mg-ilmenite and Fe metal. Rare large feldspar grains are visible and some 200-300 micron zones within the plagioclase show well-developed granulitic texture, but most of it displays a fine intergrowth of irregular grains suggestive of an early stage in the development of granulitic texture (Fig. 1k). Grains of olivine ($Fo_{52.54}$), 10-20 microns across, and a few large pyroxene grains ($En_{59}Fs_{37}Wo_4$ and $En_{44}Fs_{19}Wo_{37}$) are scattered through the plagioclase. This clast is a feldspathic ferroan granulite with low REE concentrations, similar to more mafic samples of the ferroan anorthosite suite as well as the ferroan granulites of Lindstrom and Lindstrom (1986).

The second metamorphic clast, 15459,309/346, is a poikilitic rock consisting of 60% plagioclase (An_{93}), 30% pyroxene ($En_{76}Fs_{20}Wo_4$; $En_{47}Fs_9Wo_{44}$), 9% olivine (Fo_{77}), and accessory ilmenite, chromite, zircon, and whitlockite. Fine-grained plagioclase is interspersed among long branching chains of poikilitic pyroxene (Fig. 1l). Olivine occurs linked to pyroxene chains or as minute inclusions in pyroxene. The rock was shocked after formation of the poikilitic texture. This clast is a mafic magnesian granulite with REE concentrations a factor of two higher than in typical granulitic breccias (Lindstrom and Lindstrom, 1986).

Granulitic anorthositic norites are fairly common at the Apennine Front. Anorthositic gabbro 15418 (Nord *et al.*, 1977; Lindstrom and Lindstrom, 1986) is a severely shocked example. Analyses of such clasts reported by Warren and Wasson (1978) include a REE-poor ferroan granulite and a REE-rich magnesian clast. Other clasts of metamorphic-textured anorthositic norites were found in 15459 (Ridley, 1977) and 15465 (Cameron and Delano, 1973), but only petrographic studies were reported.

Highland Impact Melt Rocks and Glasses

Twenty-five new analyses of highland impact melt rocks are presented in Table 4. The samples include the matrices of the three large impact melt breccias (15405, 15445, 15455) and clasts from the regolith breccias. Most of the clasts have been examined in thin section and found to be fine- to medium-grained impact melts. Most of the impact melts are noritic in bulk composition, having 15-20% Al_2O_3 and 8-11% FeO. MgO has not been measured in all of the samples, but existing analyses reveal variations in Mg' from 55 to 78. There are also major variations in REE and other incompatible element concentrations. REE patterns of some of the more representative melt rocks (Fig. 3d) show variations from ~20 to 300 times chondrites, with all except the lowest patterns having

TABLE 4. Compositions of Apennine Front impact melts and glasses.

	A*	A	A	A	A	A	B	B	B	B	B	C	C	D
	15459	15405	15405	15405	15459	15459	15459	15459	15435	15435	15459	15498	15498	15459
	.242	.173	.174	.175	.290	.241	.305	.329	.54-1	.54-2	.313	.192	.209	.286
TiO ₂ (%)	1.74	1.99		2.03		1.70				1.58		0.78	0.72	
Al ₂ O ₃	15.3	14.8		15.5		15.1				16.1		22.0	21.4	
FeO	10.9	10.9	10.8	10.1	9.51	10.9	10.4	10.1	8.98	9.09	6.69	6.21	6.48	9.58
MgO	10.5	7.3		8.4		13.7				11.6		8.49	8.50	
CaO	9.8	10.3	9.4	10.5	11.8	11.2	10.0	10.0	9.7	10.6	13.0	12.94	12.87	10.7
Na ₂ O	0.620	0.856	0.861	0.829	0.811	0.563	0.51	0.595	0.69	0.66	0.561	0.656	0.636	0.513
K ₂ O	<3			1.2	0.19				0.49	0.53		0.29	0.29	
Sc (ppm)	20.8	22.3	22.1	20.7	19.1	23.4	20.5	19.9	18.0	17.3	12.4	11.4	12.6	18.0
Cr	1410	1630	1580	2000	1450	1710	2420	1830	1780	1760	1230	910	900	1660
Co	20.5	18.4	17.7	20.8	23.5	38.7	37.4	30.9	22.1	30.4	22.5	18.5	16.7	30.4
Ni	120	60	45	50	170	370	350	240	100	95	85			170
Rb	22	24	29	19	17	16	12	14	14	17		13	9	9
Sr	140	190	180	150	190	200	160	120	140	170	180	200	170	180
Cs	1.27	1.05	1.05	0.75	0.55	0.60	0.38	0.53	0.62	0.57	0.16	0.23	0.22	0.30
Ba	840	880	880	680	660	600	430	460	550	480	320	330	310	270
La	95.0	83.4	87.3	67.6	67.7	64.6	49.1	44.8	44.3	45.2	39.1	34.1	27.8	24.5
Ce	260	222	229	180	181	168	132	120	129	119	103	94	75.6	64.0
Nd	140	130	137	105	110	100	79	67	84	66	62	50	42	37
Sm	40.7	37.5	38.9	29.9	31.3	29.6	22.6	20.5	22.3	20.3	18.0	15.1	12.1	11.3
Eu	2.18	2.34	2.39	2.39	2.34	2.26	1.93	1.69	1.86	1.84	2.22	1.62	1.54	1.41
Tb	9.4	7.95	8.24	6.45	6.42	6.52	4.70	4.59	5.87	4.46	3.94	3.13	2.72	2.30
Yb	29.5	27.5	28.0	21.7	20.1	19.8	15.2	15.1	15.2	15.4	11.23	10.7	10.3	7.91
Lu	4.42	3.75	3.80	2.90	2.76	2.94	2.09	2.05	2.18	2.06	1.51	1.55	1.53	1.19
Zr	1170	1100	1100	800	990	770	680	640	630	630	420	400	350	350
Hf	33.4	31.2	29.5	23.9	24.0	22.7	15.3	15.2	17.3	16.6	10.38	10.8	10.3	8.62
Ta	4.35	3.50	3.60	2.82	2.50	2.19	2.99	1.95	2.01	2.00	1.34	1.17	1.11	1.08
Th	22.0	16.0	16.2	11.6	10.5	9.55	7.32	7.71	8.75	8.16	4.81	6.70	6.10	4.94
U	5.90	4.29	4.43	3.14	2.60	2.90	2.00	2.25	2.60	2.14	1.26	1.70	1.70	1.14
Ir (ppb)	2.4	<2	<2	1.1	4.6	5.3	5.9	2.9	<3	1.2	1.6	<4	<4	3
Au	2.2	1.5	<2	<2	2.2		7.4	6.1	<1.4	<1.6	<5	<7	<4	<4

characteristic KREEP slopes and negative Eu anomalies. Many of the samples have siderophile element (Ir, Au) concentrations detectable by INAA (>2 ppb), but much lower than those of Apollo 16 POIK and VHA impact melts (Korotev, 1987b).

Ryder and Spudis (1987) divided their limited set of 14 Apennine Front impact melts into five groups (A to E) largely according to REE concentrations. The studies reported in this volume add 48 new analyses of Apollo 15 impact melts (12 in Laul et al., 1987; 11 in Ryder et al., 1987; and 25 here) for a total of 62 recent analyses of Apollo 15 melt rocks. Several of these samples have only partial major element analyses, but there is generally sufficient information to compare them with other impact melts. Using this expanded dataset, the populations of the five groups change considerably and the divisions become less distinct. Group A has increased from 3 to 11 analyses, group B from 5 to 21, group C from 5 to 8, group D from 2 to 12, and group E from 1 to 10. The numbers are somewhat misleading because some of the data represent multiple analyses of the same impact melt. Eliminating multiple analyses reduces the numbers to 8, 21, 6, 5, and 8, respectively. The group B impact melts are by far the most abundant melts at the Apennine Front. Figure 3d shows ranges of REE concentrations for each of the melt rock groups and examples of each type from the analyses presented here. The

REE concentrations are almost continuous throughout the entire suite. Whether these melt groups actually represent distinct impact melts or a continuum of melt compositions can be evaluated by comparisons of their major element compositions. The first four melt groups generally have noritic bulk compositions with 15-20% Al₂O₃ and Mg' ranging from ferroan (55-65) in the group A melts to moderately magnesian (69-78) in the other three groups. The group E melts have anorthositic norite bulk compositions (20-24% Al₂O₃), with Mg' (59-72) spanning most of the range of the group A-D melts. The REE patterns of the group E melts are distinct from the other melts, varying from LREE-enriched patterns with negative Eu anomalies to HREE-enriched patterns with positive Eu anomalies. The group A and E melts are therefore distinct from the group B-C-D melts, but a continuum appears to exist in the noritic magnesian melt rock suite.

The significance of the continuum of melt compositions encompassing the groups B-C-D melts is not well understood. These three types may be described as LKFM (low-K Fra Mauro) melts, having noritic bulk compositions similar to that of samples from the Fra Mauro formation (Apollo 14), with REE and other incompatible element ratios similar to that of KREEP, but at lower concentration levels. LKFM melt rocks of similar compositions are found at other highland sites, and are generally

TABLE 4. (continued)

	†	D	D	D	D	D	D	†	D	E	E	E	Green glass	Green glass
	15459 ,317	15445 ,244	15445 ,245	15445 ,246	15455 ,258	15455 ,259	15455 ,260	15405 ,171	15459 ,239w	15459 ,231-1	15459 ,231-2	15459 ,320	15498 ,237	15498 ,158
TiO ₂ (%)		1.24		1.62		1.71		0.38	1.76		2.14		1.11	1.64
Al ₂ O ₃		20.6		17.1		16.3		22.8	19.8		20.1		19.2	16.9
FeO	8.83	7.98	8.28	9.17	9.53	9.79	9.66	8.61	8.38	8.22	8.07	7.58	10.2	9.05
MgO		12.9		16.0		16.2		7.0	11.2		11.6		8.2	9.15
CaO	14.4	11.4	11.3	9.8	10.1	9.4	9.3	13.3	12.6	11.7	11.7	12.3	12.9	10.81
Na ₂ O	0.772	0.551	0.550	0.523	0.552	0.548	0.527	0.537	0.666	0.661	0.693	0.679	0.621	0.72
K ₂ O		<0.2	0.15	<0.7	0.14	<.6		<.8			<.3		0.44	0.44
Sc (ppm)	21.7	13.4	14.9	16.9	17.3	17.9	17.8	11.2	16.6	17.1	17.4	15.4	19.2	18.0
Cr	640	1380	1500	1940	1660	1700	1700	1130	1130	1100	1090	1000	1570	1670
Co	15.9	35.4	29.0	30.5	32.1	37.7	38.9	11.6	21.0	20.0	20.5	19.5	55.6	20.9
Ni	55	320	270	270	260	330	350	<40	110	66	82	76	830	
Rb	3.6	<9	6	5	<10	<7	<9	<12	<9		<7	<9	18	17
Sr	210	190	160	170	160	180	170	150	170	220	200	190	190	150
Cs	0.063	0.27	0.18	0.21	0.13	0.18	0.14	0.10	0.21	0.12	0.13	0.10	0.95	0.49
Ba	220	200	200	230	250	250	230	160	220	120	130	120	400	530
La	21.9	16.5	19.4	20.7	21.8	22.0	22.3	20.0	18.9	8.10	8.49	7.49	38.0	51.1
Ce	56.5	43.0	50.0	51.9	56.6	57.0	56.6	52.4	49.0	21.0	22.0	20.6	101	141
Nd	38	25	32	34	33	36	36	27	29	13	14	9.9	54	90
Sm	11.1	7.65	8.80	9.30	10.3	10.3	10.3	8.65	8.61	4.02	4.35	3.74	17.3	23.1
Eu	2.08	1.63	1.72	1.72	1.87	1.85	1.81	1.16	1.76	1.62	1.64	1.58	1.36	2.07
Tb	2.38	1.64	1.86	1.97	2.12	2.07	2.15	1.85	1.94	0.94	1.00	0.85	3.96	4.97
Yb	7.57	5.03	5.59	6.01	6.90	6.45	6.45	6.66	6.16	3.60	3.87	3.40	13.0	16.2
Lu	1.15	0.74	0.84	0.88	0.95	0.93	0.95	0.99	0.94	0.538	0.578	0.489	1.83	2.38
Zr	350	190	250	270	270	230	260	250	270	110	100	100	460	650
Hf	8.23	5.72	6.64	7.70	8.12	7.84	7.76	6.67	6.46	3.25	3.55	2.78	13.8	18.1
Ta	1.10	0.85	0.94	0.96	1.01	1.04	1.03	0.86	0.90	0.57	0.61	0.53	1.69	2.02
Th	2.82	2.85	3.26	3.00	2.82	3.32	3.45	4.73	3.05	1.38	1.46	1.60	7.78	9.0
U	0.70	0.60	0.68	0.65	0.75	0.62	0.65	1.25	0.75	0.50	0.44	0.35	2.03	2.50
Ir (ppb)	<2	3.7	2.5	2.6	2.0	3.6	2.8		1.6			1.5	2.3	
Au	<4	<2	2.1	2.5	2.2	3.2	2.4	<1		<1.4		<1.4	6.7	

Analyses by INAA, one sigma uncertainties based on counting statistics are: 1-2% for Al₂O₃, FeO, Na₂O, Sc, Cr, Co, La, Sm, Eu; 3-10% for CaO, Sr, Ba, Ce, Tb, Yb, Lu, Hf, Ta, Th; 10-25% for TiO₂, MgO, K₂O, Ni, Cs, Nd, U, Ir, Au.

* Impact melt groups indicated by letters A-E (Ryder and Spudis, 1987).

† Ungrouped impact melts.

interpreted to represent major basin impacts because they are most common at the Apollo 15 and 17 sites, which are located on the ejecta from Imbrium and Serenitatis basins. The average composition of the highlands in those regions, as measured by the orbital geochemistry experiments, is very similar to the LKFM composition. At the Apollo 16 and 17 sites, impact melt compositions cluster into distinct groups rather than form a continuum of melt compositions (McKinley *et al.*, 1984; Ryder and Wood, 1977). The clustering of a large number of samples in the Apollo 15 group B (high REE) melts suggests that group B may represent the dominant impact melt at the site. At the other end of the continuum are the low-REE group D melts, whose dominant members are 15445 and 15455, the only two large samples of LKFM impact melt returned from the Apennine Front. Their clast assemblage is restricted to mafic magnesian pristine rocks one of which has been dated at 4.5 by. (Ryder, 1985). Ryder and Bower (1977) interpret these clasts as deep crustal rocks that could only be brought to the surface by basin-sized impacts. They suggest that these impact melts are

ejecta from the Imbrium impact. The group B and D impact melts may represent the major basin impact melts at the site, and the group C melts with intermediate compositions result from smaller local impacts that mix the ejecta from the basin-forming impacts.

The group A impact melt is a ferroan melt (Mg' 55-65) that has the bulk composition of KREEP basalt. There is considerable variation in both Mg' and REE concentrations in samples of the melt, but the same variation is seen in splits of individual KREEP basalts (15382, 15386; Ryder, 1985). Group A melts appear to be fairly common at the Apollo 15 site, and include breccia 15405 as its most prominent member. The Ar-Ar age of 1.3 by. for the 15405 matrix (Bernatowicz *et al.*, 1978) is very young. This age, coupled with the variations in melt composition, suggest that samples are small local impact melts and not major basin melts, which should be more homogeneous in composition. KREEP basalt flows underlying mare basalts at the site, and at the Apennine Bench, are probably the sources of group A impact melts.

Group E melts do not represent a single impact melt, but a suite of melts that have more feldspathic bulk compositions than do the other melt groups. The more REE-rich samples have slopes parallel to that of KREEP and may represent the mixture of feldspathic highland rocks and a small amount of KREEP. The REE-poor group E melts have patterns distinct from KREEP, more similar to those of some plutonic and metamorphic rocks. There is not presently sufficient information on these melt rocks to determine whether there are distinct subgroupings of these feldspathic highland melt rocks, but an origin as impact melts of pre-Serenitatis plutonic and metamorphic highland rocks is likely for these group E melt rocks.

Two analyses of highland glasses are also presented in Table 4. The glasses are homogeneous green glasses that have noritic bulk compositions with K₂O (0.4%) and Mg' (60-65) characteristic of the moderate K Fra Mauro basalt glass in Apennine Front soils (*Reid et al.*, 1973). These glasses and a third Apollo 15 highland green glass (*Ryder et al.*, 1987) have REE concentrations in the range of group B impact melts, but their low Mg' (63) distinguishes them from group B melts (Mg' 72). These glasses may represent the average composition of Apollo 15 highland rocks, which are a mixture of magnesian basin-derived impact melts with ferroan KREEP basalts and a variety of plutonic rocks.

IMPLICATIONS OF DIVERSITY OF APENNINE FRONT ROCKS

Provenances of Apollo 15 Igneous Rocks

The Apollo 15 highland rock suite is the most diverse of the highland suites sampled by the Apollo program. The igneous rocks include members of the three major types of highland plutonic rocks, previously unidentified ferroan norites, and extrusive KREEP basalts. Metamorphic rocks are similar to the granulitic breccias found at all highland sites. A very wide variety of impact melt compositions occur at the site; some of them (groups A and E) undoubtedly are local in origin, but others (groups B and D) are probably basin-related. Evaluation of the provenances of the Apennine Front igneous rocks can be based on comparison to rocks of known provenance.

The Apollo 15 ferroan anorthosite suite is similar to that from Apollo 16 in both bulk rock and mineral compositions. Although fewer in number, the Apollo 15 ferroan samples span the range from pure anorthosite to anorthositic norite, as do the Apollo 16 ferroan samples. Recent isotopic studies have succeeded in dating these important highland rocks at 4.5 b.y. (*Hanan and Tilton*, 1987; *Lugmair*, 1987), confirming their suspected ancient age. In the generally-accepted magma ocean model (*Warren*, 1985), these ferroan anorthositic rocks make up much of the earliest outer shell of the Moon's crust and would be an important pre-Serenitatis component at Apollo 15.

Many of the Apollo 15 magnesian suite samples resemble noritic and troctolitic rocks from Apollo 17 in both mineral and bulk composition. Members of each suite have been dated as ancient (older than 4.2 b.y.). At both the Apollo 15 and

17 sites the Mg-suite rocks occur as clasts in LKFM impact melts. *Ryder and Wood* (1977) discussed these impact melts and their magnesian clasts and concluded that the Mg-suite plutonic rocks are deep crustal materials that could be brought to the surface only by basin-forming impacts. Based on a small but significant difference in melt composition they concluded that the two suites could not be derived from the same impact. They assigned the Apollo 17 highland rocks to Serenitatis and the Apollo 15 suite to Imbrium. Despite the fact that these group D impact melts are not the most abundant melt group at the site, the arguments are sound and led *Ryder and Spudis* (1987) to reiterate that conclusion. The Mg-troctolite and anorthosite presented here and one Apollo 17 troctolite (*Winzer et al.*, 1974) are enriched in incompatible elements and more closely resemble the Apollo 14 Mg-suite troctolites and anorthosites (*Lindstrom et al.*, 1984). These probably result from assimilation of KREEP components in shallower plutons.

The Apollo 15 alkali suite bears strong resemblance to the Apollo 14 alkali suite (*Goodrich et al.*, 1986) and to Apollo 16 alkali gabbroanorthosites (*Lindstrom*, 1984; *James et al.*, 1987). Members of the suite have evolved mineral compositions and abundant late-stage accessory minerals. Alkali suite rocks are an abundant highland component at the Apollo 14 site, but only minor components at the Apollo 15 and 16 sites. They occur in varied associations, in pre-Imbrium fragmental breccias at Apollo 16, and with post-Imbrium local KREEP basalts at Apollo 15. It is probable that alkali suite rocks are scattered throughout the lunar crust, perhaps in near-surface plutons that can be brought to the surface by smaller impacts.

The ferroan norites are not sufficiently similar to other known highland rocks to assign them to a specific geologic location. We might infer from the fact that they are ferroan plutonic rocks that appear to be unrelated to ferroan anorthosites that they are derived from moderately shallow plutons, but whether they are local or exotic can only be determined when we know how common they are at the Apollo 15 site. We have begun a search for noritic rocks among Apollo 15 samples to evaluate this question.

Relative Abundances of Components in the Apennine Front

The relative abundances of rock types at the Apennine Front can be approximated in several ways. The lithologic approach uses the distribution of rock types among a large number of rock fragments that have been subjected to petrologic and chemical studies. This distribution may vary with different sampling strategies. The compositional approach attempts to model the average composition of the material as a mixture of various components using least-squares mixing calculations. The results are as good as the choice of components. Ideally the two approaches should be combined, with the results of the lithologic studies being used to select components for the mixing calculations. Complications inevitably arise because intermediate rock types that may be mixtures of other rock types, such as impact melts and granulitic breccias, are often the most common components. This is indeed the case for Apennine Front samples. Three lithologic studies of Apollo 15

highland rocks (this study; *Ryder et al.*, 1987; *Simon et al.*, 1987 and *Laul et al.*, 1987) all demonstrate that impact melts are the most abundant rock type, making up about half of the nonregolith lithic fragments. As previously discussed, compositions of impact melts vary widely, as do their inferred components and origins.

Among igneous fragments, KREEP basalt is the dominant rock type in both the studies of *Ryder et al.* (1987) and *Simon et al.* (1987). KREEP basalts are post-imbrium volcanic rocks whose proportion we intended to limit by selecting KREEP-poor regolith breccia 15459 for our detailed study of the ancient Apennine Front components. The number of well-characterized Apollo 15 plutonic rocks remains small: These new studies add about 20 to the number available at the time of the Apollo 15 workshop. Most of the fragments are small and may not be representative of their rock units, but mineral compositions and clusters in bulk composition can be used to define typical compositions. Ferroan and magnesian plutonic rocks are approximately equally abundant, with alkali suite rocks a minor component except in breccia 15405. The ferroan rocks include ferroan anorthosites and anorthositic norites, but also the unusual ferroan norites, which are apparently unrelated to ferroan anorthosites. The proportions of mafic minerals in the ferroan anorthositic rocks tend to be higher than in Apollo 16 rocks. The Mg-suite rocks, especially those in impact melts 15445 and 15455, are highly magnesian members of the suite. They include both troctolitic and noritic varieties and tend to be more feldspathic than their Apollo 17 counterparts. The Apollo 15 alkali suite samples extend the differentiation trend from more primitive norite to highly evolved quartz monzodiorite. It is difficult to select appropriate plutonic components for use in compositional modeling of the Apennine Front.

Korotev (1987a) reviewed the compositional approach to the Apennine Front and showed that the selection of input components influences the conclusions. He found that compositional variations in Apollo 15 soils could be modeled as mixtures of five components: KREEP basalt, mare basalt, green glass, meteorite and an Apennine Front Soil Component (AFSC). AFSC was defined as the Apennine Front soil containing the least mare basalt. The composition of AFSC corresponds more closely to that of LKFM glass (*Reid et al.*, 1973) than either do to the compositions of individual rocks at the Apennine Front. AFSC is obviously a mixture of preexisting rock types, including the various types discussed above. The fact that a single component is sufficient to describe variations in soil composition implies that the Apennine Front rocks are well mixed and their proportions do not vary. All variations in soil composition seem to be accounted for by variations in the amounts of young volcanic products: KREEP, mare basalts and green glass.

Korotev (1987a) did not present mixing models giving the proportions of components in the AFSC, but used compositional arguments to suggest which rock types might be important components. The rocks most similar in composition to AFSC are the group D impact melts (15445, 15455), which are themselves mixtures dominated by Mg-suite and ancient KREEP components. Although generally similar in bulk composition,

these impact melts are distinctly more mafic and more magnesian than AFSC (Al_2O_3 16 versus 20%; Mg' 75 versus 65). *Korotev* showed that if the group D impact melts are an important component of the Apennine Front, there must be a corresponding ferroan component that raises the Al_2O_3 and lowers the Mg' . He concluded that ferroan anorthosite alone cannot contribute enough Fe or Mg to change the Mg' of the bulk composition and that a more mafic ferroan rock is required. He suggested anorthositic norite 15418, but added that another mafic ferroan rock could also provide the necessary constituents. The ferroan norites found in 15459 represent another such mafic ferroan rock whose bulk composition is similar to that of AFSC. The proportions of other ferroan rocks (mare basalt, KREEP, and alkali norite) are strictly limited by their high concentrations of either transition metals and REE.

Some of the relationships between regolith samples and their components can be seen in Fig. 5, a plot of Sm versus Sc for Apennine Front samples. The major types of igneous rocks form a triangle outlining the compositions of polymict rocks. Pristine plutonic rocks of the three major suites spread outward from the origin. Mare basalts and green glass plot at the high Sc, low Sm corner of the triangular array, while KREEP basalts are at the top, having high Sm and moderate Sc. Apennine Front impact melts (triangles) form arrays between the plutonic rocks and KREEP. Regolith samples from Apennine Front Stations 2, 6, and 7 are plotted as fields for the soils and individual points (zeros) for the regolith breccias (*Korotev*, 1987a, and personal communication, 1986). The arrays of regolith breccia and soil compositions extend outward from

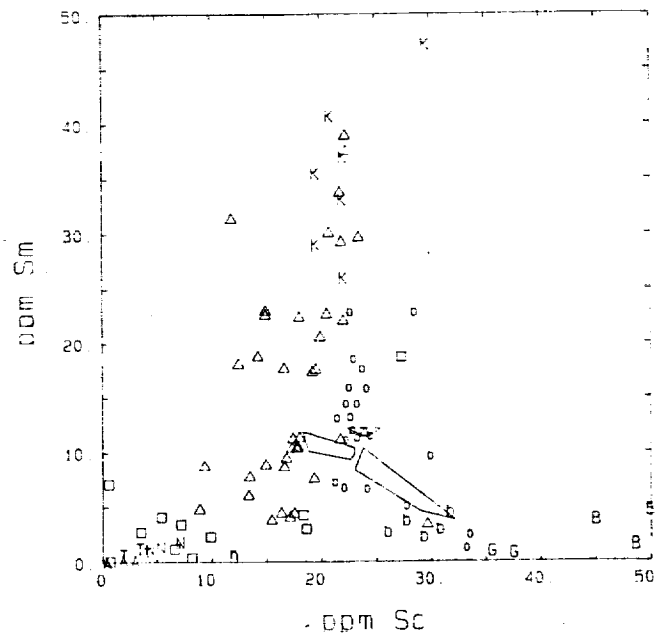


Fig. 5. Sm versus Sc for Apennine Front samples. Igneous rocks from literature data plotted by letters representing their composition: ANT-g-m=highland plutonic rocks; K=KREEP basalt, BbG=mare basalt and glass (*Ryder*, 1985). Regolith components: o = breccias, soil fields for Stations 2, 6, 7 outlined (*Korotev*, 1987a). New data: boxes=igneous rocks, triangles=impact melt rocks.

the AFSC central point toward the younger volcanic rocks: KREEP, green glass, and mare basalts. Group D melt rocks lie just to the left of the AFSC point, with group E melts below and other groups above. Various proportions of impact melts contribute most of the Sm in AFSC because the concentrations are low in the plutonic rocks. As stated above, the major element variations require significant proportions of mafic ferroan plutonic rocks. Ferroan anorthosites and Mg-suite rocks have very low Sc concentrations and need to be balanced by high Sc plutonic rocks. Ferroan norite, which plots near the group E impact melts, is the only such component. It appears likely that AFSC is a mixture of many components, among them KREEP-rich impact melts (groups B and D), Mg-suite plutonic rocks, and ferroan anorthosite, anorthositic norites, and norites. Such a complex mixture is difficult to model quantitatively, but is unlikely to be dominated by any individual igneous component.

In summary, the suite of highland rocks at the Apennine Front is the most diverse of any yet studied. Igneous rocks include members of the three major suites of highland plutonic rocks, a newly identified ferroan norite, and younger extrusive KREEP basalts. Impact melt rocks have a similarly wide range in composition, extending from those that resemble some plutonic rocks to melts of KREEP basalt composition. None of these rock types appears to dominate the average composition of the front. Diversity is a fundamental characteristic of the Apennine Front that results from its complex geologic history.

Acknowledgments. The efforts of numerous people at our four institutions were instrumental in the study. The curator's staff, Kim Willis and Charlie Galindo, extracted the clasts used in this study. Assistance with analyses was provided by R. Korotev and D. Lindstrom (WU), A. V. Murali (LPI), D. Mittlefehldt (Lockheed), and J. Wirtke (USC). Discussions of Apollo 15 rocks with G. Ryder, R. Korotev, and D. Lindstrom were invaluable. This work was supported by NASA through grants NAG 9-56 (Haskin), NAG 9-29 (Marvin) and NAG 9-169 (Shervais).

REFERENCES

- A15PET (Apollo 15 Preliminary Examination Team) (1972) The Apollo 15 lunar samples: a preliminary description. *Science*, **175**, 363-375.
- ALGIT (Apollo Lunar Geology Investigation Team) (1972) Geologic setting of the Apollo 15 samples. *Science*, **175**, 407-415.
- Bernatowicz T., Hohenberg C. M., Hudson B., Kennedy B. M., and Podosek F. A. (1978) Argon ages for lunar breccias 14064 and 15405. *Proc. Lunar Planet. Sci. Conf. 9th*, 905-919.
- Blanchard D. P., Brannon J. C., Haskin L. A., and Jacobs J. W. (1976) Sample 15445 Chemistry. In *Interdisciplinary Studies by the Imbrium Consortium*, vol. 2, pp. 60-62. Smithsonian Astrophysical Observatory, Cambridge.
- Cameron K. L. and Delano J. W. (1973) Petrology of Apollo 15 consortium breccia 15465. *Proc. Lunar Sci. Conf. 4th*, 461-466.
- Chamberlain J. W. and Watkins C., eds. (1972) *The Apollo 15 Lunar Samples*, The Lunar Science Institute, Houston. 525 pp.
- Chao E. C. T., Minkin J. A., and Thompson C. L. (1976) The petrology of 77215, a noritic impact ejecta breccia. *Proc. Lunar Sci. Conf. 7th*, 2287-2308.
- Delano J. W. (1979) Apollo 15 green glass: Chemistry and possible origin. *Proc. Lunar Planet. Sci. Conf. 10th*, 275-300.
- Dowry E., Conrad G. H., Green J. A., Hlava P. F., Keil K., Moore R. B., Nehru C. E., and Prinz M. (1973) Catalogue of Apollo 15 rake samples from stations 2 (St. George), 7 (Spur Crater), and 9a (Hadley Rille). *Institute of Meteoritics Special Publication No. 8*, University of New Mexico, Albuquerque. 75 pp.
- Ganapathy R., Morgan J. W., Krahenbuhl U., and Anders E. (1973) Ancient meteoritic components in lunar highland rocks: clues from trace elements in Apollo 15 and 16 samples. *Proc. Lunar Planet. Sci. Conf. 4th*, 1239-1261.
- Goodrich C. A., Taylor G. J., Keil K., Kallemeyn G. W., and Warren P. H. (1986) Alkali norite, troctolites and VHK mare basalts from breccia 14304. *Proc. Lunar Planet. Sci. Conf. 16th*, in *J. Geophys. Res.*, **91**, D305-D318.
- Hanan B. B. and Tilton G. R. (1987) 60025: relict of primitive lunar crust? *Earth Planet. Sci. Lett.*, **84**, 15-21.
- Haskin L. A., Blanchard D. P., Jacobs J. W., and Telander K. (1973) Major and trace element abundances in samples from the lunar highlands. *Proc. Lunar Sci. Conf. 4th*, 1275-1296.
- Haskin L. A., Lindstrom M. M., Salpas P. A., and Lindstrom D. L. (1981) On compositional variations among lunar anorthosites. *Proc. Lunar Planet. Sci. 12B*, 41-66.
- Jacobs J. W., Korotev R. L., Blanchard D. P., and Haskin L. A. (1977) A well-tested procedure for instrumental activation analyses of silicate rocks and melts. *J. Radioanal. Chem.*, **40**, 93-114.
- James O. B. (1972) Lunar anorthosite 15415: Texture, mineralogy, and metamorphic history. *Science*, **175**, 432-436.
- James O. B., Lindstrom M. M., and Flohr M. K. (1987) Petrology and geochemistry of alkali gabbronorites from lunar breccia 67975. *Proc. Lunar Planet. Sci. Conf. 17th*, in *J. Geophys. Res.*, **92**, E314-E330.
- Korotev R. L. (1985) Geochemical studies of Apollo 15 regolith breccias (abstract). In *Lunar Planetary Science XVI*, pp. 459-460, Lunar and Planetary Institute, Houston.
- Korotev R. L. (1987a) Mixing levels, the Apennine Front soil component, and compositional trends in the Apollo 15 soils. *Proc. Lunar Planet. Sci. Conf. 17th*, in *J. Geophys. Res.*, **92**, E411-E431.
- Korotev R. L. (1987b) The meteorite component of Apollo 16 noritic impact melt breccias. *Proc. Lunar Planet. Sci. Conf. 17th*, in *J. Geophys. Res.*, **92**, E491-E512.
- Korotev R. L. (1987c) National Bureau of Standards coal flyash (SRM 1633a) as a multielement standard for instrumental neutron activation analysis. *Proc. Internat. Conf. Nucl. Anal. Chem.*, in *J. Radioanal. Chem.*, in press.
- Laul J. C., Simon S. B., and Papike J. J. (1987) Chemistry and petrology of the Apennine Front, Apollo 15, Part II: Impact melt rocks. *Proc. Lunar Planet. Sci. Conf. 18th*, this volume.
- Lindstrom M. M. (1984) Alkali gabbronorite, ultra-KREEPy melt rock and the diverse suite of clasts in North Ray crater feldspathic fragmental breccia 67975. *Proc. Lunar Planet. Sci. Conf. 15th*, in *J. Geophys. Res.*, **89**, C50-C62.
- Lindstrom M. M. (1986) Diversity of rock types in Apennine Front Breccias (abstract). In *Lunar and Planetary Science XVIII*, pp. 486-487. Lunar and Planetary Institute, Houston.
- Lindstrom M. M. and Lindstrom D. J. (1986) Lunar granulites and their precursor anorthositic norites of the early lunar crust. *Proc. Lunar Planet. Sci. Conf. 16th*, in *J. Geophys. Res.*, **91**, D263-D276.
- Lindstrom M. M. and Marvin U. B. (1987) Geochemical and petrologic studies of clasts in Apennine Front breccia 15459 (abstract). In *Lunar and Planetary Science XVIII*, pp. 554-555. Lunar and Planetary Institute, Houston.
- Lindstrom M. M., Knapp S. A., Shervais J. W., and Taylor L. A. (1984) Magnesian anorthosites and associated troctolites and dunite in Apollo 14 breccias. *Proc. Lunar Planet. Sci. Conf. 15th*, in *J. Geophys. Res.*, **89**, C41-C49.

- Lugmair G. W. (1987) The age of the lunar crust: 60025-Methuselah's legacy (abstract). In *Lunar Planetary Science XVIII*, pp. 584-585. Lunar and Planetary Institute, Houston.
- Ma M.-S., Liu Y.-G., and Schmitt R. A. (1981) A chemical study of individual green glasses and brown glasses from 15426: Implications for their petrogenesis. *Proc. Lunar Planet. Sci. 12B*, 523-534.
- McKinley J. P., Taylor G. J., Keil K., Ma M.-S., and Schmitt (1984) Apollo 16: Impact melt sheets, Contrasting nature of the Cayley Plains and Descartes Mountains, and geologic history. *Proc. Lunar Planet. Sci. Conf. 14th*, in *J. Geophys. Res.*, 89, B513-B524.
- Nord G. L., Christie J. M., Lally J. S., and Heuer A. H. (1977) The thermal and deformational history of Apollo 15418. A partly shock-melted lunar breccia. *The Moon*, 17, 217-231.
- Nyquist L. E., Weismann H., Shih C.-Y., and Bansal B. M. (1977) REE and Rb-Sr analysis of 15405 quartz-monzodiorite (Super-KREEP) (abstract). In *Lunar Science VIII*, pp. 738-740. The Lunar Science Institute, Houston.
- Reid A. M., Warner J., Ridley W. I., and Brown R. W. (1973) Major element composition of glasses in three Apollo 15 soils. *Meteoritics*, 7, 395-415.
- Ridley W. I. (1977) Some petrological aspects of Imbrium stratigraphy. *Phil. Trans. Roy. Soc. Lond.*, A285, 105-114.
- Ridley W. I., Hubbard N. J., Rhodes J. M., Weismann H., and Bansal B. (1973) The petrology of lunar breccia 15445 and petrogenetic implications. *J. Geol.*, 81, 621-631.
- Ryder G. (1976) Lunar sample 15405: remnant of a KREEP basalt-granite differentiated pluton. *Earth Planet. Sci. Lett.*, 29, 255-268.
- Ryder G. (1985) *Catalog of Apollo 15 Rocks, Parts 1, 2, and 3*. Curatorial Branch Publication 72, JSC 20787. 1296 pp.
- Ryder G. (1987) Petrographic evidence for nonlinear cooling rates and a volcanic origin for Apollo 15 KREEP basalts. *Proc. Lunar Planet. Sci. Conf. 17th*, in *J. Geophys. Res.*, 92, E331-E339.
- Ryder G. and Bower J. F. (1977) Petrology of Apollo 15 black-and-white rocks 15445 and 15455-fragments of the Imbrium melt sheet? *Proc. Lunar Sci. Conf. 8th*, 1895-1923.
- Ryder G. and Spudis P. (1987) Chemical composition and origin of Apollo 15 impact melts. *Proc. Lunar Planet. Sci. Conf. 17th*, in *J. Geophys. Res.*, 92, E432-E446.
- Ryder G. and Wood J. A. (1977) Serenitatis and Imbrium impact melts: implications for large-scale layering in the lunar crust. *Proc. Lunar Sci. Conf. 8th*, 655-668.
- Ryder G., Lindstrom M. and Willis K. (1987) The reliability of macroscopic identifications of lunar coarse-fines particles and the petrogenesis of 2-4 mm particles in Apennine Front sample 15243. *Proc. Lunar Planet. Sci. Conf. 18th*, this volume.
- Simon S. B., Papike J. J., Gosselin D. C., and Lau J. C. (1986) Petrology, chemistry, and origin of Apollo 15 regolith breccias. *Geochim. Cosmochim. Acta*, 50, 2675-1591.
- Simon S. B., Papike J. J., and Lau J. C. (1987) Chemistry and petrology of the Apollo 15 Apennine Front I: KREEP basalts and plutonic rocks. *Proc. Lunar Planet. Sci. Conf. 18th*, this volume.
- Spudis P. D. (1980) Petrology of the Apennine Front, Apollo 15: implications for the geology of the Imbrium impact basin (abstract). In *Papers Presented to the Conference on Multiring Basins*, pp. 83-85, Lunar and Planetary Institute, Houston.
- Spudis P. D. and Ryder G. (1985) Geology and petrology of the Apollo 15 landing site: past, present, and future understanding. *Eos Trans. AGU*, 66, 721-726.
- Spudis P. D. and Ryder G., eds. (1986) *Workshop on the Geology and Petrology of the Apollo 15 Landing Site*, LPI Tech Rpt. 86-03, Lunar and Planetary Institute, Houston, 126 pp.
- Taylor S. R. (1982) *Planetary Science: A Lunar Perspective*. Lunar and Planetary Institute, Houston, 481 pp.
- Taylor G. J., Warner R. D., Keil K., Ma M.-S., and Schmitt R. A. (1980) Silicate liquid immiscibility, evolved lunar rocks and the formation of KREEP. In *Proc. Conf. Lunar Highlands Crust*, (R. B. Merrill and J. J. Papike, eds.) pp. 339-352. Pergamon, New York.
- Vetter S., Shervais J., and Lindstrom M. M. (1987a) Petrology of mare basalt and highland clasts from breccia 15498 (abstract). In *Lunar and Planetary Science XVIII*, pp. 1040-1041. Lunar and Planetary Institute, Houston.
- Vetter S. K., Shervais J. W., and Lindstrom M. M. (1987b) Petrology and geochemistry of olivine-normative and quartz-normative basalts from regolith breccia 15498: new diversity in Apollo 15 mare basalts. *Proc. Lunar Planet. Sci. Conf. 18th*, this volume.
- Walker D., Grove T. L., Longhi J., Stolper E. M., and Hays J. F. (1973) Origin of lunar feldspathic rocks. *Earth Planet. Sci. Lett.*, 20, 325-326.
- Warner J. L., Phinney W. C., Bickel C. E., and Simonds C. H. (1977) Feldspathic granulitic impactites and pre-final bombardment lunar evolution. *Proc. Lunar Sci. Conf. 8th*, 2051-2066.
- Warren P. H. (1985) The magma ocean concept and lunar evolution, *Ann. Rev. Earth Planet. Sci.* 13, 201-240.
- Warren P. H. and Wasson J. T. (1978) Compositional-petrographic search for pristine nonmare rocks. *Proc. Lunar Planet. Sci. Conf. 9th*, 185-217.
- Warren P. H. and Wasson J. T. (1979) The compositional-petrographic search for pristine nonmare rocks. Third foray. *Proc. Lunar Planet. Sci. Conf. 10th*, 583-610.
- Warren P. H. and Wasson J. T. (1980) Further foraging for pristine nonmare rocks. *Proc. Lunar Planet. Sci. Conf. 11th*, 431-470.
- Warren P. H., Taylor G. J., Keil K., Kallemeyn G. W., Rosener P. S., and Wasson J. T. (1983) Sixth foray for pristine non-mare rocks and an assessment of the diversity of lunar anorthosites. *Proc. Lunar Planet. Sci. Conf. 13th*, in *J. Geophys. Res.*, 88, A615-A630.
- Warren P. H., Shirley D. N., and Kallemeyn G. W. (1986) A potpourri of pristine moon rocks, including a VHK mare basalt and a unique, augite-rich Apollo 17 anorthosite. *Proc. Lunar Planet. Sci. Conf. 16th*, in *J. Geophys. Res.*, 91, D319-D330.
- Winzer S. R., Nava D. E., Schuhmann S., Kouns C. W., R. K. L. Lum, and Philpotts J. A. (1974) Major, minor and trace element abundances in samples from the Apollo 17 Station 7 Boulder: Implications for the origin of early lunar crustal rocks. *Earth Planet. Sci. Lett.*, 23, 439-444.
- Wood J. A., ed. (1976) *Interdisciplinary studies by the Imbrium Consortium, Vols. 1 & 2*, Smithsonian Astrophysical Observatory, Cambridge, 280 pp.



Olivine Vitrophyres: A Nonpristine High-Mg Component in Lunar Breccia 14321

John W. Shervais

Department of Geological Sciences, University of Tennessee, Knoxville, TN 37996 and Department of Geology, University of South Carolina, Columbia, SC 29280

Lawrence A. Taylor

Department of Geological Sciences, University of Tennessee, Knoxville, TN 37996

Marilyn M. Lindstrom*

Department of Earth and Planetary Sciences, Washington University, St. Louis, MO 63130

*Now at NASA Johnson Space Center, Code SN2, Houston, TX 77058

PREV. ANN
89A 10856

Geochemical modeling of the highlands crust has established the need for three principal components: anorthosite, KREEP, and a high-Mg component. The high-Mg component is most elusive because its presence can only be established indirectly; no pristine rocks of suitable compositions are known. Olivine vitrophyre clasts from breccia 14321 have high bulk MgO (~20 wt %) and $100 \times \text{Mg}/(\text{Mg}+\text{Fe}) = 78$, which is about the same as the cryptic Mg-component at Apollo 16. The 14321 olivine vitrophyres also have high incompatible element concentrations (~0.5 \times high-K KREEP), with REE ratios similar to KREEP (e.g., La/Lu = 22) and CaO/Al₂O₃ ratios similar to highland melt rocks. The high siderophile element concentrations of these rocks show that they are impact-generated melt rocks. Because impact melts form by total or near total melting of the target, their compositions represent the average composition of the crust, or of some portion of the crust. The high modal olivine content of the vitrophyres is not the result of accumulation, as almost all of the modal olivine has skeletal morphologies indicating rapid crystallization. Thus, the crust represented by this melt sheet is extremely mafic compared to the crust sampled by lunar surface geochemistry. Least squares modeling of the mafic component in this crust shows that it is not the same as that found at Apollo 16 (MAF, SCCRV, Primary matter), but must have a higher Mg/Fe ratio (Mg# = 84-85) and a high MgO concentration (~42 wt %). We suggest that this component is not an isolated rock type, but represents the mafic portion of some prevalent lunar rock type, e.g., Mg-rich troctolite. The mixing calculations show that the Mg-suite rocks comprise about 30% of the crust; alkali-rich lithologies are dominant (~60% of crust) in the form of KREEPy norites, alkali anorthosites, and granites. Olivine vitrophyres are higher in MgO than supposed Imbrium basin impact melts (15445 and 15455) and cannot represent melt rocks formed during this event. Pieters (1982) has shown that the central uplift in Copernicus (95 km diameter) consists largely of olivine derived from less than 10 km depth. Pre-Imbrium craters of similar size are common in the Fra Mauro region. Two of these craters ("northwest" and Fra Mauro) are less than one km from the Apollo 14 landing site, and may be the source area of the 14321 olivine vitrophyres.

INTRODUCTION

Geochemical modeling has shown that soils and breccias in the lunar highlands consist of three principal components: anorthosite, KREEP, and a high-Mg component (e.g., Wänke *et al.*, 1976; Wasson *et al.*, 1977; Korotev *et al.*, 1980). In addition, many also contain small contributions from meteorites and mare basalts. The anorthosite component used in the modeling is usually taken to be the ferroan anorthosite that characterizes the Apollo 16 site. While plagioclase-rich rocks are the dominant pristine rock type at the other highland sites, these vary from anorthosite to troctolite, and at the western sites the anorthosites are sodic. KREEP is a cryptic component that dominates incompatible element concentrations in soils and breccias and only rarely occurs as a pristine rock. Major element concentrations for KREEP are poorly constrained, but are generally thought to be noritic (Warren and Wasson, 1979).

The high-Mg component has been referred to variously as "primary matter" (Wänke *et al.*, 1976, 1977), SCCRV (Boynton

et al., 1975; Wasson *et al.*, 1977), and MAF (Korotev *et al.*, 1980). Like KREEP, the high-Mg component is also cryptic: no pristine rock types with sufficiently high Mg are known except dunite and lherzolite. However, these rocks are rare in the returned sample suites and they have Mg/Fe ratios that are too high by a factor of 2 (Korotev *et al.*, 1980).

We report here on a nonpristine rock type that may represent this illusory Mg-rich component—the olivine vitrophyres of lunar breccia 14321. These rocks, which have been described previously from thin sections (Allen *et al.*, 1979), occur as large (6.5 \times 4.5 cm) clasts in lunar breccia 14321 (Shervais and Taylor, 1984; Shervais *et al.*, 1984a, 1985a). We present the first bulk-rock major and trace element analyses of this rock type by INAA, with mineral and glass compositions by electron microprobe.

These data show that the 14321 olivine vitrophyres are impact melt rocks, as inferred by Allen *et al.* (1979), and that they probably formed by the total or near total melting of mafic-rich crustal lithologies in the Fra Mauro region. These lithologies comprise the mafic-rich portions of both Mg-rich

suite and alkali anorthosite suite plutons. The 14321 olivine vitrophyres represent the average composition of this crustal material and include much of the "anorthosite" component isolated by previous models.

PREVIOUS WORK

Lunar Breccia 14321

Lunar breccia 14321 (*alias* Big Bertha) is the largest sample returned from the Apollo 14 site and, at 9 kg, the third largest sample returned from the Moon. It was collected from the rim of Cone Crater and represents Fra Mauro formation excavated from a depth of about 60 m below the surface (Suwann *et al.*, 1977). The Fra Mauro formation was originally thought to consist of primary ejecta from the Imbrium basin, but based on comparative studies of terrestrial impact events (e.g., Hörz *et al.*, 1983), it now seems more likely that the Fra Mauro breccias consist dominantly of locally derived material entrained by secondary impacts of the primary Imbrium ejecta (Hawke and Head, 1977). This conclusion has important implications for the composition of the lunar crust at the Apollo 14 site.

A detailed petrographic study of breccia 14321 by Grieve *et al.* (1975) identified three principal lithologic components: (1) rounded fragments of pre-existing microbreccia, comprising mineral and rock fragments in a dark, fine-grained matrix; (2) igneous rock fragments of basaltic composition, ranging in texture from glassy to ophitic; and (3) a light-colored matrix that binds the clastic components.

Grieve *et al.* (1975) found that mineral fragments in the matrix have compositions similar to minerals in the mare basalts, suggesting that the matrix is dominated by comminuted basalt fragments, with a smaller component of disaggregated microbreccia. This interpretation is supported in general by chemical mixing models (Lindstrom *et al.*, 1972; Duncan *et al.*, 1975).

Olivine Vitrophyres

Olivine vitrophyres were first discovered and named by Allen *et al.* (1979) during a petrographic survey of 16 thin sections from breccia 14321. They discovered a total of 21 olivine vitrophyre clasts ranging from 0.1-14 square mm (Allen *et al.*, 1979). Bulk compositions of olivine vitrophyres were determined by modal reconstruction using average mineral and glass compositions from electron microprobe analyses. Olivine vitrophyres are distinguished from mare basalt clasts by their high modal olivine, high MgO concentrations, and low CaO/Al₂O₃ ratios. Allen *et al.* (1979) concluded that the olivine vitrophyres were impact melts of Mg-enriched highland crust and attributed their high apparent Mg/Fe partition coefficients ($K_d \approx 0.5$) to olivine accumulation in the melt.

Grover *et al.* (1980) performed piston cylinder experiments at high pressures on an average olivine vitrophyre bulk composition to determine whether or not it could be derived as an endogenous melt of the lunar interior. They found that the average olivine vitrophyre did not become multiply saturated until pressures of 25-30 kb (470-570 km). Grover

et al. (1980) concluded that olivine vitrophyres probably did not represent endogenous melts but formed near the surface as suggested by Allen *et al.* (1979). Grover *et al.* (1980) also determined equilibrium olivine/liquid partition coefficients experimentally for an olivine vitrophyre bulk composition. They found $K_d = 0.30-0.35$ and agreed with Allen *et al.* (1979) that the high apparent K_d 's for Fe/Mg partitioning resulted from olivine accumulation.

METHODS

In 1983, while the senior author was a research associate at the University of Tennessee, a new consortium study of breccia 14321 was instituted (Sbervais and Taylor, 1984). This study was to characterize the diverse assemblage of clasts present and to place these clasts within the context of our current petrologic and geochemical understanding of lunar rocks. A breccia guidebook to sample 14321 was published that documents the size and distribution of clasts (Sbervais *et al.*, 1984). We have already published our results on pristine highland lithologies (Lindstrom *et al.*, 1984) and mare basalts (Sbervais *et al.*, 1985b) that occur as clasts in breccia 14321. Further work on the microbreccia clasts and matrix is in progress (Sbervais *et al.*, 1985c; Knapp, 1986).

Previous studies of breccia 14321 were limited to thin sections or small slabs that did not represent the bulk sample (e.g., Grieve *et al.*, 1975; Duncan *et al.*, 1975; Allen *et al.*, 1979). As part of our consortium effort, all remaining subsamples of breccia 14321 greater than 10 g were examined and mapped, including two new faces formed by a saw cut through the largest subsample (Sbervais *et al.*, 1984a). Three of the largest clasts exposed on these faces are olivine vitrophyres that range up to 6.5 × 4.5 cm. Additional smaller clasts of olivine vitrophyre are distributed throughout the matrix (Sbervais *et al.*, 1984a).

Representative chips of the three largest olivine vitrophyre clasts exposed on the new west face of 14321, 37 (DA-1, DA-3, and DA-4) were extracted and split into two portions: one for whole-rock analysis and the other to make polished probe mounts (Sbervais and Taylor, 1984). Most of these clasts remain in place and are available for further study. In addition, mirror images of these clasts may be found on the east faces of 14321, 1082, 1083 and 1084 (Sbervais *et al.*, 1984a).

Whole-rock samples were analyzed for major and trace elements by INAA at Washington University based on the procedures of Lindstrom (1984), and data were reduced using the TEABAGS program of Lindstrom and Korotev (1982). Analytical uncertainties based on counting rate at the 1- σ level are as follows: 1-2% Al, Fe, Na, Sc, Cr, Mn, Co, La, Sm, Eu; 3-5% Ca, Ce, Tb, Yb, Lu, Hf, Ta, Th; 5-15% Ti, Mg, Sr, Cs, Ba, Nd, U; 15-25% K, V, Ni, Rb, Zr, Ir. The detection limit for Ir is 2 ppb.

Mineral analyses were performed using the automated MAC 400S electron microprobe at the University of Tennessee. Standards, operating procedures, and data reduction techniques are those normally used in this lab (Sbervais *et al.*, 1984b). Major element analyses of residual glass in the vitrophyres were made by broad beam (~20 microns) electron microprobe analysis with a 30 nA beam current to minimize sodium loss.



Fig. 1. Mug shot of 14321 ,37 (south face), showing new surface produced by slabbing in November, 1983. The three largest clasts exposed on this face are olivine vitrophyres, labeled DA-1, DA-3, and DA-4. Note the small light-colored clast near the pointed end of DA-3.

PETROGRAPHY AND PHASE CHEMISTRY

The distribution of olivine vitrophyre clasts in breccia 14321 is shown in Fig. 1, a photograph of the west face of sample ,37. These clasts are mapped as Dark Aphanitic (DA) because in hand-sample the olivine vitrophyres have no discernable texture and are dark greenish-brown or olive-drab in color. Three clasts from this face (DA-1, DA-3, and DA-4) were sampled (Fig. 1). DA-3 is the only true vitrophyre, consisting of about 30% olivine microphenocrysts set in a dark reddish-brown glass with traces of Fe metal (Fig. 2a). Sample DA-1 and DA-4 have similar olivine microphenocrysts set in a glassy to variolitic matrix of plagioclase, low-Ca pyroxene, augite, ilmenite, Fe-metal, and glass (Figs. 2b,c). The variolitic textures imply that these clasts experienced a slower crystallization rate than DA-3 after an initial quenching. Clast DA-1 also contains large, partially resorbed xenocrysts of olivine, plagioclase, and maskelynite (Fig. 2b), and DA-3 contains rare interclasts of anorthosite or troctolite (seen in hand-sample).

Mineral Chemistry

Olivine crystals are divided into three groups based on size and morphology: (1) microphenocrysts, (2) phenocrysts, and (3) xenocrysts. Quenching of all three samples is indicated by the size of the olivine microphenocrysts (20-100 microns) and their characteristic skeletal morphologies (Fig. 3a). Olivine microphenocrysts range in composition from Fo_{65} to Fo_{87} , but most cluster in the narrow range of Fo_{79} to Fo_{85} (Table 1). The average composition of olivine microphenocryst in DA-3, based on 50 random analyses, is Fo_{83} . The average compositions of olivine microphenocrysts in DA-1 and DA-4 are slightly lower (Fo_{81} in DA-1; Fo_{80} in DA-4), and have even more restricted compositional ranges ($Fo_{77.5}$ to Fo_{83}).

Larger euhedral to subhedral olivine grains (100-200 microns), some with internal skeletal growth structures, have cores as magnesian as Fo_{89} and zone outward to rims of Fo_{86} to Fo_{84} (Fig. 3a). We interpret these larger grains to be early-

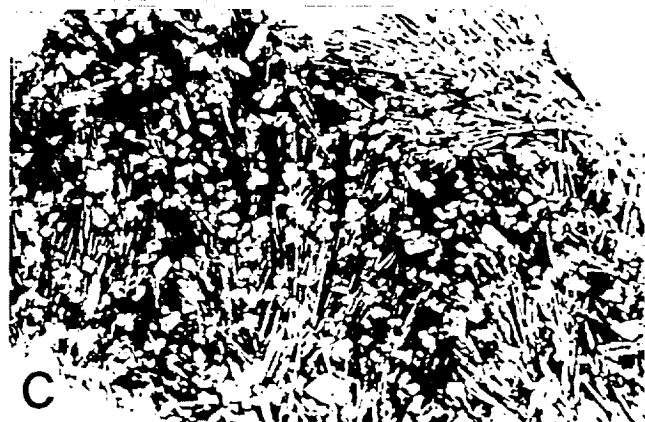
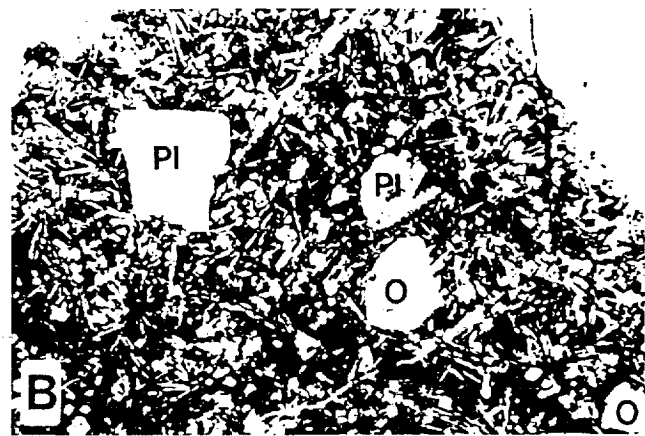
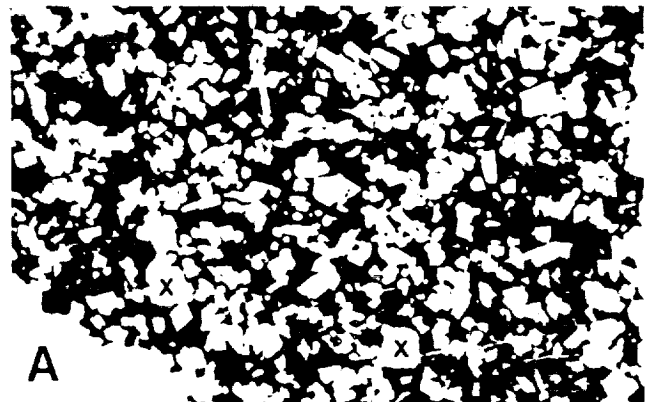


Fig. 2. Photomicrographs of olivine vitrophyre clasts from breccia 14321, all at same scale (FOV = 2.8 mm). (a) DA-3: olivine phenocrysts and microphenocrysts in glass; (b) DA-1: olivine microphenocrysts in quenched groundmass of plagioclase, pyroxene, and glass, large rounded crystals are xenocrysts of olivine (o) and feldspar (p); (c) DA-4: olivine microphenocrysts in quenched groundmass of plagioclase, pyroxene, and glass; note variolitic texture.



Fig. 3. Photomicrographs of olivine crystals in vitrophyres DA-3 and DA-1. (a) Olivine phenocryst (b) and microphenocrysts in glass, DA-3. Note the small size and delicate, skeletal morphologies of the olivine microphenocrysts. The slightly larger phenocryst has morphology similar to the microphenocrysts. FOV = 0.7 mm. (b) Olivine xenocrysts (X1, X2) surrounded by smaller microphenocrysts and phenocrysts in DA-3. Xenocryst X1 has an Fo_{87} core, Fo_{95} rim; xenocryst X2 has an Fo_{66} core, Fo_{73} rim, suggesting back-reaction with a more magnesian melt. FOV = 1.4 mm. (c) Large xenocryst of magnesian olivine with an Fo_{89} core, Fo_{84} rim in DA-1. FOV = 0.7 mm.

formed phenocrysts that did not re-equilibrate with the evolving residual melt, but zoned outwards to more Fe-rich compositions. The presence of large, magnesian phenocrysts in addition to the more common microphenocrysts implies a two-stage crystallization history.

Olivine also occurs as xenocrysts, along with plagioclase and maskelynite (Figs. 3b,c). The xenocrysts range in size from 0.2 to 0.6 mm and are generally subhedral with resorbed grain boundaries. Plagioclase and maskelynite are commonly rounded or embayed, while olivine xenocrysts have subhedral or irregular grain shapes with frittered grain boundaries. Olivine xenocrysts generally have homogenous core compositions of Fo_{87} to Fo_{90} and thin rims Fo_{84} to Fo_{86} in composition. We found one olivine xenocryst, however, with a core composition of Fo_{66} and a rim of Fo_{73} . This suggests back-reaction of an Fe-rich xenocryst with a more magnesian melt. Plagioclase and maskelynite xenocrysts range in composition from An_{83} to An_{95} and are not zoned (Table 2).

The variolitic matrices of DA-1 and DA-4 consist of sheaf-like arrays of slender plagioclase crystals (An_{79} , Ab_{19} , Or_2) that engulf the olivine phenocrysts and microphenocrysts, and are intergrown with granular aggregates of low-Ca pyroxene ($Wo_{3.5-7.5}$, En_{72}), augite (Wo_{24} , En_{44}), ilmenite, and Fe-metal. Minor residual glass is found between plagioclase laths and in nonvariolitic patches.

Residual Glass Chemistry

Residual glass was analyzed in DA-3, the only true vitrophyre. Twenty random spots were analyzed with a 20 micron beam and the results averaged (Table 3). The residual glass is alkali rich, with $Na_2O \approx 1\%$ and $K_2O \approx 0.4\%$. The $Mg\#$ [$=100 \cdot Mg/(Mg+Fe)$] is 64 (higher than most mare basalts) and the CaO/Al_2O_3 ratio = 0.69, which is typical of highland melt rocks (Vaniman and Papike, 1980). The DA-3 glass composition is compared, in Table 3, to alkali-rich mare vitrophyres found in breccia 14321. The mare vitrophyres have SiO_2 , TiO_2 , MgO , and Na_2O in the same range as the olivine vitrophyres, but they are lower in Al_2O_3 and K_2O , and higher in FeO . The mare vitrophyres have $Mg\#$ s (43-45) and CaO/Al_2O_3 ratios (0.86) that are typical of the aluminous basalts found at the Apollo 14 site. Thus, the major element chemistry of the residual glass in DA-3 clearly distinguishes it from mare vitrophyres such as those described by Sbertvais *et al.* (1985b) and confirm its highland affinities.

As noted by Allen *et al.* (1979), residual glass in the olivine vitrophyres is compositionally variable due to the quench growth of olivine. This is shown in Table 3 by representative glass analyses that span the range of observed compositions. When plotted in the Ol-An-Q ternary of Walker *et al.* (1973), the residual glass data form a field that extends from near the Ol-Px-Plg reaction point into the plagioclase stability field and away from the olivine apex (Fig. 4). Because plagioclase is not observed as a liquidus or near liquidus phase in DA-3, these data are consistent with metastable expansion of the olivine phase volume due to suppression of plagioclase nucleation during rapid crystallization, as shown by Taylor and Nabelek (1979), and Nabelek *et al.* (1978).

TABLE 1. Olivines in olivine vitrophyre clast DA-3 from breccia 14321 analyzed by electron microprobe.

	1	2	3	4	5	6	7	8
SiO ₂	37.67	38.84	38.84	39.67	39.14	39.29	36.36	37.89
FeO	24.64	19.73	16.14	14.25	12.80	14.04	33.12	25.55
MnO	0.20	0.13	0.11	0.09	0.05	0.17	0.26	0.21
MgO	37.87	42.20	44.24	46.53	48.49	47.09	30.68	36.61
CaO	0.16	0.09	0.15	0.11	0.07	0.12	0.13	0.23
Sum	100.54	100.99	99.47	100.65	100.55	100.71	100.55	100.57
<i>Cations per four oxygens</i>								
Si	0.986	0.987	0.987	0.987	0.970	0.977	0.990	0.991
Fe	0.539	0.419	0.342	0.296	0.265	0.292	0.754	0.559
Mn	0.003	0.002	0.002	0.001	0.000	0.002	0.005	0.002
Mg	1.477	1.599	1.675	1.725	1.791	1.746	1.245	1.427
Ca	0.003	0.002	0.003	0.002	0.001	0.002	0.003	0.006
Sum	3.009	3.009	3.009	3.011	3.027	3.019	3.001	2.996
% Fo	73.3	79.2	83.0	85.3	87.1	85.6	62.3	71.9

Columns 1-4 are quench olivines with skeletal habits; columns 5-6 are the core and rim of a large relict xenocryst; columns 7-8 are the core and rim of a smaller relict xenocryst that is more Fe-rich than the quench olivines.

WHOLE-ROCK GEOCHEMISTRY

Whole-rock major and trace element analyses of DA-1, DA-3, and DA-4 by INAA are presented in Table 4. The major element data are complete only for DA-3; however, for the elements analyzed, all three are virtually identical. Also shown for comparison are major element analyses of DA-3 by modal reconstruction and the Average Olivine Vitrophyre (AOV) of *Allen et al.* (1979).

The major element data for DA-3 confirm the highland affinities of the olivine vitrophyres, with high Mg# (78) and low CaO/Al₂O₃ (0.69). Mass balance calculations using an average olivine microphenocryst and the average residual glass show that the whole-rock composition may be reconstructed if we assume that olivine constitutes about 30% of the mode by weight. The best fit is obtained if we assume that part of this olivine has high Fo content (similar to the early phenocrysts and the xenocrysts) and that the rest is similar to the average microphenocryst composition (Table 4, column 5).

The AOV composition of *Allen et al.* (1979) has MgO = 24%, which is considerably higher than the concentration in DA-3 (19.2%). *Allen et al.* (1979) base their AOV composition on the four most magnesian vitrophyres they found in thin section. Since these particular clasts are all small (< 6.0 square mm), their modes may reflect nonmodal enrichment in olivine or overcounting of olivine. *Allen et al.* (1979) report six other modal reconstructions of olivine vitrophyre clasts that average around 20% MgO, and are almost identical to our analysis of DA-3. We suggest that the MgO concentration used by *Allen et al.* (1979) for their average olivine vitrophyre is too high,

and recommend our own "preferred average olivine vitrophyre" composition, based on the average of our whole rock data (Table 4).

The olivine vitrophyres studied here have nearly identical trace element concentrations (Table 4). All are greatly enriched in incompatible trace elements relative to mare basalts and

TABLE 2. Plagioclase in olivine vitrophyre clast DA-1 from breccia 14321.

	1	2	3
SiO ₂	45.18	45.29	47.41
Al ₂ O ₃	35.84	35.87	33.84
FeO	0.22	0.28	0.23
CaO	19.05	19.00	17.48
Na ₂ O	0.60	0.42	1.23
K ₂ O	0.10	0.08	0.09
Sum	100.98	100.94	100.28
<i>Cations per eight oxygens</i>			
Si	2.064	2.068	2.169
Al	1.930	1.931	1.824
Fe	0.008	0.009	0.008
Ca	0.932	0.930	0.856
Na	0.052	0.036	0.108
K	0.005	0.004	0.004
Sum	4.991	4.978	4.970
% An	94.2	95.9	88.4

TABLE 3. Residual glass in olivine vitrophyre clast DA-3 analyzed by electron microprobe with mare basalt vitrophyres from breccia 14321 (*Sbervais et al.*, 1985) shown for comparison.

	1	2	3	4	5	6	7	8
SiO ₂	49.52	49.36	49.73	49.23	49.49	0.96	47.49	47.04
TiO ₂	1.55	2.04	2.00	1.79	1.87	0.22	2.22	2.30
Al ₂ O ₃	15.98	18.22	17.75	16.99	17.64	0.77	13.28	13.33
FeO	10.18	9.25	7.59	9.52	8.43	1.06	16.74	17.17
MnO	0.20	0.13	0.15	0.14	0.13	0.04	0.27	0.27
MgO	11.96	8.78	8.09	7.56	8.34	1.18	7.63	7.16
CaO	8.92	10.68	13.05	12.09	12.18	1.45	11.41	11.41
Na ₂ O	0.75	0.95	0.98	0.86	0.99	0.18	0.81	0.92
K ₂ O	0.27	0.41	0.34	0.85	0.42	0.13	0.14	0.15
Cr ₂ O ₃	0.16	0.18	0.24	0.26	0.23	0.02	0.29	0.30
Sum	99.50	100.00	99.92	99.28	99.73	S.D.	100.28	100.05
Mg#	67.7	62.8	65.6	58.7	63.9		44.8	42.6
CaO/ Al ₂ O ₃	0.558	0.586	0.735	0.712	0.690		0.859	0.856

Columns 1-4 are representative residual glass analyses from olivine vitrophyre DA-3; column 5 is the mean of 20 glass analyses from DA-3, and column 6 is one standard deviation of this average. Column 7 is the mean of 30 glass analyses of mare vitrophyre DV-1 from breccia 14321, and column 8 is the mean of 25 glass analyses from mare vitrophyre DA-6 from breccia 14321 (*Sbervais et al.*, 1985).

pristine highlands rocks. The rare earth elements are KREEPy, with La = 170 × chondrite, Yb = 78 × chondrite, and La/Lu = 22, which is the same ratio as KREEP (Fig. 5). The other KREEPy incompatible elements (K, Rb, Hf, Th, U) show similar enrichments. Unlike KREEP, however, the olivine vitrophyres are also enriched in the compatible transition metals Sc, Co, Cr, and V. These elements are more commonly identified with either mare basalts or the cryptic mafic component of the lunar highlands.

One of the more important results of our trace element analyses is the demonstration of high siderophile element concentrations in the olivine vitrophyres. The high concentration of Ir and Ni in all three olivine vitrophyres studied here shows that these rocks represent impact melts, and they are not pristine volcanic rocks.

DISCUSSION

The data presented above confirm the hypothesis presented by *Allen et al.* (1979) that olivine vitrophyre clasts in lunar breccia 14321 represent impact melts of lunar highlands material. Their highlands affinity is shown by high Mg#, low Ca/Al ratios, and KREEPy incompatible element enrichments. Their origin by impact melting is shown by high siderophile concentrations, which implies the addition of a meteoritic component to the target. As noted by *Allen et al.* (1979) their compositions do not match any known lunar soil or regolith breccia, and cannot be modeled using common pristine rock types.

We must now face the dilemma of how to account for the mafic-rich composition of these vitrophyres. There are two possible solutions. The enrichment in mafic components may result from (1) the accumulation of olivine in a more normal

highland impact melt, or (2) from the melting of a protolith rich in the mafic component. We will address first the question of olivine accumulation, which hinges on the partitioning of Mg and Fe between olivine and the melt.

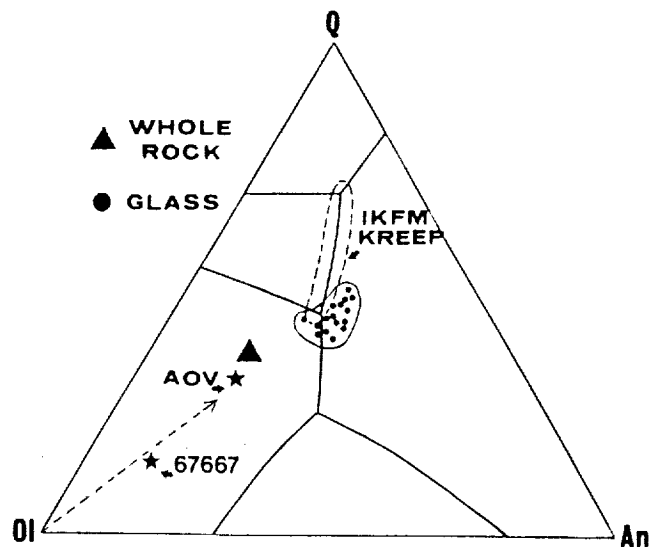


Fig. 4. Residual glass compositions from DA-3 plotted on the Ol-An-Q ternary of *Walker et al.* (1973). Shown for comparison are the average olivine vitrophyre of *Allen et al.* (1979), our preferred olivine vitrophyre whole-rock analysis, feldspathic peridotite 67667, and the field of IKFM KREEP. The residual glass data form a field that extends away from the Ol-An-Px reaction point into the plagioclase phase volume. Since plagioclase is not present in these glasses, this trend into the plagioclase phase volume suggests suppression of plagioclase nucleation due to rapid cooling rates (*Nabelek et al.*, 1978).

TABLE 4. Whole rock analyses of olivine vitrophyres from breccia 14321.

	DA-4 ,1159	DA-1 ,1180	DA-3 ,1158	MR-3	AOV*	Preferred 14321 AOV
SiO ₂	na	na	48.3	46.6	45.7	46.5
TiO ₂	na	na	1.3	1.31	1.03	1.30
Al ₂ O ₃	na	na	12.4	12.35	10.3	12.4
FeO	9.85	9.84	9.88	10.57	10.8	9.86
MnO	na	na	0.1312	0.12	0.12	0.13
MgO	na	na	19.2	19.51	24.3	19.2
CaO	8.5	7.9	7.4	8.56	6.27	7.9
Na ₂ O	0.801	0.806	0.796	0.69	0.78	0.80
K ₂ O	0.57	0.41	0.56	0.29	0.46	0.51
Cr ₂ O ₃	0.227	0.235	0.225	0.16	0.17	0.229
Sum	none	none	100.0*	100.0	99.93	98.83
<i>Trace Elements</i>						
ppm						
V			41			41
Sc	17.87	17.62	17.93			17.80
Cr	1555	1605	1537			1566
Co	34.88	38.2	33.4			35.5
Ni	310	340	240			297
Rb	18	27	20			22
Sr	134	176	157			156
Cs	0.72	0.66	0.7			0.69
Ba	790	730	780			767
La	58.9	57.1	58.7			58.2
Ce	159	156	160			158
Nd	94	92	93			93
Sm	25.4	24.	26.5			25.3
Eu	2.05	1.96	2.01			2.01
Tb	6.05	5.92	6.17			6.05
Yb	19.7	19.5	20.1			19.8
Lu	2.63	2.62	2.68			2.64
Hf	21.9	21.8	22.4			22.0
Zr	800	810	830			815
Ta	2.55	2.53	2.61			2.56
Th	11.71	11.19	11.7			11.53
U	2.82	2.92	3.08			2.94
ppb						
Ir	7.2	6.7	5.8			6.57

Major and trace elements in DA-1, DA-3, and DA-4 by INAA; major elements in MR-3 and the Average Olivine Vitrophyre (AOV*) of Allen *et al.* (1979) by modal reconstruction from electron microprobe analyses of glass and olivine. Preferred AOV is our best estimate of major and trace elements in an average olivine vitrophyre, based on averages of DA-1, DA-3, and DA-4 (except silica from MR-3).

Partitioning of Fe and Mg Between Olivine and Glass

A major problem in deciphering the origin of the 14321 olivine vitrophyres is the apparent disequilibrium in Fe/Mg partitioning between olivine and a liquid having the bulk rock composition. The bulk-rock Mg# (= 77.6) implies equilibrium with Fo₉₁ olivine, using the experimentally determined maximum $K_d = 0.35$ of Grover *et al.* (1980), or Fo₉₂ for $K_d = 0.30$. The most magnesian olivine phenocryst observed, however, is Fo₈₉, which implies that the K_d is equal to 0.5. Alternatively, this high apparent K_d may result from olivine

accumulation or kinetic factors (e.g., super-cooling of the melt; Bianco and Taylor, 1976).

Both Allen *et al.* (1979) and Grover *et al.* (1980) favor olivine accumulation to explain this discrepancy between the calculated and observed olivine composition. Allen *et al.* (1979) calculate that 25% olivine accumulation is required for equilibrium between their calculated average olivine vitrophyre and the average microphenocryst composition; less accumulation is needed if our lower MgO "preferred average olivine vitrophyre" composition is used. However, this conclusion is not consistent with the observed petrography. The vast majority

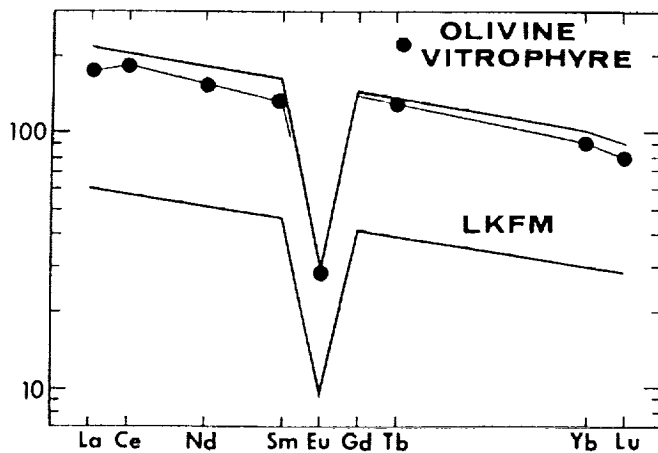


Fig. 5. Chondrite-normalized REE concentrations of our preferred average olivine vitrophyre, compared to the range of low-K Fra Mauro (LKFM) melt rocks, after *Vaniman and Papike* (1980). Olivine vitrophyres have REE concentrations at the upper extreme of the LKFM range, and are only $0.5 \times$ high-K KREEP.

of modal olivine formed by quench crystallization during rapid cooling within the melt sheet. These olivines are small and have delicate skeletal morphologies. Accumulation of such olivine crystals by gravitational settling is not possible under these circumstances.

One explanation for this discrepancy is that the apparent accumulation of olivine results from the incomplete digestion of xenocrystic olivine in the melt sheet. In this scenario, the liquid composition was never equivalent to the whole rock, which contains clasts of material entrained during flow. The major problem with this explanation is that the observed content of xenocrystic olivine is too low ($< 1\%$ modally) to account for the apparent enrichment, which requires at least 10% olivine accumulation (based on an equilibrium olivine of FO_{89} and our preferred AOV composition). Thus, while the incomplete digestion of xenocrystic olivine is a factor in this problem, it is not the complete solution.

Relationships between observed olivine compositions and calculated equilibrium values in DA-3 are shown in Fig. 6. The average olivine microphenocryst ($FO_{83.1}$) is virtually identical to the calculated olivine in equilibrium with the average residual glass ($FO_{83.5}$). Further, the range in observed olivine microphenocryst compositions is similar to the range in equilibrium olivine compositions calculated from the range in residual glass analyses (Fig. 6). The rims on most large olivines also fall within this same range. The implication is that conditions approaching equilibrium were maintained between the olivine microphenocrysts and residual liquid on a local scale near individual grains, but not on a large scale. This suggests that kinetic factors may be important in the origin of these rocks.

There are at least two possible explanations for the discrepancy between observed and calculated olivine compositions that focus on kinetic considerations: (1) the rapid quenching to form olivine microphenocrysts may have been preceded by a period of slower crystallization, during which

the larger, euhedral olivine phenocrysts formed, or (2) the earliest olivine formed by "disequilibrium" crystallization, during which the effective K_d was close to 0.5. *Donaldson et al.* (1975) and *Bianco and Taylor* (1976) have shown that effective K_d values will approach 0.5 at high cooling rates (48° to $400^\circ\text{C}/\text{hour}$) because cations are not able to diffuse through the melt fast enough to maintain bulk equilibrium at the crystal-liquid interface. This explanation implies that cooling rates were highest during initial crystallization and slowed as crystallization proceeded, consistent with the inferred cooling history of impact melt sheets (*Onorato et al.*, 1976, 1978).

It is difficult to distinguish between these hypotheses with the data presented here. The large size of the olivine phenocrysts relative to the microphenocrysts, and the presence of thin rims on the phenocrysts that are more or less in equilibrium with the adjacent glass, supports the first explanation—early crystallization at rates slow enough for the crystals to maintain bulk equilibrium with the melt, followed by more rapid crystallization. On the other hand, disequilibrium crystallization (i.e., crystallization where the effective K_d is ~ 0.5) is supported by the metastable expansion of the olivine phase volume into the plagioclase phase volume (Fig. 4). In any event, it is not necessary to invoke olivine accumulation to account for the apparent discrepancy in Fe-Mg partitioning. Olivine accumulation is not consistent with the observed textures, which must have formed by rapid "quench" crystallization.

In summary, we conclude that the high MgO concentrations observed in olivine vitrophyre bulk-rock samples is not the result of gravitational accumulation of olivine; the high MgO content of the bulk rock must be a primary characteristic of the original melt.

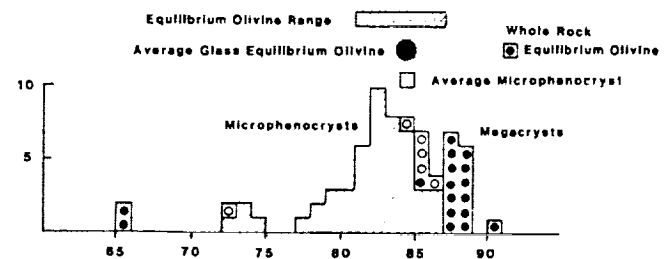


Fig. 6. Compositional data for olivine microphenocrysts (shaded), phenocrysts (open circles), and xenocrysts (closed circles) in vitrophyre DA-3, compared to the range of olivines in equilibrium with the residual glass (shaded bar), the olivine in equilibrium with the average residual glass (large filled circle), the average olivine microphenocryst (open square), and the olivine in equilibrium with the whole rock (filled circle in square). Note that the range of olivine in equilibrium with residual glass and the olivine in equilibrium with the average glass (based on $K_d = 0.33$) correspond to the observed range in olivine microphenocryst compositions and the average microphenocryst composition, respectively. This implies that equilibrium was maintained on a local scale, but not throughout the rock.

Olivine Vitrophyres and the Highland Mafic Component

All geochemical models of the soils and breccias in the lunar highlands have demonstrated the need for a mafic component that is not represented by any of the common lunar rock types. Mare basalts cannot fulfill this role because, although they are rich in mafic elements, their Mg/Fe ratio is too low. Dunite and lherzolite are more magnesian, but they are exceedingly rare and their Mg/Fe ratios are too high by a factor of 2 (Korotev *et al.*, 1980). The most recent suggestion is the postulate of Ringwood *et al.* (1987) that the mafic component at Apollo 16 derives from ancient komatiite lava flows.

The Mg content of the 14321 olivine vitrophyres is much higher than "normal" lunar soils or regolith breccias (e.g., Lau *et al.*, 1982; Jerde *et al.*, 1987) and presumably contains a higher proportion of the elusive mafic component. Because of their high MgO concentrations and intermediate Mg/Fe ratios, the 14321 olivine vitrophyres cannot be modeled as simple mixtures of the more common, felsic highland lithologies (anorthosite, norite, troctolite).

Least squares mixing models using both major and trace elements show that our "preferred" average olivine vitrophyre can be modeled as mixtures of various cryptic mafic components (e.g., SCCRV, MAF) plus KREEP, anorthosite, and an "extra lunar" (meteorite) component. Most models require ~30-35% mafic component, 50-55% KREEP, 8-10% anorthosite, and about 1.5% meteorite (Table 5). The fits are poor, however, and cannot be improved by adding other components such as mare basalt. The problem is exacerbated if we use a mafic component derived from Apollo 14 regolith breccias ("SCCRV-14"; Jerde *et al.*, 1987) because the MgO content of this component (~20% MgO) is the same as the 14321 vitrophyres. This leaves no room for the KREEP component, which must be over 50% to account for the high incompatible trace element concentrations.

A major problem with all of the mafic components calculated previously is that their Mg/Fe ratios and MgO concentrations are too low to reproduce the 14321 olivine vitrophyre composition when mixed with the large proportion of KREEP required to balance the trace element data. One solution to this problem is to calculate a mafic component that is tailored to the 14321 vitrophyres, using the same iterative technique as Wasson *et al.* (1977) and Korotev *et al.* (1980). The results of this exercise are shown in Table 7 as "MAF-14."

The major differences between MAF-14 and the other mafic components are its MG# (= 84) and its MgO concentration (~42 wt %), both of which are significantly higher than SCCRV, MAF, and Primary matter. Our preferred AOV comprises about 30% MAF-14, 53% KREEP, 13% alkali anorthosite, and 2% extra lunar component (Table 5). The Mg-rich nature of MAF-14 compared to other calculated mafic components must represent a real difference in the composition of mafic rocks that contribute to this component. This difference reflects the Mg-rich nature of the western highlands crust compared to the Apollo 16 highlands. In the next section, we attempt to relate this cryptic Mg-rich component to pristine rock types that constitute the western highlands crust.

Olivine Vitrophyres and the Pristine Highland Rocks

Previous studies of Apollo 14 breccias have established that Mg-suite troctolites and anorthosites, alkali anorthosites and norites, and mare basalts are the most common pristine rock types found at that site (Hunter and Taylor, 1983; Warren *et al.*, 1983a,b; Shervais *et al.*, 1983, 1984b, 1985b; Lindstrom *et al.*, 1984). Less common, but still important from a petrogenetic standpoint, are granite and ilmenite norites/gabbros, both of which may be associated with the alkali suite (Shervais and Taylor, 1986; James *et al.*, 1987). Dunite, pyroxenite and ferroan anorthosite are rare at the Apollo 14 site.

TABLE 5. Mixing results for Preferred 14321 AOV with various mafic components derived from the literature and by unmixing of our preferred AOV composition.

Component	Mix 1	Mix 2	Mix 3	Mix 4	Mix 5	Mix 6
SCCRV	31.1%	35.0%	-	-	-	-
MAF	-	-	34.7%	33.4%	-	-
MAF-14	-	-	-	-	29.4%	30.1%
KREEP	46.4%	38.9%	42.9%	45.1%	53.7%	52.1%
Meteorite	1.65%	1.68%	1.41%	1.42%	1.71%	1.70%
Granite	3.14%	2.98%	2.77%	1.51%	1.49%	0.76%
FAN	11.6%	-	11.9%	-	10.9%	-
ALKAN	-	17.0%	-	12.2%	-	13.5%
Sum	94.0%	95.5%	93.6%	93.6%	97.2%	98.1%
Chi-sq	23.5	19.4	26.1	27.4	5.6	4.3

Mafic components are SCCRV (Wasson *et al.*, 1977), MAF (Korotev *et al.*, 1980), and MAF-14 (derived here). Results for the Primary matter of Wänke *et al.* (1977) are similar to those of SCCRV. Other components are KREEP (Warren and Wasson, 1979), FAN (Wasson *et al.*, 1977), ALKAN (14305,400; Shervais *et al.*, 1984b), meteorite (Boynston *et al.*, 1975), and granite (14321,1198; unpublished data). MAF-14 derived by successive approximations to provide reasonable match to bulk MgO and Mg#. KREEP adjusted to higher SiO₂ (49.5%) and TiO₂ (2.0%) to provide better fits.

The composition of olivine and plagioclase xenocrysts in the 14321 vitrophyres provide important clues concerning the constitution of the source rocks. Olivine xenocrysts are mostly magnesian (FO_{87} to FO_{90}), but one ferroan olivine is also found (FO_{66}). Plagioclase/maskelynite xenocrysts span a wide range of compositions, from $AN_{83.6}$ to $AN_{94.6}$ (Table 2). These xenocrysts reflect a range in parent rock types that corresponds to the common pristine rock types at the Apollo 14 site: Mg-suite troctolites (calcic plagioclase, magnesian olivine), alkali anorthosites or gabbronorites (sodic plagioclase), and possibly mare basalt (ferroan olivine). Ferroan anorthosite (calcic plagioclase, ferroan olivine) may be present also, but is not required. The correspondence between the inferred parent lithologies and rock types common in the Apollo 14 sample suite supports the idea that local crust was sampled by the impact.

Geochemical studies of Apollo 14 pristine rocks have shown that these lithologies are generally enriched in incompatible trace elements relative to similar rocks from other sites (*Warren et al.*, 1983a,b; *Sbervais et al.*, 1983, 1984b, 1985b; *Lindstrom et al.*, 1984). Least squares mixing models using pristine rock compositions from the Apollo 14 site show that the preferred average olivine vitrophyre may be modeled with moderate success as a mix of KREEP (~50-60%), dunite (~25-30%), mare basalt (~10-12%), granite (~0-2%), anorthosite (8-12%), and an extra lunar component (~2%). The exact proportions vary somewhat, depending on the type of anorthosite used (Table 6). Mare basalt is required to account for the high Sc, V, Fe, and Ti; small amounts of granite help raise the Si content of the mix.

The high concentration of KREEP derived from the mixing models is required by the incompatible trace element data. Olivine vitrophyres have K, REE, P, and Hf concentrations 10× to 200× higher than most pristine highland rocks, and about half that of high-K KREEP. Because Apollo 14 alkali anorthosite has higher REE, K, and Na concentrations than FAN, slightly lower KREEP contents are necessary when alkali anorthosite

is used in place of FAN as the anorthosite component (Table 6). Regardless of which anorthosite is used, however, the overall chemistry of the mix is strongly dominated by KREEP.

We suggest that the mixing components used here do not necessarily represent distinct components in the lunar crust. As discussed by *Korotev et al.* (1980), the cryptic mafic component (dunite in this case) may represent the mafic portion of some prevalent lunar rock type. If we mix dunite with anorthosite, the result is an Mg-rich troctolite (Table 7) that probably represents the average composition of Mg-suite rocks melted in the impact event. Alkali-rich lithologies are most likely represented by the KREEP component, which has affinities to alkali anorthosites, norites, and ilmenite gabbronorites. These rocks have an average major element composition that is roughly equivalent to norite and similar to high-K KREEP, and their trace elements are dominated by a KREEPy overprint, so they may easily be represented in the mixing models by a single component.

Mixing models that use only these two components (Mg-rich troctolite and KREEP) plus an extra lunar component provide good solutions (Table 6) that suggest the proportions of Mg-suite and alkali suite rocks in the Apollo 14 crust. Alkali suite rocks predominate by a two-to-one ratio over Mg-suite rocks, approximately the inverse found for pristine rocks. The difference may be explained by the common occurrence of KREEP as an extrusive rock (*Shirley and Wasson*, 1981), or from the exclusion of the nonpristine KREEPy granulitic norites, which are probably the most common alkali suite lithology.

Implications for the Composition of the Western Lunar Crust

Studies of terrestrial impact melt sheets have shown that they have extremely homogeneous compositions due to turbulent mixing of the superheated melt phase with entrained clasts (*Simonds et al.*, 1976, 1978). Further studies have shown that most of the melt sheet is confined to the crater cavity,

TABLE 6. Mixing results for Preferred 14321 olivine vitrophyre using pristine highland lithologies from Apollo 14.

Component	Mix 1	Mix 2	Mix 3	Mix 4	Mix 5	Mix 6
Dunite	23.7%	23.7%	24.4%	24.3%	-	-
MGTRC	-	-	-	-	32.9%	33.7%
FAN	8.2%	-	-	-	0.33%	-
Magan	-	9.9%	-	-	-	-
ALKAN	-	-	10.8%	10.6%	-	-
KREEP	53.2%	51.0%	48.9%	51.0%	51.7%	61.2%
Meteorite	1.83%	1.80%	1.83%	1.83%	1.80%	1.80%
Granite	1.65%	1.79%	1.41%	-	1.72%	-
Mare	8.2%	8.6%	10.0%	9.3%	8.3%	-
Sum	96.8%	96.7%	97.4%	97.0%	96.7%	96.7%
Chi-sq	4.3	3.7	2.5	2.45	3.7	4.3

MGTRC derived from mix of dunite (72%) and Mg-suite anorthosite (28%). Components are same as Table 5, except dunite and Magan from *Lindstrom et al.* (1984) and mare from *Sbervais et al.* (1985b).

although ejected melt may be transported as far as one crater diameter (Howard and Wilshire, 1975; Hörz et al., 1983). This implies a relatively local origin for melt rocks. Melt rocks that remain within the crater cavity may be redistributed by later impacts.

The 14321 olivine vitrophyres are anomalously mafic compared to average lunar crust calculated from surface chemistry (e.g., Adler and Trombka, 1977; Taylor and Jakes, 1974; Taylor, 1982) and compared to the Apollo 14 regolith, which averages about 9.5% MgO (Laul et al., 1982). Since surface geochemistry is skewed towards surface lithologies (e.g., Ryder and Wood, 1977), these data imply that the mafic

TABLE 7. Cryptic components derived from 14321 vitrophyres.

	MAF-14	MGTRC
Wt %		
SiO ₂	42.0	41.4
TiO ₂	0.4	0.116
Al ₂ O ₃	1.20	9.195
FeO	15.0	8.30
MgO	41.0	36.78
CaO	0.8	5.42
Na ₂ O	0.25	0.165
K ₂ O	0.05	0.035
ppm		
Sc	30	4.35
Cr	2800	434
Co	40	45.5
Ni	120	64.4
La	0.2	9.72
Ce	0.54	24.7
Sm	0.12	4.16
Eu	0.10	0.75
Yb	0.13	2.73
Lu	0.02	0.472
Hf	0.10	1.745

component of lunar crust must reside at deeper crustal levels. The outstanding question is, how deep?

The generation of mafic-rich impact melts is commonly thought to require a basin-forming impact large enough to sample the deeper crustal levels where mafic-rich protoliths are thought to dominate (e.g., Ryder and Bower, 1977). The only basin close enough to the Apollo 14 site to be a reasonable candidate, however, is the Imbrium basin. Olivine vitrophyres are too high in MgO, however, to represent Imbrium basin impact melt; the best-documented samples of Imbrium basin impact melt (15445 and 15455) contain only 13% to 14% MgO (Ryder and Bower, 1977).

Pieters (1982) has reported spectral reflectance data that show that the central peak of Copernicus is dominated by dunite, which we have shown may represent the mafic component in the 14321 olivine vitrophyres. Extrapolation of data on cratering dynamics to a crater the size of Copernicus (~96 km) suggests that the central peak material was excavated from depths of up to 10 km (Pieters, 1982; Pieters and Wilhelms, 1985). Thus, the mafic component is closer to the surface in some areas than one would assume from the surface

chemistry data. Pieters and Wilhelms (1985) attribute this near-surface enrichment in mafic material to removal of the early ferroan crust by ballistic erosion during basin-forming impacts (e.g., the Procellarum basin event).

Hawke and Head (1977) made an extensive survey of pre-Imbrium craters in the Fra Mauro region. They found four craters ("northwest," "central," "site," and Fra Mauro) that are close enough to the Apollo 14 landing site to deposit significant amounts of impact melt at the site. Only two of these ("northwest" and Fra Mauro) are large enough (95 to 136 km in diameter) to generate impact melt deep enough to involve mafic rocks like those inferred to underlie Copernicus (95 km diameter) by Pieters (1982). There are many other potential source craters that are farther away, but the lack of shock features in the olivine vitrophyre clasts argues against emplacement by later impacts into an already solid melt sheet.

The enrichment in KREEP observed in Apollo 14 soils, breccias, and orbital geochemistry must extend to at least 12-17 km depth in the Apollo 14 crust, based on the estimated maximum depths of excavation calculated by Hawke and Head (1977) for Fra Mauro and "northwest" craters. KREEPy element concentrations are as high in the 14321 olivine vitrophyres as they are in the Apollo 14 regolith, despite the high concentration of mafic components in the vitrophyres. The implication here is that KREEP is an important component in the intermediate crust, where it is part of the indigenous rock suite. This deeper crustal KREEP may exist in the form of KREEPy norite plutons (e.g., Ryder and Wood, 1977; Ryder, 1976; Warren et al., 1983a,b; Lindstrom et al., 1984; Shervais and Taylor, 1986).

The mixing models calculated here for the olivine vitrophyres show that granite remains a minor but important mixing component at the Apollo 14 site, consistent with its observed modal abundance in the A-14 pristine rock suite, in the A-14 regolith, and in A-14 regolith breccias (Warren et al., 1983; Simon et al., 1982; Jerde et al., 1987). The inferred abundance of granite in A-14 regolith breccias (Jerde et al., 1987) and in the 14321 vitrophyres (1-2 wt %) is much higher than that estimated for A-14 regolith (0.3-0.5 wt %; Shervais and Taylor, 1983; Jerde et al., 1987). This suggests that granite may also be more common deeper in the crust, probably in association with noritic plutons of the alkali-rich suite (e.g., Ryder, 1976; James, 1980).

CONCLUSIONS

The data presented here show that the olivine vitrophyres of lunar breccia 14321 are impact melt rocks, as proposed by Allen et al. (1979). These rocks are unusual because they are exceptionally rich in both KREEP and a high-Mg mafic component. KREEPy trace elements are present in concentrations approximately 0.5 times the high-K KREEP component of Warren and Wasson (1979). The high MgO concentration of the vitrophyres is manifest by skeletal quench crystals of olivine that constitute approximately 30% of the mode.

Mixing calculations show that the mafic component of the 14321 olivine vitrophyres is more magnesian than cryptic mafic components isolated at the Apollo 16 site (SCCRV, MAF, Primary

matter) and cannot be modeled by any mixture that uses these cryptic components. Mixing calculations based on pristine highland lithologies require about 25% dunite and 10% anorthosite, along with KREEP, granite, and extra lunar material. Since dunite is not a common rock type, we suggest that its components occur combined with "anorthosite" as Mg-suite troctolite. Alkali-rich lithologies are represented by KREEP and minor granite.

The absence of ferroan anorthosite from this assemblage is consistent with a crust that is locally dominated by later Mg-suite and alkali-suite plutons. Since dense Mg-suite magmas are not likely to be emplaced at shallow levels in a ferroan anorthosite crust, the emplacement of Mg-rich material close enough to the surface to be sampled by 100-km size craters probably requires that the early ferroan crust was thinned or removed by ballistic erosion during basin-forming impacts (e.g., *Shervais and Taylor, 1986; Pieters and Wilhelms, 1985*).

The importance of impact melt rocks in deciphering lunar crustal origins should not be overlooked in the current fervor for pristine rocks. Many important rock types may not be sampled in their pristine state because they formed on the lunar surface during the later stages of accretion, or because they occur deep within the crust and are only sampled by large impacts which destroy their pristinity. The merits of nonpristine rocks for understanding the origin of the lunar crust are aptly demonstrated by the data presented here on the 14321 olivine vitrophyres.

Acknowledgments. This paper benefited from useful discussions with J. W. Delano. Logistical support was provided by the Planetary Materials Curatorial Staff, and especially Rene Martinez. This work was supported by NASA grants NAG 9-62 (L. A. Taylor), NSG 9-56 (L. A. Haskin), and NAG 9-169 (J. Shervais).

REFERENCES

- Adler J. and Trombka J. (1977) Orbital chemistry—lunar surface analysis from the X-ray and gamma ray remote sensing experiments. In *Chemistry of the Moon, Phys. Chem. Earth, 10*, 17-43.
- Allen F. M., Bence A. E., Grove T. L. (1979) Olivine vitrophyres in Apollo 14 breccia 14321: Samples of the high-Mg component of the lunar highlands. *Proc. Lunar Planet. Sci. Conf. 10th*, 695-712.
- Bianco A. and Taylor L. A. (1976) Cooling rate experimentation on olivine normative mare basalts: effects of FeO content on mineral texture and chemistry. *Geol. Soc. Am., Abstracts with Programs*, 8, 778.
- Boynton W. V., Baedeker P. A., Chou C.-L., Robinson K. L., and Wasson J. T. (1975) Mixing and transport of lunar surface materials: Evidence obtained by the determination of lithophile, siderophile, and volatile elements. *Lunar Sci. Conf. 6th*, 2241-2259.
- Donaldson C., Usselman T., Williams R., and Lofgren G. (1975) Experimental modeling of the cooling history of Apollo 12 olivine basalts. *Proc. Lunar Planet. Sci. Conf. 6th*, 843-869.
- Duncan A. R., McKay S. M., Stoesser J. W., Lindstrom M. M., Lindstrom D. J., Fruchter J. S., and Gales G. A. (1975) Lunar polymict breccia 14321: a compositional study of its principal components. *Geochim. Cosmochim. Acta*, 39, 247-260.
- Grieve R. A. F., McKay G. A., Smith H. D., and Weill D. F. (1975) Lunar polymict breccia 14321: a petrographic study. *Geochim. Cosmochim. Acta*, 39, 229-246.
- Grover J. E., Lindsley D. H., and Bence A. E. (1980) Experimental phase relations of olivine vitrophyres from breccia 14321: the temperature and pressure dependence of Fe-Mg partitioning for olivine and liquid in a highlands melt-rock. *Proc. Lunar Planet. Sci. Conf. 11th*, 179-196.
- Hawke R. and Head J. W. (1977) Pre-Imbrium history of the Fra Mauro region and Apollo 14 sample provenance. *Proc. Lunar Sci. Conf. 8th*, 2741-2761.
- Hörz F., Ostertag R. and Rainey D. (1983) Bunte breccia of the Ries: continuous deposits of large impact craters. *Rev. Geophys. Space Phys.*, 21, 1667-1725.
- Howard K. A. and Wilshire H. G. (1975) Flows of impact melt at lunar craters. *J. Res. U.S. Geological Survey*, 3, 237-251.
- Hunter R. H. and Taylor L. A. (1983) The magma ocean from the Fra Mauro shoreline: An overview of the Apollo 14 crust. *Proc. Lunar Planet. Sci. Conf. 13th*, in *J. Geophys. Res.*, 88, A591-A602.
- James O. B. (1980) Rocks of the early lunar crust. *Proc. Lunar Planet. Sci. Conf. 11th*, 365-393.
- James O. B., Lindstrom M. M., and Flohr M. K. (1987) Petrology and geochemistry of alkali gabbroanorthites from lunar breccia 67975. *Proc. Lunar Planet. Sci. Conf. 17th*, in *J. Geophys. Res.*, 92, E314-E330.
- Jerde E., Warren P. H., Morris R. V., Heiken G., and Vaniman D. T. (1987) A potpourri of regolith breccias: "New" samples from the Apollo 14, 16, and 17 landing sites. *Proc. Lunar and Planet. Sci. Conf. 17th*, in *J. Geophys. Res.*, 92, E526-E536.
- Knapp S. A. (1986) *Petrogenesis of Apollo 14 Lunar Breccia 14321*. M.S. Thesis, University of Tennessee. 118 pp.
- Korotev R. L., Haskin L. A., and Lindstrom M. M. (1980) A synthesis of lunar highlands compositional data. *Proc. Lunar Planet. Sci. Conf. 11th*, 395-429.
- Laul J. C., Papike J. J. and Simon S. B. (1982) The Apollo 14 regolith: chemistry of cores 14210/14211 and 14220 and soils 14141, 14148, 14149. *Proc. Lunar Planet. Sci. Conf. 13th*, in *J. Geophys. Res.*, 87, A247-A259.
- Lindstrom D. J. and Korotev R. L. (1982) TEABAG: computer programs for instrumental neutron activation analysis. *J. Radioanal. Chem.*, 70, 439-458.
- Lindstrom M. M. (1984) Alkali gabbroanorthitic, ultra-KREEPy melt rock and the diverse suite of clasts in North Ray Crater feldspathic fragmental breccia 67975. *Proc. Lunar Planet. Sci. Conf. 15th*, in *J. Geophys. Res.*, 90, C50-C62.
- Lindstrom M. M., Duncan A. R., Fruchter J. S., McKay S. M., Stoesser J. W., Gales G. G., and Lindstrom D. J. (1972) Compositional characteristics of some Apollo 14 clastic materials. *Proc. Lunar Sci. Conf. 3rd*, 1201-1214.
- Lindstrom M. M., Knapp S. A., Shervais J. W., and Taylor L. A. (1984) Magnesian anorthosites and associated troctolites and dunite in Apollo 14 breccias. *Proc. Lunar Planet. Sci. Conf. 15th*, in *J. Geophys. Res.*, 89, C41-C49.
- Nabelek P. I., Taylor L. A. and Lofgren G. E. (1978) Nucleation and growth of plagioclase and development of texture in a high-alumina basaltic melt. *Proc. Lunar Planet. Sci. Conf. 9th*, 725-741.
- Onarato P., Uhlmann D., and Simonds C. (1976) Heat flow in impact melts: Apollo 17 station 6 boulder and some applications to other breccias and xenolith laden melts. *Proc. Lunar Planet. Sci. Conf. 7th*, 2449-2467.
- Onarato P., Uhlmann D., and Simonds C. (1978) The thermal history of the Manicougan impact melt sheet, Quebec. *J. Geophys. Res.*, 83, 2789-2798.
- Pieters C. M. (1982) Copernicus crater central peak: lunar mountain of unique composition. *Science*, 215, 59-61.
- Pieters C. M. and Wilhelms D. E. (1985) Origin of olivine at Copernicus. *Proc. Lunar Planet. Sci. Conf. 15th*, in *J. Geophys. Res.*, 90, C415-C420.

- Ringwood A. E., Seifert S., and Wänke H. (1987) A komatiite component in Apollo 16 highland breccias: implications for the nickel-cobalt systematics and bulk composition of the moon. *Earth Planet. Sci. Lett.*, **81**, 105-117.
- Ryder G. (1976) Lunar sample 15405: remnant of a KREEP basalt-granite differentiated pluton. *Earth Planet. Sci. Lett.*, **29**, 255-268.
- Ryder G. and Bower J. F. (1977) Petrology of Apollo 15 black-and-white white rocks 15445 and 15455—fragments of the Imbrium melt sheet? *Proc. Lunar Planet. Sci. Conf 8th*, 1895-1923.
- Ryder G. and Wood J. A. (1977) Serenitatis and Imbrium impact melts: implications for large scale layering in the lunar crust. *Proc. Lunar Planet. Sci. Conf 8th*, 655-668.
- Servais J. W. and Taylor L. A. (1983) Micrographic granite: More from Apollo 14 (abstract). *Lunar and Planetary Science XIV*, pp. 696-697. Lunar and Planetary Institute, Houston.
- Servais J. W. and Taylor L. A. (1984) Consortium breccia 14321: Petrology of mare basalts and olivine vitrophyres (abstract). *Lunar and Planetary Science XV*, pp. 766-767. Lunar and Planetary Institute, Houston.
- Servais J. W. and Taylor L. A. (1986) Petrologic constraints on the origin of the Moon. In *Origin of the Moon* (W. K. Hartman, R. J. Phillips, and G. J. Taylor, eds.), pp. 173-202. Lunar and Planetary Institute, Houston.
- Servais J. W., Taylor L. A., and Laul J. C. (1983) Ancient crustal components in the Fra Mauro breccias: implications for igneous processes. *Proc. Lunar Planet. Sci. Conf. 14th*, in *J. Geophys. Res.*, **88**, B177-B192.
- Servais J. W., Knapp S., and Taylor L. A. (1984a) *Breccia guidebook No. 7: 14321*. NASA-JSC Publication #69, Planetary Materials Branch, 57 pp.
- Servais J. W., Taylor L. A., Laul J. C., and Smith M. R. (1984b) Pristine highland clasts in consortium breccia 14305: Petrology and geochemistry. *Proc. Lunar Planet. Sci. Conf. 15th*, in *J. Geophys. Res.*, **89**, C25-C40.
- Servais J. W., Taylor L. A., and Lindstrom M. M. (1985a) Olivine vitrophyres—a nonpristine high-Mg component in lunar breccia 14321 (abstract). In *Lunar and Planetary Science XVI*, pp. 771-772. Lunar and Planetary Institute, Houston.
- Servais J. W., Taylor L. A., and Lindstrom M. M. (1985b) Apollo 14 mare basalts: petrology and geochemistry of clasts from consortium breccia 14321. *Proc. Lunar Planet. Sci. Conf. 15th*, in *J. Geophys. Res.*, **90**, C375-C395.
- Servais J. W., Knapp S., Taylor L. A., and Lindstrom M. M. (1985c) Petrology and geochemistry of microbreccia clasts and matrix in lunar breccia 14321 (abstract). In *Lunar and Planetary Science XVI*, pp. 767-768. Lunar and Planetary Institute, Houston.
- Shirley D. and Wasson J. T. (1981) A mechanism for the extrusion of KREEP. *Proc. Lunar Planet. Sci. 12B*, 965-978.
- Simon S. B., Papike J. J., Laul J. C. (1982) The Apollo 14 regolith: Petrology of cores 14210/14211 and 14220 and soils 14141, 14148, and 14149. *Proc. Lunar Planet. Sci. Conf. 13th*, in *J. Geophys. Res.*, **87**, A232-A246.
- Simonds C., Warner J., Phinney W., and McGee P. (1976) Thermal model for impact breccia lithification: Manicougan and the moon. *Proc. Lunar Planet. Sci. Conf 7th*, 2509-2528.
- Simonds C., Floran R., McGee P., Phinney W., and Warner J. (1978) Petrogenesis of melt rocks, Manicougan impact structure, Quebec. *J. Geophys. Res.*, **83**, 2773-2788.
- Swann G. A., Bailey N. G., Batson R. M., Eggleton R. E., Hait M. H., Holt H. E., Larson K. B., Reed V. S., Schaber G. G., Sutton R. L., Trask N. J., Ulrich G. E., and Wilshire H. G. (1977) Geology of the Apollo 14 landing site in the Fra Mauro highlands. *U.S. Geological Survey Prof. Pap.*, **880**, 103 pp.
- Taylor S. R. (1982) *Planetary Science—a lunar perspective*. Lunar and Planetary Institute, Houston. 481 pp.
- Taylor S. R. and Jakes P. (1974) The geochemical evolution of the Moon. *Proc. Lunar Sci Conf. 5th*, 1287-1305.
- Taylor L. A. and Nabelek P. I. (1979) Effects of kinetics on the crystallization sequences in basalts (abstracts). In *Lunar and Planetary Science Conference X*, pp. 1212-1213. Lunar and Planetary Institute, Houston.
- Vaniman D. T. and Papike J. J. (1980) Lunar highland melt rocks: Chemistry, petrology and silicate mineralogy. *Proc. Conf. Lunar Highlands Crust* (J. J. Papike and R. B. Merrill, eds.), pp. 271-337.
- Walker D. (1983) Lunar and terrestrial crust formation. *Proc. Lunar Planet. Sci. Conf. 14th*, in *J. Geophys. Res.*, **88**, B17-B25.
- Walker D., Grove T. L., Longhi J., Stolper E. M., and Hays J. F. (1973) Origin of lunar feldspathic rocks. *Earth Planet. Sci. Lett.*, **20**, 325-336.
- Wänke H., Baddenhausen H., Blum K., Cendales M., Dreibus G., Hofmeister H., Kruse H., Jagoutz E., Palme C., Spettel B., Thacker R., and Völcek E. (1977) On the chemistry of lunar samples and achondrites: Primary matter in the lunar highlands, a re-evaluation. *Proc. Lunar Planet. Sci. Conf 8th*, 2191-2213.
- Wänke H., Palme H., Kruse H., Baddenhausen H., Blum K., Cendales M., Dreibus G., Hofmeister H., Jagoutz E., Palme C., Spettel B., Thacker R. (1976) Chemistry of lunar highland rocks: a refined evolution of the composition of the primary matter. *Proc. Lunar Sci. Conf. 7th*, 3479-3499.
- Warren P. H. and Wasson J. T. (1979) The origin of KREEP. *Rev. Geophys. Space Phys.*, **17**, 73-88.
- Warren P. H., Taylor G. J., Keil K., Kallemeyn G. W., Rosener P. S., and Wasson J. T. (1983a) Sixth foray for pristine nonmare rocks and an assessment of the diversity of lunar anorthosites. *Proc. Lunar Planet. Sci. Conf. 13th*, in *J. Geophys. Res.*, **88**, A615-A630.
- Warren P. H., Taylor G. J., Keil K., Kallemeyn G. W., Shirley D., and Wasson J. T. (1983b) Seventh foray: whitlockite-rich lithologies, a diopside bearing troctolitic anorthosite, ferroan anorthosites, and KREEP. *Proc. Lunar Planet. Sci. Conf. 13th*, in *J. Geophys. Res.*, **88**, A615-A630.
- Wasson J. T., Warren P. H., Kallemeyn G. W., McEwing C. E., Mittlefehldt D. W., and Boynton W. V. (1977) SCCRV, a major component of highland rocks. *Proc. Lunar Planet. Sci. Conf. 8th*, 2237-2252.



HIGHLAND CRUST AT THE APOLLO 14 SITE: A REVIEW

SI-9/
170681

p. 10

John W. Shervais, Department of Geological Sciences, University of South Carolina,
Columbia SC 29208

Recent petrologic studies of pristine nonmare samples from the Apollo 14 site have demonstrated the unique character of the western highlands crust. Many of the lithologies which occur here are not found at other highland sites or represent unique variations of more common lithologies. Rare highland samples found at the Apollo 12 site have petrologic and geochemical affinities with the Apollo 14 highland suite and the two sites taken together constitute what can be called the Western Highland Province. Rocks of the Western Highland Province are geochemically distinct from similar lithologies found at eastern highland sites (Apollo 15, Apollo 16, Apollo 17, and the Luna sites) -- a fact which adds further complications to current petrogenetic models for the lunar crust (e.g., [1]; [2]; [3]). Nonetheless, an understanding of how the Western Highlands Province formed and why it differs from highland crust in the east is crucial to our overall understanding of primordial lunar differentiation and petrogenesis.

OCCURRENCE: Highland plutonic rocks at the Apollo 14 site occur only as clasts in the crystalline-matrix Fra Mauro breccia (e.g., 14304, 14305, 14321) or in younger regolith breccias (e.g., 14312, 14318). Many of these clasts have rims of an older, dark breccia matrix attached, which shows that these rocks have been effected by at least two or three episodes of brecciation. Texturally the clasts vary from cataclasites with no surviving primary textures, to texturally pristine clasts with well preserved igneous textures. The texturally pristine clasts are generally chemically pristine as well, unless they have been invaded by thin glass veins of melt rock. Many texturally pristine clasts are known only from thin section and electron microprobe study, and no chemical data are available. Pristinity of the cataclasites must be evaluated chemically using siderophile element concentrations and the cut-off values for siderophile contamination suggested by Warren and Wasson [4].

LITHOLOGIES: Three distinct suites of plutonic rock are important at the Apollo 14 site: the Magnesian suite, the Alkali suite, and a variety of evolved lithologies. The Magnesian suite can be further subdivided into the olivine-bearing magnesian troctolite association (which includes troctolite, anorthosite, dunite, and pyroxene-bearing troctolites) and the less abundant magnesian norite association (which includes norites, olivine norites, gabbro-norites, and ilmenite gabbros/norites). Ferroan anorthosites ("FAN"), which dominate highland suites in some eastern provinces (Apollo 15, Apollo 16) are rare in the Western Highland Province. Each of these suites, including FAN, will be considered here in order of their relative abundance.

MAGNESIAN SUITE

Magnesian Troctolite Association: The magnesian troctolite association includes a variety of olivine-bearing rocks characterized by relatively calcic plagioclase compositions (An₉₃₋₉₆) and a range in olivine compositions (Fo₇₅₋₉₀). Troctolite is the most common lithology in this association, with modes around 30-40% olivine and 60-70% plagioclase ([1]; [5]; [2]; [6]; [7]). More mafic compositions with 50-60% olivine are less common (e.g., [7]; [11]), but troctolitic anorthosites with 10-15% olivine and 85-90% plagioclase are widespread ([5]; [8]; [9]). A few troctolites also contain minor enstatite and diopside. Other important members of the Apollo 14 magnesian troctolite association include magnesian anorthosite, dunite, and pyroxene-rich troctolite.

Magnesian anorthosites are relatively new additions to the Mg-rich suite ([9]; [7]). These rocks are characterized by plagioclase-rich modes (90-99% plagioclase) with mineral compositions similar to the Mg-troctolites: An₉₄₋₉₇ plagioclase with minor Fo₈₄₋₉₀ olivine. An REE-rich Ca-phosphate phase (probably whitlockite) forms a large, 500 x 120 micron, anhedral grain in one of these anorthosites ([7] [19]) and may contain almost all of the REE found in this samples.

Dunite is another rare but important member of the magnesian troctolite association. Two small dunite clasts have been found to date: one in breccia 14321 ([7]), the other in breccia 14304 ([11]). Both consist of nearly pure Fo₈₈₋₈₉ olivine with almost no compositional variation either within or between the two clasts.



Two *pyroxene-rich troctolite* clasts have also been found. One is an anorthositic troctolite with 80% plagioclase, 15% olivine, and 5% diopside, the other is a mafic troctolite with 46% plagioclase, 47% olivine, 7% enstatite, and minor Cr-pleonaste [8,9,10]. Mineral compositions are similar in both, with An94-95 plagioclase, Fo88-89 olivine, and pyroxene Mg#s ($= 100 \cdot \text{Mg}/(\text{Mg} + \text{Fe})$) of 90. The Mg-rich compositions of the olivines and coexisting pyroxenes indicates that the parent magmas reached pyroxene saturation early in their fractionation history, prior to extensive olivine fractionation. In addition, the stable coexistence of olivine-enstatite and enstatite-spinel (both in discrete grains and in enstatite-spinel symplectites) indicates that crystallization occurred relatively deep in the crust, where the four-phase assemblage ol-plg-opx-sp was stable [8,9,10].

Hunter and Taylor [5] were first to notice a compositional gap between two troctolite subgroups (figure 1). Group I troctolites tend to have more mafic-rich modes and more magnesian phase compositions (olivine Fo85-90); Group II troctolites are more felsic modally and have more Fe-rich mineral compositions (olivine Fo74-81). All of the minor lithologies discussed above plot with the Group I troctolites. Only one sample of Group II troctolite has been analyzed chemically (14321 c2 -- [2]). Its incompatible element abundances are in the same range as the more numerous Group I troctolites.

Magnesian Norite Association: The magnesian norite association contains a diverse assemblage of rocks referred to as ilmenite gabbros, ilmenite norites, and gabbronorites [3,5,8,11]. Only four clasts have been described so far that can be considered unequivocally part of the Mg-suite: norite 14063 ,61 [5], gabbronorite 14304 ,125 [11], olivine norite 14318 ,149 [6], and olivine norite 14305 ,489 [12]. These rocks have modes with subequal portions of plagioclase and pyroxene -- generally pigeonite with minor augite. Ilmenite is a common accessory phase in some of these clasts, along with Ti-spinel, Fe-metal, and troilite. Plagioclase compositions are around An87-90 and mafic silicates have Mg#s between 70-75. One a plot of An content of plagioclase versus Mg# of mafic silicate (figure 1), these rocks plot between rocks of the magnesian troctolite association and the alkali suite.

Several clasts in breccias 14303, 14304, and 14305 are gabbronorites with An90-95 plagioclase and relatively Fe-rich mafic silicates with Mg#s 65-70 [8,11,12]. These rocks generally have orthocumulate or mesocumulate textures, with primocrysts of plagioclase and pigeonite surrounded by post-cumulus feldspar, pigeonite, augite, ilmenite, and Ti-spinel. Their modes are similar to the magnesian norites described above, but they plot *below* the Mg-suite field on an An-Mg# diagram, between the magnesian norites and the ferroan anorthosite field (figure 1). This is the same region where Apollo 14 mare basalts plot, suggesting that some of these gabbronorites may be cumulates derived from aluminous pigeonite basalts (e.g., [8]). Potential mare cumulates are characterized by high modal ilmenite and Ti-rich ($\text{TiO}_2 > 0.5 \text{ wt\%}$) cumulus pigeonites. These rocks also fall on calculated fractionation trends for Mg-suite parent magmas [13] and may be related to the Group II troctolites by fractional crystallization. Gabbronorites with Ti-poor pigeonite and low modal ilmenite may thus be related to more magnesian members of the Mg-suite.

ALKALI SUITE

Alkali Anorthosite/Norite Association: The Alkali suite was first recognized by Warren and Wasson [4] and subsequent studies established it as the second most common highland rock association at the Apollo 14 site [2,5,6,8,9,10]. This suite was once thought to be unique to the Western Highlands Province, but similar alkali gabbronorites are now known from the Apollo 16 site [7,14]. The most common lithologies are anorthosite and norite or gabbronorite; olivine norites are rare.

Alkali anorthosites were the first alkalic highland lithology recognized [1]. Seven true alkali anorthosites are known from Apollo 14 [1,5,9,10,11]. These rocks are characterized by modes of 95-100% plagioclase (An76-86) with minor pigeonite, augite, K-feldspar, ilmenite, silica, whitlockite, and Fe-metal. Mafic silicates have Mg#s 50-70, with the higher Mg#s being augite. Plagioclase primocrysts are up to 1.5 mm across; accessory phases are generally much smaller. Whitlockite (an REE-rich Ca-phosphate) occurs either as interstitial grains or as small inclusions in plagioclase primocrysts (indicating Ca-saturation) and may comprise up to 2% modally.



Alkali norites are another common alkalic lithology -- at least six clasts are currently recognized [5,6,8,10,11]. These rocks typically contain 75-85% modal plagioclase (An80-85), but more mafic clasts with 14-40% plagioclase are known. Pigeonite or hypersthene are the most common mafic phases, and may occur either as cumulus primocrysts or as post-cumulus crystals interstitial to plagioclase. Augite, K-feldspar, ilmenite, and whitlockite are common post-cumulus accessory phases; Mg#s in the mafic silicates are typically the same as in the alkali anorthosites (53-63 in pigeonite, 64-68 in augite). Whitlockite is found in most alkali norites and may comprise up to 35% of the mode [10]. As a result, REE in these clasts exhibit a wide range in concentrations.

Two *alkali olivine norites* have been described [12,14]. These rocks contain about 65% modal plagioclase, 25% orthopyroxene or pigeonite, and 5-10% olivine modally, with minor ilmenite, whitlockite, and troilite. Plagioclase compositions are typical of the alkali suite (An78-83), but the mafic silicate compositions are Mg-rich compared to typical alkali norites and anorthosites, with olivine Fo70-80 and pyroxene Mg#s 75-85 (figure 1).

EVOLVED LITHOLOGIES

The most common evolved lithology at Apollo 14, commonly referred to as "lunar granite", is a granophyric intergrowth of quartz and alkali feldspar, either alone, with sodic plagioclase (An60-80). The alkali feldspar vary from nearly pure orthoclase (Or95 Ab5) to a ternary feldspar (Or45 Ab25) which plots in the forbidden zone in a feldspar ternary [15,16,27]. In one small granite clast orthoclase and ternary feldspar both occur as granophyric intergrowths with quartz [27]. Accessory minerals include pigeonite, augite, ferroaugite, fayalite, ilmenite, zircon, and Ca-phosphates (apatite, whitlockite). Variations in mineral assemblages and in mineral compositions (e.g., BaO in alkali feldspars, Mg# in mafics) indicate that at least four distinct parent magmas are involved.

The only age data available at the Apollo 14 site on highland lithologies are from lunar granite 14321, 1027 [16,28]. This granite has been dated at 4.1 Ga using Rb/Sr isochron techniques [28]. Its $^{87}\text{Rb}/^{86}\text{Sr}$ and $^{87}\text{Sr}/^{80}\text{Sr}$ ratios are the highest yet measured on any lunar material [28].

Granite clasts are relatively common at the Apollo 14 site, which suggests that granite differentiates of mafic plutons are a common and important crustal component in the Western Highlands Province. Based on the abundance of K,Si-rich glasses in Apollo 14 soils and regolith breccias, granites are estimated to comprise 0.5% to 2% of the crust here [17,27].

FERROAN ANORTHOSITES

Ferroan anorthosites are rare at the Apollo 14 site. Only one clast of ferroan anorthosite has been characterized chemically and petrographically [6]. This clast is a monomict cataclasite which consists of nearly 100% plagioclase (An95.5) with relict grains up to 1.3 mm across. Olivine (Fo69) is the only mafic phase.

GEOCHEMISTRY OF THE WESTERN HIGHLANDS PROVINCE

Plutonic rocks of the Western Highlands Province are characterized by high concentrations of incompatible trace elements compared to their eastern counterparts. This characteristic applies to the only FAN clast analyzed to date, as well as to rocks of the magnesian and alkali suites [6]. Despite the fact that whole rock analyses of Apollo 14 plutonic rocks are very sensitive to accessory mineral contents due to the small size of most analyzed samples (< 100 mg), the observed enrichment of incompatible elements in these rocks appears to reflect a fundamental geochemical characteristic of the Western Highlands Province, and is not a spurious effect of sampling problems.

HIGHLAND CRUST AT APOLLO 14 Shervais, J. W.

Troctolites, anorthosites, and dunites of the magnesian suite are characterized by a wide range in REE concentrations, with La ranging from 15x to 700x chondrite (figure 2). The highest REE concentrations are found in magnesian anorthosites that contain abundant whitlockite [7,19]. More realistic estimates of crustal composition may be obtained from rocks with the lowest REE contents, but even these are much more enriched than comparable Mg-suite rocks from the east. In addition, parent magma REE concentrations of 3000x (for La) to 1500x (for Lu) chondrite are implied by whitlockite/liquid partition coefficients and the high REE concentrations found in the accessory whitlockite [7,19]. The calculated parent magma REE concentrations are about 10x KREEP --- far to high to have precipitated the observed primitive mineral compositions [7,9,19]. Lindstrom and others [7,19] suggest that the whitlockites may not be in equilibrium with the Mg-suite parent magma. They envisage formation of the phosphates after crystallization from metasomatic fluids which penetrate the rock from below. The source of this fluid and its physical nature (aqueous ? magmatic ?) is not yet resolved.

Rocks of the alkali anorthosite suite are characterized by a similar wide range in REE concentrations, with La from 35x to 600x chondrite (figure 3). As noted in the Mg-suite plutonic rocks, the highest incompatible element concentrations seem to occur in samples with high modal whitlockite and apatite (e.g., [10]). REE concentrations in accessory Ca-phosphate phases are similar to those observed in the Mg-suite rocks -- about 10,000x chondrite. Again, the parent magma composition implied by these concentrations is unrealistically high. In addition, major element compositions of the minerals in the alkali suite are much more evolved than minerals in the Mg-suite rocks, but their accessory phases have nearly identical trace element contents. Clearly, there is no simple explanation to this apparent paradox.

Chemical differences between rocks of the Western Highlands Province and nonmare plutonic rocks from the east are clearly illustrated by a plot of Sm (an incompatible MREE) and Eu (an MREE which is compatible with plagioclase under the reducing conditions found on the moon). Figure 4 shows data for ferroan anorthosites, eastern Mg-suite rocks, western Mg-suite rocks, and western alkalic rocks. Ferroan anorthosites and eastern Mg-suite rocks are characterized by low concentrations of Eu (.5 to 1.0 ppm) and a wide range of Sm concentrations, with Sm in FAN < 0.3 ppm and Sm in the eastern Mg-suite rocks > 0.5 ppm (figure 4). Western Mg-suite rocks have a range in Sm similar to the eastern troctolites (from 2 to 100 ppm Sm) but are enriched in Eu relative to the eastern rocks. Alkali anorthosites are even richer in Eu, with 2 to 10 ppm Eu in rocks with the same Sm content as the Magnesian suite.

ORIGIN OF THE WESTERN HIGHLAND PROVINCE

The high Sm concentrations which characterize plutonic rocks of the Western Highland Province also result in low Ti/Sm and Sc/Sm ratios [1]. These ratios are sub-chondritic, as in KREEP, and suggest derivation of western plutonic suites from an evolved crustal or upper mantle source. Alternatively, these low ratios may reflect the assimilation of residual urKREEP by magmas parental to Mg-suite rocks (e.g., [20]). However, if the incompatible element-rich magnesian suite troctolites, anorthosites, and dunites of Apollo 14 crystallized from Mg-rich magmas that were severely contaminated with urKREEP [20], where did the alkali suite magmas come from ??

Several scenarios can be envisioned for the origin of the western magnesian and alkali suite highland rocks. All of these models have certain attractive features, but none are entirely consistent with what we currently know about the western highland suite. Some possibilities include:

- (1) The Mg-suite and alkali suites represent distinct parent magmas, derived from different parts of the lunar mantle, each of which assimilated variable amounts of urKREEP prior to crystallization. This model begs the question of ultimate source, and does not address why there are two distinct parent magmas. It does seem consistent with the gap between the alkali suite and troctolites of the Mg-suite, and with the steep apparent fractionation trends seen in the magnesian troctolite association and in the alkali suite (figure 1). This steep trend in the alkali suite is accentuated by the recent discoveries of primitive olivine norites with typical alkalic plagioclase compositions.

- (2) The alkali suite represents Mg-suite magma which has evolved by AFC processes; its high alkali and trace element contents are attributed to relatively large fractions of assimilation. This model has the advantage of one parent magma, and seems in general consistent with the overall trend of the Mg-suite in figure 1. It does not explain, however, why both suites have the same range in trace element concentrations, or why the alkali suite has higher Eu concentrations than either the Mg-suite or KREEP -- fractional crystallization of plagioclase and KREEP assimilation should both act to lower Eu in a residual magma derived from the Mg-suite. It is also puzzling why there are so few Mg-suite norites intermediate to the alkalic rocks and the Mg-troctolites (figure 1). If variable contamination of a single magma was operative, a continuous trend in compositions would be expected.
- (3) The alkali suite represents cumulate rocks which crystallized from a KREEP parent magma. This magma was assimilated by Mg-suite parent magmas before they crystallized, or penetrated already crystallized Mg-suite plutons to enrich them metasomatically. It is not clear if the alkali suite cumulate rocks are consistent with this origin, but it does offer an attractive explanation to the contrasts in major and trace element compositions observed between the two suites.

The origin of the evolved lithologies cannot be established with any certainty [15,16,17,27]. Lunar granites are characterized by V-shaped REE patterns with LREE and HREE concentrations 100-200 times chondrite, MREE 100 times chondrite, and significant negative Eu anomalies [15,16,17]. Dickinson and Hess [29] have shown that lunar granites cannot form from KREEP parent magmas because overall REE concentrations are too low in the granites, and because KREEP has a steep negative HREE slope, while granites have a shallow positive slope. Other potential parent magmas include mare basalt, the alkali suite parent magma, and the Mg-suite parent magma [15,16,17,30,31]. The V-shaped REE patterns have been attributed to apatite fractionation [17], but fractional crystallization alone cannot create the observed major and trace element characteristics. In particular, the high K/La ratios of lunar granites seem to require silicate liquid immiscibility at some point in the fractionation history [15,16,17,27,30,31].

WHERE DO WE GO FROM HERE ?

Despite the tremendous increase since 1980 in geochemical and petrologic data on the Western Highlands Province, there are still large gaps in our understanding of how the western crust formed, and why it is different from the eastern crust. Since much of this uncertainty revolves around KREEP, a major priority should be detailed studies which focus on the origin of KREEP, its geochemistry, and its phase relations. In addition, age data is virtually nonexistent on highland lithologies at Apollo 14. Age data are critical to understanding how the alkali suite and Mg-suite rocks are related to one another, and to the aluminous mare basalts which are common at this site (e.g., [21,22,23]). The Apollo 14 aluminous mare basalts range in age from 3.75 to 4.3 Ga -- the same age inferred for many highland crustal rocks [24,25,26]. The relationship between this early mare volcanism and crust forming-processes needs to be thoroughly explored. In addition to these efforts, more data are needed on the variety of highland rock types present at the Apollo 14 site, with special emphasis on integrating whole rock chemistry with phase chemistry (e.g., [19]). The question of possible metasomatism must be addressed, including the specific transport mechanism and the source of the metasomatic fluid.

The unique nature of the highland suite at Apollo 14 provides an exciting opportunity to investigate variations in the lunar crust which formed during the earliest stages of lunar differentiation and perhaps earlier, during accretion. Understanding the origin of these primordial variations in the lunar crust will increase our understanding of how planetary crusts form and evolve, and should give us important insights into the early evolution of the Earth as well.



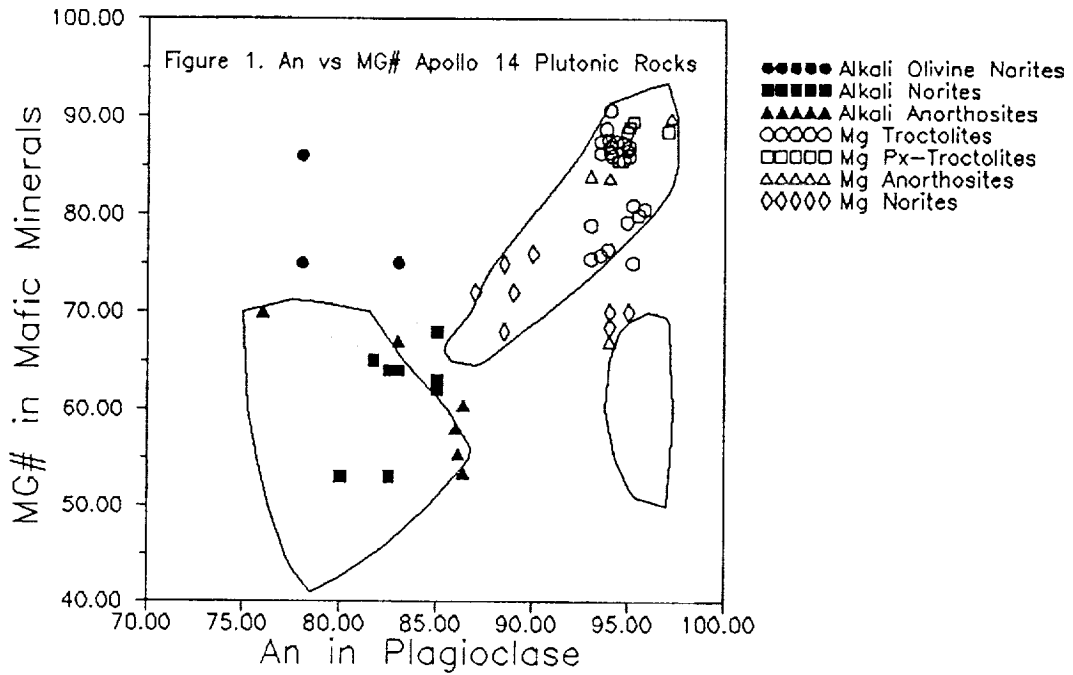


Figure 1. An in plagioclase versus MG# in mafic mineral for plutonic rocks from the Apollo 14 site. Mg-suite rocks are shown in open symbols, as are norites which plot between the Mg-suite data field and the FAN data field. Alkali suite rocks are shown in filled symbols.

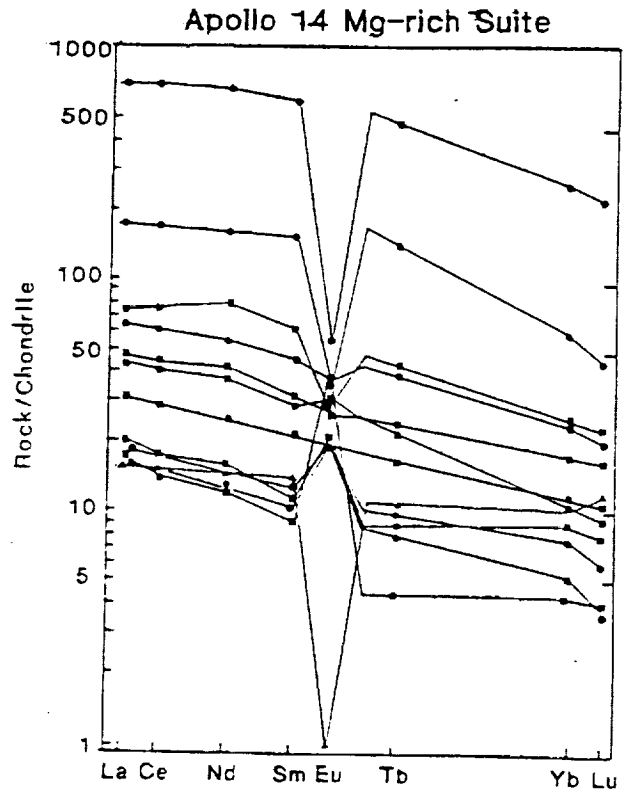


Figure 2. Chondrite-normalized REE patterns for Magnesian suite troctolites (squares), anorthosites (circles), and a dunite (triangle). After Shervais and Taylor, 1985.

HIGHLAND CRUST AT APOLLO 14
 Shervais J. S.

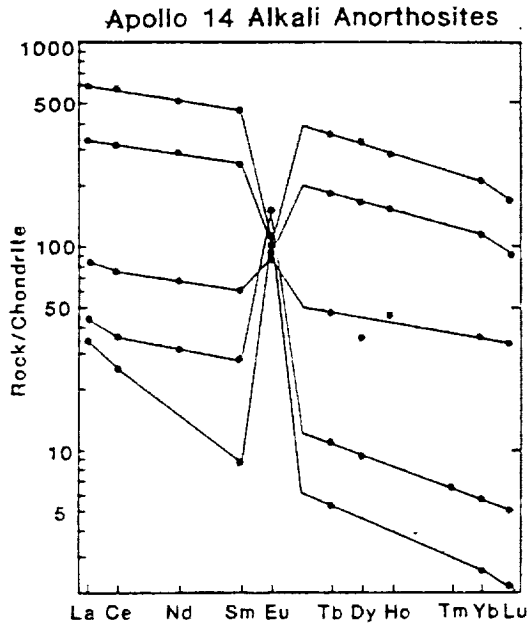
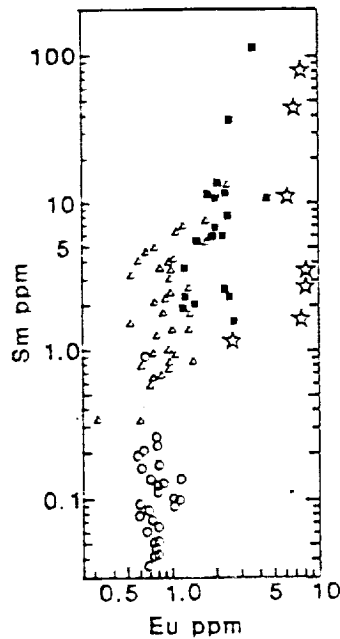


Figure 3. Chondrite-normalized REE patterns for representative alkali suite anorthosites and norites. After Shervais and Taylor, 1985.

Figure 4. Sm vs Eu plot, with data for eastern ferroan anorthosites (open circles), eastern Mg-suite rocks (open triangles), western Mg-suite rocks (filled squares), and western alkali suite rocks (Stars). Western rocks are characterized by higher concentrations of Eu relative to Sm than equivalent eastern rocks.



REFERENCES

- [1] Warren P.H. and Wasson J.T. (1980) Further foraging for pristine nonmare rocks: Correlations between geochemistry and longitude. *Proc. Lunar Planet. Sci. Conf. 11th*, pp. 431-470.
- [2] Warren P.H., Taylor G.J., Keil K., Marshall C., Wasson J.T. (1981) Foraging westward for pristine nonmare rocks: Complications for petrogenetic models. *Proc. Lunar Planet. Sci. 12B*, pp. 21-40.
- [3] Shervais, J.W. and Taylor, L.A. (1986) Petrologic constraints on the origin of the Moon; in W.K. Hartman, R.J. Phillips, and G.J. Taylor (eds) *Origin of the Moon*, LPI Houston, 173-202.
- [4] Warren P.H. and Wasson J.T. (1977) Pristine nonmare rocks and the nature of the lunar crust. *Proc. Lunar Sci. Conf. 8th*, pp. 2215-2235.
- [5] Hunter, R.H. and Taylor, L.A. (1983) The magma ocean from the Fra Mauro shoreline: An overview of the Apollo 14 crust; *Proc. 13th Lunar and Planet. Sci. Conf., J. Geophys. Res. Supl.*, 88, A591-A602.
- [6] Warren P.H., Taylor G.J., Keil K., Kallemeyn G.W., Rosener P.S., and Wasson J.T. (1983a) Sixth foray for pristine nonmare rocks and an assessment of the diversity of lunar anorthosite. *Proc. Lunar Planet. Sci. Conf. 13th*, in *J. Geophys. Res.*, 88, A615-A630.
- [7] Lindstrom, M.M., Knapp, S.A., Shervais, J.W. and Taylor, L.A. (1984) Magnesian anorthosites and associated troctolites and dunite in Apollo 14 breccias; *Proc. 15th Lunar and Planet. Sci. Conf., J. Geophys. Res. Supl.*, 89, C41-C49.
- [8] Shervais J.W., Taylor L.A., and Laul J.C. (1983) Ancient crustal components in the Fra Mauro breccias. *Proc. Lunar Planet. Sci. Conf. 14th*, in *J. Geophys. Res.*, 88, B177-B192.
- [9] Shervais J.W., Taylor, L.A., Laul J.C., and Smith M.R. (1984) Pristine highland clasts in consortium breccia 14305: Petrology and geochemistry. *Proc. Lunar Planet. Sci. Conf. 15th*, in *J. Geophys. Res.*, 89, C25-C40.
- [10] Warren, P.H., Taylor, G.J., Keil, K., Kallemeyn, G.W., Shirley, D. and Wasson, J.T. (1983b) Seventh foray: whitlockite-rich lithologies, a diopside bearing troctolitic anorthosite, ferroan anorthosites, and KREEP, *Proc. 14th Lunar and Planet. Sci. Conf., J. Geophys. Res. Supl.*, 88, A615-A630.
- [11] Goodrich C.A., Taylor, G.J., Keil, K., Kallemeyn, G.W., and Warren, P.H. (1986) Alkali norite, troctolites, and VHK mare basalts from breccia 14304. *Proc. Lunar Planet. Sci. Conf. 16th*. In *J. Geophys. Res.* 91, D305-D318.
- [12] Neal C.R., Taylor, L.A., and Lindstrom, M.M. (1987) Petrology and geochemistry of highland clasts from Apollo 14 breccias 14303, 14305, and 14321, *Proc. Lunar Planet. Sci. Conf. 18th*, pp. 709-711.
- [13] Longhi, J. (1982) Effects of fractional crystallization and cumulus processes on mineral composition trends of some lunar and terrestrial rock series, *Proc. Lunar Planet. Sci. Conf. 13th*, in *J. Geophys. Res.*, 87, A54-A64.
- [14] James O.B., Lindstrom M.M., and Flohr M.K., (1987) Petrology and geochemistry of alkali gabbro-norites from lunar breccia 67975, *J. Geophys. Res.*, 92, E314-E330.
- [15] Warren, P.H., Jerde E.A., and Kellemeyn G.W., (1987) Pristine moon rocks: A "Large" felsite and a metal-rich ferroan anorthosite, *J. Geophys. Res.*, 92, E303-E313.

1. The first part of the document discusses the importance of maintaining accurate records of all transactions and activities. It emphasizes that proper record-keeping is essential for ensuring transparency and accountability in financial operations. This section also highlights the role of internal controls in preventing fraud and errors.

2. The second part of the document focuses on the implementation of robust risk management strategies. It outlines various risk assessment techniques and provides guidance on how to identify, measure, and mitigate potential risks. The text stresses the need for a proactive approach to risk management to protect the organization's assets and reputation.

3. The third part of the document addresses the importance of effective communication and reporting. It discusses the need for clear and concise communication channels and the role of regular reporting in keeping stakeholders informed. This section also touches upon the importance of maintaining accurate financial statements and providing timely updates to investors and other interested parties.

4. The final part of the document concludes by summarizing the key points discussed and reiterating the importance of adhering to these principles. It encourages organizations to continuously review and improve their internal controls and risk management practices to stay ahead of potential challenges and ensure long-term success.

- [16] Warren P.H., Taylor G.J., Keil K., Shirley D.N., and Wasson J.T. (1983c) Petrology and geochemistry of two large granite clasts from the moon. *Earth Planet. Sci. Lett.*, 64, 175-185.
- [17] Salpas P. Shervais J.W., and Taylor L.A. (1985) Petrogenesis of lunar granites: The result of apatite fractionation (abstract). In *Lunar and Planetary Sciences XVI*, pp. 726-727. Lunar and Planetary Institute, Houston.
- [18] Jerde, E., Warren, P.H., Morris, R.V., Heiken, G. and Vaniman, D.T. (1987) A potpourri of regolith breccias: "New" samples from the Apollo 14, 16, and 17 landing sites; Proc. 17th Lunar and Planet. Sci. Conf., *J. Geophys. Res. Supl.*, 92, E526-E536.
- [19] Lindstrom M., Crozaz G., Zinner E., (1985) REE in phosphates from lunar highlands cumulates: an ion probe stude (abstract), in *Lunar and Planetary Science XVI*, pp. 493-494, Lunar and Planetary Institute, Houston.
- [20] Warren P.H. (1988) The origin of pristine KREEP: Effects of mixing between UrKREEP and the magmas parental to the Mg-rich cumulates, *Proc. 18th Lunar and Planetary Sci. Conf.*, pp. 233-241.
- [21] Dickinson T., G.J. Taylor, K. Keil, R.A. Schmitt, S.S. Hughes, and M.R. Smith, (1985) Apollo 14 aluminous mare basalts and their possible relationship to KREEP, *Proc. Lunar Planet. Sci. Conf. 15th*, in *J. Geophys. Res.*, 90, C356-C374.
- [22] Shervais J.W., L.A. Taylor, and M.M. Lindstrom (1985a) Apollo 14 mare basalts, petrology and geochemistry of clasts from consortium breccia 14321, *Proc. Lunar Planet. Sci. Conf. 15th*, C-375-395.
- [23] Shervais J.W., L.A. Taylor, and J.C. Laul (1985b) Mare basalt petrogenesis: an important link in very high potassium (BHK) basalt, *Proc. Lunar Planet. Sci. Conf. 16th*, in *J. Geophys. Res.*, 90, in press.
- [24] Shih C.-Y., Nyquist I.E., Bogard D.D., Bansal B.M., Weismann H., Johnson P., Shervais J.W., and Taylor L.A. (1986) Geochronology and petrogenesis of Apollo 14 Very High Potassium mare basalts. *Proc. Lunar Planet. Sci. Conf. 16th*, in *J. Geophys. Res.*, 91, D214-D228.
- [25] Shih C.-Y., Nyquist I.E., Bogard D.D., Dasch E.J., Bansal B.M., and Weismann H. (1987) Geochronology of high-K aluminous mare basalt clasts from Apollo 14 breccia 14303. *Geochim. Cosmochim. Acta*, in press.
- [26] Taylor L.A., J.W. Shervais, R.H. Hunter, C.Y. Shih, L. Nyquist, B. Bansal, J. Woden, and J.C. Laul (1983) Pre-4.2 AE mare basalt volcanism in the lunar highlands, *Earth Planet. Sci. Lett.*, 66, 33-47.
- [27] Shervais, J.W. and L.A. Taylor (1983b) Micrographic granite: more from Apollo 14 (abstract), in *Lunar and Planetary Science XIV*, pp. 696-697, Lunar and Planetary Institute, Houston.
- [28] Shih, C.-Y., L.E. Nyquist, D.D. Bogard, B.M. Bansal, H. Weismann, J.W. Shervais, and L.A. Taylor, Age and petrogenesis of VHK basalts, *Proc. Lunar Planet. Sci. Conf. 16th*, in *J. Geophys. Res.*, 90, in press, 1985.
- [29] Dickinson, J.E. and P.C. Hess (1983) Role of whitlockite and apatite in lunar felsite. *Lunar and Planetary Science XIV*, pp. 158-159, Lunar and Planetary Institute, Houston.
- [30] Neal, C.R. and L.A. Taylor (1987) Lunar granite: an enigma with a new perspective. *Lunar and Planetary Science XVIII*, pp. 704-705, Lunar and Planetary Institute, Houston.

- [31] Taylor, G.J., R.D. Warner, K. Keil, M.S. Ma, and R.A. Scmitt (1980) Silicate liquid immiscibility evolved lunar rocks and the formation of KREEP. *Proc. Conf. Highlands Crust*, Merrill and Papike, eds, pp. 339-352, Pergamon, New York.



*52-91**170682**P-4*

WHOLE ROCK MAJOR ELEMENT CHEMISTRY OF KREEP BASALT CLASTS IN LUNAR BRECCIA 15205: IMPLICATIONS FOR THE PETROGENESIS OF VOLCANIC KREEP BASALTS.

Scott K. Vetter, Department of Geology, Centenary College, Shreveport, LA, 71104 and John W. Shervais, Department of Geological Sciences, University of South Carolina, Columbia, SC, 29208.

KREEP basalts are a major component of soils and regolith at the Apollo 15 site. Their origin is controversial: both endogenous (volcanic) and exogenous (impact melt) processes have been proposed, but it is now generally agreed that KREEP basalts are volcanic rocks derived from the nearby Apennine Bench formation [1-5]. Because most pristine KREEP basalts are found only as small clasts in polymict lunar breccias, reliable chemical data are scarce [5-8]. The primary aim of this study is to characterize the range in chemical composition of pristine KREEP basalt, and to use these data to decipher the petrogenesis of these unique volcanic rocks.

Lunar breccia 15205 is a polymict regolith breccia that consists of approximately 20% KREEP basalt clasts and 20% quartz-normative basalt clasts in a KREEP-rich matrix [9]. The clasts range up to 1 cm in size, but most are considerably smaller. Seventeen fragments of pristine KREEP basalt were extracted from the remaining large subsamples of 15205, however, due to their small size (< 5 mm), only 13 were large enough for whole rock analysis. These clasts were analyzed for trace element geochemistry by INAA [7]. After the irradiated samples were cool enough to ship, they were transferred to the University of South Carolina for fused bead electron microprobe analysis (EMPA). The samples were removed from their silica glass tubes, powdered, and fused in Mo foil boats prior to analysis for 12 major and minor elements on a Cameca SX-50 electron microprobe. Eight clasts (including 3 too small for whole rock analysis) were prepared as polished probe mounts for petrographic examination and mineral analysis.

PETROGRAPHY AND MINERAL CHEMISTRY: 15205 KREEP basalt clasts are characterized petrographically by 45-50 vol% plagioclase, 40-50 vol% pyroxene, and mesostasis. Most are medium to coarse-grained basalts with textures grading from ophitic or subophitic to intersertal within the same rock. The irregularly distributed mesostasis consists of K-rich glass, K-feldspar, silica, Ca-phosphate, and ilmenite. Ilmenite occurs as discrete slender grains between the coarser silicate phases; other mesostasis phases form granular patches. Plagioclase ranges in composition from An78 to An88. Pyroxene have pale tan magnesian pigeonite cores (En76 Wo4 to En67 Wo5) with rims of greenish ferroan pigeonite or augite pyroxene (En42 Wo15 - En33 Wo39). One clast has a fine-grained, variolitic texture consisting of quenched pyroxene (En69 Wo5 - En49 Wo25) with an opaque glass and ilmenite between the varioles.

WHOLE ROCK GEOCHEMISTRY: The major element data presented here show that KREEP basalt clasts from 15205 span a limited range in composition compared to earlier studies [e.g., Irving, 1], but are essentially identical in compositional range to the KREEP basalts analyzed by Ryder [6]. Calculated Mg#'s range from 53 to 66 (MgO = 6.4 to 11.3 wt%) (Table 1). SiO_2 , TiO_2 , K_2O , and P_2O_5 all increase with decreasing MgO, whereas FeO, CaO, and Al_2O_3 show little or no change throughout the range of MgO contents (Figure 1). Based on these relationships, a parent liquid can be postulated similar in composition to 15205,140 from which the other samples may be derived by fractional crystallization (sample ,158 is more primitive, but appears not to represent a liquid composition). Deviations from pure fractional crystallization trends may be caused by non-representative sampling of the small, coarse-grained clasts [e.g., 7]. This view is supported by the trace element data [7], which show little or no correlation with major element fractionation indices. Lindstrom et al. [7] have suggested that the observed scattering in trace elements concentrations could result from small variations in mesostasis distribution, and that all of these samples may come from a single flow. This interpretation (derived from a single lava flow) is at odds with the observed major element variations, which are similar to those seen in terrestrial magma suites.

DISCUSSION: Fractional crystallization models can be tested using least squares mixing models with an assumed or calculated parent magma composition and observed or hypothetical liquidus phases. Calculations take the form parent = daughter + liquidus phases, and reasonable solutions are assumed to have squared residual sums < 1.0 . Calculations using ,140 as the assumed parent magma and the observed liquidus phases (Opx, Plag) fail to obtain good fits ($r^2 = 3$). Good fits are obtained when olivine is added to the fractionating assem-

1. The first part of the document discusses the importance of maintaining accurate records of all transactions. It emphasizes that proper record-keeping is essential for the integrity of the financial system and for the ability to detect and prevent fraud. The text notes that records should be kept for a sufficient period to allow for a thorough audit and to provide a clear history of the organization's financial activities.

2. The second part of the document outlines the specific requirements for record-keeping. It states that all transactions must be recorded in a clear and concise manner, using a standardized format. The records should be organized in a way that allows for easy retrieval and analysis. Additionally, the document stresses the importance of ensuring that the records are secure and protected from unauthorized access or tampering.

3. The third part of the document discusses the role of the auditor in verifying the accuracy of the records. It explains that the auditor's primary responsibility is to ensure that the records are complete and correct. This involves reviewing the records on a regular basis and comparing them to the underlying transactions. The auditor should also be vigilant in identifying any discrepancies or irregularities that may indicate a potential problem.

4. The fourth part of the document provides guidance on how to handle any discrepancies or irregularities that are identified. It advises that any such findings should be reported immediately to the appropriate authorities and that the records should be corrected as soon as possible. The document also notes that the auditor should maintain a detailed record of any such findings and the actions taken to resolve them.

5. The fifth and final part of the document concludes by reiterating the importance of maintaining accurate records and the role of the auditor in ensuring their integrity. It emphasizes that proper record-keeping is a fundamental responsibility of all those involved in the financial system and that the auditor's role is crucial in maintaining the trust and confidence of the public.

KREEP basalt in 15205
VETER and SHERVAIS

blage ($r^2 = 0.7$ to 0.9), with 72% total fractionation required to obtain the most evolved compositions (38% plag, 27% opx, 7% olivine). Plagioclase dominates the fractionating assemblage, in keeping with the high alumina content of KREEP basalts. A problem with these solutions is that olivine is not observed as phenocrysts in KREEP basalts, nor do they appear to be olivine saturated in a silica-olivine-plagioclase ternary plot [e.g., 5]. The lack of modal olivine may be due to resorption of early formed olivine during slow cooling.

CONCLUSIONS: KREEP basalt clasts from breccia 15205 appear to represent a fractionation series related to a common parent magma. The range in major element compositions is too large to form by non-representative sampling of a single flow, but the lack of correlation between major elements and trace elements suggests that mesostasis distribution in these coarse-grained samples does not represent magmatic compositions.

Table 1. Whole rock geochemistry of KREEP basalt clasts in 15205

	.146	.131	.132	.142b	.163	.135	.148	.161B	.133	.165	.167	.158	.140
SiO ₂	51.27	50.34	51.25	51.83	50.04	51.03	50.78	50.66	50.98	52.88	50.15	48.34	49.75
TiO ₂	2.07	1.99	1.92	1.78	2.38	2.07	2.20	2.03	2.41	2.13	1.94	2.22	1.40
Al ₂ O ₃	16.09	15.38	16.28	16.33	14.61	15.78	15.87	16.98	16.81	15.38	15.92	15.37	16.90
FeO	10.17	10.71	9.79	9.31	11.52	10.15	10.23	9.85	9.97	10.11	10.33	10.80	9.65
MnO	0.18	0.16	0.15	0.11	0.18	0.12	0.15	0.18	0.14	0.14	0.15	0.16	0.14
MgO	7.33	8.81	8.49	8.79	8.19	8.85	8.53	8.27	8.41	7.18	8.32	11.31	10.45
CaO	10.31	10.11	10.10	10.06	10.16	9.97	10.14	10.58	10.23	9.70	9.98	9.43	9.67
Na ₂ O	0.87	0.81	0.84	0.78	0.81	0.81	0.82	0.79	0.82	0.91	0.78	0.72	0.78
K ₂ O	0.67	0.54	0.58	0.55	0.65	0.56	0.54	0.37	0.67	0.83	0.49	0.34	0.40
P ₂ O ₅	0.35	0.29	0.22	0.23	0.54	0.29	0.41	0.16	0.47	0.44	0.30	0.23	0.11
Cr ₂ O ₃	0.27	0.34	0.32	0.31	0.29	0.31	0.32	0.31	0.26	0.28	0.33	0.43	0.36
Sum	99.56	99.48	99.92	100.08	99.36	99.94	99.95	100.18	99.16	99.98	99.68	99.15	99.60
Mg#	56.22	59.48	60.74	62.71	53.90	60.85	59.77	59.94	53.43	55.88	61.67	65.11	65.87

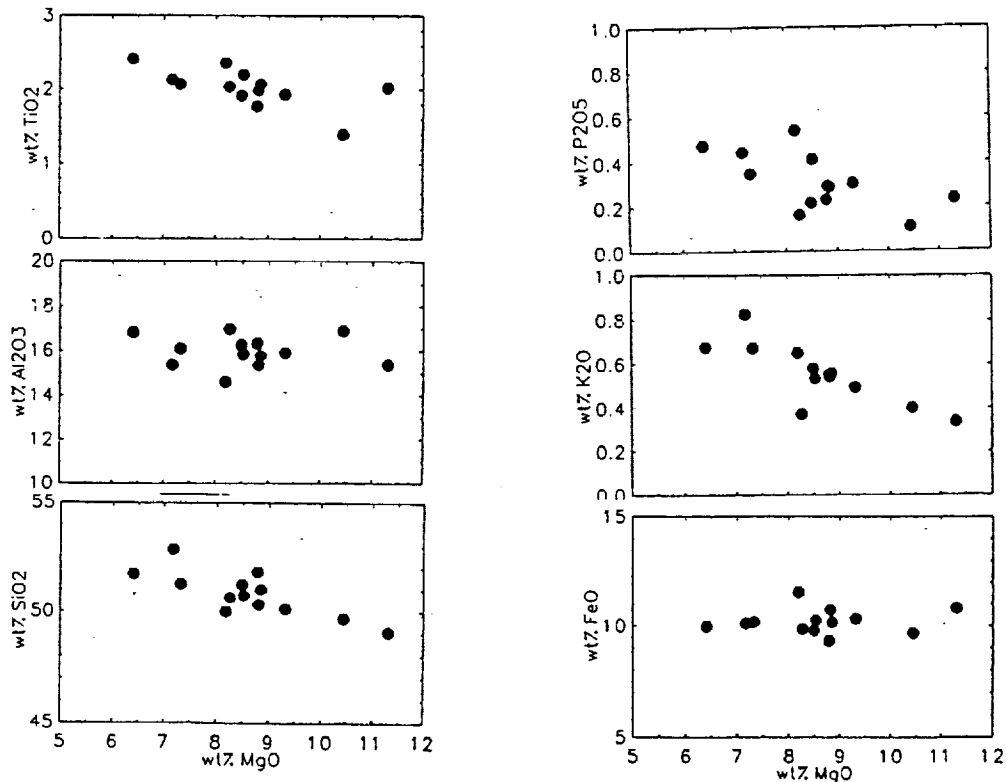
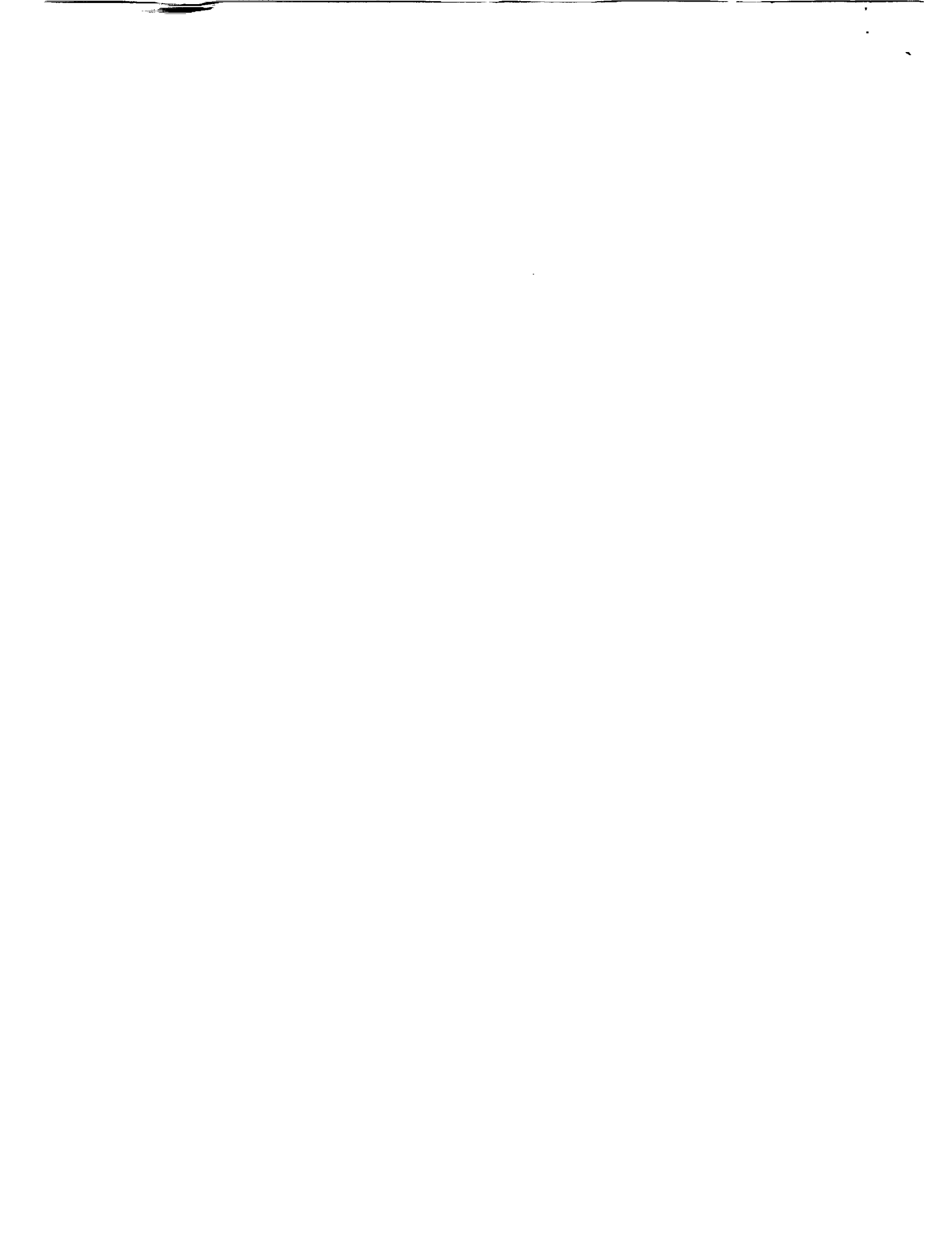


Figure 1. MgO-variation diagrams for KREEP basalt clasts from lunar breccia 15205.

REFERENCES: [1] Irving (1977) PLSC 8th, 2433. [2] Spudis and Hawke (1986) LPI Tech. Rpt. 86-03, 105. [3] Dymek (1986) LPI Tech. Rpt. 86-03, 52. [4] Ryder (1987) PLSC 17th, E331. [5] Ryder (1989) LPSC XX, 936. [6] Shervais and Vetter (1989) LPSC XX, 1000. [7] Lindstrom et al. (1989) LPSC XX, 578. [8] Ryder (1988) LPSC XIX, 1011. [9] Dymek et al. (1974) PLPSC 5th, 235-260. [10] Shervais et al. (1990) PLPSC 20th, 109-126.



N15

53-91

170683

MAJOR ELEMENT CHEMISTRY OF APOLLO 14 MARE BASALT CLASTS AND HIGHLAND PLUTONIC CLASTS FROM LUNAR BRECCIA 14321: COMPARISON WITH NEUTRON ACTIVATION RESULTS. SHERVAIS, John W., Department of Geological Sciences, University of South Carolina, Columbia SC 29208 and VETTER, Scott K., Department of Geology and Geography, Centenary College, Shreveport, LA 71104.

Studies of lithic components in lunar breccias have documented a wide variety of rock types and magma suites which are not found among large, discrete lunar samples. Rock types found exclusively or dominantly as clasts in breccias include KREEP basalts [1,2], VHK mare basalts [3,4], high-alumina mare basalts [5,6], olivine vitrophyres [7], alkali anorthosites [8-10], and magnesian anorthosites and troctolites [8-12]. These miniature samples are crucial in petrogenetic studies of ancient mare basalts and the highlands crust of the western nearside, both of which have been battered by basin-forming impacts and no longer exist as distinct rock units [13].

Despite the importance of these clasts for petrogenetic models of mare basalt and highland evolution, many have not been analyzed for major element chemistry because of their small size. As a result, systematic chemical data are not available for most samples, which have only been studied by instrumental neutron activation analysis (INAA). Activation analysis has the advantage of producing excellent data for a large number of trace elements (including REE) and a few major elements (FeO, Al_2O_3 , Na_2O) from small analytical samples. The primary disadvantage of INAA is that several important major elements cannot be analyzed accurately (MgO, TiO_2 , K_2O), and SiO_2 cannot be determined at all. Several of these major elements produce short-lived isotopes which require special irradiation and counting techniques (Al_2O_3 , MgO, TiO_2); as a result, these are not determined routinely. When these elements are determined, it is customary to calculate " SiO_2 " by difference, assuming the major elements sum to 100 percent by weight. As a result, dunites and troctolites may have calculated SiO_2 as low as 34-36 wt%, despite the fact that they consist of Fo88 olivine and An94 plagioclase [12]. These problems may be overcome by using fused bead electron microprobe analysis for major elements in conjunction with INAA for trace elements and selected major elements [e.g., 8-11]. Fused bead EMP analysis produces results comparable in quality to X-ray fluorescence analysis when basaltic samples are analyzed [B. Schuraytz, pers. comm., 1990], and can be applied to samples as small as 10 milligrams. Since INAA samples generally range from 10 to 100 mg in mass, both techniques can be applied to the same sample, either by splitting a homogenized powder, or by serial analysis (INAA followed by fused bead EMPA).

We present here fused bead EMPA major element data for mare and highland clasts found in lunar breccia 14321. These clasts have already been analyzed for trace elements and selected major elements by INAA [5,7,12]. This data set represents the first complete major element for these samples, which we compare to the INAA major element results.

ANALYTICAL TECHNIQUES: A total of 20 clasts from breccia 14321 were studied here by fused bead EMPA. These clasts include 11 mare basalts [5], 3 olivine vitrophyres [7], 3 Mg-troctolites [12], 2 Mg-anorthosites [12], and one dunite [12]. All samples were powdered by hand in an agate mortar prior to fusion in a dry nitrogen atmosphere [14]. The powders were fused in molybdenum foil boats, and the fused samples analyzed for 12 elements on a Cameca SX-50 EMP at the University of South Carolina. Standards included a natural basaltic glass similar in composition to lunar low-Ti mare basalts (VG2; SiO_2 , Na_2O , CaO, TiO_2 , FeO), plagioclase (Al_2O_3), microcline (K_2O), ilmenite (MnO), fused MgO, chromite, apatite (P_2O_5), and molybdenum metal (to monitor dissolution of Mo into the fused glass). The basaltic glass standard VG2 was analyzed periodically to monitor analytical drift; results for all elements were generally within 1% of the accepted values.

RESULTS: Our fused bead EMPA results are shown in figure 1 compared to the published INAA results. All of the INAA data were produced in one lab by the same analyst (Dr. M.M. Lindstrom at Washington University), so there is no interlaboratory bias in either data set. Silica in the INAA data set was calculated by difference for "complete" analyses.



Major Element Chemistry: Shervais J. W. et al.

Differences between the two data sets are generally smallest for those elements which can be measured accurately by INAA: Al_2O_3 , FeO , MnO , Na_2O , and CaO (figure 1). Fused bead EMPA for Na_2O are systematically 5-10% lower than the INAA results, suggesting that Na was mobilized under the electron beam. INAA results for TiO_2 and MgO are systematically too high by 15% to 20% on average, while K_2O and SiO_2 show significant scatter to both high and low values. Cr_2O_3 values correspond well for the mare basalts, but show significant differences in the highland samples.

CONCLUSIONS: Fused bead EMPA provides superior analytical results for the major elements SiO_2 , TiO_2 , MgO , and K_2O on small samples extracted from lunar breccias. This method can be applied to samples which have been irradiated for INAA and compliments the data obtained by INAA. Fused bead EMPA eliminates the need for "rabbit runs", which are used primarily to obtain data for the major elements Al, Mg, and Ti. These data will allow us to refine petrogenetic models for 14321 mare basalts and highland rocks, and expand the range of clast sizes from which complete geochemical data may be obtained.

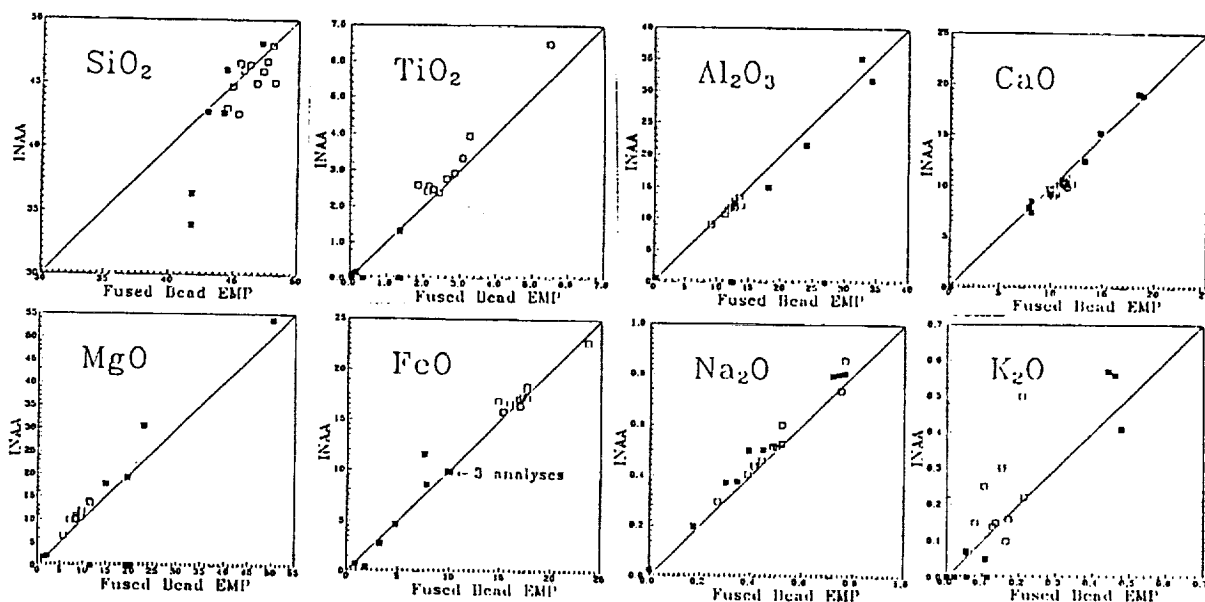


Figure 1. Fused bead EMPA of lithic clasts from lunar breccia 14321, compared to INAA results on the same samples [5,7,12]. Solid symbols = highland plutonics and melt rocks; open symbols = high-Al mare basalts. Correlations are good for Al, Ca, Fe, and Na, but poor for other elements.

REFERENCES: [1] Ryder, G. (1988) LPS XIX, 1011-1012; Ryder, G. (1989) LPSC XX, 936-937. [2] Shervais, J.W. and Vetter, S.K. (1989) LPS XX, 1000-1001. [3] Shervais J.W., et al., (1985b) J. Geophys. Res., 90, D3-D18. [4] Neal C.R., et al., (1988a) PLPSC 18th, 121-137. [5] Shervais J.W., et al., (1985a) J. Geophys. Res., 90, C375-C395. [6] Dickinson, T., et al., (1985) J. Geophys. Res., 90, C365-C374. [7] Shervais, J.W., et al., (1988) PLPSC 18th, 45-58. [8] Warren, P.H., et al., (1983a) PLPSC 13th, J. Geophys. Res. Suppl., 88, A615-A630. [9] Warren, P.H., et al., (1983b) PLPSC 14th, J. Geophys. Res. Suppl., 88, A615-A630. [10] Shervais, J.W., et al., (1984b) PLPSC 15th, J. Geophys. Res. Suppl., 89, C25-C40. [11] Warren, P.H., et al., (1986) PLPSC 16th, J. Geophys. Res. Suppl., 91, D319-D330. [12] Lindstrom, M.M., et al., (1984) PLPSC 15th, J. Geophys. Res. Suppl., 89, C41-C49. [13] Shervais, J.W. (1989) in Taylor, G.J. and Warren, P.H., eds., Workshop on Moon in Transition: Apollo 14, KREEP, and Evolved Lunar Rocks, LPI Tech. Report 89-03, 118-127. [14] Shervais, J.W., et al., (1990) PLPSC 20th, 109-126.

[Faint, illegible text covering the majority of the page]

[Faint, illegible text at the bottom of the page]

AUTO-METASOMATISM OF THE WESTERN LUNAR HIGHLANDS: RESULT OF CLOSED SYSTEM FRACTIONATION AND MOBILIZATION OF A KREEPY TRAPPED LIQUID. SHERVAIS, John W., Department of Geological Sciences, University of South Carolina, Columbia SC 29208 and VETTER, Scott K., Department of Geology and Geography, Centennial College, Shreveport, LA 71134. p-4

The discovery of REE-rich phosphates (dominantly whitlockite) in pristine, non-mare rocks of the western lunar nearside (Apollo 14, Apollo 12, and most recently, Apollo 17) has created a paradox for lunar petrologists. These phases are found in feldspar-rich cumulates of both the Mg-suite and the Alkali suite, which differ significantly in their mineral chemistries and major element compositions [1-7]. Despite the differences in host rock compositions, whitlockites in both suites have similar compositions, with LREE concentrations around 21,000 to 37,000 x chondrite [1-5]. Simple modeling of possible parent magma compositions using the experimental whitlockite/liquid partition coefficients of Dickinson and Hess [8] show that these REE concentrations are too high to form from normal lunar magmas, even those characterized as "urKREEP" [1-5].

These phosphates pose two separate problems: how to account for KREEPy trace element characteristics in primitive rocks of the Mg-suite (plagioclase An₉₄) [3,4], and how to account for the occurrence of whitlockites with similar compositions in more evolved rocks of the alkali suite (plagioclase An₈₂) [1-7]. Proposals which focus on the effects of KREEP assimilation by the parent magmas can explain the presence of KREEPy trace element patterns in both primitive Mg-suite rocks and evolved Alkali suite rocks, but they cannot resolve the "concentration problem" [1-4,7]. Similarly, previous proposals for the influx of an REE-rich metasomatic fluid have failed to address the question of how this fluid is derived, and where it comes from [2-4,7]. In contrast, Neal and others [5,6] have recently proposed that metasomatism of western highland cumulates occurs by the process of "REEP-frac metasomatism", where their hypothetical REEP-frac component forms by silicate liquid immiscibility fractionation of an urKREEP parent magma. This urKREEP represents extreme magma ocean fractionation, and the REEP-frac component is considered to enter the highland cumulates after crystallization is complete [5,6].

We present here an alternative hypothesis, which we proposed orally at the LPSC XXI, whereby REE-rich whitlockites in both suites form through a process of auto-metasomatism. By this we refer to metasomatic fluids derived from closed system fractionation of KREEPy trapped liquids which are mobilized along grain boundaries and fractures shortly before complete crystallization and thermal equilibration of the cumulates. The occurrence of KREEPy trapped liquids in both suites is attributed to assimilation of KREEPy wall rocks or mixing with a KREEP-rich residual magma [1-4,7]. Alternatively, the Alkali suite cumulates may have formed from a KREEP parent magma [7].

Petrographic evidence for metasomatic origin: Whitlockites of the Mg-suite occur most commonly as subequant interstitial grains in anorthosites, troctolites, or norites [3-5]. In the magnesian anorthosite 14321,1211/1273 [3,4], whitlockite occurs in a zone of recrystallized plagioclase with a polygonal-mosaic texture which cuts across large, finely twinned plagioclase primocrysts. In the Alkali suite, whitlockites occur both interstitially

CONFIDENTIAL - SECURITY INFORMATION

AUTO-METASOMATISM OF LUNAR HIGHLANDS: J.W. SHERVAIS and S.K. VETTER

[1,9] and, rarely, as inclusions in plagioclase primocrysts [2]. The whitlockite inclusion in 14305,400 was originally interpreted to require a parent magma saturated in phosphate early in its crystallization history [2]. A closer examination, however, shows that this inclusion occurs along a healed fracture in the plagioclase primocryst, as shown by the offset in twin lamellae. Thus, the evidence seems to suggest that whitlockite formed late in the crystallization history of the rocks (unsurprisingly), and possibly after initial crystallization was more-or-less complete. While the petrographic data do not confirm a metasomatic origin for the whitlockite, they are compatible with such an interpretation.

Whitlockite saturation and REE enrichment factors: Dickinson and Hess [8] show that whitlockite saturation varies with P_2O_5 concentration, SiO_2 , and temperature. They show that, in basaltic rocks, whitlockite saturation requires around 4.5 wt% P_2O_5 ; at slightly higher silica contents and lower temperatures which may be appropriate for KREEP, Warren et al [1] estimate whitlockite saturation at about 3.2 wt% P_2O_5 . These saturation levels are 4x to 6x higher than estimated for high-K KREEP [9]. This would require 75% to 85% closed system fractionation of a KREEPy trapped liquid component. By comparison, Neal and others [5] calculate that the liquid from which these whitlockites crystallized was 4x to 10x more enriched in REE than typical KREEP compositions. Since bulk partition coefficients for the REE are probably $\ll 0.1$ before whitlockite saturation, this would require 75% to 90% closed system fractionation -- about the same enrichment required for whitlockite saturation. Thus, it appears that the similarity of whitlockite compositions in Mg-suite and alkali suite cumulates is a function of the similar enrichment factors for P_2O_5 and REE, assuming a trapped liquid component with KREEPy trace element ratios. Differences in P_2O_5 and REE concentrations in the respective trapped liquids (i.e., dilute KREEP vs concentrated KREEP) control only the amount of closed system fractionation required. This may explain the more common occurrence of whitlockite in alkali suite cumulates relative to Mg-suite rocks.

Auto-metasomatism and heterogeneous phase distribution: An important aspect of this model is that mobilization of the metasomatic fluids leads to a heterogeneous distribution of accessory phases which control incompatible trace element concentrations. Analysis of small, non-representative samples leads to trace element concentrations and ratios which are not representative of the initial magma or of simple closed system crystallization. Depending on the length scale of metasomatism, the average sample size required to recapture the trace element systematics of the magma system could be quite large. The fact that many whole rock samples of pristine highland cumulates *do* retain relatively consistent trace element systematics suggests that this process, while important locally, does not control the trace element geochemistry of the highlands.

References: [1] Warren et al, 1983, *PLPSC 14* in *JGR* 88, B151-B164. [2] Shervais et al, 1984, *PLPSC 15* in *JGR* 89, C25-40. [3] Lindstrom et al, 1984, *PLPSC 15* in *JGR* 89, C41-49. [4] Lindstrom et al., 1985, *LPS XVI*, 493-494. [5] Neal et al, 1990, *LPS XXI*, 863-864. [6] Neal & Taylor, 1990, *LPS XXI*, 851-852. [7] Shervais, 1989, *LPI Tech. Report 89-03*, Lunar and Planetary Institute, Houston, 118-127. [8] Dickinson & Hess, 1982, *LPS XIII*, 172-173. [9] Warren, 1988, *LPI Tech. Report 89-03*, Lunar and Planetary Institute, Houston.

1
2
3
4
5
6
7
8
9
10
11
12
13
14
15
16
17
18
19
20
21
22
23
24
25
26
27
28
29
30
31
32
33
34
35
36
37
38
39
40
41
42
43
44
45
46
47
48
49
50
51
52
53
54
55
56
57
58
59
60
61
62
63
64
65
66
67
68
69
70
71
72
73
74
75
76
77
78
79
80
81
82
83
84
85
86
87
88
89
90
91
92
93
94
95
96
97
98
99
100

POLYTOPIC VECTOR ANALYSIS IN IGNEOUS PETROLOGY: APPLICATION TO LUNAR PETROGENESIS. SHERVAIS, J.W. and EHRlich, R., Department of Geological Sciences, University of South Carolina, Columbia, SC 29208.

Lunar samples represent a heterogeneous assemblage of rocks with complex inter-relationships that are difficult to decipher using standard petrogenetic approaches. These inter-relationships reflect several distinct petrogenetic trends as well as thermo-mechanical mixing of distinct components. Additional complications arise from the unequal quality of chemical analyses and from the fact that many samples (e.g., breccia clasts) are too small to be representative of the system from which they derived.

Polytopic vector analysis (PVA) is a multi-variate procedure used as a tool for exploratory data analysis [1-3]. PVA allows the analyst to classify samples and clarifies relationships among heterogeneous samples with complex petrogenetic histories. It differs from orthogonal factor analysis in that it uses non-orthogonal multivariate sample vectors to extract sample endmember compositions. The output from a Q-mode (sample based) factor analysis is the initial step in PVA. The Q-mode analysis, using criteria established by Miesch [4] and Klován and Miesch [5], is used to determine the number of endmembers in the data system. The second step involves determination of endmembers and mixing proportions with all output expressed in the same geochemical variable as the input. The composition of endmembers is derived by analysis of the variability of the data set. Endmembers need not be present in the data set, nor is it necessary for their composition to be known a priori. A set of any endmembers defines a "polytope" or classification figure (triangle for a three component system, tetrahedron for a four component system, a "five-tope" in four dimensions for five component system, et cetera).

Given the dimensionality of the polytope from the Q-mode analysis, the polytope is derived by an iterative process. These procedures are basically exercises in Euclidian geometry. The initial polytope is defined as either the vertices of the K most mutually extreme samples or as k points within the data cloud roughly parallel to the shape of the data cloud. Points lying outside the initial polytope are reported as having negative mixing proportions for one or more endmembers. If this occurs, the polytope iteratively expands and rotates until convergence occurs or the maximum number of iterations is reached. A solution is not guaranteed - and sometimes solutions may diverge.

Inspection of the results for intermediate iterations identifies those samples which are difficult to accommodate within a polytope. Often, the reasons for this are readily apparent in that a subset might represent a distinct subpopulation totally unrelated to the rest of the samples or a subpopulation with extreme geochemical values due to small sample size or analytical error. Discrete subsets can also be detected by the fact that they contain endmembers which are un-needed in the other samples. Such evaluation permits breaking the data into subsets for further analysis. Endmembers variability within a subset often reflects degree of fractionation and assimilation. If major, minor, and trace elements are included in the analysis, the composition of endmembers describes the partitioning of trace elements with respect to majors and minors.

Analysis of two lunar sample data sets (mare, highland) illustrate the manner in which PVA allows classification and analysis of such heterogeneous data.



Pristine Highland Cumulates from Western Nearside: Our analysis of cumulate plutonic rocks focused on breccia clasts from the Apollo 14 and Apollo 12 sites [7-10]. The sample set consisted of 31 samples containing 21 chemical elements. All but six samples are related to the Mg-suite (mostly troctolites with a few norites and peridotites); the last six were alkali suite anorthosites and norites. The initial Q-mode analysis indicated that a five endmember solution was best, but that Si and Ba were poorly recovered by back-calculation from that solution. This reflects the fact that these elements are poorly determined analytically; in fact, silica was typically derived by difference from INAA analyses. The Q-mode analysis also indicated that a small subset of samples (primarily alkali anorthosites) would be slightly biased by a five-EM solution. The five EMs represent approximate compositions of olivine (dunite), olivine-pyroxene mix, An100 plagioclase with abundant trace elements, An100 plagioclase with few trace elements, and An86 plagioclase with moderate trace elements. Ultramafic samples commonly fell outside the polytope (large negative mixing proportions). Most Mg-suite samples are characterized by roughly 2:1 ratios of An100 plagioclase to An86 plagioclase EMs producing An95 compositions, with variable amounts of the "dunite" EM to make troctolite. The alkali suite samples are dominated by the An86 plagioclase EM, with small contributions from the trace element-rich "pyroxene" EM. Using just the major elements alone, only a three EM solution can be obtained and was petrologically viable but uninteresting.

Lunar Mare Basalts: When all mare basalts are considered as a class (121 samples with 22 chemical elements), Q-mode analysis of variance suggests that a five EM solution is required. Two of these EMs represent basaltic compositions which bracket mare basalt compositions, Two represent fictive extracts (armalcolite, plagioclase, olivine combinations), and one represents a KREEP-rich ferrobasalt. Thus, our preliminary results suggest that the KREEP component in mare basalts is an Fe-rich ferrobasalt with very low MgO that is fractionated with respect to pristine KREEP 15386. Further work is in progress to determine relations among primitive basalt compositions to constrain mantle source variations.

[1] Full et al, 1981, *J. Math. Geol.*, 13, 331-344. [2] Full et al, 1982, *J. Math. Geol.*, 14, 259-270. [3] Ehrlich and Full, 1987, in *Use and Abuse of Statistical methods in the Earth Sciences*, W.B. Size (ed), Oxford U. Press, 33-46. [4] Miesch, 1976, *USGS Prof. Paper 574-G*, 47 pp.. [5] Klován and Miesch, 1976, *Comp. Geosci.*, 1, 161-178. [6] Klován and Imbrie, 1971, *J. Inter. Assoc. Math. Geol.*, 3, 61-78. [7] Warren et al, 1983, *PLPSC 14 in JGR 88*, B151-B164. [8] Shervais et al, 1984, *PLPSC 15 in JGR 89*, C25-40. [9] Lindstrom et al, 1984, *PLPSC 15 in JGR 89*, C41-49. [10] Shervais, 1989, *LPI Tech. Report 89-03*, Lunar and Planetary Institute, Houston, 118-127. [11] Shervais and Vetter, 1990, *LSC XXI*, 1142-1143.



56-91

170686

THE WESTERN HIGHLAND PROVINCE AT THE APOLLO 14 SITE

John W. SHERVAIS, Department of Geological Sciences, University of South Carolina,
Columbia SC 29208

Recent petrologic studies of pristine nonmare samples from the Apollo 14 site have demonstrated the unique character of the western highlands crust. Many of the lithologies which occur here are not found at other highland sites or represent unique variations of more common lithologies. Rare highland samples found at the Apollo 12 site have petrologic and geochemical affinities with the Apollo 14 highland suite and the two sites taken together constitute what can be called the Western Highland Province. Rocks of the Western Highland Province are geochemically distinct from similar lithologies found at eastern highland sites (Apollo 15, Apollo 16, Apollo 17, and the Luna sites)--a fact which adds further complications to current petrogenetic models for the lunar crust. Nonetheless, an understanding of how the Western Highlands Province formed and why it differs from highland crust in the east is crucial to our overall understanding of primordial lunar differentiation and petrogenesis (e.g., [1-3]).

MAGNESIAN SUITE: The Magnesian suite consists of two distinct groups, the olivine-bearing magnesian troctolite association (which includes troctolite, anorthosite, dunite, and pyroxene-bearing troctolites) and the less abundant magnesian norite association (which includes norites, olivine norites, gabbronorites, and ilmenite gabbros/norites). The magnesian troctolite association includes a variety of olivine-bearing rocks; troctolite is the most common lithology, but troctolitic anorthosites and anorthosites are also widespread [1-9]. Mafic compositions are rare: only two dunites and a few small mafic troctolites have been found, as well as two pyroxene-rich troctolites have been found. The magnesian norite association contains a diverse assemblage of rocks referred to as ilmenite gabbros, ilmenite norites, and gabbronorites. Only four clasts have been described so far that can be considered unequivocal part of the Mg-suite. Other gabbronorite clasts have mineral compositions that plot below the Mg-suite field on an An-Mg# diagram (figure 1), in the same region where Apollo 14 mare basalts plot [7,8,10].

ALKALI SUITE: The Alkali suite was first recognized by Warren and Wasson [1] and subsequent studies established it as the second most common highland rock association at the Apollo 14 site. This suite was once thought to be unique to the Western Highlands Province, but similar alkali gabbronorites are now known from the Apollo 16 site. The most common lithologies are anorthosite (7 clasts) and norite or gabbronorite (6 clasts). Two olivine norites have been found; these may represent primitive cumulates from the alkali suite parent magma [1,4,8,9,10].

EVOLVED LITHOLOGIES: The most common evolved lithology at Apollo 14 is a granophyric intergrowth of quartz and alkali feldspar commonly referred to as "lunar granite". Accessory minerals include pigeonite, augite, ferroaugite, fayalite, ilmenite, zircon, and Ca-phosphates. Variations in mineral assemblages and in mineral composition (e.g., BaO in alkali feldspars, MG# in mafics) indicate that at least four distinct parent magmas are involved. Based on the abundance of K,Si-rich glasses in Apollo 14 soils and regolith breccias, granites are estimated to comprise 0.5% to 2% of the crust here.

FERROAN ANORTHOSITES: Ferroan anorthosites are rare at the Apollo 14 site. Only one clast of ferroan anorthosite has been characterized chemically and petrographically.

GEOCHEMISTRY OF THE WESTERN HIGHLANDS PROVINCE: Plutonic rocks of the Western Highlands Province are characterized by high concentrations of incompatible trace elements compared to their eastern counterparts [1-10]. Chemical differences between rocks of the Western Highlands Province and nonmare plutonic rocks from the east are clearly illustrated by Sm and Eu. Ferroan anorthosites and eastern Mg-suite rocks are characterized by low concentrations of Eu (.5 to 1.0 ppm) and a wide range of Sm concentrations, with Sm in FAN < 0.3 ppm and Sm in the eastern Mg-suite rocks > 0.5 ppm (figure 4). Western Mg-suite rocks have a range in Sm similar to the eastern troctolites (Sm=2 to 100 ppm) but are enriched in Eu relative to the eastern rocks (Eu=1-5 ppm). Alkali anorthosites are even richer in Eu (Eu=2 to 10 ppm) in rocks with the same Sm content as the Magnesian suite.

ORIGIN OF THE WESTERN HIGHLAND PROVINCE: The high Sm concentrations which characterize plutonic rocks of the Western Highland Province also result in low Ti/Sm and Sc/Sm ratios. These ratios are sub-chondritic, as in KREEP, and suggest derivation of western plutonic suites from an evolved crustal or upper mantle source. Alternatively, these low ratios may reflect the assimilation of residual urKREEP by magmas parental of Mg-suite rocks [9]. However, if the incompatible element-rich magnesian suite troctolites, anorthosites, and dunites of Apollo 14 crystallized from Mg-rich magmas that were severely contami-



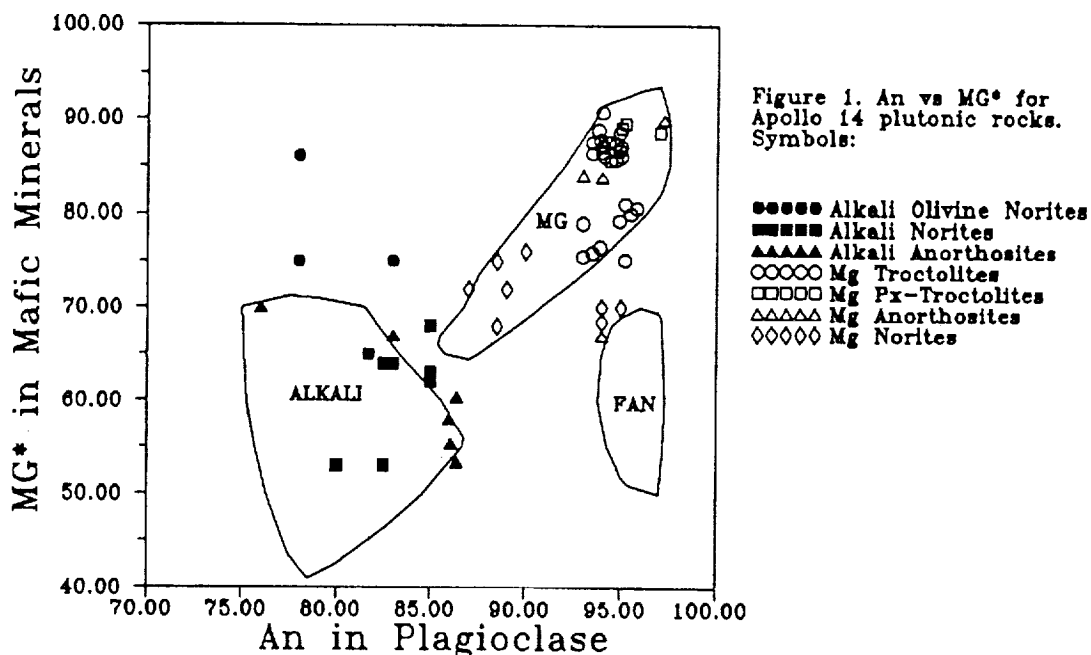
nated with urKREEP, where did the alkali suite magmas come from?? Several scenarios can be envisioned for the origin of the western magnesian and alkali suite highland rocks. All of these models have certain attractive features, but none are entirely consistent with what we currently know about the western highland suite. Some possibilities include:

(1) The Mg-suite and alkali suites represent distinct parent magmas, derived from different parts of the lunar mantle, each of which assimilated variable amounts of urKREEP prior to crystallization. This model begs the questions of ultimate source, and does not address why there are two distinct parent magmas. It does seem consistent with the gap between the alkali suite and troctolites of the Mg-suite, and with the steep apparent fractionation trends seen in the magnesian troctolite association and in the alkali suite (figure 1). This steep trend in the alkali suite is accentuated by the recent discoveries of primitive olivine norites with typical alkalic plagioclase compositions.

(2) The alkali suite represents an Mg-suite magma which has evolved by AFC processes; its high alkali and trace element contents are attributed to relatively large fractions of assimilation. This model has the advantage of one parent magma, and seems in general consistent with the overall trend of the Mg-suite in figure 1. It does not explain, however, why both suites have the same range in trace element concentrations, or why the alkali suite has higher Eu concentrations than either the Mg-suite or KREEP - fractional crystallization of plagioclase and KREEP assimilation should both act to lower Eu in a residual magma derived from the Mg-suite. It is also puzzling why there are so few Mg-suite norites intermediate to the alkalic rocks and the Mg-troctolites (figure 1). If variable contamination of a single magma was operative, a continuous trend in compositions would be expected.

(3) The alkali suite represent cumulate rocks which crystallized from a KREEP parent magma. This magma was assimilated by Mg-suite parent magmas before they crystallized, or penetrated already crystallized Mg-suite plutons to enrich them metasomatically. It is not clear if the alkali suite cumulate rocks are consistent with this origin, but it does offer an attractive explanation to the contrasts in major and trace element compositions observed between the two suites.

REFERENCES: [1] Warren and Wasson (1980) Proc. Lunar Planet. Sci. Conf. 11th, pp. 431-470; [2] Warren et al (1981) Proc. Lunar Planet. Sci. 12B, pp. 21-40; [3] Shervais and Taylor (1986) Origin of the Moon, 173-202; [4] Hunter and Taylor (1983) Proc. 13th Lunar and Planet. Sci. Conf., JGR Supl., 88, A591-A602; [5] Warren et al (1983) Proc. Lunar Planet. Sci. Conf. 13th, in JGR 88, A615-A630; [6] Lindstrom et al (1984) Proc. 15th Lunar and Planet. Sci. Conf., JGR Supl. 89, C41-C49; [7] Shervais et al (1983) Proc. Lunar Planet. Sci. Conf. 14th, in JGR 88, B177-B192; [8] Shervais et al (1984) Proc. Lunar Planet. Sci. Conf. 15th, in JGR 89, C25-C40; [9] Warren et al (1983) Proc. 14th Lunar and Planet. Sci. Conf., JGR Supl., 88, A615-A630; [10] Goodrich et al (1986) Proc. Lunar Planet. Sci. Conf. 16th in JGR 91, D305-D318.





57-91

170687

p. 2

LUNAR MARE VOLCANISM: MIXING OF DISTINCT, MANTLE SOURCE REGIONS WITH KREEP-LIKE COMPONENT

John W. SHERVAIS and Scott K. VETTER, Department of Geological Sciences, University of South Carolina, Columbia SC 29208

Mare basalts comprise less than 1% of the lunar crust, but they constitute our primary source of information on the moon's upper mantle. Compositional variations between mare basalt suites reflect variations in the mineralogical and geochemical composition of the lunar mantle which formed during early lunar differentiation (4.5-4.4 AE). Three broad suites of mare basalt are recognized: very low-Ti (VLT) basalts with $\text{TiO}_2 < 1$ wt%, low-Ti basalts with $\text{TiO}_2 = 2-4$ wt%, and high-Ti basalts with $\text{TiO}_2 = 10-14$ wt% [1-3]. Important subgroups include the Apollo 12 ilmenite basalts ($\text{TiO}_2 = 5-6$ wt%) [4], aluminous low-Ti mare basalts ($\text{TiO}_2 = 2-4$ wt%, $\text{Al}_2\text{O}_3 = 10-14$ wt%) [5-7], and the newly discovered Very High potassium (VHK) aluminous low-Ti basalts, with $\text{K}_2\text{O} = 0.4-1.5$ wt% [8-10]. The mare basalt source region has geochemical characteristics complementary to the highlands crust, and is generally thought to consist of mafic cumulates from the magma ocean which formed the felsic crust by feldspar flotation. The progressive enrichment of mare basalts in Fe/Mg, alkalis, and incompatible trace elements in the sequence VLT basalt \rightarrow low-Ti basalt \rightarrow high-Ti basalt is explained by the remelting of mafic cumulates formed at progressively shallower depths in the evolving magma ocean. This model is also consistent with the observed decrease in compatible element concentrations and the progressive increase in negative Eu anomalies [11].

Despite the appeal of this simple model there is increasing evidence that more complex scenarios are required. The hybridization of Fe- and incompatible element-rich late magma ocean cumulates with more magnesian early magma ocean cumulates seems necessary to explain the major and trace element compositions of the mare basalt source region: mare basalts are too magnesian to be derived from a magma ocean cumulate formed after >95% fractional crystallization, but such high degrees of fractional crystallization are needed to create the necessary trace element rich source [12, 13]. This hybridization is gravitationally driven since the late magma ocean cumulates are more Fe-rich and denser than the underlying magnesian cumulates. Recent hybridization models generally assume three end members: early magnesian cumulates with low Ti (dominantly olivine + Opx), late Fe,Ti-rich cumulates (Cpx + ilmenite), and a late magma ocean trapped-liquid component similar to KREEP in composition [13, 14]. These end members are mixed in various proportions to create the range in observed mare basalt compositions.

Recent studies of the Apollo 14 aluminous mare basalt suite have revealed a wide variety of previously unknown mare basalt types, many of which seem to require assimilation as an important process in their petrogenesis [5-10]. Two main components have been identified: KREEP, the incompatible element-rich mafic component concentrated in soils and impact breccias [5-7], and lunar granites [8-10]. The Apollo 14 aluminous basalt suite is important because it has many compositional characteristics intermediate between normal, low-alumina mare basalts and high-Ti mare basalts. Apollo 14 high-alumina basalts have high MG#s (similar to low-Al, low-Ti basalts), high alkali and incompatible trace element contents (similar to high-Ti basalts or higher), and compatible trace elements intermediate between high and low Ti basalts [15]. In a cumulate remelting model, these characteristics suggest a mantle source region which lies above the normal low-Ti basalt source and below the high-Ti basalt source. In addition, Apollo 14 high-Al basalts are also high in CaO, suggesting either plagioclase assimilation [12] or plagioclase in the source region.

When data for all mare basalt types (including Apollo 14 aluminous mare basalts and VHK basalts) is plotted on ratio-ratio or ratio-element plots, two distinct trends are observed (figures 1,2). One trend is defined by low-Ti basalts *sensu lato* (including VLT, VHK, and high-Al, low-Ti basalts); the other trend is defined by the high-Ti basalt suite. Both trends resemble hyperbolic mixing curves [16] whose incompatible element-rich end points asymptotically towards KREEP. There is little or no overlap between the two trends, however, and their incompatible element-poor asymptotes point to distinct end-member compositions. If these curves are considered simple mixing hyperbolas, up to 65% assimilation of KREEP is indicated. Alternatively, these curves may be due to fractional crystallization, as suggested by fractionation trends on MG# plots. If so, the trends toward a KREEP-like composition suggest that this composition may represent an incompatible element-rich end member mixed into the mare basalt source prior to melting. Fractionation of phase assemblages with bulk distribution coefficients similar to the refractory mineral assemblage will drive the melt composition towards the KREEP-like mixing component.



Shervais, J.W. and Vetter, S.K.

These observations suggest that the compositional variations observed in mare basalts result from a complex source hybridization process similar to that suggested by Hughes et al [13]. In this scenario a late stage magma ocean component similar in composition to KREEP sinks into earlier magma ocean cumulates and the resulting mixture undergoes partial melting to form the mare basalt parent magmas. These magmas subsequently undergo fractional crystallization to create the observed fractionation trends. The major difference between our model and previous models such as Hughes et al [13] is that the KREEPy component mixes with distinct low-Ti and high-Ti mantle source regions, and that there is no significant mixing between these two source regions (e.g., figures 1,20). The physical process by which the KREEP component mixes with the cumulate mantle rocks is uncertain; the KREEPy component may sink as solid blocks of crystalline material or as a liquid. For this material to sink, it must have been an Fe-rich precursor to KREEP and not true "urKREEP", whose density is lower than that of mare basalt.

REFERENCES: [1] Papike et al (1976) Rev. Geophys. Space Phys. 14, 475-540; [2] BVSP (1981) Pergamon Press, 951 pp; [3] Head (1976) Rev. Geophys. Space Phys. 14, 265-300; [4] James and Wright (1972) Geol. Soc. America Bull., 83, 2357-2382; [5] Shervais et al (1985) Proc. 15th Lunar Planet. Sci. Conf., Jour. Geophys. Res., 90, C375-C395; [6] Dickinson et al (1985) Proc. 15th Lunar Planet. Sci. Conf., J. Geophys. Res., 90, C365-C374; [7] Neal et al (1988) Proc. 18th Lunar & Planet. Sci. Conf., 139-1153; [8] Shervais et al (1985) Proc. 16th Lunar Planet. Sci. Conf., Jour. Geophys. Res., 90, D3-D18; [9] Shih et al (1986) Proc. 16th Lunar and Planet. Sci. Conf., J. Geophys. Res., 91, D214-D228; [10] Neal et al (1988) Proc. 18th Lunar Planet. Sci. Conf., 121-137; [11] Taylor & Jakes (1974) Proc. Lunar Sci. Conf. 5th, 1287-1305; [12] Kesson & Ringwood (1976) Earth Planet. Sci. Lett., 30, 155-163; [13] Hughes et al (1989) Proc. 19th Lunar Planet. Sci. Conf., 175-188; [14] Binder (1985) Proc. 16th Lunar Planet. Sci. Conf., J. Geophys. Res., 90, D19-D30; [15] Shervais & Taylor (1984) Origin of the Moon, 173-201; [16] Langmuir et al (1978) Earth Planet. Sci. Lett., 37, 380-390.

Fig. 1. Ti/Sm vs Sm for mare basalts from all sites. High-Ti basalts plot along the upper mixing curve, low-Ti basalts along the lower curve.

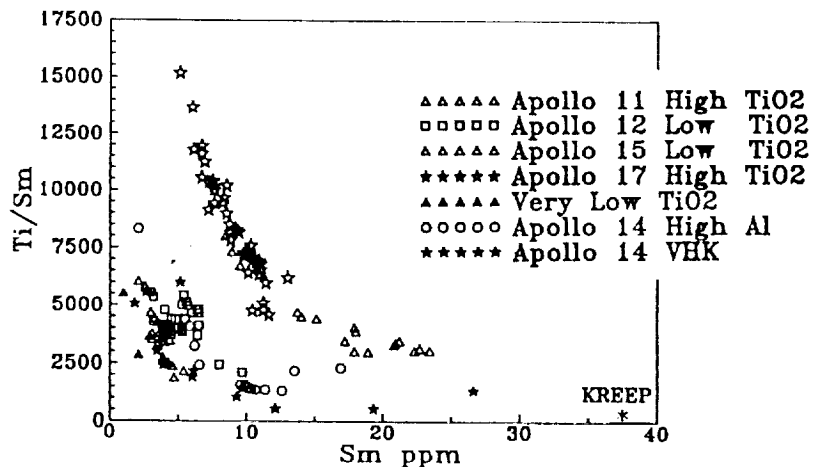
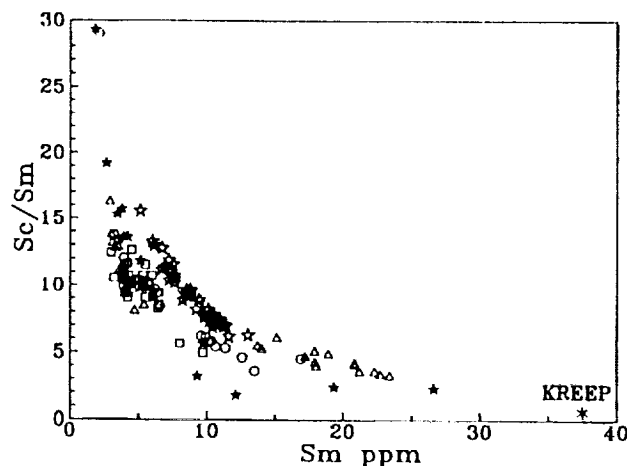


Fig. 2. Sc/Sm vs Sm for mare basalts from all sites. Same symbols as figure 1.





A DYNAMIC MELTING MODEL FOR THE ORIGIN OF APOLLO 15 OLIVINE-NORMATIVE AND QUARTZ-NORMATIVE MARE BASALTS.

17068P

P-2

Scott K. VETTER and John W. SHERVAIS, Department of Geological Sciences, University of South Carolina, Columbia, SC, 29208.

Early studies of mare basalts from the Apollo 15 site established that two distinct groups are represented: the olivine-normative basalts (ONB) and the quartz-normative basalts (QNB) [1-3]. The ONB and QNB suites are distinguished petrographically by their phenocryst assemblages (the ONBs are olivine-phyric, the QNBs are generally pyroxene-phyric) and chemically by their major element compositions: the QNBs are higher in SiO₂ and MgO/FeO, and lower in FeO* and TiO₂ than ONBs with similar MgO contents. Experimental data [2,4-7] show that the QNB suite is derived from a more magnesian, olivine-normative parent magma, a conclusion which is supported by the recent discovery of high-SiO₂ olivine-normative basalt clasts in breccia 15498 [8]. The high-SiO₂ ONBs fall on olivine control lines with primitive QNBs, and least-squares mixing calculations are consistent with the high-SiO₂ ONBs being parental to the more evolved QNB suite [8]. We include these high-SiO₂ ONBs as part of the "QNB suite" in this discussion. Our major element modeling results [8] also are consistent with the conclusions of earlier studies [2,3] which showed that the ONB and QNB suites cannot be related to one another by low pressure crystal fractionation. The combination of high Mg#, high SiO₂, and low TiO₂ in the QNB suite precludes a relationship to the ONB suite by simple removal of liquidus minerals (olivine and pigeonite).

Despite these significant differences in petrography and major element composition, both groups have nearly identical trace element concentrations and chondrite-normalized abundance patterns (Figure 1). The major question to be addressed by any petrogenetic model for Apollo 15 mare basalts is how to form mare basalt suites with distinctly different major element characteristics but nearly identical trace element compositions. The similarity in trace element concentrations imply compositionally similar source regions and similar percent melting, but these conclusions are not easily reconciled with the observed differences in major element compositions, which require sources with distinct mineralogies or large differences in percent melt.

PREVIOUS MODELS: The mare basalt source region has geochemical characteristics that are complementary to the highlands crust, and it is generally thought to comprise mafic cumulates from the magma ocean [9]. Early models of mare basalt petrogenesis, suggested that remelting of these cumulates at different depths resulted in the observed mare chemistries [9]. Despite the appeal of this simple model, there is increasing evidence that more complex scenarios are required. More recent models of mare basalt petrogenesis have stressed two dominant themes: (1) the assimilation of crustal components, e.g., KREEP [10-15], and (2) melting of complex hybrid source regions [16,17].

Binder [10] suggests that all mare basalts have undergone modification by a KREEPY component, but this model has only been applied in detail to aluminous mare basalts from the Apollo 14 site [10-15]. A major problem with this type of model is that the assimilation of KREEP tends to both enrich the LREE and MREE relative to the HREE. KREEP assimilation models which succeed at Apollo 14 site will not work at Apollo 15 because the Apollo 15 basalts have LREE/MREE slopes < 1. The Apollo 15 basalts also have low overall concentrations of incompatible elements which differ little between the two main suites present. These suites differ mainly in their major element chemistry (unlike the Apollo 14 basalts, which have nearly identical major element compositions). We have tried a variety of KREEP assimilation models on the Apollo 15 mare basalts and none have proved satisfactory.

Hughes et al. [17] have recently presented detailed, quantitative models that account for Apollo 15 ONBs by melting of hybrid source regions. These regions are complex mixtures of early magma ocean cumulates, late magma ocean cumulates, and trapped liquid. The trapped liquid component is late magma ocean with a KREEP-like composition, so these models are similar to the assimilation models in effect, but differ in concept. Hughes et al. [17] apply their model to Apollo 15 green glass, yellow-brown glass, and ONBs, but do not address the more subtle differences observed between the ONB and QNB suites.

DYNAMIC MELTING MODEL: We propose that the salient chemical characteristics of the Apollo 15 olivine normative and quartz normative mare basalt suites can be derived from a dynamic melting model without KREEP assimilation. In this model, melt extraction from the mantle source region is incomplete and 5-10% of the melt produced during each melting event is retained in the source region as dikes and veins [18]. During subsequent melting events, trace element concentrations are controlled by remelting of the dikes, whereas major elements are controlled by phase proportions and compositions in the refractory residuum. This model allows repeated melting of the same source region without total depletion of the incompatible trace elements. Because the refractory residuum is enriched in MgO and depleted in SiO₂ during melting, subsequent melts derived from this region tend to be more mafic and silica-undersaturated.

Three general situations were tested using this approach: (1) Cpx-rich cumulate source in equilibrium with late lunar magma ocean (LMO) ($L_a = 30 \times$ chondrite), (2) Olivine + Opx-rich cumulate with 20% Cpx in equilibrium with late LMO ($L_a = 30 \times$ chondrite), and (3) Olivine/Opx/Cpx cumulate in equilibrium with an early LMO ($L_a = 10 \times$ chondrite). All of our models share the following

10

10

characteristics: (1) Nine trace elements were included in the calculations (five REE, Ba, Th, Sc, Ti); (2) Following Nyquist et al. [19], a fractionated LMO was used (La/Lu = 2x chondrite); (3) Non-modal melting dominated by pyroxene; (4) We assume that 2-10% of the first stage melt was retained in the source as dikes/veins; (5) The high-SiO₂ ONBs are taken to be parental to the more evolved QNB suite; (6) In each case, the QNB parent magma (= high-SiO₂ ONB) is assumed to be the first melt extracted from the source, and the normal low-SiO₂ ONBs are generated by re-melting of the refractory source region.

Figure 2 shows the results of our modeling compared to observed Apollo 15 mare basalt suites. Model 1 (Cpx-rich source with late LMO) produces observed trace element concentrations in the QNB parent magma after 25% melting. Remelting of the refractory residue (plus 10% dikes) produces the relative trace element concentrations of the ONB suite after 20% melting; matching the absolute concentrations requires about 25% fractional crystallization. Model 2 (olivine-rich source with late LMO) matches the QNB parent magma after 5% to 7% melting. Primitive ONBs are produced by an additional 5-7% melting of the residue (plus 5-9% dikes). Model 3 (olivine-rich source with early LMO) produces the overall shape of the trace element patterns after 4% melting, but the absolute abundances are too low; approximately 50% fractional crystallization is required to produce the correct absolute abundances. Re-melting of this mantle residuum (plus 5% dikes) can produce the ONB suite pattern, but up to 50% fractional crystallization is required to match the observed concentrations (Figure 2b).

Our results show that the dynamic melting model can be applied over a wide range of mantle compositions to successfully model mare basalt suites which have similar trace element abundances. It seems clear that model 1 is the most robust because the amount of melting significantly exceeds the amount of trapped/retained magma in the source, so we are not merely remelting the retained magma. However, Nyquist et al [19] have suggested that the Rb/Sr systematics of Apollo 15 ONBs require a source with only 20% Cpx. This constraint favors models 2 and 3 - which differ mainly in their LMO component. Model 3 may be applicable to a non-hybrid, magma ocean cumulate source region, whereas models 1 and 2 will probably require some hybridization to match the major element characteristics of these basalts. We are currently attempting to model major element variations during partial melting of the LMO cumulates to further constrain these calculations.

REFERENCES [1] Rhodes J.M. and Hubbard N.J. (1973) Proc. Lunar Planet. Sci. Conf., 4th, 1127-1148; [2] Chappell B.W. and Green D.H. (1973) EPSL, 18, 237-246; [3] Dowty E., et al. (1973) Proc. Lunar Planet. Sci. Conf., 4th, 423-444; [4] Humphries et al., (1972) The Apollo 15 Lunar Samples, 103-107; [5] Lofgren (1975) Lunar Science VI, 515-517; [6] Longhi et al (1972) The Apollo 15 Lunar Samples, 131-134; [7] Grove T. and Walker D. (1977) Proc. Lunar Sci. Conf. 8th 1501-1520; [8] Vetter et al. (1988) Proc. Lunar Planet. Sci. Conf. 18th, 255-271; [9] Taylor, S.R. and Jakes, P. (1974) Proc. Lunar Sci. Conf. 5th, 1287-1305; [10] Binder, A.B. (1985) Proc. Lunar Planet. Sci. Conf. 16th, D19-D30; [11] Shervais J. et al, (1985) Jour. Geophys. Res., 90, C375-C395; [12] Shervais J. et al, (1985) Jour. Geophys. Res., 90, D3-D18; [13] Shih, C-Y. et al, (1986) Proc. Lunar Planet. Sci. Conf. 16th, J. Geophys. Res., 91, D214-D228; [14] Dickinson, T. et al, (1985) Proc. Lunar Planet. Sci. Conf. 15th, 90, C365-C374; [15] Neal C.R., et al (1988) Proc. Lunar Planet. Sci. Conf. 18th, 121-137; [16] Ringwood A. and Kesson S. (1976) Proc. Lunar Sci. Conf. 7th, 1697-1772; [17] Hughes et al. (1989) submitted Geochim. Acta Chem.; [18] Langmuir C. et al. (1977) EPSL 36, 133-156; [19] Nyquist L. et al. (1977) Proc. Lunar Sci. Conf. 8th 1383-1415.

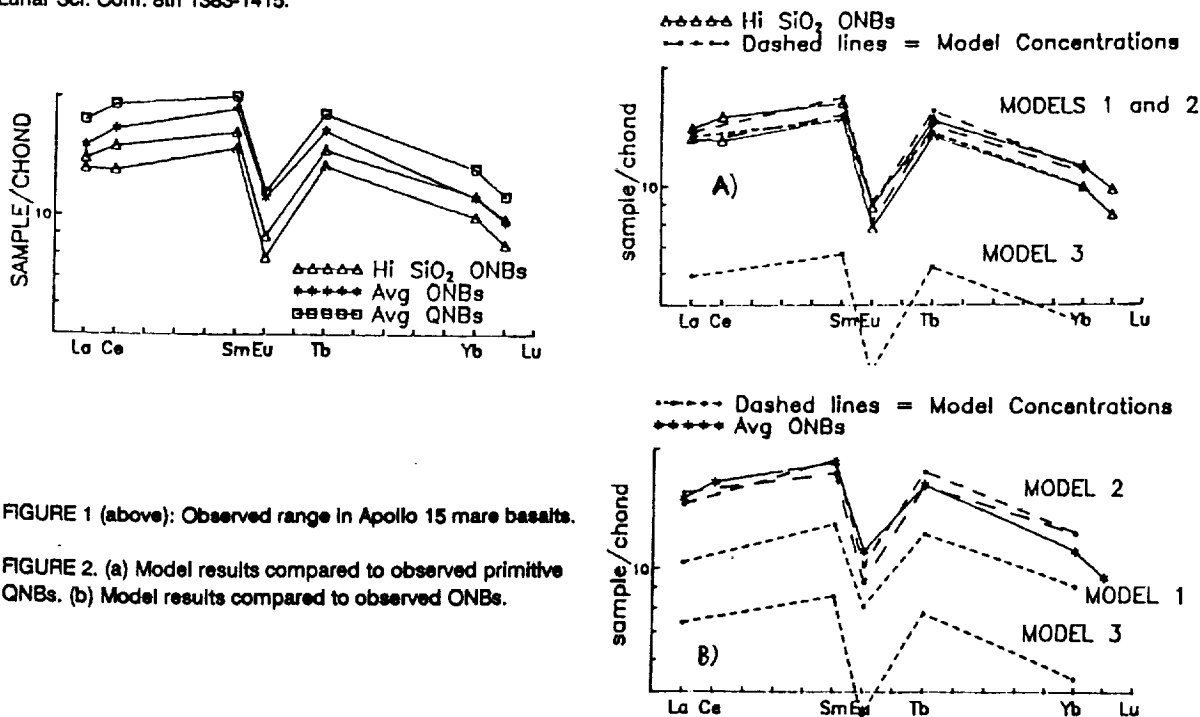


FIGURE 1 (above): Observed range in Apollo 15 mare basalts.

FIGURE 2. (a) Model results compared to observed primitive QNBs. (b) Model results compared to observed ONBs.



59-91
N 94 424 372
170689
P. 2**MELT ROCK COMPONENTS IN KREEPY BRECCIA 15205 – PETROGRAPHY AND MINERAL CHEMISTRY OF KREEP BASALTS AND QUARTZ-NORMATIVE MARE BASALTS.**

John W. Shervais and Scott K. Vetter, Department of Geological Sciences, University of South Carolina, Columbia, SC

Many current models for the origin of lunar highland rocks feature as an essential component the assimilation of KREEPy material by primitive magmas parental to the Mg-rich suite and alkali suite plutonic rocks (e.g., [1]). Similar models have also been proposed for the origin of various mare basalt suites [2,3,4,5]. However, any model which considers assimilation of KREEP an important petrologic process must sooner-or-later deal with the question: what is KREEP? Because pristine KREEP basalts are rare, and most known samples are small (e.g., 15382/15386), the geochemical variability of KREEP basalts is poorly known. Other KREEP compositions which are commonly used in these models include the hypothetical "high-K KREEP" component of Warren and Wasson [6], which is derived from Apollo 14 soil data, and the "superKREEP" quartz-monzodiorite 15405 [7].

Lunar breccia 15205 is a polymict regolith breccia that consists of approximately 20% KREEP basalt clasts and 20% quartz-normative basalt clasts in a KREEP-rich matrix [8]. Bulk rock mixing calculations show that this sample comprises about 84% KREEP [9]. The clasts range up to 1 cm in size, but most are considerably smaller. The primary aim of this study is to characterize pristine KREEP basalts petrographically, to establish the range in chemical compositions of KREEP basalts, and to test models that have been proposed for their origin. In addition, we may be able to extend the compositional range recognized in the quartz-normative basalt suite and cast some light on its origin as well. Preliminary whole rock geochemical data on the KREEP basalts are presented in a companion paper by M.M. Lindstrom and co-workers [10]. We concentrate here on the petrography and mineral chemistry of these clasts, and the implications these data have for the origin of the different melt rock suites.

METHODS: Twenty-three rock fragments were extracted from the remaining large subsamples of 15205 in the Pristine Sample Lab at JSC. Six of these represent sample pairs from the same clast, so only twenty unique clasts are represented. Because of their small size (commonly ≤ 5 mm ϕ), only sixteen were large enough for whole rock analysis; these data are reported by Lindstrom et al [10]. Twelve fragments representing ten clasts were prepared as polished probe mounts for petrographic examination and mineral analysis. Mineral analyses were carried out on a Cameca SX-50 Electron Microprobe at the University of South Carolina using natural and synthetic mineral standards.

PETROGRAPHY AND MINERAL CHEMISTRY

KREEP BASALTS: Seven of the ten clasts studied here are KREEP basalts characterized petrographically by modes that are rich in plagioclase (~45-50 vol%) compared to typical mare basalts. Dymek et al [8] recognized 5 textural varieties of KREEP basalt in their detailed petrographic study of serial thin sections from 15205, but all the KREEP basalt clasts extracted for this study are (with one exception) medium to coarse-grained basalts with textures that grade from ophitic or subophitic to intersertal within the same rock. The finer-grained varieties consist of slender plagioclase laths up to 0.4 x 0.08 mm in size, intergrown with somewhat larger, blocky pyroxene grains. Coarser-grained varieties have blockier plagioclase (0.8 x 0.3 mm) that is only partly included in pyroxene and may grade into an intergranular texture. Regardless of grain size, almost all of the ophitic/subophitic KREEP basalts contain an irregularly distributed mesostasis consisting of K-rich glass, K-feldspar, silica, Ca-phosphate, and ilmenite. Ilmenite, the only ferromagnesian oxide found in the KREEP basalts, also occurs as discrete slender grains between the coarser silicate phases. Pyroxene in the KREEP basalts ranges from pale tan magnesian pigeonite cores (En76 Wo4 to En67 Wo5) to rims of greenish ferroan pigeonite or augite (En42 Wo15 - En33 Wo39) (figure 1). As noted by Dymek et al. [8], some pyroxenes in the coarse-grained KREEP basalts also zoned inward to fill hollow cores (En58 Wo8). Plagioclase ranges in composition from An 78 to An 88 – more sodic than the plagioclase in mare basalt.

One KREEP basalt clast is texturally distinct from the others. This pale-grey colored clast (B1) consists of a fine-grained, variolitic intergrowth of slender quench pyroxene (En69 Wo5 - En49 Wo25) and plagioclase (An79-An85) with an opaque black glass and ilmenite between the varioles. Despite its textural similarity to rapidly-cooled mare basalts, it can be distinguished as a KREEP basalt by the occurrence of K-feldspar in the groundmass, the lack of spinel-phase oxides, and its KREEPy trace element composition [10].

MARE BASALTS: Four clasts of mare basalt were extracted from breccia 15205 for this study, but only three are available for petrographic study. Two are pyroxene-phyric basalts with fine-grained, variolitic groundmass, the third is a medium-grained ophitic/subophitic olivine-phyric basalt. Phenocrysts in the pyroxene-phyric basalts typically form large, elongate grains up to 1.5 x 0.3 cm in size, many of which contain hollow cores filled with the groundmass assemblage. The pyroxene phenocrysts have pigeonitic cores (En71 Wo4 to En66 Wo6) which zone outwards to ferroan pigeonite or subcalcic augite rims (En19 Wo15 - En37 Wo35) (figure 2). The variolitic groundmass consists dominantly of pyroxene-rich varioles with less abundant intergrown plagioclase, separated by an opaque glass and accessory oxide phases (chromian ulvospinel, ilmenite). Groundmass pyroxenes are more Fe-rich than the phenocrysts (En25 Wo10 - En5 Wo24) and many plot within the forbidden zone on the pyroxene quadrilateral (figure 2). Plagioclase occurs only in the groundmass as slender needles intergrown with the pyroxene-rich varioles. It is generally more calcic than plagioclase in the KREEP basalts, ranging from An83 to An92 in composition, and forms only 25-35 vol% of the mode.

The single ophitic-textured olivine-phyric basalt consists of blocky pyroxene grains 0.2-0.8 mm ϕ (50-55 vol% of mode) which enclose somewhat smaller, randomly-oriented plagioclase laths $\leq 0.4 \times 0.05$ mm in size (25-30 vol% of mode). The small Fo50-55 olivine phenocrysts up to 0.4 mm ϕ are jacketed by pigeonite, similar to other olivine-phyric members of the QNB suite (e.g., [11-13]). The larger blocky pyroxenes have pigeonite cores (En58 Wo9) that zone outwards to augite or ferroan pigeonite (En40 Wo30 - En25 Wo18); smaller interstitial pyroxenes have compositions similar to these rims (figure 2). Plagioclase in this basalt is more calcic than the other basalt samples (An89 - An92) and exhibits a more restricted range in composition. Accessory phases include Ti-rich Cr-spinel, chromian ulvospinel, ilmenite, Fe-metal, and troilite.

DISCUSSION

KREEP BASALTS: All of the KREEP basalts studied here are (with one exception) texturally and mineralogically the same, with only minor variations in grain size and mode. Grain size variations do not exceed those found within single flows of slowly cooled terrestrial basalts, consistent with the idea that all of the medium to coarse grained KREEP basalt samples studied here represent fragments derived from a single lava flow. This interpretation is supported by the limited range in mineral compositions observed, which is approximately the same for all of the medium/coarse-grained KREEP basalts. The most obvious difference between these basalts petrographically is in the proportion of mesostasis present, which ranges from almost zero up to 15 or 20 vol% of the mode. These variations are not surprising when the small size and coarse textures of these clasts is considered. As noted by Lindstrom et al [10], these modal variations in the mesostasis could easily account for the range in trace element concentrations observed in the KREEP basalt clasts studied here, according to the short-range unmixing model of [14-15]. The fine-grained KREEP basalt studied here may represent the quickly cooled outer portion of this same flow, but the extreme textural difference seems more consistent with its origin in a separate flow. Nonetheless, its trace element composition is identical to the other KREEPy basalts.

MARE BASALTS: Two of the mare basalts studied here are pyroxene-phyric basalts with nearly identical groundmass textures and similar ranges in mineral chemistry; these clasts may represent different pieces of a single, quartz-normative basalt flow. Texturally, they resemble typical pyroxene vitrophyres of the QNB suite [11-13]. The olivine-phyric basalt is petrographically similar to olivine-phyric basalts of the QNB suite - a relationship suggested by the occurrence of pigeonite mantles on the olivine. It cannot be from the same flow as the pyroxene-phyric QNBs, however, because those rocks are no longer saturated with olivine.

REFERENCES: [1] Warren, P.H. (1968) Proc. 18th Lunar Planet Sci Conf., 233-242; [2] Shervais J.W., et al (1985) Jour. Geophys. Res., 90, C375-C395; [3] Dickinson, T. et al, (1985) Proc. 15th Lunar Planet. Sci. Conf., J. Geophys. Res., 90, C365-C374; [4] Neal C.R. et al, (1988) Proc. 18th Lunar and Planetary Science Conf., 139-153; [5] Binder, A.B. (1985) 16th Lunar Planet. Sci. Conf., J. Geophys. Res., 90, D19-D30; [6] Warren, P.H. and Wasson, J.W. (1979) Rev. Geophys. Space Phys., 17, 2051-2083; [7] Taylor, G.J., et al. (1980) Proc. Lunar Highlands Crust, Papike and Merrill, eds, 339-352; [8] Dyrnek, R.F., et al. (1974) Proc. 5th Lunar Sci. Conf., 235-260; [9] Schonfeld (1975) Lunar Science VI, 712-714; [10] Lindstrom, M.M., et al, (1989) this volume; [11] Rhodes J.M. and Hubbard N.J. (1973) Proc. Lunar Planet Sci. Conf., 4th, 1127-1148; [12] Papike J.J., et al. (1976) Rev. Geophys. Space Phys., 14, 475-540; [13] Vetter et al (1988) Proc. 18th Lunar and Planetary Science Conf., 255-271; [14] Lindstrom M.M. and Haskin L.A. (1978) Proc. Lunar Sci. Conf., 9th, 465-486; [15] Lindstrom M.M. and Haskin L.A. (1981) Geochim. Cosmochim. Acta, 45, 15-31.

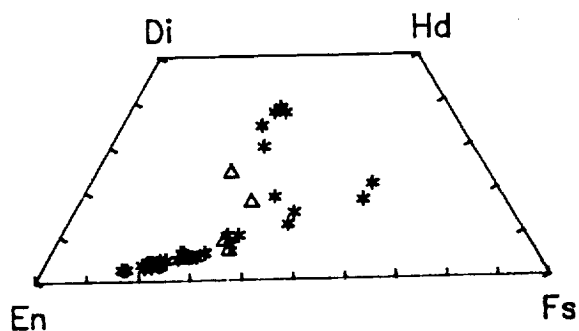


Figure 1. Pyroxene compositions in 15205 KREEP basalts. Ophitic/subophitic KREEP = *, Variolitic KREEP = triangle.

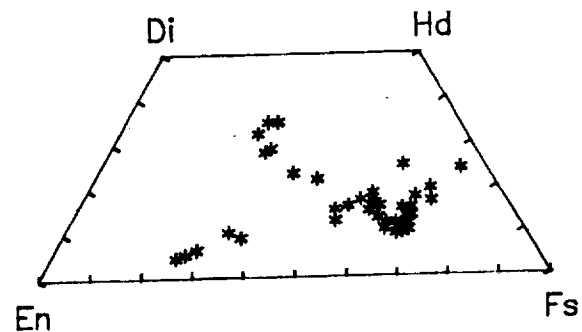
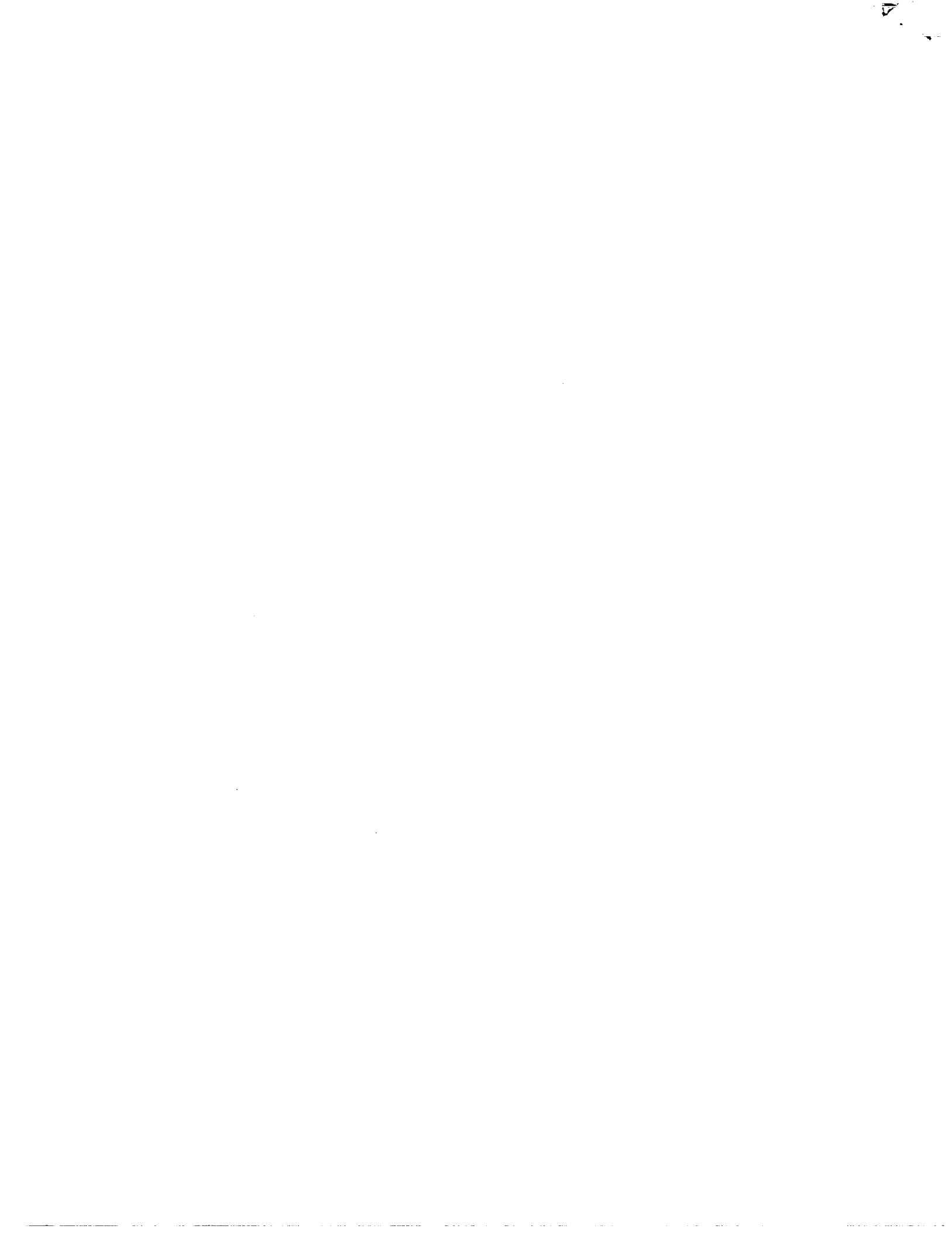


Figure 2. Pyroxene compositions in the QN mare basalts.



HETEROGENEITY IN SMALL ALIQUOTS OF APOLLO 15 OLIVINE NORMATIVE BASALT:
IMPLICATIONS FOR BRECCIA CLAST STUDIES.170690
P-2John W. SHERVAIS and Scott K. VETTER, Univ. of South Carolina, Columbia, SC 29208, and
Marilyn M. LINDSTROM, SN2/NASA-JSC, Houston, TX, 77058.

Most of the recent advances in lunar petrology are the direct result of breccia pull-apart studies, which have identified a wide array of new highland and mare basalt rock types that occur only as clasts within the breccias. These rocks show that the lunar crust is far more complex than suspected previously, and that processes such as magma mixing and wall-rock assimilation were important in its petrogenesis. These studies are based on the implicit assumption that the breccia clasts, which range in size from a few mm to several cm across, are representative of the parent rock from which they were derived. In many cases, the aliquot allocated for analysis may be only a few grain diameters across. While this problem is most acute for coarse-grained highland rocks, it can also cause considerable uncertainty in the analysis of mare basalt clasts. Similar problems arise with small aliquots of individual hand samples (e.g., Ryder and Steele, 1987).

We report here on our study of sample heterogeneity in 9 samples of Apollo 15 olivine normative basalt (ONB) which exhibit a range in average grain size from coarse to fine (15536, 15537, 15538, 15546, 15547, 15548, 15598, 15605, and 15636). Seven of these samples have not been analyzed previously, one has been analyzed by INAA only (15605; Ma et al, 1978), and one has been analyzed by XRF+INAA (15636; Compston et al, 1972; Fruchter et al, 1972). Our goal is to assess the effects of small aliquot size on the bulk chemistry of large mare basalt samples, and to extend this assessment to analyses of small breccia clasts.

METHODS: Five samples were received as 2 aliquots of 150 mg each taken from different parts of the parent sample; the other four were received as single 200 mg fragments, each of which were split into two 100 mg aliquots before crushing. Each aliquot was powdered in an agate mortar and divided into two splits: 70-100 mg for INAA (selected major and trace elements) and 30-50 mg for fused bead EMP analysis (major elements). All samples were studied petrographically in thin section, and phase compositions were determined by EMP analysis.

RESULTS: All of the samples are low-SiO₂ ONBs typical of the Apollo 15 site; seven are olivine microgabbros, the other two are medium to fine-grained olivine-phyric basalts. Olivine (Fo65 to Fo30) is the primary liquidus phase and occurs as subhedral to rounded grains which may be jacketed by pyroxene. Plagioclase most commonly occurs as large, poikilitic laths that enclose both pyroxene and olivine. Several samples contain mafic-rich clots up to several mm across which have little or no feldspar. Late phases include fayalite, ilmenite, spinel, cristobalite, whitlockite, and K,Si-rich glass. The late phases are commonly associated spatially, and in the coarser-grained samples (15547, 15636) they are concentrated in the mafic-rich clots. All of the phases are relatively Fe-rich relative to the A-15 QNB suite; phase compositions are shown in figure 1.

Major element analyses of aliquots from the same sample generally agree within analytical uncertainty, except for samples 15547 and 15636. These samples are higher in Fe, Ti, P₂O₅, and La than the other samples, and corresponding aliquots exhibit large differences in composition (figure 2). These differences are shown in figure 3 as the function Δ/σ , where Δ equals the deviation of the samples from their mean and σ is the average analytical uncertainty (one sigma). Total analytical uncertainty (at the two sigma level) is shown by the dashed line. Three samples (15536, 15537, and 15605) shown no variation at the 2 sigma level, and four samples (15538, 15546, 15548, 15598) show minor differences between aliquots (one or two elements vary at the 3 sigma level). There is no consistent relationship to grain size - fine and coarse-grained samples are present in each group. The largest variations are shown by 15547 and 15636, in which aliquots differ by up to 14 sigma from the mean (figure 3). Short count trace element data exhibit more scatter than do the major elements, and differences between aliquots can be substantial, even when major element differences are small. These differences cannot be quantified, however, until more reliable long count data become available.

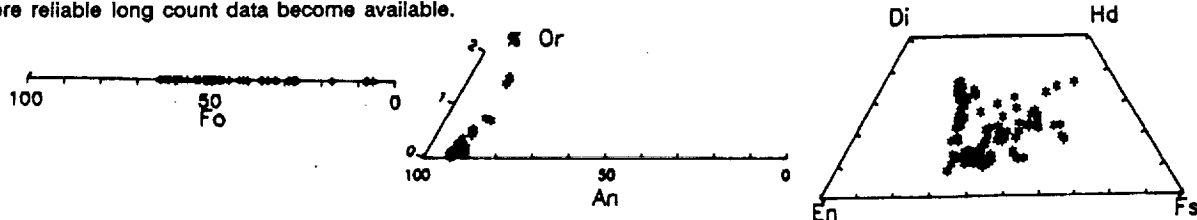


Figure 1. Olivine, pyroxene, and plagioclase compositions in Apollo 15 olivine basalts.



DISCUSSION : The dispersion of chemical data about a mean of replicate analyses is caused by (1) analytical uncertainty and (2) sample heterogeneity on a scale larger than the sample size. When viewed in terms of analytical uncertainty at the two sigma level, most of aliquot pairs in this study are identical or nearly identical in major element composition, regardless of grain size or texture. The two samples which exhibit large differences between aliquot pairs are characterized by heterogeneous distribution of mafic-minerals and late-forming mesostasis phases. Figure 4 is a BSE image of a typical mesostasis clot in 15636 containing fayalite, ilmenite, cristobalite, glass, and apatite, surrounded by zoned pyroxene and plagioclase. The mesostasis phases contain most of the Fe (fayalite, ilmenite), Ti (ilmenite), P (apatite), and REE (apatite) found in the sample. The positive correlation between these elements seen in figure 2 implies that the chemical heterogeneity exhibited by 15547 and 15636 is due largely to the heterogeneous distribution of late-forming mesostasis phases. Similar coarse-grained microgabbro samples in which these phases are more evenly distributed do not show significant chemical dispersion, and even the small aliquots studied here are representative for the major elements. Trace elements seem to be more sensitive, and detailed geochemical modeling based trace element concentrations in very small samples may be subject to large uncertainties. Because the sample aliquots studied here are about the same size as most aliquots of breccia clasts, the same conclusions will apply to clast studies.

References:

- Compston et al (1972) A-15 Lunar Samples, 347-351.
Ma et al (1978) PLPSC 9, 523-533.
Ryder, G. and Steele, A. (1987) LPS XVIII, 862.

Figure 2. Whole rock chemical variations in aliquots of Apollo 15 olivine basalt. Note positive correlation of Fe, Ti, P, and La (below).

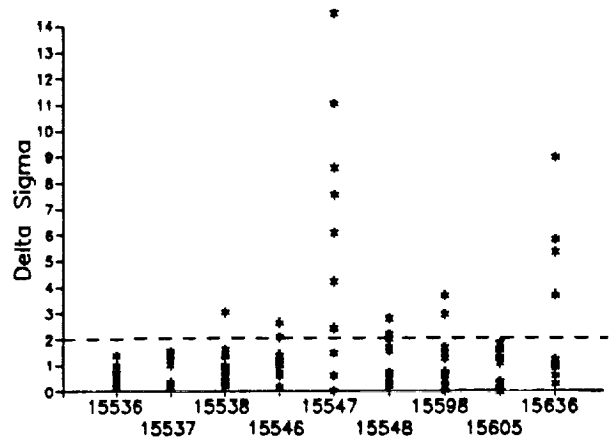
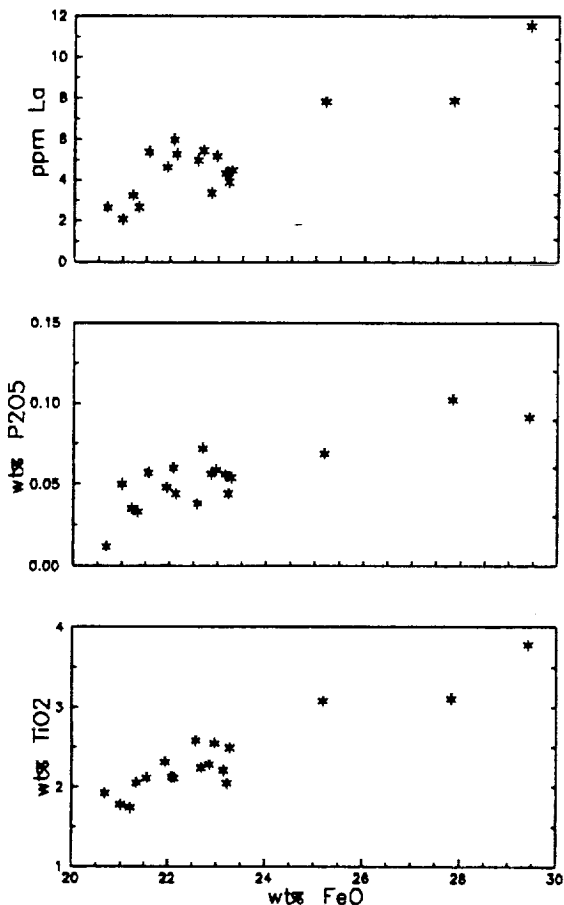


Figure 3. Chemical dispersion of olivine basalt aliquots relative to analytical uncertainty. Function Δ/σ equals deviation of analysis from mean, divided by uncertainty for that element (above).



Figure 4. BSE image of mesostasis clot in 15636. Bright = Fayalite; dark grey = feldspar, cristobalite, and glass; light grey = whitlockite; zoned grey = pyroxene. Bar scale = 200 microns.

